

**An Investigation of
Coxsackie and Adenovirus Receptor
in the Human Pancreatic Beta Cells**

Eseoghene Ifie

Doctor of Philosophy

July 2018

An Investigation of Coxsackie and Adenovirus Receptor in the Human Pancreatic Beta Cells

Submitted by Eseoghene Ifie to the University of Exeter as a thesis for the degree of Doctor of Philosophy in Medical Studies in July 2018.

This thesis is available for Library use on the understanding that it is copyright material and that no quotation from the thesis may be published without proper acknowledgement.

I certify that all material in this thesis which is not my own work has been identified and that no material has previously been submitted and approved for the award of a degree by this or any other University.

.....

ABSTRACT

Human pancreatic beta cells are susceptible to infection by enteroviruses, especially Coxsackie B viruses, and such infections could contribute to the development of Type 1 diabetes. Enteroviruses gain entry via cell surface receptors, one of which, the Coxsackie and Adenovirus receptor (CAR), is a transmembrane cell adhesion protein which serves as a key entry receptor for Coxsackie B viruses and is thought to be localised mainly within regions where contacts are formed between adjacent cells. CAR exists as at least 5 isoforms and this study has examined their expression profile and distribution in the human pancreas utilising; formalin-fixed paraffin-embedded pancreatic sections from non-diabetic individuals, type 1 diabetes patients and a human tissue microarray. Isolated human islets, human pancreatic beta and ductal cell lines were also studied. Immunological and molecular approaches were employed to examine the expression and cellular localisation of the known CAR isoforms in human pancreas.

One specific isoform of CAR (CAR-SIV) with a unique C terminal PDZ binding domain, was highly expressed in human beta cells at the protein level. Surprisingly, it was distributed in a punctate manner mainly within the cytoplasm of the cells, rather than at the cell surface. In human beta cells, within the cytoplasm CAR-SIV co-localised with ZnT8, PC1/3 and insulin but less so with proinsulin suggesting that CAR-SIV is associated with insulin secretory granules. Immunogold labelling and electron microscopic analysis revealed that CAR-SIV is localised both to maturing insulin secretory granules and to fully mature, dense-core (insulin) secretory granules. Intriguingly, CAR-SIV colocalises and interacts with a cytosolic protein, PICK1, which plays a role in the budding, maturation and

trafficking of insulin secretory granules. On this basis, a model is proposed whereby CAR-SIV and PICK1 interact to regulate the maturation and trafficking of insulin secretory granules. Overall, this study suggests that the specialised role and subcellular localisation of CAR-SIV in human beta cells may contribute to their sensitivity to enteroviral infection following externalisation of the protein at the cell surface, during insulin exocytosis.

Table of Contents

ABSTRACT	3
LIST OF FIGURES	11
LIST OF TABLES	15
ACKNOWLEDGEMENT	17
ABBREVIATIONS	18
PUBLICATIONS	23
CHAPTER 1	
Introduction.....	24
1.1 Brief history of diabetes mellitus	25
1.2 Diabetes mellitus	26
1.2.1 Type 1 diabetes (T1D).....	27
1.2.2 Other forms of diabetes.....	28
1.2.3 Immune mediated Type 1 diabetes.....	31
1.3 Pancreas	34
1.3.1 Islets of Langerhans.....	35
1.3.2 Studying the beta cell.....	38
1.3.3 Insulin granule biogenesis.....	38
1.3.4 Insulin secretion	41
1.3.5 Alternate signals for insulin secretion	44
1.3.6 Insulin granule pools	45
1.3.7 Exocytosis.....	46
1.3.7.1 Fusion pore opening	47
1.3.8 Endocytosis	50
1.4 Human enteroviruses and Type 1 diabetes	52
1.5 Mechanism of virus-induced autoimmune T1D	57
1.5.1 Direct beta cell damage	57
1.5.2 Persistent enteroviral infection	58
1.5.3 Molecular mimicry	59
1.6 Enterovirus receptors	59
1.7 The Coxsackievirus and adenovirus receptor (CAR)	61
1.7.1 Structure of CAR.....	64
1.7.2 CAR expression in cells and tissues	67
1.7.3 CAR Post-translational modifications	68
1.7.9 CAR interacting protein partners	70
1.7.10 Mechanism of Coxsackievirus entry through CAR.....	73

1.8 AIMS	75
CHAPTER 2	
Materials and Methods.....	76
2.1 Source of reagents	77
2.2 Cell culture	79
2.2.1 Passaging of cell line	80
2.3 Isolated human Islets.....	80
2.4 Tissue samples	81
2.4.1 Microtomy	82
2.5 Immunostaining reagents	83
2.6 Immunocytochemistry (ICC)	84
2.6.1 Cells and fixation.....	84
2.6.2 Staining.....	84
2.7 Immunohistochemistry (IHC)	85
2.8 Immunofluorescence microscopy	87
2.8.1 Imaging.....	87
2.9 Cryoimmunogold electron microscopy (Cryo-EM).....	88
2.10 RNA analysis.....	88
2.10.1 RNA purification	88
2.10.2 RNA or DNA estimation	89
2.10.3 cDNA (Complementary DNA) synthesis.....	89
2.10.4 Primer design.....	89
2.11 polymerase chain reaction (PCR).....	90
2.12 DNA sequencing	90
2.13 RT-Real Time PCR.....	91
2.14 Laser capture microdissection of human islets	91
2.15 RNAseq.....	93
2.16 Protein analysisby Western blotting	93
2.16.1 Sample preparation.....	93
2.16.2 Protein estimation	94
2.16.3 Electrophoresis and protein transfer.....	94
2.16.4 Antibody probing	95
2.16.5 Detection of proteins	96
2.17 Flow cytometry	96
2.17.1 Cell preparation.....	97
2.17.2 Extracellular staining of surface antigen.....	97
2.17.3 Intracellular staining of antigen.....	97

2.18 Proximity ligation assay (PLA)	98
2.19 Co-immunoprecipitation.....	99
2.19.1 Cell lysate preparation	99
2.19.2 Precipitation of Immune complexes.....	99
2.20 DNA cloning	100
2.20.1 Agar plates.....	100
2.20.2 Bacterial transformation and plasmid purification	100
2.20.3 Glycerol storage.....	101
2.21 Transient transfection of purified plasmid	101
2.21.1 Identification of a suitable transfection reagent for the human pancreatic beta cell line 1.1B4	102
2.21.2 Transient transfection of CAR-SIV Myc construct into the human pancreatic beta cell line 1.1B4.	106
2.22 Site directed mutagenesis	111
2.22.1 Restriction digest	113
2.22.2 Direct sequencing confirming successful site directed mutagenesis.....	114
2.23 Human growth hormone assay (HGH).....	116
2.24 Statistical analysis	119

CHAPTER 3

Characterisation of CAR isoforms in the human beta cell and pancreas.....	120
3.1 Introduction	121
3.2 Results	123
3.2.1 RT-PCR detection of mRNA encoding specific CAR isoforms in human pancreatic islets and human beta cell lines	123
3.2.2 TaqMan qRT-PCR detection of mRNA encoding specific CAR isoforms in isolated and laser captured micro-dissected human pancreatic islets	128
3.2.3 RNAseq and RT-PCR detection of mRNA encoding specific CAR isoforms and effect on cytokine treatment in human pancreatic islets and human beta cell lines	133
3.2.4 Detection of CAR isoform protein expression in human pancreatic tissue by immunohistochemistry	139
3.2.5 Detection of CAR isoform protein expression by immunofluorescence analysis in human pancreatic tissue.....	145
3.2.6 Detection of other CAR isoforms by immunofluorescence analysis in human pancreatic tissue.....	148
3.2.7 CAR isoform expression by Western blotting	152
3.2.8 Detection of ADAM10 expression in isolated human islets, human pancreatic tissue and beta cell line EndoC-βH1	155

3.2.9 Comparison of CAR CT and CAR RmcB antisera in human pancreatic tissue and the human pancreatic beta cell line 1.1B4.....	157
3.2.10 CAR-SIV isoform expression in the human pancreas.....	159
3.2.11 CAR-SIV isoform expression in the pancreas of Type 1 diabetes patients	164
3.2.12 CAR-SIV isoform expression in the pancreas of Type 2 diabetes patients	167
3.2.13 Differential staining of CAR-SIV isoform in mouse and human pancreas tissue	168
3.3 Discussion.....	173
3.3.1 Expression of transmembrane CAR isoform in isolated human islets and beta cell lines.....	173
3.3.2 Expression of soluble CAR isoform in isolated human islets and pancreatic beta cell lines.....	174
3.3.3 Cytokine treatment has no effect in CAR isoform expression in the isolated human islets and EndoC-βH1 cells	175
3.3.4 CAR isoform expression in the human pancreatic tissue.....	176
3.3.5 CAR isoform protein expression in the isolated human islets and pancreatic beta cell lines.....	177
3.3.6 CAR isoform expression in autoantibody positive individuals without diabetes and individuals with Type 2 Diabetes	179
3.3.7 Differential CAR isoform expression in mouse and human pancreatic tissue	180
3.3.8 Summary:	181

CHAPTER 4

Characterisation of CAR antisera using human pancreas tissue beta and ductal cells.....	182
4.1 Introduction	183
4.2 Results	185
4.2.1 Trial of CAR antisera in human pancreatic ductal cell line.....	185
4.2.2 Detection of CAR surface expression in the human pancreatic beta and ductal cell line model	188
4.2.3 Detection of intracellular CAR expression in the human pancreatic beta and ductal cell line models.....	191
4.2.4 Bioinformatics prediction of CAR-SIV isoform structural orientation within a cell.....	193
4.2.5. Flow cytometry detection of CAR orientation in the human pancreatic beta cell model (EndoC-βH1).....	195
4.2.6 CAR-SIV isoform immunolabelling in normal and cancerous human tissues	200
4.3 Discussion.....	205

4.3.1 CAR CT, CAR ECD and CAR RmcB antisera differentially label the human pancreatic ductal cell (PANC-1)	205
4.3.2 The extracellular domain of CAR is present on the surface of human pancreatic beta and ductal cell lines	205
4.3.3 CAR CT antiserum staining suggests that CAR-SIV is present in intracellular compartments in human pancreatic beta and ductal cells	208
4.3.4 CAR orientation in EndoC- β H1 cell line.....	208
4.3.5 CAR-SIV is differentially expressed in normal and cancerous human tissues	210
4.3.6 Differential CAR-SIV and CAR-TVV expression in normal and cancerous human tissues by RNAseq.....	210

CHAPTER 5

Subcellular localisation of CAR-SIV in human beta cell of the pancreas.....214

5.1 Introduction	215
5.2 Results	216
5.2.1 Cellular localisation of CAR-SIV in the human pancreatic beta cell	216
5.2.2 Co-localisation of CAR-SIV with insulin secretory granule (ISG) proteins in the beta cell	219
5.2.3 Pearson's correlation coefficient (PCC) quantifies the colocalisation between CAR-SIV and the secretory granule proteins	223
5.2.4 Manders correlation coefficient (MCC) quantifies the colocalisation between CAR-SIV and the secretory granule proteins	225
5.2.5 Cryo-immunogold electron microscopy (Cryo-EM) of CAR-SIV and ZnT8 in the insulin granule.....	229
5.2.6 Morphometric quantification of CAR-SIV labelling density.....	232
5.2.7 CAR-SIV immunogold labelling at different stages of insulin granule maturation.....	233
5.2.8 Detection of PICK1 protein expression in human pancreatic tissue by immunohistochemistry	236
5.2.9 PICK1 detection by immunofluorescence and confocal immunofluorescence microscopy	239
5.2.10 Pearson's correlation coefficient and Mander's correlation coefficient quantifies the colocalisation of PICK1, CAR-SIV and Insulin.....	242
5.2.11 PICK1 expression by Western blotting analysis	244
5.2.12 Do PICK1 and CAR-SIV interact in the human pancreatic beta cell?	246
5.3 Discussion.....	251
5.3.1 CAR-SIV colocalises with insulin in human pancreatic beta cells	251
5.3.2 CAR-SIV is present in both immature and mature insulin secretory granule proteins.....	251

5.3.3 CAR-SIV colocalises and interacts with PICK1 in the insulin secretory granule	255
CHAPTER 6	
Investigation of the role of CAR-SIV in the human beta cell.....	264
6.1 Introduction	265
6.2 Results	265
6.2.1 Confirming the generated wildtype CAR-SIV and truncated CAR-SIV mutant constructs	265
6.2.2 Detection of CAR CT and CAR RmcB antisera binding in transfected cells using a proximity ligation assay	270
6.2.3 CAR-SIV colocalises with insulin in wild-type CAR-SIV construct in the human pancreatic beta cell line 1.1B4	273
6.2.4 Investigating insulin secretion in transfected 1.1B4 cells	275
6.2.5 Effects of transfection with CAR-SIV on human growth hormone (hGH) release from 1.1B4 cells	277
6.2.6 Investigation of the human growth hormone (hGH) system in the rodent pancreatic INS-1E cell line.....	281
6.2.7. Immunocytochemical detection of human growth hormone (hGH) and CAR-SIV in the human pancreatic beta cell line 1.1B4	285
6.3 Discussion.....	287
6.3.1 Generation of wild-type and mutant CAR-SIV constructs	287
6.3.2 Validation of the specificity of the CAR CT antiserum using the mutant CAR-SIV construct	287
6.3.3 CAR-SIV overexpression did not impact on insulin granule secretion in this model-but is it the right model?	288
6.3.4 Future work to assess the effect of CAR-SIV in insulin secretion	289
CHAPTER 7	
Conclusion.....	291
7.0 Summary.....	292
7.0.1 The localisation of CAR-SIV may explain the susceptibility of human beta cells to enteroviral infection.....	293
7.0.2 CAR-SIV may have a role in vesicle maturation and trafficking in human pancreatic beta cells	295
7.1 Limitation of study	298
7.2 Future Work	298
APPENDIX.....	301
REFERENCES.....	306

LIST OF FIGURES

CHAPTER 1

<i>Figure 1.1 Worldwide current and projected cases of diabetes.</i>	26
<i>Figure 1.2 Architectural difference in islet organisation of beta and alpha cells in human and mouse pancreas</i>	37
<i>Figure 1.3 Biogenesis of insulin granules.</i>	40
<i>Figure 1.4 Insulin secretion pathway.</i>	43
<i>Figure 1.5 Exocytosis mechanism of insulin secretion</i>	49
<i>Figure 1.6 Endocytosis proposed mechanism.</i>	51
<i>Figure 1.7 Structure and genome of Enterovirus.</i>	53
<i>Figure 1.8 Structure of the CAR protein and isoform.</i>	63
<i>Figure 1.9 Similarities and differences between the protein sequence of CAR-SIV and CAR-TVV.</i>	66
<i>Figure 1.10 CAR and interacting protein partners.</i>	72
<i>Figure 1.11 Mechanism of CVB entry into cells.</i>	74

CHAPTER 2

<i>Figure 2.1 Morphology of isolated human islets</i>	81
<i>Figure 2.2 Immunocytochemical staining with chromogranin and insulin antisera in EndoC-βH1 cell line</i>	85
<i>Figure 2.3 Immunocytochemical analysis showing pMax-GFP vector transfected in 1.1B4 cells utilising different transfection reagents.</i>	103
<i>Figure 2.4 Avalanche-Omni reagent has a 20% transfection efficiency when compared to Fugene transfection reagent in the 1.1B4</i>	105
<i>Figure 2.5 RT-PCR confirms the overexpression of CAR-SIV and not CAR-TVV in 1.1B4 cells transfected with CAR SIV-Myc.</i>	107
<i>Figure 2.6 Immunocytochemical analysis demonstrates low expression of CAR-SIV in transfected CAR-SIV Myc 1.1B4 cells.</i>	108
<i>Figure 2.7 Western blot analysis confirms low expression of CAR-SIV in transfected CAR-SIV Myc-tag 1.1B4 cells</i>	110
<i>Figure 2.8 Pipeline of site directed mutagenesis</i>	112
<i>Figure 2.9 Restriction digest confirms the wild-type CAR-SIV vector.</i>	114
<i>Figure 2.10 Direct sequencing confirmation of the generation of CAR-SIV wild type and truncated CAR-SIV constructs by insertion of mutation.</i>	115
<i>Figure 2.11 Pictorial diagram of human Growth Hormone secretion process.</i>	118

CHAPTER 3

<i>Figure 3.1 CAR-SIV or CAR-TVV transmembrane isoforms are amplified in isolated human islet and 1.1B4.</i>	124
<i>Figure 3.2 Isoform specific RT-PCR analysis revealed that CAR-SIV is more abundant than CAR-TVV from two independent isolated human islets.</i>	126
<i>Figure 3.3 CAR-SIV and CAR-TVV isoform is confirmed in isolated human islets.</i>	127
<i>Figure 3.4 Schematic diagram displaying the location of TaqMan probes and primers for each of the five CAR isoforms.</i>	129
<i>Figure 3.5 CAR-SIV and CAR-TVV is expressed in both isolated and LCM human islets</i>	131
<i>Figure 3.6 Visualisation of human islets for laser capture microdissection (LCM)</i>	132

Figure 3.7 RNAseq analysis demonstrates higher expression of CAR-SIV compared to CAR-TVV and low expression of CAR4/7	134
Figure 3.8 RT-PCR confirms the soluble CAR4/7 isoform expression in isolated human islets and 1.1B4 cell line	136
Figure 3.9 RNAseq analysis confirms no effect of cytokines on levels of mRNA of CAR isoforms.....	138
Figure 3.10 Schematic diagram of CAR antisera immunoreactivity against CAR protein	139
Figure 3.11 CAR isoforms are detected in the islet and exocrine pancreas utilising CAR (NT and ECD) antisera in NDA pancreas.	141
Figure 3.12 CAR isoform is detected in the islet and not in the exocrine tissue utilising CAR CT antiserum in NDA pancreas.	142
Figure 3.13 CAR isoform expression estimated by reciprocal intensity demonstrates that staining with CAR CT antisera detects high levels of CAR expression in the islets and not in the exocrine.....	144
Figure 3.14 The CAR-SIV isoform is absent in some endocrine cells of the islets.....	145
Figure 3.15 Immunofluorescence images demonstrate that CAR-SIV is present in the beta cells	147
Figure 3.16 Representative immunofluorescence microscopy images of CAR isoforms in the islet	150
Figure 3.17 Immunofluorescence images provide independent confirmation of CAR-SIV isoform in the beta cells from an autoantibody positive non-diabetic case.....	151
Figure 3.18 Western blot analysis utilising the CAR CT and CAR ECD antisera detects CAR-SIV in isolated human islets, 1.1B4, EndoC- β H1 and PANC-1 cell lines	153
Figure 3.19 ADAM10 is expressed in isolated human islets and EndoC- β H1.....	156
Figure 3.20 CAR RmcB antiserum epitope recognises the extracellular domain of CAR protein	157
Figure 3.21 Comparison of the CAR CT and CAR RmcB antisera in the human pancreatic tissue and in the human pancreatic beta cell line 1.1B4.....	158
Figure 3.22 Consistent expression of CAR-SIV isoform in the islets of non-diabetes cases from neonates to adulthood.	160
Figure 3.23 Consistent expression of CAR-SIV isoform and insulin in beta cells in non diabetic pancreas.....	161
Figure 3.24 CAR isoforms expression in the ductal cells of the human pancreas.....	163
Figure 3.25 CAR-SIV is expressed in only the insulin containing islets of Type 1 diabetes cases and not in insulin deficient islets.	165
Figure 3.26 CAR-SIV is present only in insulin containing islet (ICI) and is absent in insulin deficient islets (IDI)	166
Figure 3.27 Expression of CAR-SIV is not altered in a pancreas from a Type 2 diabetes case.....	168
Figure 3.28 Differential enteroviral VP1 protein expression in CVB infected human and mouse pancreatic tissue	169
Figure 3.29 Differential immunostaining with CAR CT and CAR ECD antisera in mouse pancreas tissue.....	171
Figure 3.30 Alignment of the human and mouse CAR-SIV isoform.....	172

CHAPTER 4

Figure 4.1 Schematic diagram of CAR antisera (CAR NT, CAR ECD, CAR RmcB and CAR CT) immunoreactivity against CAR protein.....	184
Figure 4.2 Staining with CAR RmcB and CAR CT, but not CAR ECD, antisera detects CAR in PANC-1 cell line	187
Figure 4.3 CAR expression is detected on the surface of cells by staining with CAR RmcB antisera	190
Figure 4.4 CAR-SIV isoform is detected intracellularly by staining with the CAR CT antisera in EndoC- β H1, 1.1B4 and PANC-1 cells.....	192
Figure 4.5 Bioinformatics prediction of the orientation of the CAR-SIV isoform with bioinformatic tool (Protter).....	194
Figure 4.6 CAR orientation is detected utilising staining with anti-CAR RmcB and anti-CAR CT in the human pancreatic beta cell EndoC- β H1.....	197
Figure 4.7 Staining with CAR RmcB suggests that the CAR-SIV isoform is present both on the surface of the cells and in an intracellular compartment.....	198
Figure 4.8 CAR-SIV isoform distribution and cellular localisation in normal and cancerous human tissues.	201
Figure 4.9 CAR-SIV isoform expression in normal and cancerous human tissues. ...	202
Figure 4.10 RNAseq analysis confirming the expression profile of CAR-SIV, CAR-TVV and CAR4/7.....	204
Figure 4.11 A model of CAR proteolysis, with molecular weights of the resulting fragments indicated.	207
Figure 4.12 CAR-SIV orientation in the beta cell....	209

CHAPTER 5

Figure 5.1 CAR-SIV colocalises with insulin in FFPE isolated human islets.....	217
Figure 5.2 CAR-SIV colocalises with insulin in insitu human pancreas	218
Figure 5.3 CAR-SIV colocalises with insulin secretory granule proteins in the beta cell.	220
Figure 5.4 CAR-SIV shows a partial colocalisation with proinsulin and no colocalisation with glucagon secretory granule proteins in the human islet.	222
Figure 5.5 Pearson's correlation coefficient (PCC) demonstrating an association between CAR-SIV and insulin secretory granule protein.....	224
Figure 5.6 Mander's correlation coefficient (MCC) demonstrating the proportion of CAR-SIV that associates with insulin secretory granule proteins	226
Figure 5.7 Mander's correlation coefficient (MCC) demonstrates that CAR-SIV associates more with insulin but less with proinsulin.....	228
Figure 5.8 Cryo-immunogold electron microscopy revealed that CAR-SIV and ZnT8 is localised to the insulin granule	230
Figure 5.9 Cryo-immunogold electron microscopy.	231
Figure 5.10 Cryo-immunogold electron microscopy quantification.....	233
Figure 5.11 Cryo-immune EM analysis of insulin granules at different stages of maturation.....	235
Figure 5.12 Cryo-EM analysis of pancreatic tissue with unconjugated gold particles	236
Figure 5.13 PICK 1 is expressed in the islet of normal human pancreatic tissue.....	238
Figure 5.14 CAR-SIV colocalises with PICK1 and insulin in the beta cell in normal pancreas tissues.....	240

Figure 5.15 Confocal microscopy coupled with hyvolution imaging demonstrates a close association of CAR-SIV and PICK1 in insulin granule of normal human pancreas.	241
Figure 5.16 Pearson correlation coefficient and Manders correlation coefficient demonstrating the extent of CAR-SIV colocalisation with PICK1 and insulin.	243
Figure 5.17 Schematic diagram of PICK1 antisera with epitope recognition sites against the PICK1 protein. Adapted from (Xu and Xia, 2006).....	245
Figure 5.18 Confirmation of PICK1 expression in isolated human islets and pancreatic beta cell lines EndoC-βH1 and 1.1B4.	245
Figure 5.19 Immunoprecipitation of PICK1 and CAR-SIV independently from EndoC-βH1 with different antisera.	247
Figure 5.20 Co-immunoprecipitation of CAR pulls down PICK1.	249
Figure 5.21 Co-immunoprecipitation of PICK1 weakly pulls down CAR.	250
Figure 5.22 Proposed CAR-SIV orientation in the insulin secretory granule.	258
Figure 5.23 Pictorial diagram of CAR-SIV and PICK1 binding.....	260
Figure 5.24 Model for CAR-SIV, PICK1 and ICA69 insulin granule maturation and trafficking.	262

CHAPTER 6

Figure 6.1 Full length CAR-SIV isoform is overexpressed in wild-type CAR-SIV and not in truncated CAR-SIV mutant constructs in 1.1B4 cell line	266
Figure 6.2 Confirmation of the CAR CT antiserum detecting only the full length CAR-SIV isoform.	267
Figure 6.3 Representative flow scatter plot confirming labelling with CAR RmcB and CAR CT antisera in CAR-SIV transfected 1.1B4 cells.....	269
Figure 6.4 Proximity ligation assay demonstrates the binding of CAR CT and CAR RmcB in the different CAR-SIV constructs	271
Figure 6.5 Schematic diagram of both CAR constructs	272
Figure 6.6 CAR-SIV co-localises with insulin in the wild-type CAR-SIV transfected 1.1B4 cells.	274
Figure 6.7 Effect of different combinations of insulin secretion stimuli on human Growth Hormone (hGH) release in hGH transfected 1.1B4 cells.	276
Figure 6.8 Effect of the different CAR-SIV constructs on human growth Hormone (hGH) release in 1.1B4 cells.....	278
Figure 6.9 Effect of the equal ratio of human growth hormone (hGH) and different CAR-SIV constructs on hGH release in 1.1B4 cells.....	280
Figure 6.10 hGH is released in INS1E cells co-transfected with 0.5µg of hGH and 0.3µg empty constructs.....	281
Figure 6.11 The hGH release from the hGH transfected 1.1B4 cells is similar to the INS1-E cells.....	282
Figure 6.12 Insulin is present in many more INS-1E cells than expressed hGH.	283
Figure 6.13 hGH co-localises with insulin in some, but not in all INS-1E cells.....	284
Figure 6.14 ICC staining reveals hGH partial co-localisation with CAR-SIV in insulin containing beta cells in 1.1B4 cells.	286

CHAPTER 7

<i>Figure 7.1 Proposed model of enteroviral entry in the beta cell through CAR-SIV.....</i>	<i>294</i>
<i>Figure 7.2 CAR-SIV and PICK1 interaction in the beta cell may be involved in the maturation and trafficking of the insulin secretory vesicle.....</i>	<i>297</i>

CHAPTER 8

<i>Figure 8.1 Map of the pCMV6 vector</i>	<i>302</i>
<i>Figure 8.2 Map of the pCMV6 empty vector.....</i>	<i>303</i>
<i>Figure 8.3 Site directed mutagenesis strategy creating the Wild-type CAR-SIV and truncated CAR-SIV mutant construct</i>	<i>305</i>

LIST OF TABLES

CHAPTER 1

<i>Table 1.1 Summary of mutations, conditions and agents that can lead to diabetes.....</i>	<i>30</i>
<i>Table 1.2 Endocrine and exocrine cells of the pancreas and specific hormone secreted. (↑) increase (↓) decrease</i>	<i>36</i>
<i>Table 1.3 Receptors utilised by enterovirus serotypes</i>	<i>61</i>
<i>Table 1.4 CAR isoforms from NCBI and UniProt database</i>	<i>63</i>

CHAPTER 2

<i>Table 2.1 Buffer-solutions and components</i>	<i>78</i>
<i>Table 2.2 Cell lines and sources</i>	<i>79</i>
<i>Table 2.3 List of primary antibodies utilised in this study.....</i>	<i>83</i>
<i>Table 2.4 Secondary antibodies and DAPI utilised for immunofluorescence and immunocytochemistry</i>	<i>83</i>
<i>Table 2.5 List of immunostaining reagents.....</i>	<i>84</i>
<i>Table 2.6 List of secondary antibodies for Western blotting</i>	<i>96</i>

CHAPTER 3

<i>Table 3.1 Primer sequence to target both CAR-SIV and CAR-TVV.....</i>	<i>124</i>
<i>Table 3.2 Primer sequence specific for CAR-SIV and CAR-TVV isoform.....</i>	<i>126</i>
<i>Table 3.3 TaqMan probe sequence for the five CAR isoforms</i>	<i>128</i>
<i>Table 3.4 Isolated human islet donors</i>	<i>129</i>
<i>Table 3.5 RIN values of LCM human islets (nPOD) donor</i>	<i>132</i>
<i>Table 3.6 Primer sequence targeting the CAR soluble isoforms</i>	<i>135</i>
<i>Table 3.7 CAR antisera and their predicted CAR isoforms.....</i>	<i>148</i>
<i>Table 3.8 Summary of CAR antisera staining pattern using the semi-quantitative method</i>	<i>151</i>
<i>Table 3.9 Autoantibody positive, type1 diabetes and normal cases</i>	<i>151</i>

CHAPTER 4

<i>Table 4.1 Summary of the utility of CAR antisera in different assays (+ suitable, -not suitable).....</i>	<i>183</i>
<i>Table 4.2 Validation of CAR antisera with different assays</i>	<i>199</i>

CHAPTER 5

<i>Table 5.1 Secretory granule proteins and their localisation in endocrine cells.....</i>	<i>219</i>
<i>Table 5.2 PCC analysis of CAR-SIV and secretory granule proteins.....</i>	<i>225</i>
<i>Table 5.3 MCC analysis of CAR-SIV, insulin and proinsulin proteins</i>	<i>228</i>
<i>Table 5.4 Pearson and Manders correlation coefficient of CAR-SIV association with PICK1 and insulin</i>	<i>244</i>
<i>Table 5.5 Proteins interacting with CAR-SIV.....</i>	<i>255</i>

CHAPTER 6

<i>Table 6.1 Summary of the validation of the specificity of CAR CT antiserum with the wild-type and truncated CAR-SIV constructs</i>	<i>272</i>
---	------------

APPENDIX

<i>Table 8.1 Tissue Samples, Patient Information.....</i>	<i>301</i>
<i>Table 8.2 Primers used for site directed mutagenesis.....</i>	<i>304</i>

ACKNOWLEDGEMENT

I would like to wholeheartedly thank my supervisors Dr Sarah Richardson and Prof. Noel Morgan for their mentorship and guidance in the entirety of this project. With their enthusiasm and passion for research, both have inspired me and taught me grit and resilience in order to evolve as a scientist. Thank you for the extensive feedback and constructive criticisms while writing my thesis.

I am utterly grateful to Dr Mark Russell and Dr Pia Leete for their support from the very first day I started my PhD and Dr Shalinee Dhayal who assisted me through the last stage.

To our collaborators (in Finland, Belgium and Italy) and funders “FFWG, UEMS, JDRF, nPOD, Diabetes UK” as well as the donors and their family, thank you.

I would also like to thank every single member of the IBEX team both past and present for the pleasant and friendly vibrant lab environment; Afi, Trish, Nikki, the entire team and level 4 labs.

I would like to specially thank Felice Dileo for his kindness, immense support and encouragement.

To my lovely siblings (Mamu, Ochuko, Nyerhovwo and Ejiro), words cannot express my deepest gratitude for your support throughout this journey.

Finally, I would love to thank my dearest parents Mr and Mrs U.N Ifie who are irreplaceable and have gone beyond to make this dream become a reality. For believing in me when I found it so difficult to believe in myself. I am extremely grateful for your sacrifices and investment in me.

To God almighty for the strength and grace to start and complete this degree.

ABBREVIATIONS

ADS	Antibody diluting solution
ADST	Antibody diluting solution with Triton X-100
ATP	Adenosine triphosphate
BCA	Bicinchoninic acid
BSA	Bovine serum albumin
BT-IgSF	Brain-testis Immunoglobulin superfamily
cAMP	Cyclic adenosine monophosphate
CAR	Coxsackie and adenovirus receptor
CLMP	CAR like membrane protein
CD	Cluster of differentiation
CCR5	C-C chemokine receptor type 5
CHO	Chinese hamster ovary
CPE	Carboxypeptidase
CT	C terminus
CTLA4	Cytotoxic T lymphocyte associated protein 4
CTX	Cortical thymocyte marker in Xenopus
CVB	Coxsackievirus B
DAF	Decay accelerating factor
DiviD	Diabetes virus detection
DKA	Diabetic ketoacidosis
EADB	Exeter Archival Diabetes Biobank
EBV	Epstein-Barr virus 1
ECD	Extracellular domain
EDTA	Ethylenediaminetetraacetic acid

EM	Electron microscopy
EPAC	Exchange protein directly activated by cAMP
ER	Endoplasmic reticulum
ESAM	Endothelial cell selective adhesion molecule
FACS	Fluorescence activated cell sorting
FBS	Fetal bovine serum
Fd	Forward
FFPE	Formalin fixed paraffin embedded
GADA	Glutamic acid decarboxylase
GIP	Glucose dependent insulinotropic peptide
GLUT	Glucose transporter
GLP1	Glucagon like peptide 1
GLP2	Glucagon like peptide 2
HEV	Human enteroviruses
hGH	Human growth hormone
HLA	Human Leucocyte Antigen
HRP	Horseradish peroxidase
IAA	Insulin autoantibody
IAPP	Islet amyloid polypeptide
IA-2A	Protein tyrosine phosphatase related IA-2 molecule
IBMX	3-isobutyl-1-methylxanthine
ICA	Islet cell autoantibodies
ICAM-1	Intercellular Adhesion Molecule 1
ICC	Immunocytochemistry
ICD	Intracellular cytoplasmic domain

IDF	International diabetes federation
IF	Immunofluorescence
IGSF	Immunoglobulin superfamily
IHC	Immunohistochemistry
IL2RA	Interleukin-2-receptor alpha chain
INS	Insulin
IP3	Inositol triphosphate
ISG	Insulin secretory granule
JAMs	Junctional adhesion molecules
KATP	ATP sensitive potassium
LADA	Latent autoimmune diabetes
LB	Luria broth
LCM	Laser captured micro-dissected
LDCV	Large dense core vesicles
LDS	Lithium dodecyl sulfate
MCC	Manders correlation coefficient
MDCK	Madin-Darby Canine Kidney Cells
MHC	Major histocompatibility complex 1
MODY	Maturity onset diabetes of the young
NDA	Non diabetes adult
NOD	Non obese diabetes
nPOD	network of Pancreatic Organ donor
NT	N terminus
PBMC	Peripheral blood mononuclear cell
PBS	Phosphate buffered saline
PC	Prohormone convertase

PCC	Pearson's correlation coefficient
PDZ	PSD-95 (Post Synaptic Density Protein), DlgA (Drosophila Disc Large Tumor Suppressor) and ZO-1(Zonula Occludens-1 Protein)
PE	Phycoerythrin
PFA	Paraformaldehyde
PKA	Protein kinase A
PP	Pancreatic polypeptide
PTPN22	Protein tyrosine phosphatase non-receptor type 22
PVDF	polyvinylidene difluoride
PVR	Poliovirus receptor
RIN	RNA integrity number
RRP	Readily releasable pool
RER	Rough endoplasmic reticulum
RT-PCR	Reverse transcriptase polymerase chain reaction
SEM	Standard error of the mean
STWS	Scott's tap water substitute
SNARE	Soluble NSF Attachment protein Receptor
T1D	Type 1 diabetes
T2D	Type 2 diabetes
TAE	Tris base, acetic acid, EDTA
TBE	Tris, borate, EDTA
TBS	Tris-buffered saline
TBST	Tris-buffered saline with Tween 20
TCR	T cell receptor
TGN	trans-Golgi network
TM	Transmembrane

RER	Rough endoplasmic reticulum
RRP	Readily releasable pool
RV	Reverse
SEM	Standard error of the mean
SJL/J	Swiss Jim Lambert
SNAP25	Synaptosomal associated protein of 25kDa
TBST	Tris buffered saline + tween
TIRF	Total internal reflection fluorescence
UAG	Unacylated Ghrelin
UTR	Untranslated region
VAMP2	vesicle associated membrane protein 2
VDCC	Voltage gated Ca ²⁺ channels
VP	Viral capsid protein
ZO-1	Zonula occludens-1
ZnT8	Zinc transporter 8

PUBLICATIONS

Ifie E, Russell M.A, Dhayal S, LeeteP, Sebastiani G, Nigi L, Dotta F, Marjomäki V, Eizirik D.L, Morgan N.G &. RichardsonS.J (2018) Unexpected subcellular distribution of a specific isoform of the Coxsackie and Adenovirus Receptor, CAR-SIV, in human pancreatic beta cells. *Diabetologia* Nov; 61(11): 2344-2355

Jmii H, Halouani A, Elmastour F, **Ifie E**, Richardson S.J, Sane F, Mokni M, Aouni M, Hober D, Jaïdane H (2016) Central nervous system infection following vertical transmission of Coxsackievirus B4 in mice. *FEMS Pathogens and Disease* Sep 20; 74 (8).ftw096.

CHAPTER 1

Introduction

1.1 Brief history of diabetes mellitus

In 400 B.C Sushruta, an Indian physician described polyuria (a symptom of type 1 diabetes) as sweet urine disease and documented “that black ants were attracted to the urine” of affected individuals. This was recognised as the first recorded symptom of diabetes. The term “diabetes” originated from a Greek word (meaning “to syphon”), reflecting how individuals with the disease produce large volumes of urine. The term “Diabetes Mellitus” was later coined by a physician Thomas Willis in 1674, he described the word “Mellitus” (Latin to mean “sweet like honey”) as a feature of the urine of people with diabetes (von Engelhardt, 1989).

It was not until the late 1800’s that a connection between diabetes and the pancreas was established after German physicians Joseph von Mering and Oskar Minkowski noticed that dogs developed diabetes after the pancreas was surgically removed. This breakthrough discovery led to research centred on the isolation of pancreatic extract from animals that could treat diabetes (v. Mering and Minkowski, 1890). The extract now known as “insulin” was isolated by a surgeon, Fredrick Banting, and a medical student Charles Best, in the laboratory of Prof. John Macloed in Toronto, Canada. Experiments on diabetic dogs showed that this extract caused a drop in blood glucose levels and the disappearance of glucose in urine (Banting et al., 1922).

In 1922, the first patient, an extremely ill young boy received insulin which lowered his blood glucose levels and he began to gain weight (Banting et al., 1922). Over the next 60 years, our understanding of the insulin molecule was refined, and insulin collected from animals to treat humans was terminated due to the advancement of recombinant human insulin (Ahmed, 2002).

1.2 Diabetes mellitus

Diabetes mellitus is “a complex metabolic disorder characterised by abnormally high levels of blood glucose (hyperglycaemia) as a result of dysfunction in either insulin secretion, insulin signalling or both” (American Diabetes Association, 2010). In 2013, the International Diabetes Federation (IDF) <https://www.idf.org/> predicted that globally, 1 in 10 people will be diagnosed with some form of diabetes and that about 382 million people were living with the disease, this is expected to markedly increase to 600 million by 2035.

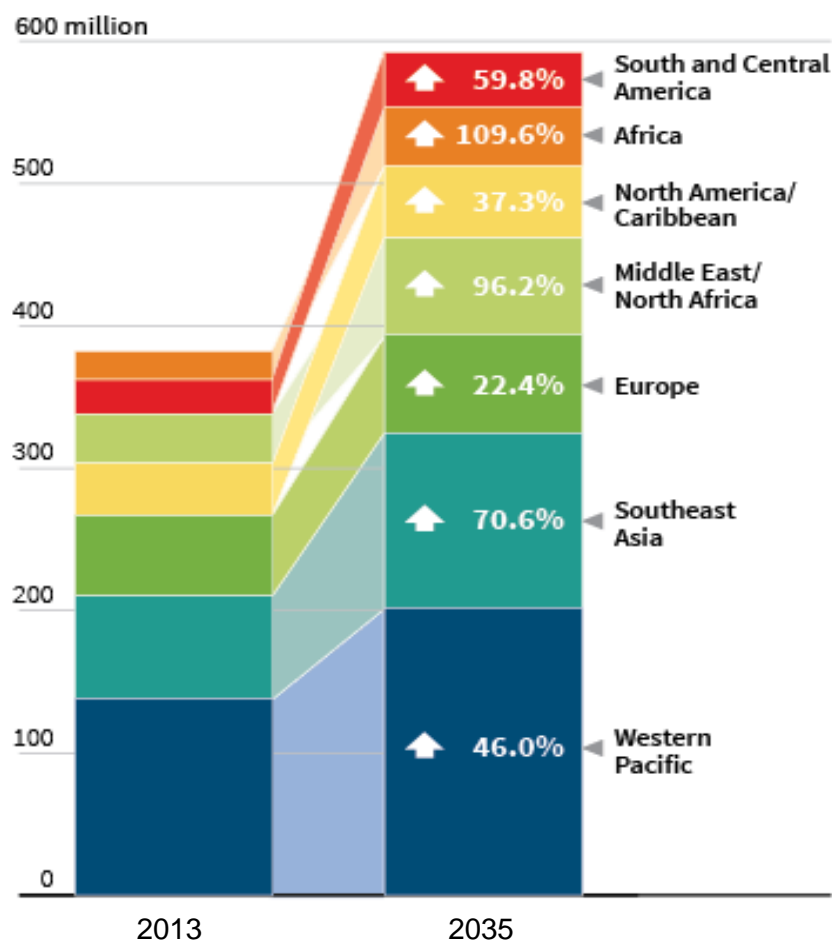


Figure 1.1 Worldwide current and projected cases of diabetes.

Chart showing diabetes cases in 2013 and an estimated increase of diabetes cases in the world by 2035 (white arrow represent estimated % increase). International Diabetes Federation (IDF), *Diabetes Atlas 6th edition* (2013), <https://www.idf.org/e-library/epidemiology-research/diabetes-atlas/19-atlas-6th-edition.html>

The Diabetes UK charity in 2017 <https://www.diabetes.org.uk/professionals/position-statements-reports/statistics>, reported that in the UK alone, 3.7million people aged 17yrs or older had been diagnosed with the disease with an estimated 10% with Type 1 diabetes and 90% with Type 2 diabetes. Interestingly, there were large variations within the country with some cities having the highest prevalence of type 1 and type 2 diabetes.

Previously, it was indicated that there were two forms of diabetes mellitus; autoimmune type 1 diabetes (T1D) and non-autoimmune type 2 diabetes (T2D) (Canivell and Gomis, 2014). However, as research advances many forms of diabetes mellitus are emerging. The American Diabetes Association recently classified diabetes into type 1 diabetes, type 2 diabetes, gestational diabetes mellitus and other specific forms of diabetes (American Diabetes Association 2010, 2018) which are summarised in Table 1.1

1.2.1 Type 1 diabetes (T1D)

Type 1 diabetes is subdivided into immune mediated, latent autoimmune diabetes (LADA) and idiopathic diabetes. Immune mediated type 1 diabetes previously termed “insulin dependent” or “juvenile-onset diabetes” occurs as a result of autoimmune destruction of the pancreatic beta cells. The terms were abolished when it became evident that not all individuals with autoimmune diabetes were either juvenile or exhibited an absolute insulin requirement (Leslie et al., 2006). Immune mediated type 1 diabetes is the focus of this thesis and is described in more detail in section 1.2.3.

LADA refers to individuals with adult onset autoimmune diabetes who may not initially require insulin treatment. This type of diabetes has also been called a

slow progressing insulin dependent diabetes (Kobayashi et al., 1993) or type 1.5 diabetes (Naik and Palmer, 2003). Three features have been defined for the diagnosis of LADA; adult age at diagnosis, the presentation of circulating autoantibodies and the delay from diagnosis for the requirement of insulin dosage to manage hyperglycaemia (Leslie et al., 2006).

Individuals with idiopathic T1D have no evidence of autoantibodies presentation but have strong genetic association, mostly observed in African and Asian lineage. Individuals also have almost complete insulin deficiency and are liable to diabetic ketoacidosis (American Diabetes Association, 2010)

1.2.2 Other forms of diabetes

Other forms of diabetes include Type 2 diabetes, gestational diabetes, neonatal and maturity onset diabetes of the young (MODY).

Type 2 diabetes is reported to account for 90-95% of all diabetes and was termed “non-insulin dependent diabetes” or “adult onset diabetes”. People with type 2 diabetes generally present as overweight or obese with relative insulin deficiency and peripheral insulin resistance (American Diabetes Association 2010, 2018). Type 2 diabetes results from a defect in beta cell insulin secretory function which is insufficient to compensate for insulin resistance (Lebovitz, 1999). In some individuals, T2D diagnosis may be missed for many years because hyperglycaemia may develop gradually over decades.

Gestational diabetes mellitus (GDM) is defined as glucose intolerance diagnosed during pregnancy, and it is characterised by the insufficiency of the pancreatic beta secretory function to meet the body’s insulin requirement (Buchanan et al., 2007). Women with gestational diabetes are at an increased risk of also

developing type 2 diabetes, cardiovascular disease and other metabolic syndromes (Poola-Kella et al., 2018).

Neonatal diabetes is a form of monogenic diabetes that occurs from the inheritance of a mutation in a single gene. These mutations are found in genes that regulate beta cell function and are diagnosed in children within the first 6 months of life (Hattersley et al., 2009). Maturity onset diabetes of the young (MODY) is also a form of monogenic diabetes that comprises of a group of clinically heterogeneous mutations that trigger beta cell dysfunction, with an autosomal dominant mode of inheritance (Shields et al., 2010), normally diagnosed before 25years of life. The subtypes of Neonatal and Maturity onset diabetes of the young with known mutations as well as other conditions that can lead to diabetes are summarised in Table 1.1 below

Table 1.1 Summary of mutations, conditions and agents that can lead to diabetes

Known mutations in Neonatal Diabetes	Known mutations associated with MODY	Diseases of the exocrine pancreas	Endocrinopathies	Drugs or chemicals that can induce diabetes
KCNJ11	HNF-4 α (MODY 1)	Pancreatitis	Acromegaly	Nicotinic acid
INS	GCK (MODY 2)	Cystic fibrosis	Cushing's syndrome	Glucocorticoids
ABCC8	HNF-1 α (MODY 3)	Neoplasia	Glucagonoma	Diazoxide
FOXP3	IPF-1 (MODY4)	Hemochromatosis	Hyperthyroidism	β -adrenergic agonist
GATA6	HNF-1 β (MODY 5)	Pancreatectomy	Aldosteronoma	Thiazides
EIF2AK3	NeuroD1 (MODY6)			Pentamidine

Adapted from (Carmody et al., 2015, Association, 2010)

1.2.3 Immune mediated Type 1 diabetes

Globally, about 500,000 young people under the age of 15 are estimated to have type 1 diabetes and the incidence is rising, in Europe this increase is most clear in young children (Patterson et al., 2014). It has been forecast that the incidence of T1D in developed countries will double in children under the age of 5 between 2005 and 2020 (Patterson et al., 2009).

Type 1 diabetes develops from the selective destruction of the insulin producing pancreatic beta cells by autoimmune attack (Anderson and Bluestone, 2005). Analysis of post mortem pancreas tissue samples from recent onset T1D patients revealed that the destruction is linked to the infiltration of CD8⁺ cytotoxic T cells, CD4⁺ helper T cells, CD20⁺ B lymphocytes cells and CD68⁺ macrophages termed “insulinitis” (Willcox et al., 2009). CD8⁺ T cells have long been known as the major effectors of pancreatic beta cell destruction from studies of non-obese diabetes (NOD) mice (a rodent model of Type 1 diabetes), which demonstrates that mice do not progress to diabetes in the absence of cytotoxic CD8⁺ T cells (Katz et al., 1993). These CD8⁺ T cells are activated by the interaction of their T-cell receptors (TCRs) with the MHC1 (Major histocompatibility complex 1), expressed on all nucleated cells. These activated CD8⁺ T cells can directly kill cells by the production of perforins, pore forming proteins, and granzymes, proteases that digest intracellular proteins or by Fas-Fas ligand mediated pathway (Trivedi et al., 2016, Graham et al., 2012).

The classical symptoms of T1D are polyuria, polyphagia, polydipsia, weight loss, weakness and recurrent infections (Atkinson and Eisenbarth, 2001). One major complication of T1D especially for some children and adolescents is the initial presentation with diabetic ketoacidosis (DKA). Adults may have modest

hyperglycaemia, which may be exacerbated by environmental factors triggering severe hyperglycaemia and diabetic ketoacidosis (Dabelea et al., 2014). The consequence of the disease is that patients have to rely on lifelong exogenous insulin administration due to the failure in insulin production from the destroyed beta cells.

In most individuals, the preclinical phase of the disease is usually characterised by the presence of one or more circulating autoantibodies (early immunological markers) in the serum which can appear between a few weeks to several years before onset (Ziegler et al., 2013). These circulating autoantibodies are targeted against beta cell autoantigens including those reactive to insulin (IAA), glutamic acid decarboxylase (GADA), protein tyrosine phosphatase-related IA-2 molecule (IA-2A) and Zinc transporter 8 (ZnT8) (Hyöty, 2002).

Genetic predisposition plays an important role, with more than 50 candidate genes associated with risk of disease development (Santin and Eizirik, 2013). About 40-50% of the genetic risk of T1D derives from human leucocyte antigen (HLA) alleles located on chromosome 6. The *HLA* class II haplotypes (*HLA-DRB1*, *HLA-DQA1* and *HLA-DQB1 loci*) in particular show the strongest association with T1D (Noble and Erlich, 2012, de Beeck and Eizirik, 2016). The *HLA* class II region encodes membrane proteins expressed on the surface of antigen presenting cells (B lymphocytes, macrophages and dendritic cells) that are involved in the processing and presentation of exogenous antigens to CD4+ T helper cells (Gillespie, 2006). Other mapped candidate genes across the genome include cytotoxic T lymphocyte associated protein 4 (*CTLA4*); protein tyrosine phosphatase non-receptor type 22 (*PTPN22*), insulin (*INS*), interleukin-2-receptor alpha chain (*IL2RA*), C-C chemokine receptor type 5 (*CCR5*) *e.t.c* (Todd, 2010)

Importantly though, the 1.5% annual increase in disease incidence cannot be explained by genetics alone as only a proportion of individuals with the genetic risk eventually go on to develop the disease (Atkinson et al., 2015). Also, the concordance rate observed between monozygotic twin study is only 30-50% and less than 5% of genetically predisposed individuals develop T1D (Redondo et al., 1999, Patterson et al., 2012) implying that both genetic and environmental factors may contribute to the disease. A range of potential environmental factors have been linked to triggering T1D, such as; enhanced reactivity to cow's milk introduced early in infancy which was evident in children who later went on to develop T1D (Luopajarvi et al., 2008), greater weight gain in early life (Hyppönen et al., 2001, Elding Larsson et al., 2016) and lower serum levels of vitamin D binding protein (Blanton et al., 2011).

Recently, it has also been suggested that a correlation exists between the gut microbiome and type 1 diabetes. This was shown in a study where analysis of the microbiome from duodenal mucosa biopsied from people with type 1 diabetes was composed of reduced levels of Proteobacteria (*Escherichia*, *Salmonella*, *Helicobacter*) and increased Firmicutes (*Bacilli* and *Streptococcus*) when compared to healthy control individuals (Pellegrini et al., 2017).

Viruses such as Epstein-Barr virus 1 (EBV), cytomegaloviruses, parechoviruses, rotaviruses, mumps virus, reovirus, retroviruses, rubella virus, enteroviruses and congenital rubella have also been implicated (Jun and Yoon, 2004, Coppieters et al., 2012). In particular, the human enterovirus family seem to have the strongest association (Yeung et al., 2011, Rodriguez-Calvo et al., 2016) and are considered by many, the prime environmental trigger for the disease. What is clear though is that there is a complex interplay between genetic predispositions, a dysregulated

immune system and environmental factors, each of which contribute in part to type 1 diabetes disease pathogenesis.

1.3 Pancreas

The pancreas is an organ with a head, neck, body and tail and is part of the gastrointestinal system that lies in the upper abdomen behind the stomach (Longnecker, 2014). It is highly vascularised and is innervated with sympathetic, parasympathetic and afferent nerve fibres that are closely associated together as they move through the pancreas (Love et al., 2007, Ahrén, 2000, Rodriguez-Diaz and Caicedo, 2013, Lindsay et al., 2006).

The pancreas has two distinct tissues (endocrine and exocrine) that have important metabolic and digestive functions. The endocrine pancreas is organised into the islets of Langerhans, and these structures comprise approximately 1-2% of the pancreas mass. The islets produce and secrete hormones into the blood to regulate energy metabolism (Longnecker, 2014). The exocrine tissue is composed of lobules with acinar cells surrounded by ducts (Pandol, 2011). These cells synthesize and secrete digestive enzymes and bicarbonate, respectively, into the duodenum (initial part of the small intestine). Importantly, most studies of the pancreas come from extensive research in mice models which is still the most studied animal model due to the difficulties in obtaining human pancreas tissues.

1.3.1 Islets of Langerhans

The islets of Langerhans were originally described as “small cells of almost perfect homogeneous content and of a polygonal form, with round nuclei without nucleoli, mostly lying together in pairs or small groups” by Paul Langerhans, a medical student in Berlin in 1869 (Sakula, 1988).

The islets of Langerhans are highly vascularised micro-organs which are supplied with approximately 10-fold more volume of blood than the entire exocrine tissue. The intra-islet microcapillary comprises 7-8% of the total islet volume (Henderson and Moss, 1985, Saito et al., 1979). It is estimated that the average adult human pancreas contains one to two million islets (Hellman, 1959, Stefan et al., 1982), and these structures are more concentrated in the tail compared to the head or neck (Mann and Bellin, 2016).

Five different endocrine cells make up the islets and respond to changes in plasma nutrient level by releasing a balanced mixture of specific hormones into the portal vein (Smeets, 2015). These cell types and their distribution in the islet include the alpha (α) cells (20%), beta (β) cells (70%), delta (δ) cells (<10%), ghrelin or epsilon (ϵ) cells (<1%) and F or pancreatic polypeptide (PP) cells (<5%). Upon receiving an appropriate stimulus these cells would secrete glucagon, insulin, somatostatin, ghrelin and pancreatic polypeptide respectively (Elayat et al., 1995, El-Gohary and Gittes, 2018). Apart from specific hormone product, non-hormonal products with varying functions are also secreted by these cells (Marrif and Al-Sunousi, 2016) described in Table 1.2

Table 1.2 Endocrine and exocrine cells of the pancreas and specific hormone secreted.
 (↑) increase (↓) decrease

Pancreatic Cells	Hormone Secreted	Function
Beta (β)	Insulin Amylin or Islet Amyloid polypeptide (IAPP)	↓plasma glucose ↓pancreatic enzymes ↓gut gastric emptying
Alpha(α)	Glucagon Glucagon like peptide (GLP1 and GLP2)	↑plasma glucose ↑insulin secretion and sensitivity ↓glucagon secretion
Delta(δ)	Somatostatin	Inhibits insulin and glucagon secretion
F PP	Pancreatic polypeptide	Reduces food intake and the rate of gastric emptying
Epsilon (ε)	Ghrelin (AG). Unacylated Ghrelin (UAG)	Inhibits insulin release and increases appetite
Acinar cells	Alpha-amylase, proteases and lipases	Promote digestion in the gut
Duct cells	Secrete mucus, bicarbonate	Promotes digestion

Adapted from (Marrif and Al-Sunousi, 2016)

Importantly, the overall islet architecture may differ between human and rodent islets. Human islets are composed of layers of beta cells sandwiched between alpha cells. These are then folded in structures with vessels circulating along both sides. The beta cells also have cytoplasmic extensions (yellow arrows; *Figure 1.2A*) intercalated between alpha cells implying that beta cells are able to reach the vasculature (*Figure 1.2A*). Also, either a heterologous beta-alpha cell contact or homologous beta-beta cell contact is predominant in human islets (Bosco et al., 2010). In contrast, rodents islets tend to be organised into a core-mantle unit favouring homologous beta-cell to beta-cell contacts in the core and alpha-alpha cell contacts in the mantle surrounding the periphery which are in close association with vasculature (Bosco et al., 2010) as shown in *Figure 1.2B*.

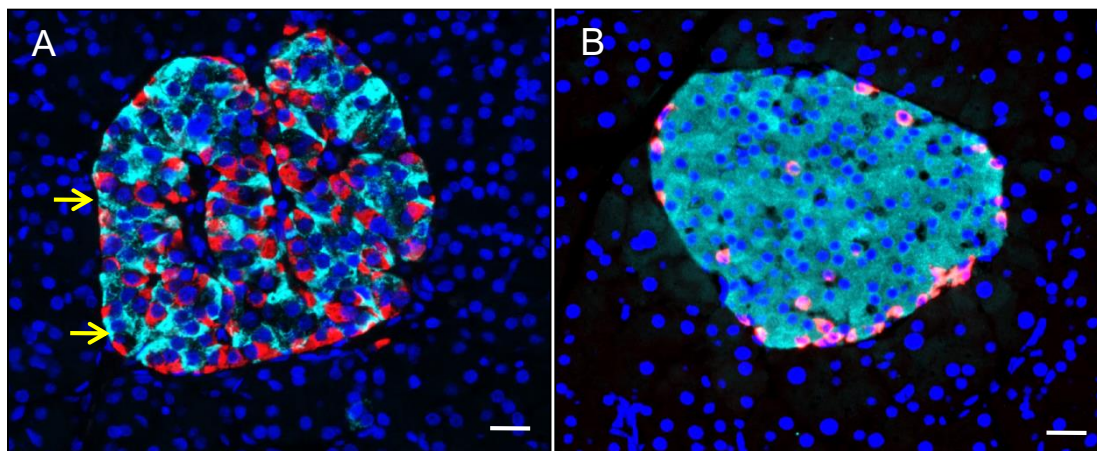


Figure 1.2 Architectural difference in islet organisation of beta and alpha cells in human and mouse pancreas

Immunofluorescence images showing (A) Human islets displaying layers of beta cells (light blue) sandwiched between alpha cells (red) enriched layers, beta cells also have cytoplasmic extensions intercalated between alpha cells (yellow arrows) (B) mouse islet organised with beta-beta cell in the core and alpha cells in the mantle surrounding the periphery. Nuclei are in dark blue. Scale bar 25 μ m

1.3.2 Studying the beta cell

In 1908, Lane identified the “beta cells” by staining guinea pig pancreas sections with an alcoholic solution, Bensley’s neutral gentian (Lane, 1907, Bensley, 1914). It is estimated that about a 100×10^6 beta cells are present in the pancreas (Weir and Bonner-Weir, 2013). The pancreatic beta cell functions as a sensor of extracellular glucose and produces appropriate amounts of insulin to decrease the blood glucose to a physiological level (Marrif and Al-Sunousi, 2016). As shown previously in Table 1.2, the beta cell also produces islet amyloid polypeptide (IAPP) also known as amylin. Amylin reduces food intake by slowing gastric emptying and promoting satiety (Reda et al., 2002). In mouse islet studies, amylin was shown to be packaged in and released from insulin granules (Kahn et al., 1990). Insulin and IAPP gene promoters have both been shown to be regulated by the transcription factor, PDX1 (MacFarlane et al., 1994, MacFarlane et al., 2000).

1.3.3 Insulin granule biogenesis

Studies with electron microscopy analysis estimated that about 11,000 insulin granules are present in a single beta cell of mouse pancreas (Dean, 1973, Olofsson et al., 2002) and the characteristic morphological feature of the insulin secretory granule has been observed by transmission electron microscopy to have a central dense core with a surrounding halo (Olofsson et al., 2002, Orci et al., 1986).

The biogenesis of insulin (see *Figure 1.3*) begins with the synthesis of preproinsulin on the ribosomes in the rough endoplasmic reticulum (RER) and proinsulin is formed when the signal peptide sequence is cleaved off (by signal

peptidase) (Dodson and Steiner, 1998). According to Yang *et al* (2010), it is in the ER (endoplasmic reticulum) lumen that proinsulin is folded into a globular protein, a disordered structure comprising of native-like insulin and C-peptide (Yang *et al.*, 2010). Properly folded proinsulin is then assembled in COPII vesicles which are subsequently transported from the ER to the trans-Golgi network (Fang *et al.*, 2015). Here, proinsulin is assembled into Zn²⁺ and Ca²⁺ containing hexamers (Dunn, 2005) and packaged in clathrin coated vesicles before budding off as an immature granule to begin the maturation process.

An ATP-dependent proton pump in the granule is reported to be responsible for the acidification of the insulin secretory vesicle (Davidson *et al.*, 1988). As the vesicles mature they become more acidic which facilitates the sequential proteolytic cleavage of proinsulin by the endoprotease PC1/3 (which cleaves the B-C junction of the proinsulin peptide sequence), and then PC2 (which cleaves the A-C junction of the proinsulin peptide sequence) (Furuta *et al.*, 1997, Goodge and Hutton, 2000). Carboxypeptidase E enzyme (CPE) trims the carboxyl terminal two-basic amino acids yielding mature insulin and C peptide (Hutton, 1994, Tokarz *et al.*, 2018). This process converts proinsulin to mature insulin and C peptide (Naggert *et al.*, 1995). Following the actions of prohormone convertase and carboxypeptidase, the insulin within the secretory granule binds to zinc enabling the crystallisation of insulin and the formation of dense core insulin structures (Ashcroft and Ashcroft, 1992, Dunn, 2005).

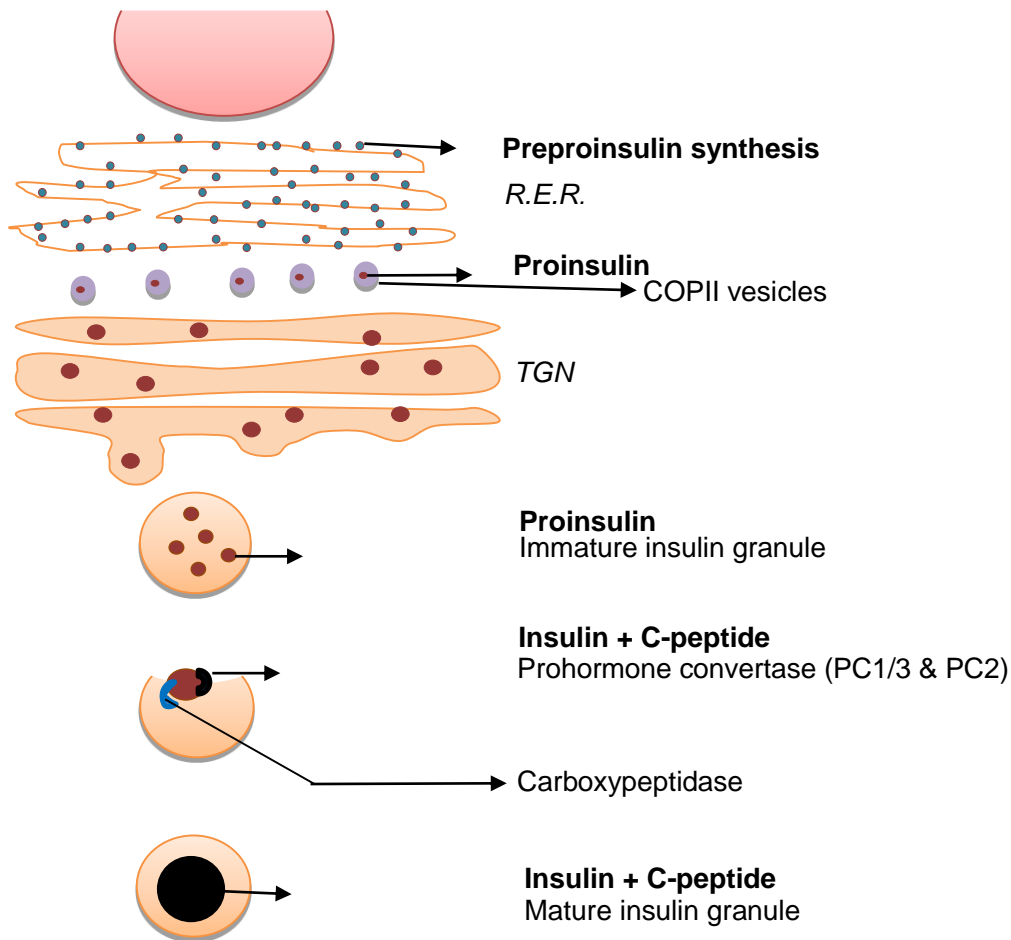


Figure 1.3 Biogenesis of insulin granules.

Preproinsulin synthesis initiates on the ribosomes of the rough endoplasmic reticulum (RER). The signal peptide is cleaved and proinsulin is translocated into the ER lumen and proinsulin is then transported to the trans-Golgi network (TGN). Immature insulin granules then bud off the trans-Golgi network. Pro-insulin within the immature granules undergoes proteolytic cleavage to form insulin which forms insulin crystals when bound to zinc.

1.3.4 Insulin secretion

Insulin secretion has been intensively studied in rodent and human pancreas and it is well established that the beta cell is a glucose sensor with a physiological function to secrete insulin (Ashcroft and Rorsman, 1989, Ashcroft and Rorsman, 2012, Doyle and Egan, 2007).

The process of insulin secretion (*Figure 1.4*) initiates when there is a postprandial rise in plasma glucose levels which elicits the uptake of glucose into the beta cell through the low affinity glucose transporter (GLUT1/3) in humans and (GLUT2) in mouse (Thorens, 1992). Cytosolic glucose is then metabolised through the glycolytic pathway to generate glucose-6-phosphate by glucokinase through an ATP dependent reaction. Glucokinase catalyses the rate limiting step in the process (Newgard and McGarry, 1995, De Vos et al., 1995) and thus is described to play a central role as a “glucose sensor” (Matschinsky, 1990). The production of glucose-6-phosphate then drives further metabolism leading to the generation of an increase in the ATP:ADP ratio (Rorsman et al., 2000, Cook et al., 1988).

Studying ionic currents using patch clamp experiments has established that two types of ion channels are present in the pancreatic beta cell. These ion channels are pivotal for insulin secretion initiation in response to glucose: ATP sensitive K⁺ channels (K_{ATP}-channels) and voltage-gated Ca²⁺ channels (VDCC) (Rorsman and Renström, 2003).

At low glucose, the K_{ATP} channel maintains the membrane potential at its resting potential (-70mv) and an increase in ATP generation induces the closure of the K_{ATP} channels which prevents K⁺ efflux and causes depolarisation of the plasma membrane. This change in membrane potential initiates the opening of the voltage dependent Ca²⁺ channels which facilitates the influx of extracellular

calcium (Ca^{2+}) into the beta-cell. The increase in cytosolic Ca^{2+} induces insulin granule release, the key step in exocytosis (Rorsman and Braun, 2013, Shibasaki et al., 2004).

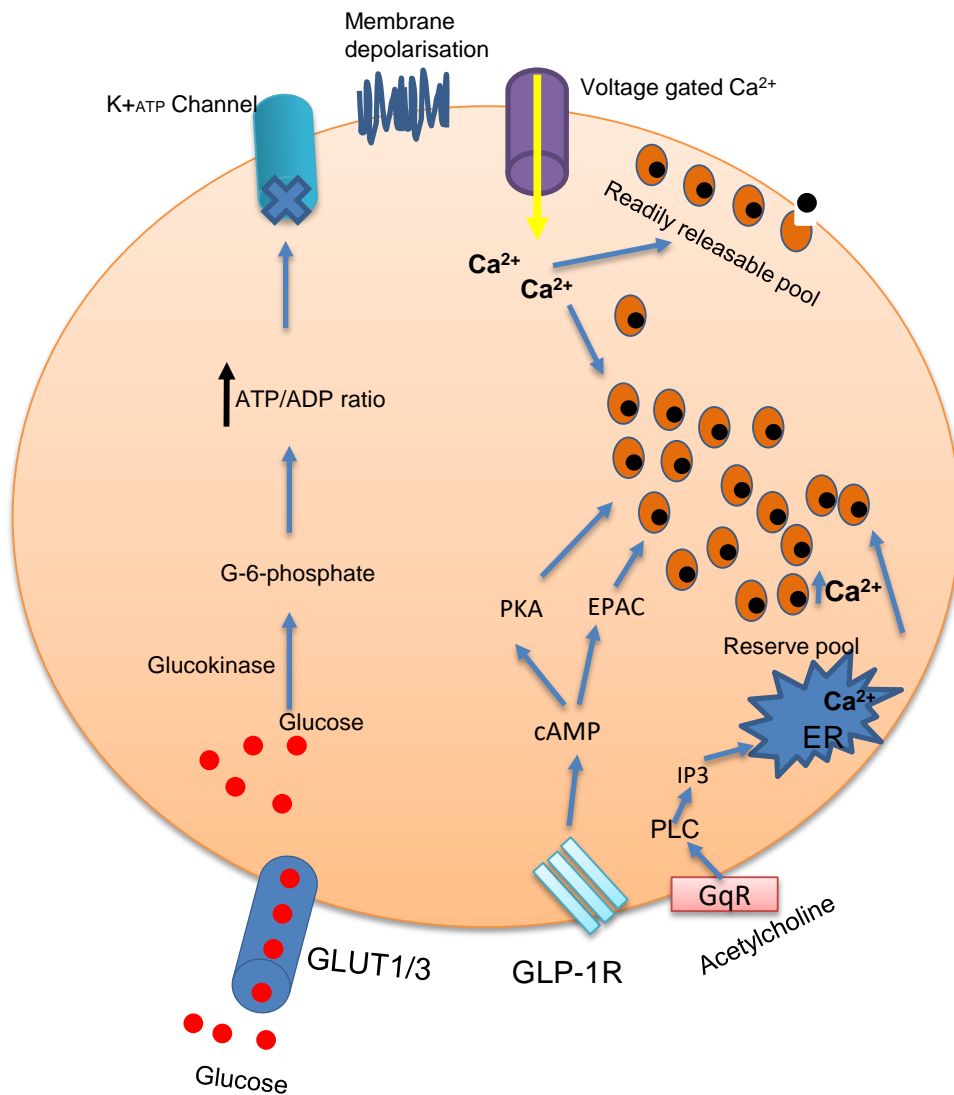


Figure 1.4 Insulin secretion pathway.

Glucose enters into the human beta cell through the GLUT1/3 transporter and becomes metabolised via the glycolytic pathway facilitating an increase in intracellular ATP. This increase leads to the closure of the K_{ATP} channels inducing depolarisation of the membrane. This change in membrane potential initiates the opening of the voltage-gated Ca²⁺ channels, Ca²⁺ then enters leading to rise in cytosolic Ca²⁺ levels for insulin granule release. Another pathway that potentiates insulin secretion is the cAMP pathway, where an activation of GLP-1R leads to increase in cAMP facilitating the activation of protein kinase A (PKA) and exchange protein directly activated by cAMP (Epac) which then induces biphasic insulin secretion. Alternatively, activation of the GqR induces an increase in phospholipase C (PLC) activity thereby increasing the intracellular levels of inositol triphosphate (IP₃) leading to Ca²⁺ release from the calcium store in the ER.

1.3.5 Alternate signals for insulin secretion

Insulin release from beta cells can be regulated by secretagogues such as endogenously produced hormones, neurotransmitters and pharmacological agents which can either enhance or negatively regulate insulin secretion. This section will focus more on the potentiation of insulin secretion through cyclic adenosine monophosphate (cAMP) signalling pathway.

After the absorption of a meal, two main incretin hormones GLP-1 (glucagon like peptide-1) and GIP (glucose dependent insulinotropic peptide) are secreted by the intestinal L- and K-cells respectively in response to the local rise in glucose and these have been shown to potentiate insulin secretion (Doyle and Egan, 2007). GLP-1 and GIP act on specific G protein coupled receptors expressed on the plasma membrane of beta cells, which when activated increase adenylyl cyclase activity and enhance the subsequent activity of cAMP dependent second messenger pathway members, protein kinase A (PKA) and exchange protein directly activated by cAMP (EPAC) (Holz, 2004). These factors then act to regulate protein phosphorylation and increase the recruitment of secretory granules resulting in the potentiation of biphasic insulin release (Henquin and Nenquin, 2014). The biphasic insulin secretion includes a first phase rapid release of insulin followed by a second sustained phase of insulin secretion (Henquin et al., 2002). Importantly, pharmacological agents such as forskolin and IBMX (3-isobutyl-1-methylxanthine) can be used to raise cyclic AMP levels (Alasbahi and Melzig, 2012, Fehmann and Habener, 1992) and artificially stimulate the potentiation pathway.

Additional agents known to amplify insulin secretion by alternate pathways, include acetylcholine, which is a non-fuel secretagogue released by intra-

pancreatic nerves. Acetylcholine acts through the Gq coupled receptor (GqR) and activates phospholipase C (PLC), which subsequently leads to the generation of inositol triphosphate (IP₃), and results in the release of calcium stores from the endoplasmic reticulum. This elevation in cytosolic calcium levels increases the number of readily releasable insulin granules at the plasma membrane (Ahrén, 2000, Gilon and Henquin, 2001)(*Figure 1.4*)

Whilst all of the above pathways absolutely require ATP generation in order to amplify secretion, the addition of a compound such as KCl bypasses the need for glucose metabolism and the ATP induced K⁺ channel. KCl acts by directly inducing membrane depolarisation enabling the opening of the voltage gated dependent Ca²⁺ channel to permit Ca²⁺ influx (Hatlapatka et al., 2009).

1.3.6 Insulin granule pools

It is proposed that there are two populations of intracellular insulin secretory granule; a readily releasable pool (RRP) which are docked close to the plasma membrane for immediate insulin release (Rorsman and Renström, 2003) (*Figure 1.4*). The second population of granules, which are important for maintaining secretion over an extended period, are known as “the reserve pool”. These are situated in the cytoplasm and are recruited in an AMPK and kinesin-1 dependent manner to the cell periphery (McDonald et al., 2009)(*Figure 1.4*). For insulin granules to reach the plasma membrane, depolymerisation (coordinated reorganisation and remodelling) of the cytoskeleton F-actin network has to occur (Kalwat and Thurmond, 2013) before granules are docked to the plasma membrane for eventual secretion.

The readily releasable pool accounts for about 1-5% of the insulin granules which undergo release without further modification after stimulation and is thought to be responsible for the rapid release (the first phase) of insulin secretion (Neher, 1998). This pool is closely aligned to the plasma membrane and undergoes a calcium dependent release.

The reserve pool (mediating the second phase of insulin secretion) occurs at a much slower rate and accounts for 95-99% of the granules. These granules must first undergo priming/mobilization which requires ATP, Ca^{2+} and time dependent reactions prior to their release.

These two phases of glucose stimulated insulin secretion are said to yield “biphasic” insulin secretion. In the first phase, glucose stimulated insulin secretion last between 4 to 15mins (Nesher and Cerasi, 2002, Gaisano, 2014) and once depleted, the second phase insulin secretion occurs (Rorsman et al., 2000).

1.3.7 Exocytosis

Exocytosis of insulin secretory granules involves distinct steps; the tethering of the insulin secretory granules to the release site of the plasma membrane (Verhage and Sørensen, 2008, Lang, 1999, Barg et al., 2008), docking, referring to the movement of the granule and priming, which entails the assembly of SNARE complexes in preparation for the release of insulin (Eliasson et al., 2008).

It is established that the SNARE proteins such as v-SNARE protein VAMP2 (vesicle associated membrane protein2) associate with the insulin granules and form complexes that attach to the plasma membrane proteins syntaxin, synaptosomal associated protein of 25kDa (SNAP25) and t-SNARE proteins (Hou et al., 2009). The zippering of the complex allows for the overall opening of

the fusion pore (Lou and Shin, 2016). Very recently, with high resolution total internal reflection fluorescence (TIRF) microscopy, the voltage dependent K⁺ channel, Kv2.1 was shown not only to be involved in the depolarisation of the membrane but to form clusters on the plasma membrane and also bind with the C terminus of syntaxin 3 to recruit secretory granules from the reserve pool (Greitzer-Antes et al., 2018)

The SNARE proteins aid in exocytosis by bringing the vesicle membrane into close contact with the plasma membrane (Bruns and Jahn, 2002). The conformational changes that occur provide the energy to elicit membrane fusion, but it has been noted that the SNARE proteins are not sufficient to account for the Ca²⁺ dependent exocytosis in secretory cells. Synaptotagmin has been implicated in calcium regulated exocytosis in the beta cell (Gut et al., 2001). However, it remains unclear which isoform of this protein is involved as some synaptotagmin isoforms have been shown by peptide inhibition experiments to mediate calcium regulated exocytosis and knock down experiments have shown that other isoforms may exert the same effect implying that many isoforms could be involved in this process (Gut et al., 2001, Iezzi et al., 2004)

1.3.7.1 Fusion pore opening

As discussed in the previous section the secretory vesicles have to fuse with the plasma membrane for insulin to be released and there are two general fusion mechanisms proposed which include: “Full fusion” and “Kiss and Run” shown in Figure 1.5.

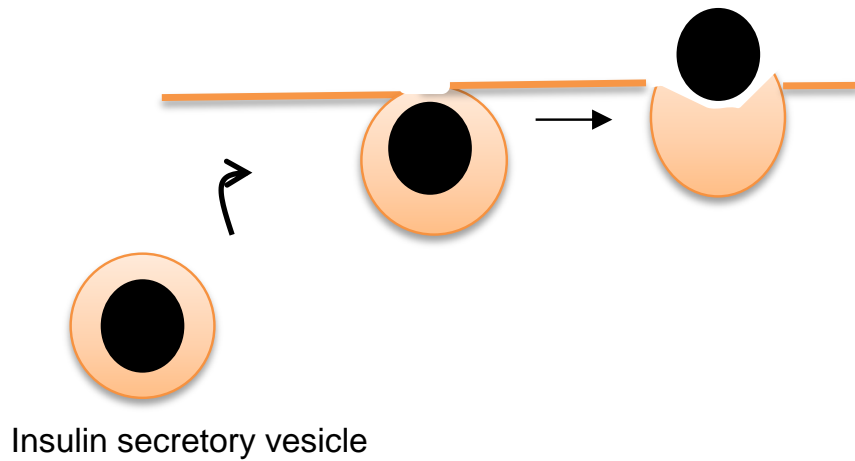
Full fusion entails the complete fusion of the insulin secretory vesicle membrane with the exterior of the beta cell plasma membrane resulting in the complete

emptying of the granule contents (Akerblom and Knip, 1998, Hastoy et al., 2017). Granule fusion has been studied extensively in pancreatic beta cell using two main methods. Studies using two photon excitation imaging techniques have involved the incubation of isolated mice islets in an extracellular dye that will not be taken up until stimulation of these islet cells. Stimulation then causes the extracellular dye to be taken up through the fusion pore which occurs when the secretory granule fuses with the plasma membrane. The granule then emits a bright fluorescence spot signifying exocytosis (Hoang Do and Thorn, 2015, Takahashi et al., 2002). Secondly, capacitance measurements analyse single beta cells and fusion of the plasma membrane and secretory membrane lead to an increase in membrane area which can be monitored electrically. Since insulin granules are estimated to be about 300-400nm in diameter the changes in membrane capacitance can be measured when vesicle fusion occurs (Neher, 1998). Both methods are powerful tools but they have met with some criticism in that no differentiation can be made between exocytosis and endocytosis mechanism (Hou et al., 2009)

The 'kiss and run' mechanism is a form of partial fusion in which transient pores open between the insulin secretory granule membrane and beta cell plasma membrane allowing only partial release of the granule contents and an abrupt closing of the pore (Tsuboi and Rutter, 2003, MacDonald et al., 2006). By utilising TIRF microscopy Rutter and Tsuboi (2003) demonstrated the formation of transient fusion pores without any fusion of the secretory granules and plasma membrane. Studies by Macdonald *et al* (2006) in rat beta cells also revealed the formation of transient fusion pores and these allowed the passage of ATP but not insulin, which was too big to penetrate. The authors suggested that kiss and run

exocytosis may serve to mediate selective release of small vesicles rather than large vesicles.

A. Full fusion



B. Kiss and Run

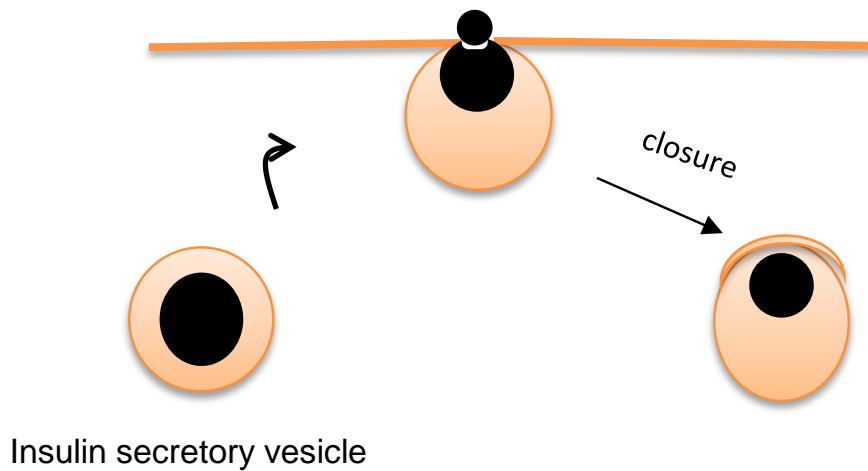


Figure 1.5 Exocytosis mechanism of insulin secretion

(A) full fusion depicting the complete fusion of the insulin membrane vesicle with the exterior of the beta cell plasma membrane resulting in the complete removal of the granule content (black circle) (B) kiss and run displaying partial fusion of the insulin membrane vesicle with the beta cell plasma membrane resulting in only partial release of the granule content (small black circle) followed by an abrupt closure of the pore

1.3.8 Endocytosis

Once insulin is released, the secreted membrane must be recaptured back into the beta cell by endocytosis and three mechanisms which are similar to exocytosis have been suggested (*Figure 1.6*)

The first type is the “kiss and run” where there is a transient fusion pore opening between the granule membrane and the plasma membrane allowing only a partial release of the granule contents. This is immediately followed by the closure and retrieval of the granule membrane back inside the cell (Tsuboi and Rutter, 2003).

Alternatively, there may be a complete integration of granule membrane and the plasma membrane (termed “full fusion”) and this extra membrane is recaptured as a clathrin coated vesicle into the cell by clathrin mediated endocytosis.

A third mechanism “Semi-fusion” has also been proposed in which there is a large opening between the granule lumen and the outside of the cell without disrupting the granule membrane for the eventual retrieval of its membrane after insulin is secreted (Taraska et al., 2003)

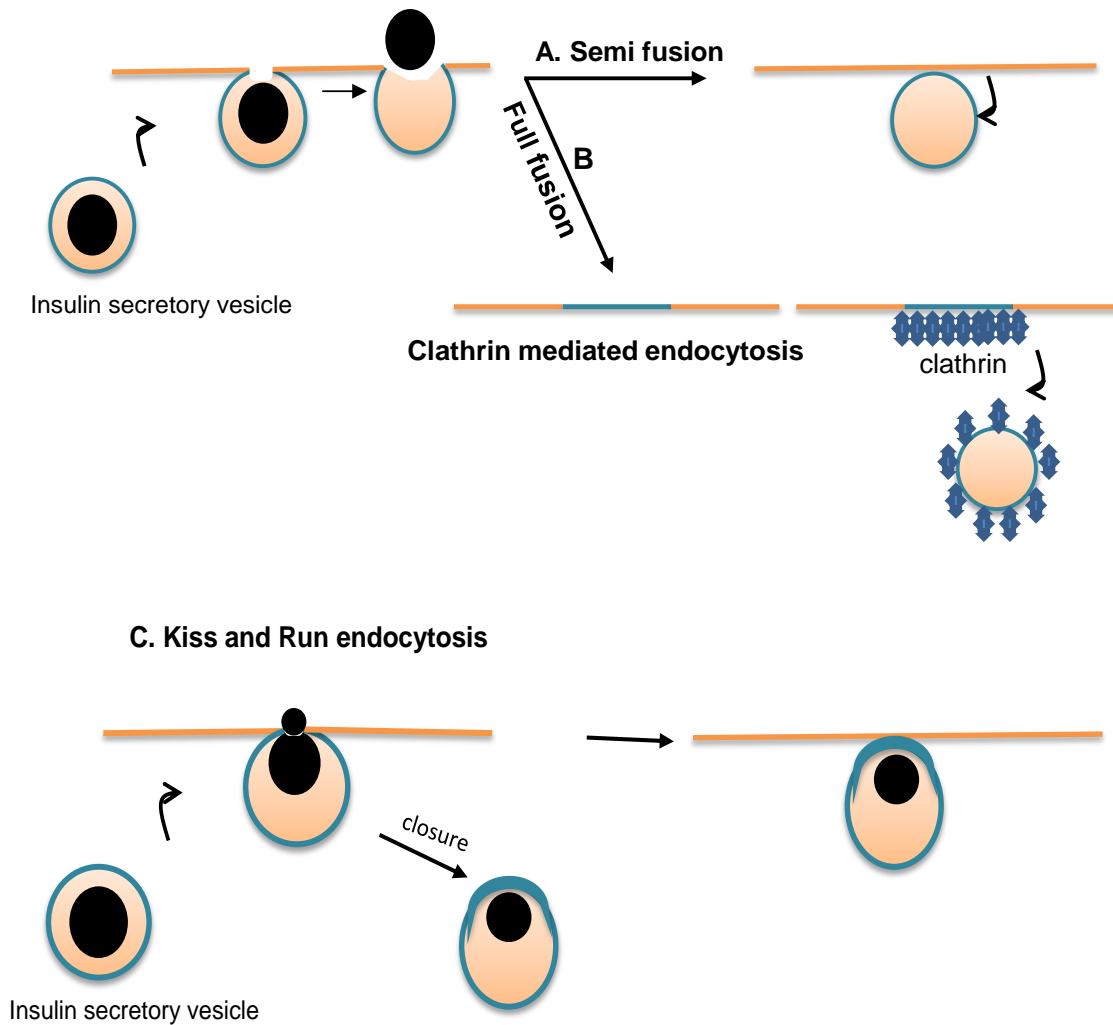


Figure 1.6 Endocytosis proposed mechanism

(A) Semi-fusion entails a large opening between the granule lumen and the exterior of the beta cell membrane without disrupting the granule membrane for the retrieval of its membrane (B) Full fusion displays a complete integration of the plasma membrane through a clathrin mediated endocytosis (C) Kiss and Run entails the partial release of the granule content followed by an immediate closure and retrieval of the granule membrane back into the cell.

1.4 Human enteroviruses and Type 1 diabetes

Human enteroviruses (HEV) are ubiquitous and circulate commonly, especially in young children. Most infections are asymptomatic, however, these viruses can cause serious illness such as post poliomyelitis syndrome, amyotrophic lateral sclerosis, chronic myocarditis and pancreatitis and in the worst cases they can be lethal (Rhoades et al., 2011). They are easily transmitted through the faecal-oral route replicating mostly in the intestine and secondarily in the pancreas (Jaidane and Hober, 2008).

HEV belong to the *Picornaviridae* family and are non-enveloped with a single-stranded positive (+) sense RNA genome of roughly 7500bases. The virion RNA has a viral protein (VPg) covalently linked to it and this acts as a primer for RNA replication. The genome contains a single open reading frame with a 5' untranslated region (UTR), that contains a type 1 internal ribosome entry site (IRES) for cap-independent translation; the P1 region, which encodes the structural polypeptides; the P2 and P3 regions, which encode the non-structural proteins required for replication and a 3'-end poly(A) tail. The structural proteins include (VP1-4) in the P1 region and the non-structural proteins (2A-2C and 3A-3D) in the P2 and P3 region.

In an acute lytic infection, after the delivery of the positive sense (+) viral RNA genome into the cytosol, the viral genome is translated to the single polyprotein which then undergoes cleavage by viral proteases (2A^{pro} and 3C^{pro}) to release structural and non-structural viral proteins (Linden et al., 2015). The four structural proteins adopt an icosahedral capsid structure with four viral capsid proteins consisting of VP1, VP2, VP3 (making up the outer surface of the capsid) and VP4 located inside the capsid (*Figure 1.7*). The icosahedral capsid protein

protects the viral RNA genome and is important in mediating cellular attachment (Hober et al., 2013). The non-structural proteins (2A-2C and 3A-3D) mediate the replication of the viral RNA genome to produce a negative-strand which is used as a template for the synthesis of positive-strand RNA. Newly synthesized positive stranded RNA molecules then either undergo another round of translation and replication or are packaged into viral capsid proteins to form new infectious particles (Linden et al., 2015).

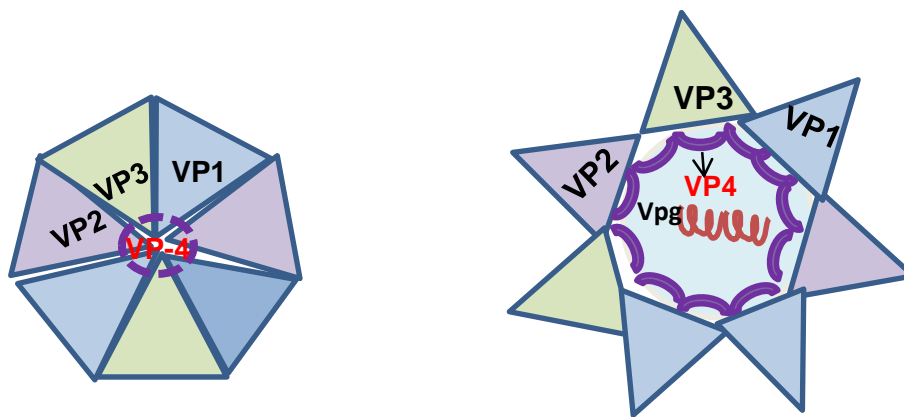


Figure 1.7 Structure and genome of Enterovirus.

Left panel displays the closed viral capsid comprising of the structural proteins VP1-3 present on the outside with VP4 inside. Right panel displays the open viral capsid with genome linked to a Vpg protein

Circumstantial epidemiological evidence suggests that enteroviruses, particularly members of the Coxsackievirus B family, may be involved in the development of type 1 diabetes (Coppieters et al., 2012). As far back as the late 1960's, human enteroviruses were implicated in the development of type 1 diabetes when Gamble and Taylor (1969) demonstrated an increased frequency of neutralising antibodies to Coxsackievirus B4 (CVB4) in newly diagnosed patients (Gamble et al., 1969). Then in 1979, a strain of CVB4 was isolated from the pancreas of a

child who died from diabetic ketoacidosis, which was able to induce T1D in mice (Yoon et al., 1979). A later study with Swiss Jim Lambert (SJL/J) mice, showed that 6 weeks after CVB4 infection, mice developed hyperglycaemia and importantly this correlated with GAD autoantigen positivity in 90% of the mice, implying that Coxsackie B viruses may trigger and/ or amplify islet autoimmunity (Gerling et al., 1991).

Serological and epidemiological studies in children from five European countries reported that antibodies against CVB1, another member of the CVB family, were more frequent in diabetic children than amongst carefully matched control children (Oikarinen et al., 2014). Moreover, enteroviral RNA has been detected in the peripheral blood of recent-onset T1D patients (Schulte et al., 2010). Coxsackie B virus infection has also been linked to the initiation of islet autoimmunity in several studies (Hyöty, 2016). Recently, for example, the appearance of neutralising antibodies against CVB1, which is indicative of a recent infection with this virus, were identified more frequently in the serum of children who later (in the next few months) developed IAA (insulin autoantibodies) (Sioofy-Khojine et al., 2018).

A meta-analysis of 24 studies with 4,448 participants prompted the conclusion that enteroviral infection is detected ten-times more frequently in patients with recent-onset T1D than in matched controls. Importantly, it was elevated four-fold in autoantibody positive (non-diabetic) patients, suggesting that such infections may be causal to, rather than a secondary consequence of islet autoimmunity (Yeung et al., 2011).

The human pancreatic beta cells are known to be susceptible to enteroviral infection and this has been demonstrated in several *in vitro* and *in vivo* studies.

The study by Elshebani *et al* (2007) revealed that infection of isolated human islets with four enterovirus strains isolated from families with T1D, resulted in increased enterovirus replication (EV-RNA), evident from three days to seven days post-infection (Elshebani et al., 2007). Importantly, they also reported that glucose stimulated insulin secretion in infected cells, 3 days after infection, was reduced when compared to non-infected control islets (Elshebani et al., 2007).

In mice, it was shown that when isolated human islets were transplanted in mice and later infected with a CVB4 strain, that diabetes was developed in these mice after three weeks (Gallagher et al., 2014). In addition, analysis of the human islets from infected mice revealed statistical significant decrease in insulin at both the RNA and protein level (Gallagher et al., 2014). In neonates, it was also shown that islets are susceptible to CVB infection when *in situ* hybridization with a CVB-specific probe detected the presence of an acute coxsackievirus infection in the pancreas particularly in the islets of five of the nine cases of these infants examined (Foulis et al., 1997). Interestingly, infection was observed mostly in the islets with limited restriction to the exocrine pancreas (Foulis et al., 1997). In contrast, a study in neonatal mouse, showed that infection with CVB was found specifically in the exocrine pancreas (Hilton et al., 1992) implying that there is differential CVB tissue tropism in the human (targeting the islets) and mouse pancreas (targeting the exocrine tissue).

More direct evidence of pancreas infection in human type 1 diabetes was provided by utilising *in situ* hybridization in pancreases from type 1 diabetes patients which revealed the presence of enteroviral RNA in the islets which was absent in non-diabetes cases (Ylipaasto et al., 2004). This was also confirmed, in 2009 when pathological studies provided evidence that a small number of beta cells express the enteroviral capsid protein VP1, in 44 of 72 (61%) recent-onset

T1D post mortem pancreas samples from the Exeter Archival Diabetes Biobank (Richardson et al., 2009). In contrast, VP1 positive cells were seen only rarely in control cases (Richardson et al., 2009). These findings have since been replicated in two further cohorts, the nPOD collection which uses a standard procedure to ensure consistency in recovery and processing of samples. In these pancreas sections, VP1 positive cells were detected in 80% of cases in islet cells in which insulin containing islets were present (Richardson et al., 2013). In addition, in the Norwegian DiViD cohort, Krogvold *et al* (2015) revealed the presence of enteroviral RNA and capsid protein (VPI) in pancreatic islet cultures and islet tissue from living people recently diagnosed (3-9 weeks) with T1D (Krogvold et al., 2015).

In the above studies, the low level of infection observed in type 1 diabetes patients (i.e very few viral protein positive cells and/ or low levels of viral RNA) contrasts with the levels observed in an acute infection setting (e.g. CVB-infected neonates) and the results are indicative of a low level persistent infection. One mechanism, through which persistent infection can occur, is via naturally occurring deletions of the 5' terminal end of the coxsackievirus genome resulting in a loss of cytopathic effect (Kim et al., 2005, Chapman et al., 2008, Tracy et al., 2015). This phenomenon has been observed in human heart samples and results in a reduced replication rate of the virus when compared to the full length virus (Tracy et al., 2015). It was further shown that inoculation of the NOD mouse with CVB3 resulted in an initial acute infection and that the terminally deleted virus could however be detected from day 21 onwards in the heart and pancreas. In contrast, the full length virus levels dropped over time, with only the terminally deleted virus still detectable on day 35. Despite the persistence of the viral RNA in the pancreas, no cytolytic virus activity could be detected (Tracy et al., 2015).

This terminally deleted 5' form of the virus genome has also been demonstrated in other tissues such as the heart, in both mice and humans (Kim et al., 2005, Chapman et al., 2008). These “terminally deleted viruses” have replicative-defective ability that rarely forms functional infectious virions that can infect adjacent cells. In non-lytic slow replication, there are equal numbers of positive and negative strand viral RNA with very little synthesis of the complete viral particles expressing the structural capsid proteins (Cunningham et al., 1990, Klingel et al., 1992, Tam and Messner, 1999). For this reason, these viruses persist in the host cells replicating very slowly over a long duration which concurs to what is observed in type 1 diabetes islets where a low number of VP1 immunopositive beta cells are detected with no extensive cell lysis (Morgan and Richardson, 2014).

1.5 Mechanism of virus-induced autoimmune T1D

1.5.1 Direct beta cell damage

Enterovirus infection can directly lead to the malfunction of the insulin producing beta cell and can induce beta cell lysis. *In vitro* studies in isolated human islets infected with enterovirus have revealed efficient viral replication in the beta cells that coincided with a significant increase in cytopathic effect and a reduction in insulin gene expression. No effect on glucagon gene expression was observed, confirming the susceptibility of beta cells to enteroviral infection (Frisk and Diderholm, 2000, Anagandula et al., 2014b). Lysis of infected beta cells will release beta cell antigens that *in vivo* will be taken up by phagocytic cells and antigen presenting cells and can subsequently lead to the activation of an

autoimmune response against beta cell antigens in at-risk individuals (Richardson and Horwitz, 2014)

1.5.2 Persistent enteroviral infection

A series of events by which a persistent infection in the beta cells could lead to autoimmune type 1 diabetes has been proposed. Following an initial acute infection with an enterovirus which causes direct damage to beta cells (described above), release of beta cell antigens and the appearance of islet autoimmunity occur in individuals who are at risk of developing type 1 diabetes. It is proposed that in certain individuals (potentially determined by their genetic background) that they are unable to efficiently clear the infection and a slowly replicative persistent infection of the pancreatic beta cells can occur. This infection can be sensed by intracellular pattern recognition receptors (PRRs), which subsequently activate antiviral signalling pathways, which includes the secretion of anti-viral interferons (IFNs). These IFNs can, amongst other functions, induce the hyperexpression of MHC class 1 on the surface of beta cells and other neighbouring endocrine cells. This is a hallmark feature in the pancreas of individuals with Type 1 diabetes (Richardson et al., 2016). Hyperexpression of MHC1 can lead to the aberrant presentation of beta cell antigen and the recruitment of the islet auto-reactive immune cells to the islets and the subsequent destruction of the beta cells, facilitating the progression towards type 1 diabetes (Richardson et al., 2014, Morgan and Richardson, 2014).

1.5.3 Molecular mimicry

This hypothesis proposes that there may be potential cross reactivity between the epitopes of islet cell autoantigens and viral proteins. This happens as a result of similarities in amino acid sequence. There are speculations that the immune response directed against the viral antigen results in the production of cytotoxic T lymphocytes which can also recognise the islet cells, evoking beta cell death. In support of the potential for molecular mimicry, a study by Atkinson *et al* (1994) revealed that PBMCs (peripheral blood mononuclear cell) from individuals at increased risk of diabetes or with recent onset type 1 diabetes had responsiveness to GAD (an islet autoantigen) peptides (amino acid region 247-279) which was not observed in healthy controls. Interestingly, this region shared similarity to the Coxsackie B virus protein P2-C (Atkinson *et al.*, 1994). However, it was later shown that the homology between these two epitopes was not associated with any functional consequence (Schloot *et al.*, 2001). The role of molecular mimicry in Type 1 diabetes is still under debate, but many believe it to be an unlikely scenario (Coppieters *et al.*, 2012)

1.6 Enterovirus receptors

Very early on in the 1960's it was reported that the presence of specific surface receptors (virus attachment sites) on the cell membrane was an important feature for virus sensitive cells and tissue tropism (Kunin, 1964). It was further demonstrated that these viral receptors may be essential for viral tropism; since in aged mice the enterovirus receptor expression was downregulated and this correlated directly with decreased viral sensitivity, with most of the adult mice tissues being resistant, except for limited infection in the brain (Kunin, 1964). In

contrast, new born mice tissues, which exhibited higher enterovirus receptor expression were exquisitely sensitive to infection with multiple Coxsackie virus strains (Kunin, 1964).

A number of cell surface receptors utilised for viral attachment and entry have been identified for different enterovirus serotypes (Table 1.3). Importantly, the enteroviral receptor known as the Coxsackievirus and adenovirus receptor (CAR) is expressed in host cells and mediates infection by Coxsackie B viruses (CVB1-6). An additional cell surface receptor decay accelerating factor (DAF) has also been identified to facilitate the binding of some members of the CVB viruses, but it is not sufficient to sustain a productive infection (Bergelson et al., 1997, Tomko et al., 1997, Shafren et al., 1995). Chinese hamster ovary (CHO) cells are not normally permissive to CVB infection, however, Bergelson *et al* (1997) demonstrated that if CAR was transfected into these cells that they became susceptible to these viruses (Bergelson et al., 1997). In another study, radiolabelled experiments with CVB3 and CVB4 showed that murine CAR transfected CHO cells (homologous to human CAR), resulted in increased virus titre and viral cytopathic effect which was not evident in control integrin $\alpha 2$ subunit transfected CHO cells (Bergelson et al., 1997). Also, Martino *et al* (2000) demonstrated that CAR transfected CHO cells sustained high levels of viral production when infected with CVB1-6 reference strains and clinical isolates which was not observed in non-CAR transfected CHO cells (Martino et al., 2000).

As many of the molecular and epidemiological studies implicate CVB viruses in type 1 diabetes and CAR plays a significant role in mediating viral attachment, entry and infection of these, I felt it was fundamentally important to investigate the presence of CAR in the human pancreas.

Table 1.3 Receptors utilised by enterovirus serotypes

Receptors	Enterovirus and serotypes	References
PVR	Poliovirus(PV)1-3	(Mendelsohn et al., 1989)
CAR	Coxsackievirus B1-6	(Bergelson et al., 1997)
ICAM-1	Coxsackievirus A21, A13,A18	(Shafren et al., 1997)
α V β 3 integrin	Coxsackievirus A9	(Berinstein et al., 1995)
DAF	Coxsackievirus B1,B3 and B5 Echovirus 3,6,7,11,13,20,21,24,29,33	(Bergelson et al., 1994, Shafren et al., 1995)

1.7 The Coxsackievirus and adenovirus receptor (CAR)

CAR is a type 1 transmembrane cell adhesion and tight junction protein that is utilised as a primary viral receptor by two distinct types of viruses; the Coxsackie B viruses (CVB) and most adenoviruses (Tomko et al., 1997, Cohen et al., 2001b, Bergelson et al., 1997, Excoffon et al., 2004).

Human CAR was first isolated by Bergelson *et al* (1997) as a protein encoded by a gene (*CXADR*) with 7 exons (Bergelson et al., 1997). Through a process of alternative splicing, CAR can be spliced into at least 5 different isoforms in humans (*Figure 1.8*, Table 1.4) and 3 isoforms in mice (Bergelson et al., 1998, Thoelen et al., 2001, Chen et al., 2003).

In humans, only two of the splice variants have a transmembrane domain; these two variants are retained by cells within membranes and can bind other CAR molecules, viruses and are able to sustain a productive infection. These two isoforms include “CAR-SIV” (also named CAR^{EX7}, HCAR1, SIV or α CAR) a 7 exon encoded isoform, which is the mice equivalent of mCAR2 and an 8 exon

encoded isoform “CAR-TVV” (also named CAR^{EX8}, HCAR5 or TVV), which is the mice equivalent of mCAR1. The two transmembrane isoforms in humans were named according to the terminal end of their amino acids (“SIV” and “TVV”) which harbours a specific protein-protein interaction domain. This domain is known as PDZ, which signifies the first letter of the initial three proteins discovered (post-synaptic density protein (PSD95), drosophila disc large tumor suppressor (DIG1) and zonula occludens-1 proteins (ZO-1) binding domain. The mouse isoforms were named according to the order they were discovered (Bergelson et al., 1998, Excoffon et al., 2010). The other three isoforms are generated by exon skipping and are soluble, as they do not contain the transmembrane domain, and are called CAR 4/7 (CAR β), CAR 3/7 (γ) and CAR 2/7 (δ) dependent on the exon splicing events. These isoforms can be secreted from cells, are capable of binding extracellular CAR and can prevent CVB3 infection (Dörner et al., 2004, Thoelen et al., 2001, Excoffon et al., 2014) by binding the sequestering virus away from susceptible cells

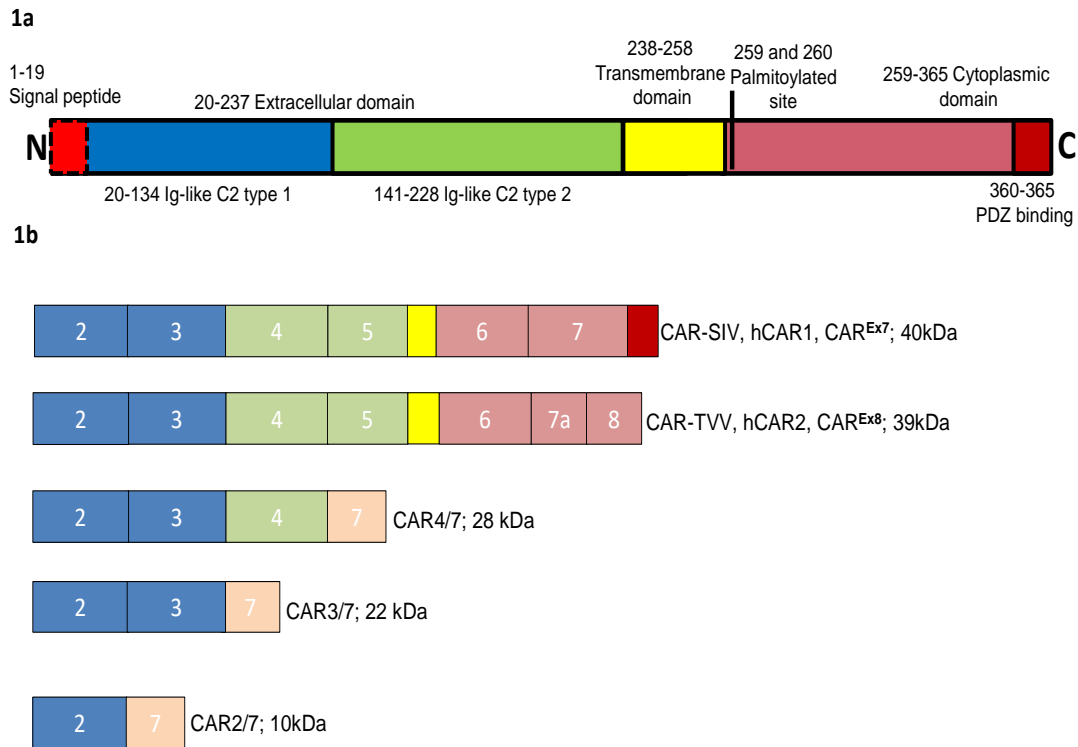


Figure 1.8 Structure of the CAR protein and isoform.

(1a) In CAR protein structure the signal peptide in the N terminus (red box, broken lines) is cleaved off to yield a mature protein with an extracellular domain (ECD) comprising 2 immunoglobulin (Ig)-like domains, type 1 and type 2 (blue and green). The transmembrane domain (TM; yellow) bridges the ECD and cytoplasmic domain (light salmon) terminating with a PDZ binding domain (brick red) (1b) CAR exon maps for the 5 differentially spliced isoforms. Isoforms CAR-SIV and CAR-TVV contain the transmembrane domain. The soluble isoforms CAR4/7, CAR3/7 and CAR2/7 reflect exons inclusion or exclusion and they all lack the transmembrane domain.

Table 1.4 CAR isoforms from NCBI and UniProt database

CAR Isoforms	NCBI nucleotide ID	UniProt ID
CAR-SIV	NM_001338.4	P78310-1
CAR-TVV	NM_001207066.1	P78310-6
CAR 4/7	NM_001207063.1	P78310-5
CAR 3/7	NM_001207064.1	P783104
CAR 2/7	NM_001207065.1	P783103

1.7.1 Structure of CAR

CAR is a 46kDa protein composed of an N-terminus signal peptide (ND), an extracellular domains (ECD) consisting of two Ig-like domain, transmembrane region (TM) and an intracellular cytoplasmic domain (ICD) shown in Figure 1.8 (Bergelson et al., 1997, Tomko et al., 1997).

CAR is classified as a member of the proteins belonging to the CTX (cortical thymocyte marker in *Xenopus*) subfamily of the immunoglobulin superfamily (Igsf) (Chrétien et al., 1998). Members of the subfamily include junctional adhesion molecules (JAMs), endothelial cell selective adhesion molecule (ESAM), brain-testis IgSF (BT-IgSF), CAR like membrane protein (CLMP), CTX and A33 (Schreiber et al., 2014, Matthäus et al., 2017). This family is structurally composed of an extracellular domain with a variable (V-type) D1 and a constant (C-type) D2, a single transmembrane domain followed by a cytoplasmic domain of varying length (Philipson and Pettersson, 2004)

Similarity exists between the human and mouse CAR protein with 91% amino acid identity within the extracellular domain, 77% within the transmembrane and up to 95% within the cytoplasmic domain (Cohen et al., 2001b).

CAR-SIV is the principal isoform of CAR encoding 365aa which differs from CAR-TVV (352aa) only within the last portion of their cytoplasmic domain (*Figure 1.9*). The C' terminus end of CAR-SIV contains 26 unique amino acids encoded by exon 7, while CAR-TVV contains 13 unique amino acids encoded by exon 7a and exon 8. The C terminus of both transmembrane isoforms encodes a consensus type 1 PDZ binding domain, a motif enclosing four amino-acid protein interaction sites at the terminal end (X-(S/T)-X-φ) where X represents any amino acid and φ

any hydrophobic aminoacid; GSIV (Gly-Ser-Ile-Val) and ITVV (Ile-Thr-Val-Val) (Excoffon et al., 2010, Excoffon et al., 2014).

The C terminus also encodes a peptide recognition site for the clathrin adaptor protein (AP), ³¹⁸**YNQV**³²¹, which is common to both CAR-SIV and CAR-TVV and a distinct basolateral sorting motif ³⁴⁵**LSRMG**³⁴⁹ only found in CAR-SIV, which is essential for basolateral targeting. This was confirmed in a study where truncated CAR mutants were shown to be localised to the apical surface of polarised Madin-Darby canine Kidney Cells (MDCK cells) (Cohen et al., 2001a). In that study, a tyrosine residue based at position 318 was also demonstrated as a sorting signal ³¹⁸**YNQV**³²¹. Mutation of that tyrosine residue resulted in differential targeting to the apical membrane of polarised MDCK cells, confirming its importance in basolateral sorting (Cohen et al., 2001a). The differences between CAR-SIV and CAR-TVV protein sequence is displayed in Figure 1.9 below.

```

CAR-SIV  MALLLCFVLLCGVDFARSLISITTPPEEMIEKAKGETAYLPCKFTLSPEDQGPLDIEWLIS
60
CAR-TVV  MALLLCFVLLCGVDFARSLISITTPPEEMIEKAKGETAYLPCKFTLSPEDQGPLDIEWLIS
60
*****

CAR-SIV  PADNQKVDQVIILYSGDKIYDDYYPDLKGRVHFTSNDLKSGDASINVTNLQLSDIGTYQC
120
CAR-TVV  PADNQKVDQVIILYSGDKIYDDYYPDLKGRVHFTSNDLKSGDASINVTNLQLSDIGTYQC
120
*****

CAR-SIV  KVKKAPGVANKKIHLVVLVKPSGARCYVDGSEEIGSDFKIKCEPKEGSLPLQYEWQKLS
180
CAR-TVV  KVKKAPGVANKKIHLVVLVKPSGARCYVDGSEEIGSDFKIKCEPKEGSLPLQYEWQKLS
180
*****

CAR-SIV  SQKMPTSWLAEMTSSVISVKMASSEYSGTYSCTVRNRVGSQCLLRLNVVPPSNKAGLIA
240
CAR-TVV  SQKMPTSWLAEMTSSVISVKMASSEYSGTYSCTVRNRVGSQCLLRLNVVPPSNKAGLIA
240
*****

CAR-SIV  GAIIGTLLALALIGLIIFCCRKKRREEKMEKEVHHDIREDVPPPKSRTSLARSYIGSNHS
300
CAR-TVV  GAIIGTLLALALIGLIIFCCRKKRREEKMEKEVHHDIREDVPPPKSRTSLARSYIGSNHS
300
*****

CAR-SIV  SLGSMSPSNMEGYSKTQYNQVPSSEDFERTPQSPTLPPAKVAAPNLSRMGAIPVMIPAQSK
360
CAR-TVV  SLGSMSPSNMEGYSKTQYNQVPSSEDFERTPQSPTLPPAKFKYPYKTDG--ITVV-----
352
*****. * : * *:

CAR-SIV  DGSIV 365
CAR-TVV  ----

```

KEY

PDZ domain 362SIV365, 349TVV352
C 259 & 260-palmitoylation
N 106 D1 DOMAIN, N201 D2 DOMAIN- glycosylation on asparagine residues
Tyrosine Y269,294,313,318& Threonine T290, serine S293 residues, S306,
323, 332
YNQV peptide recognition for basolateral targeting
345 LSRMG 349 Sorting motif
D1 c41-c120disulfide bounds
D2 c162-c212 disulfide bounds

Figure 1.9 Similarities and differences between the protein sequence of CAR-SIV and CAR-TVV

1.7.2 CAR expression in cells and tissues

A recent review by Matthäus *et al* (2017) concluded that CAR is developmentally regulated with tissue-specific expression in several organs, such as the heart, brain, testis, pancreas, kidney and intestine (Matthäus *et al.*, 2017). In mice, CAR can be detected by IHC in the ectoderm, as early as embryonic day (ED) 6.5 (Hotta *et al.*, 2003). As the embryonic mice develop CAR can be found abundantly in the brain, skeletal and heart muscles (Honda *et al.*, 2000a, Loustalot *et al.*, 2016) but expression becomes more restricted at later developmental stages. This pattern of expression may explain the extreme sensitivity of neonatal mice to CVB-infection (Hilton *et al.*, 1992, Jmii *et al.*, 2016). Knockout of CAR (Dorner *et al.*, 2005) resulted in embryonic death between ED11.5 and ED13.5, highlighting the critical importance of CAR in early developmental events, particularly within the heart. Additionally, cardiac specific CAR knockout mice resulted in abnormal atrioventricular conduction in the heart, which is essential in regulating blood flow in the heart (Lim *et al.*, 2008). In adult mice, CAR expression is predominantly found on polarised epithelial cells lining the body cavities (Raschperger *et al.*, 2006) which fits with its role as a tight junction protein. In terms of CAR expression in the pancreas, studies of CAR knockout adult mice revealed dilated intestines and atrophy of the exocrine tissue, with an almost complete lack of acinar cells. The islets, however, appeared unaffected (Pazirandeh *et al.*, 2011).

CAR developmental importance in human brain has not been reported but it has been shown to be present abundantly in the brain, specifically in the hippocampus region, responsible for long term memory (Yonelinas, 2013). In contrast, CAR was shown to be downregulated in the hippocampus in patients with Alzheimer's disease (Zussy *et al.*, 2016). In another study, CAR was detected in the choroid

plexus cells of the brain, which are involved in the synthesis of cerebrospinal fluid circulating the brain (Persson et al., 2006). In addition, CAR has also been shown to be expressed in the human pituitary gland (Persson et al., 2006).

CAR expression in the human heart is similar to the situation in mice, in that there is a low-level expression in the normal adult heart. In contrast, CAR expression was observed to be higher in patients with dilated cardiomyopathy (Noutsias et al., 2001) implying that patients with this disease could be more susceptible to CVB infection. CAR has also been demonstrated to be localised to cell-cell junctions in polarised human airway epithelial cells (Cohen et al., 2001b, Excoffon et al., 2010). Due to CAR's localisation to cell-cell contact it has been shown to play a structural role in cell adhesion (Excoffon et al., 2004).

In cancerous cells, low levels of CAR have been revealed, for example in normal bladder tissue, CAR have been shown to be downregulated at both the RNA and protein level in cancerous bladder tissue (Sachs et al., 2002, Jee et al., 2002). The consequence of low-level CAR expression in cancer cells may result in a loss in cell adhesion giving an advantage for cancerous cells to easily metastasise. In support of this, when CAR was overexpressed in human bladder cancer cells, there was an inhibition in further cell proliferation (Okegawa et al., 2001) implying that an increase in CAR expression may negatively regulate proliferation in cancerous cells.

1.7.3 CAR Post-translational modifications

Many proteins undergo palmitoylation which facilitate targeting to lipid rafts that are enriched in cholesterol and sphingomyelin (Levental et al., 2010). Using radiolabelled fatty acids it was demonstrated that the cysteine residues, C²⁵⁹ and

C²⁶⁰, in the cytoplasmic tail of CAR can be palmitoylated (van't Hof and Crystal, 2002). It was further shown in COS7 cells that if these cysteine residues were mutated that labelling by radiolabelled palmitate was prevented. MDCK cells expressing these mutants showed altered localisation, being found more prominently in the perinuclear region and throughout the plasma membrane, in contrast to the basolateral localisation of CAR that was normally observed in these cells with wild-type CAR (van't Hof and Crystal, 2002). Although, the cytoplasmic tail is essential for palmitoylation, another study observed that CAR was still localised to lipid rich microdomains when the transmembrane and cytoplasmic tail were replaced with a non-lipid raft protein (Excoffon et al., 2003) suggesting that the CAR ECD may be, in part, mediating CAR localisation.

N-Glycosylation plays pivotal roles in protein folding, conformation and stability (Mitra et al., 2006) and there are two N-glycosylation sites in the CAR ECD domain “N¹⁰⁶ in D1” and “N²⁰¹ in D2”. These have been confirmed by the generation of single and double glycosylation deficient mutants at these sites in COS-7 cells. Western blotting confirmed the loss of glycosylation by the detection of lower fragments in the mutants when compared to the glycosylated wild-type CAR which migrated at 46kDa (Excoffon et al., 2007). Cell adhesion assays revealed that mutations of both these glycosylation sites prevented CAR-CAR homophilic interactions, as evidenced by the lack of clumping cells in double deficient mutants when compared to wild type or single glycosylation deficient mutants. However, the lack of glycosylation did not alter CAR junctional localisation (Excoffon et al., 2007).

In addition, CAR also has two potential phosphorylation sites, threonine²⁹⁰ and serine²⁹³, within the C terminus. Protein kinase C delta (PKC δ) has been shown to phosphorylate these residues in human bronchial epithelial cells, and this

process is augmented by treatment of the cells with the phosphatase inhibitor (Calyculin A, CalA) and activator of protein kinase, phorbol 12,13-dibutyrate (PDBu) (Morton et al., 2013). In addition, pull down assays revealed that CAR binds directly to PKC δ . Importantly, knockdown of PKC δ reduced CAR's molecular weight in cells treated with Cal A or PDBu, indicative of a lack of phosphorylation at these residues. The phosphorylation of CAR has been shown to mediate the recruitment of E-cadherin, an adhesion protein, to cell-cell junctions (Morton et al., 2013). This was further shown using CAR mutants that could not be phosphorylated which significantly disrupted E-cadherin junctional localisation (Morton et al., 2013)

Recently, CAR was also found to undergo ubiquitination when cells were treated with cycloheximide (a protein translation inhibitor) and cytokines (IFN γ + TNF). This induced down regulation of CAR levels by ~40% in GC-2spd cells (a mouse germ cell line). This suggests that cytokines can promote CAR degradation via a ubiquitin-mediated pathway (Gao and Lui, 2014). In support of this, blocking of the proteasome pathway, using lactacystin (a proteasome inhibitor) demonstrated that when cells were pre-treated with IFN γ + TNF, that CAR could be immunoprecipitated with ubiquitin antibody. The specific residues that are ubiquitinated have still not yet been identified (Gao and Lui, 2014)

1.7.9 CAR interacting protein partners

A range of scaffolding PDZ containing proteins (*Figure 1.10*) are known to interact with the PDZ binding domain of CAR-SIV and CAR-TVV in several cells and a selection of these are described below.

Co-immunoprecipitation and cryo-EM studies have revealed that the CAR-SIV isoform interacts with and colocalises with ZO-1 at the apical region of tight junctions in the human colonic cell line (T84) (Cohen et al., 2001b). Furthermore, in CAR-CHO cells, CAR was found to recruit ZO-1 to cell-cell junctions (Cohen et al., 2001b). CAR-SIV also interacts with MAGI-1b and PSD-90; immunocytochemical analysis revealed a shift from cytoplasmic to the junctional colocalisation (Excoffon et al., 2004). The CAR-TVV isoform also interacts with PSD90, however interaction with MAGI-1b results in a loss of CAR-TVV expression and implies that binding to MAGI-1b targets this particular isoform for degradation (Excoffon et al., 2010).

The Ligand of Numb protein X2 (LNX2) which is important in Notch signalling also has been shown to interact with CAR in human embryonic kidney cells (HEK 293) (Mirza et al., 2005). CAR-SIV has also been shown to interact with PICK1 in polarised COS-7 cells and immunocytochemistry revealed significant colocalisation of both proteins at the perinuclear and membrane regions which was lost when the terminal PDZ-binding domain of "SIV" was deleted (Excoffon et al., 2004). In contrast, CAR-TVV does not interact with PICK1 and immunocytochemistry revealed a lack of colocalisation of both proteins in the same polarised COS-7 cells (Excoffon et al., 2010)

Utilising pull down and mutation analysis, murine CAR1 (TVV) and connexin 45 (a gap junction protein) were shown to interact in whole murine heart extracts. This interaction was confirmed to be mediated by the PDZ binding domain because deletions of either mCAR1 PDZ-binding domain (TVV) or deletions of connexin 45 PDZ domain prevented their interaction with one another (Lim et al., 2008).

CAR also binds to a series of different proteins involved in cell adhesion for example junctional adhesion molecules (JAMs) which include (JAM-L and JAM-C), but this interaction involves the extracellular domain. These interactions play an important role in maintaining cell-cell contacts, facilitate cell migration across tight junctions and can regulate neutrophil trans-epithelial migration across epithelial tight junctions (Zen et al., 2005, Mirza et al., 2012). Importantly, the interacting partners for CAR-SIV and CAR-TVV can differ and so this will likely impart different functional properties for each of the isoforms.

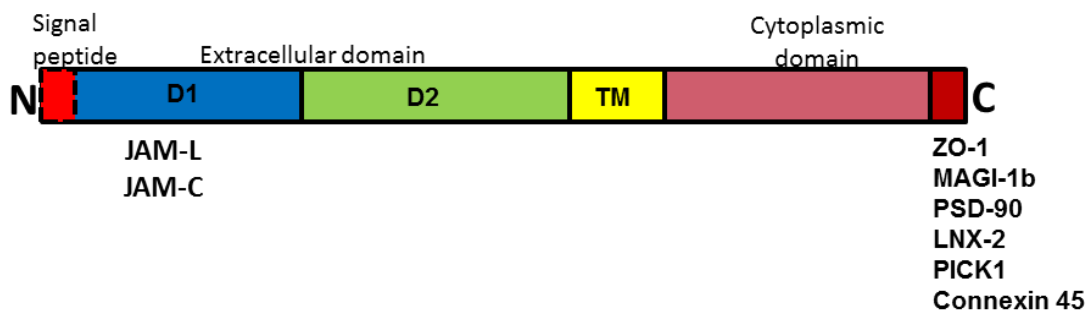


Figure 1.10 CAR and interacting protein partners.

The CAR protein structure includes a signal peptide in the N terminus (red box, broken lines) which is cleaved off to yield mature CAR protein. This includes an extracellular domain (ECD) comprising 2 immunoglobulin (Ig)-like domains, D1 (blue) and D2 (green). The transmembrane domain (TM; yellow) bridges the ECD and cytoplasmic domain (light salmon) terminating with a PDZ binding domain in the C terminus (brick red). JAM-L and JAM-C proteins can bind to domain D1 of CAR protein while ZO-1, MAGI-1b, PSD-90, LNX-2, PICK1 and Connexin 45 can bind to the PDZ binding domain (red box) in the C terminus

1.7.10 Mechanism of Coxsackievirus entry through CAR

Coxsackievirus B members interact with cell surface receptor CAR via a canyon-like depression region on the infectious viral capsid. This interaction forms the initial CVB-CAR binding complex. At physiological temperatures, the binding of CAR to this region induces a conformational change in the capsid that initiates tighter binding (Fields et al., 2007, Organtini et al., 2014). This conformational change of the native infectious virion involves the movement of the three capsid proteins (VP1, VP2 and VP3) resulting in the formation of particle called the “A particle” (destabilised infectious particle). This process induces the expansion of the capsid and the extension of the N terminus of VP1 which inserts into the membrane to form a channel composed of five amphipathic helices (allowing the virion to interact with the membrane). The release of a myristate VP4 group then results in pore formation (Baggen et al., 2018). Viral RNA is then released from the virion through these pores (yielding an empty particle) and is translocated into the cytoplasm for initiation, translation and replication (Hogle, 2002) as described in section 1.4 and Figure 1.11

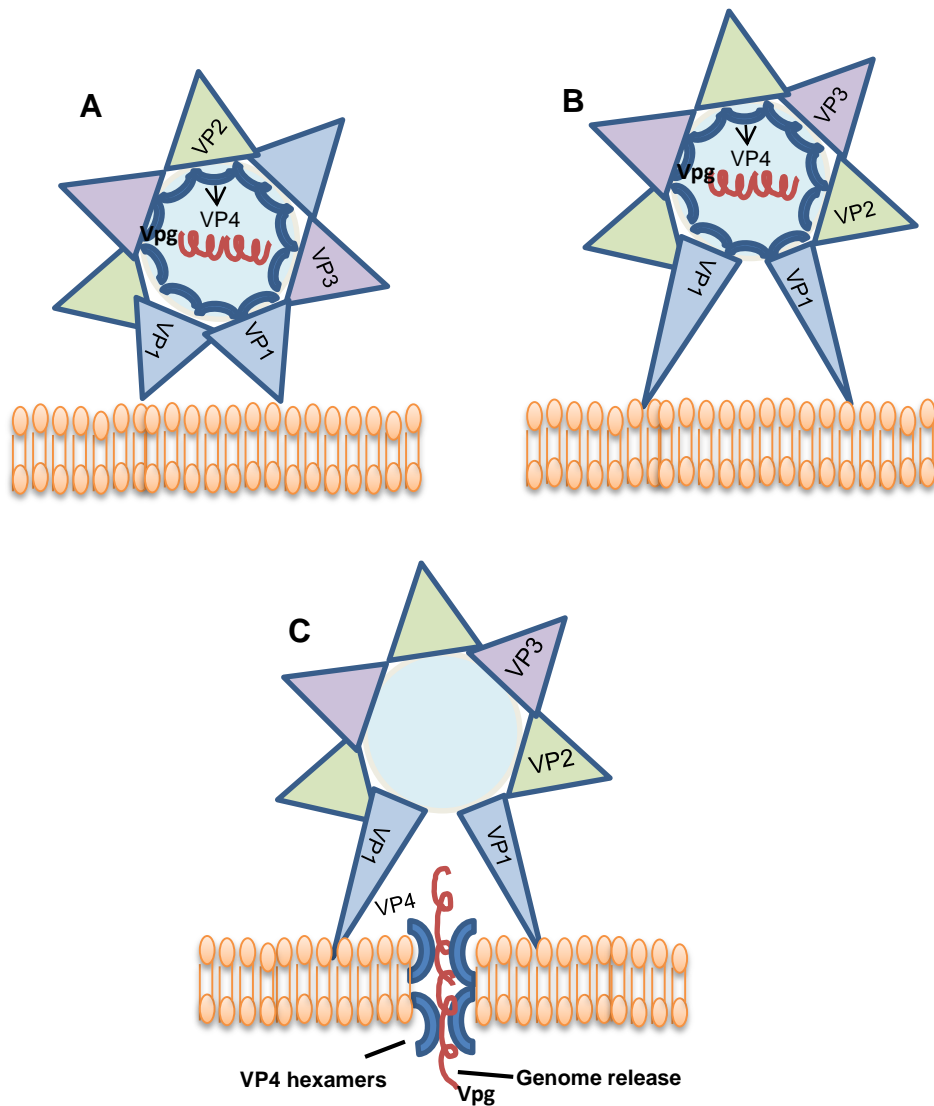


Figure 1.11 Mechanism of CVB entry into cells.

(A) CVB binds to CAR present on the cell plasma membrane forming a CVB-CAR binding complex (B) The binding of the complex then induces a conformational change in the capsid that involves the movement of the capsid proteins (VP1-4) resulting in "A particle" formation and the extension of VP1 initiates tighter binding. (C) A myristate VP4 group is released resulting in pore formation for the viral genome to be released into the cell

1.8 AIMS

The Coxsackievirus and adenovirus receptor serves as a key entry receptor for CVBs. These viruses have a clear propensity to infect human pancreatic beta cells and mounting evidence implicates them in the development of type 1 diabetes. Relatively little is known about CAR expression in human pancreas and as CAR exists in multiple different isoforms, each with a different subcellular localisation and function, it is imperative that this be investigated further. The overall aim of this thesis was to investigate the expression of CAR isoforms in human pancreas with the following sub-aims:

- To study the profile of CAR isoform expression at the RNA and protein level in human pancreas *in situ* and in cultured pancreatic beta and ductal cell lines (Chapter 3)
- To characterise the isoform specificity of various antisera raised against CAR and to evaluate their utility as tools to explore CAR expression in cells and tissues (Chapter 4)
- To examine the subcellular localisation of CAR in human islet cells and to develop a model explaining its normal physiological role (Chapter 5 & 6).

CHAPTER 2

Materials and Methods

2.1 Source of reagents

This chapter describes the range of general materials and scientific methods used in this study but more specific details concerning primers, antibodies and chemicals are described in subsequent chapters.

Cell culture solutions were mostly from Sigma-Aldrich (Dorset, UK), Lonza (Slough, UK), and Fisher Scientific (Loughborough, UK). Plastic wares for cell culture and other experiments were acquired from Greiner Bio-One (Stonehouse, UK). Alcohols were purchased from Honey-well laboratory (Seelze, Germany). General laboratory consumables were purchased from Alpha laboratories (Eastleigh, UK) and Fisher scientific (Loughborough, UK) or Sterilin (Newport, UK).

Reagents for sample preparation for immunostaining were mostly from Sigma-Aldrich, except for HistoClear (National Diagnostic, Nottingham, UK) and Xylene (Genta Medical, York, UK)

The kit for cDNA synthesis was from Promega (Southampton, UK), PCR gels, Master Mix (Fisher Scientific) and ladders (DNA, Protein) for electrophoresis and Western blotting were purchased from Fermentas (York, UK) and Geneflow (Lichfield, UK) respectively. Restriction enzymes were supplied by Promega (Southampton, UK) and New England Biolabs (Hitchin, UK).

All components of the buffer-solutions including concentration and pH are presented in Table 2.1

Table 2.1 Buffer-solutions and components

Buffer	Components
FACS buffer	2% (v/v) FBS in PBS
4% PFA	4% (w/v)PFA in PBS pH 7.4
ADS	100mmol/l lysine, 10% donor calf serum and 0.02% sodium azide
ADST	100mmol/l lysine, 10% donor calf serum, 0.02% sodium azide and 0.2% (v/v) Triton X-100
1% Saponin (Permeabilisation buffer)	1% (w/v) saponin in PBS
Lysis buffer (Western blotting)	20mmol/l Tris, 150mmol/l NaCl, 1mmol/l EDTA and 1% (v/v)Triton X-100 (pH 7.4)
Lysis buffer (Co-immunoprecipitation)	50mmol/l Tris (pH7.5), 137mmol/l NaCl, 5mmol/l EDTA, 1mmol/l EGTA, 1% Triton, 10µg/ml protease inhibitor and 10µg/ml phosphatase inhibitor cocktail 2 & 3
BCA protein assay	Solution A: Na ₂ CO ₃ , NaHCO ₃ , biocinchonic acid and Na ₂ C ₄ H ₄ O ₆ in 0.1 N NaOH Solution B: 4% CuSO ₄ .5H ₂ O
LDS sample buffer(4x)	4000mmol/l glycerol, 560mmol/l Tris Base, 420mmol/l Tris HCL, 300mmol/l lithium dodecyl sulphate, 2mmol/l EDTA, 0.075% Serva Blue G250, 0.025% Phenol red
Transfer buffer	25mmol/l Tris, 190mmol/l glycine, 20% (v/v) methanol (pH 8.3)
TBS	137mmol/l NaCl, 2.6mmol/l KCl, 49.5 mmol/l Tris (pH 7.6)
TBST	TBS and 0.05% (v/v)Tween 20 (pH 7.6)
DreamTaq Green PCR Master Mix(2X)	DreamTaq DNA Polymerase, 2X DreamTaq Green buffer, dNTPs and 4 mmol/l MgCl ₂ , 4 x 1.25ml Nuclease free water
TBE buffer	80mmol/l Tris, 40mmol/l boric acid and 0.2mmol/l EDTA (pH8.0)
TAE buffer	40mmol/l Tris, 18mmol/l acetic acid, 1 mmol/l EDTA (pH 8.0)
Krebs Ringer Buffer	125mmol/l NaCl, 4.74mmol/l KCl, 1mmol/l CaCl ₂ , 1.2mmol/l KH ₂ PO ₄ , 1.2mmol/l MgSO ₄ , 5mmol/l NaHCO ₂ , 25mmol/l HEPES

2.2 Cell culture

Details of the cell lines used in the present study are provided in Table 2.2

Table 2.2 Cell lines and sources

Cell lines	Source
EndoC-βH1	Pancreatic β cell line derived from a human fetal pancreatic bud initially transfused with a lentiviral vector expressing the viral protein SV40LT and then transplanted for differentiation into functional islets under the kidney capsules of the SCID mice model (Ravassard et al., 2011)
1.1B4 ECACC 10012801	Hybrid cell line generated from the fusion of isolated human beta cells and PANC-1 ductal cells (McCluskey et al., 2011)
PANC-1 ECACC 87092802	Epithelial ductal cell line derived from a pancreatic carcinoma of a 56 year old Caucasian male (Lieber et al., 1975)
HeLa ECACC 93021013	Immortalized cell line from a 30 year old black female who died of cervical cancer (Lucey et al., 2009)
HEK293T ECACC 14050801	Derived from the exposure of human primary embryonic kidney cells to fragments of adenovirus type 5 DNA (Graham et al., 1977)
INS-1E	Isolated beta cells from induced rat transplantable insulinoma (Asfari et al., 1992)

The human beta cell line EndoC-βH1 (kindly provided by Dr. Robert Scharfmann, University of Paris, France) was cultured in Dulbecco's Modified Eagle's Medium (DMEM) low glucose 1g/L (5.5mmol/l glucose), 2%(w/v) bovine serum albumin (fraction V), 50μmol/l β-mercaptoethanol, 5.5μg/ml transferrin, 6.7ng/ml sodium selenite, 10mmol/l nicotinamide supplemented with penicillin (100units/ml) and streptomycin (100μg/ml). Cells were seeded at 1.75×10^6 /ml on an extracellular

matrix (ECM) with fibronectin coated T25 flasks and were sub-cultured every 7-9 days. Half of the culture medium was replaced every 3-4 days.

The 1.1B4 cell line was a gift (from Prof. Peter Flatt, University of Ulster, Ireland) and was cultured in 2g/L glucose (11mmol/l RPMI 1640 medium supplemented with 10%(v/v) fetal bovine serum (FBS), 2mmol/l glutamine, 100U/ml penicillin and 100µg/ml streptomycin. This cell line was routinely cultured in a filter screw cap flask on a growth area of 75cm² in which the surface had been treated for improved cell adhesion. INS-1E cell was cultured similarly to the 1.1B4 cells but with the addition of 50µm β-mercaptoethanol.

All other cell lines were cultured in DMEM medium containing 10% (v/v) FBS, 2mmol/l glutamine, 100U/ml penicillin and 100µg/ml streptomycin. Cell lines were maintained in an incubator set at 5% CO₂, 37°C and 100% humidity. All cells were mycoplasma negative.

2.2.1 Passaging of cell line

All cell lines (except EndoC-βH1, which is described above) were sub-cultured upon reaching 70-80% confluency. Cells were washed in warm sterile phosphate buffered saline (PBS) from (Lonza, Slough, UK), incubated with 0.25% Trypsin-EDTA (Fisher Scientific) for 5mins at 37°C to detach adhered cells from flask bottom. Cells were then centrifuged at 1500rpm for 5mins and one tenth of cells were seeded in new culture vessel.

2.3 Isolated human Islets

Isolated human islets were obtained from either Oxford or Worcester centre for islet transplantation. On arrival, islets (*Figure 2.1*) were cultured for 24hrs at 37°C

for their recovery before being fixed in 4% (w/v) PFA in PBS overnight at 4°C for immunostaining or stored at 80°C for RNA extraction.

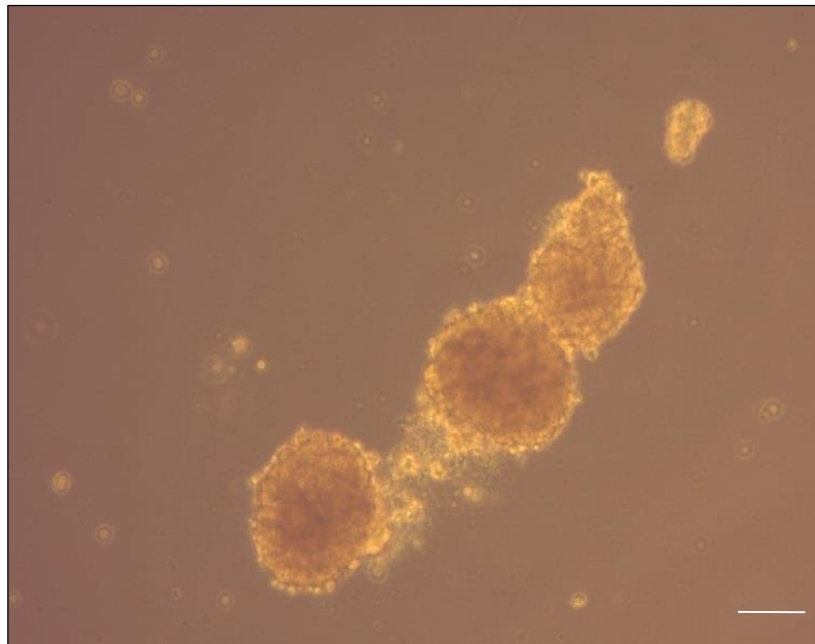


Figure 2.1 Morphology of isolated human islets
Bright field image showing islets obtained from the Oxford islet transplantation centre. Scale bar 25µm

2.4 Tissue samples

Formalin-fixed paraffin embedded (FFPE) pancreas sections were available from three cohorts: the Exeter Archival Diabetes Biobank (<http://foulis.vub.ac.be/>), the network of Pancreatic Organ donor with Diabetes (nPOD; <https://www.jdrfnpod.org/>) and the Diabetes virus detection study (DiViD). Analysis was performed on tissue from 21 non-diabetic controls (age range: 4-47years) and 10 individuals with type 1 diabetes (age range: 6-47years) detailed in Appendix, Table 8.1.

The Exeter archival diabetes biobank consists of a large UK cohort of post mortem fixed paraffin embedded (FFPE) pancreas tissue collected in the 1980's by Prof. Alan Foulis (Glasgow). These samples consist of patients recently diagnosed (<18 months) with type 1 diabetes at the time of autopsy and it remains the largest collection of "recent onset" T1D patients samples in the world.

nPOD was initiated in 2007 by the Juvenile Diabetes Research Foundation (JDRF), it consists of organs from heart beating donors that cannot be used for transplantation. The materials consist of donors with diabetes, at risk of diabetes (detected by the presence of autoantibodies) and no diabetes (control cases).

DiViD cohort is a collection of pancreatic tail tissue harvested using laparoscopic techniques from 6 living type 1 diabetes patients at the Oslo University hospital in Norway. The study was terminated as a result of the complications that developed in a few of the patients post-surgery.

The Tissue microarray (TMA) was provided as a kind gift from Prof. Alan Foulis (Glasgow) comprising of normal and cancerous human tissues.

2.4.1 Microtomy

Formalin fixed paraffin embedded tissues embedded in blocks were sliced at 4µm thickness to yield serial sections. Sections were then allowed to float on a water bath (Raymond A. Lamb, Eastbourne, UK) at 37°C and tissues were fixed on SuperFrost Plus slides (Fisher scientific) harbouring a positive charge that will attract the negative charge of the proteins in the tissues. Slides were allowed to dry in the slide drier (Raymond A. Lamb) for 24hrs.

2.5 Immunostaining reagents

Reagent sources, primary and secondary antibodies utilised are listed in the tables below.

Table 2.3 List of primary antibodies utilised in this study

Primary Antibodies	Company	Catalogue Number	species
CAR CT	Abcam	Ab100811	Rabbit
CAR ECD	Abcam	Ab180761	Rabbit
CAR NT	Abcam	Ab189216	Rabbit
Insulin	Dako	A056401-2	Guinea pig
Glucagon	Abcam	Ab10988	Mouse
Proinsulin	Abcam	Ab8301	Mouse
ZnT8	R & D	MAB7936	Mouse
PC1/3	Abcam	Ab55543	Mouse
CAR RmcB	Merck	05-644	Mouse
PICK1	Santa Cruz	SC-7452	Mouse
PICK1	Abcam	Ab133773	Rabbit
PICK1	Abcam	Ab3420	Rabbit
PICK1 L20/8	Biologend	830901	Mouse
Chromogranin	Abcam	Ab15160	Rabbit
MYC	Sigma	M4439	Mouse
Mouse IgG	Dako	X0931	Mouse
Rabbit IgG	Vector		Rabbit
GAPDH	Proteintech	60004-1-Ig	mouse
B-ACTIN	Sigma	A5441	Mouse

Table 2.4 Secondary antibodies and DAPI utilised for immunofluorescence and immunocytochemistry

AlexaFluor	Company	Catalogue number
Secondary antibodies		
568 Goat Anti-Guinea pig IgG	Invitrogen	A11075
488 Goat Anti-Mouse IgG	Abcam	Ab150113
488 Goat Anti-Rabbit IgG	Abcam	Ab150077
555 Goat Anti-Mouse IgG	Abcam	Ab150114
555 Goat Anti-Rabbit IgG	Invitrogen	A21429
647 Goat Anti-Guinea pig	Invitrogen	A21450
DAPI (4'6 diamidino-2-phenylindole)	Fisher	D1306

Table 2.5 List of immunostaining reagents

Product and Supplier	Catalogue number
Dako Real peroxidase blocking solution	S2023
Dako envision HRP Rabbit Mouse A	K5007
Dako Substrate buffer B	K5007
Dako envision DAB Chromogen C	K5007
Dako Antibody Diluent	S2022
Dako Normal Goat Serum	S1000
Dako Haemotoxylin	S2020
Dako Fluorescent mounting medium	S3023880
DPX Mounting medium	S06522

2.6 Immunocytochemistry (ICC)

2.6.1 Cells and fixation

Cells in routine culture were counted and seeded at a density of 1×10^5 cells/ml onto sterilised glass coverslips in a 24 well plate. Cells were then left to adhere between 4hrs to 24hrs. Thereafter, cells were treated and incubated appropriately. After incubation, cells were fixed by the addition of cold 4% (w/v) paraformaldehyde (PFA) for 10mins, washed in PBS twice and left in PBS at 4°C until required.

2.6.2 Staining

Cells were removed from PBS and either permeabilised with ADST or non-permeabilised with ADS (*Table 2.1*) for 30mins. The ADST/ADS was removed and cells were incubated with primary antibody for overnight at 4°C. Cells were washed five times in PBS and incubated with secondary antibody and DAPI (4'6

diamidino-2-phenylindole; stains the nuclei) at the appropriate concentration. Slides were washed in PBS (5 times) and mounted with cells facing downwards onto a small drop of Dako fluorescent mountant. Samples were left to dry in a dark box and viewed under an Upright fluorescence microscope. Figure 2.2 (below) shows an immunohistochemical staining of anti-insulin and anti-chromogranin in EndoC- β H1 cells.

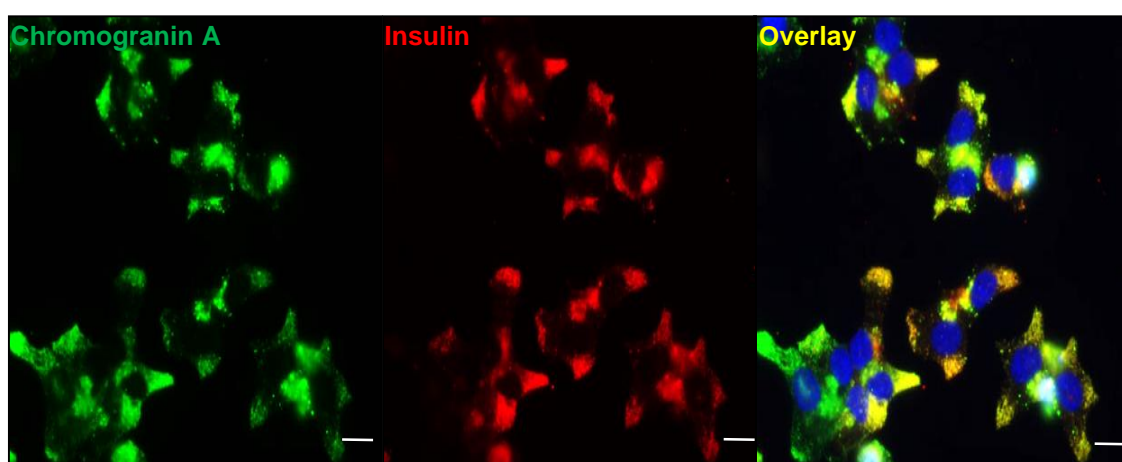


Figure 2.2 Immunocytochemical staining with chromogranin and insulin antisera in EndoC- β H1 cell line

EndoC- β H1 cells express both chromogranin A (green) and insulin (red) in the EndoC- β H1. Nuclei were stained using DAPI (blue). Data are representative of images from three replicates. Scale bar 25 μ m

2.7 Immunohistochemistry (IHC)

In preparation for staining, formalin-fixed paraffin-embedded (FFPE) tissue was first de-waxed by immersing slides in 2x5min steps of histoclear in glass coplin staining jars (Fisher) or samples fixed with mercuric chloride were placed in 0.5% (v/v) iodine in xylene followed by a further 5min incubation with xylene. Tissue samples were then re-hydrated in a series of ethanol (100% ethanol, 90% (v/v) ethanol, 70% (v/v) ethanol, 100% methanol) respectively and in distilled water for

5mins. For antigen retrieval (AR), tissue samples were immersed in an aqueous solution of 10mmol/l citrate buffer (pH 6) and incubated for 20mins at high temperature in the microwave. AR is a critical step which is thought to revive the immunoreactivity of tissue samples previously dampened by fixation technique (Shi et al., 1991). Although, the exact mechanism of how AR facilitates this recovery is still not well understood. After AR, slides were left to cool for at least 20mins and then blocked with normal goat serum to minimise background staining (Daneshtalab et al., 2010). After which tissues were incubated with primary antibody at the optimised dilution in antibody diluent solution for 1hour or overnight as appropriate. Tissues were washed three times in TBS (Tris buffered saline and incubated with peroxidase block to inhibit any endogenous peroxidase activity in tissues thereby preventing non-specific staining. The secondary antibody conjugated to horseradish peroxidase (HRP) enzyme was added to tissues for 30mins. Slides were washed three times in TBS and 3,3' diaminobenzidine (DAB) substrate solution was added to the tissue for 10mins. DAB reacts with HRP to produce a precipitate (brown in colour) that is insoluble in alcohol and water. Slides were then washed in ddH₂O for 5mins, nuclei were counter-stained with haematoxylin for 1min and washed for 5 mins in running H₂O. Blueing was achieved with STWS (Scott's tap water substitute) followed by a 5 mins incubation with ddH₂O, then copper sulphate and finally ddH₂O. Dehydration of slides was carried out in 50%(v/v), 70%(v/v), 90%(v/v), 100% (twice in) ethanol and Histoclear (twice). Mounting media (DPX) was then mounted on slides with tissues and left to dry overnight and visualised under the bright field microscope (Nikon eclipse, Surrey, UK)

2.8 Immunofluorescence microscopy

To examine multiple antigens within the same section, samples were probed in a sequential manner with either two or three primary antibodies after samples had undergone dewaxing and blocking (normal goat serum) step as detailed in (Section 2.7). Primary antibody in antibody diluent was incubated for 1 hour at room temperature; tissues were washed in PBS (thrice) in plastic slide staining jars. Secondary antibody conjugated to fluorescent dyes incubated in antibody diluent was added onto slides for 1hr in the dark at room temperature. DAPI was used to stain the nuclei and slides were washed in PBS before being mounted with the Dako fluorescent mounting media. Labelling of the antigen-antibody complex was visualised by a fluorescence microscope.

2.8.1 Imaging

For the visualisation of stained antigens in immunohistochemical images, bright field image acquisition was performed on a Nikon 50i Microscope (Surrey, UK). For immunofluorescence, images were captured either with a Leica AF6000 microscope (Leica, Milton Keynes, UK) or a Leica SP8 confocal microscope. With the Leica AF6000 microscope, images were processed using the standard LASX Leica software platform or the Leica SP8 confocal microscope coupled with Hyvolution 2 deconvolution software (Scientific Volume Imaging bv, Netherlands). Colocalisation analysis of the stained antigen was measured using a JACoP plugin from image J version 1.48, Java 1.6.0_20; (<https://imagej.nih.gov/ij/plugins/track/jacop2.html>)

2.9 Cryoimmunogold electron microscopy (Cryo-EM)

For Cryo-EM, human samples were treated as described (Slot and Geuze, 2007). Briefly, human pancreas tissue samples from nPOD (6227, 6229 and 6330) were fixed in 4% (w/v) PFA, cut into small pieces and immersed in 2300mmol/l sucrose in PBS at 4°C. The samples were placed on metal stubs, frozen in liquid nitrogen and thin cryosections were cut and protected with sucrose/methyl cellulose films. For immunogold labeling, the protective layer was first melted in gelatin coated dishes at 37°C and then washed with 0.1%(w/v) glycine in PBS. Then grids were incubated in PBS containing 1%(w/v) BSA with the anti-CAR CT, anti-insulin, anti-proinsulin and anti-ZnT8 antibodies for 45 minutes at room temperature. Protein A-gold (diameters 10 or 5 nm; G. Posthuma, Utrecht) diluted in 0.1%(w/v) BSA in PBS was added onto the grids for 20 min followed by washes with 0.1%(w/v) BSA/PBS and PBS alone. In double labeling studies, antibodies were added sequentially with their respective protein A gold conjugate, between incubations the sections were incubated briefly with 1% glutaraldehyde. The sections were then stained with 2% neutral uranyl acetate in water for 5min and then embedded for 10 min on ice with 2% methyl cellulose containing 0.4% uranyl acetate. The stained sample was examined with a Jeol 1400 microscope. *Courtesy of Dr. Varpu Marjomaki, University of Jyvaskyla, Finland.*

2.10 RNA analysis

2.10.1 RNA purification

Cells between 70-80% confluent were washed twice in PBS and RNA was extracted using RNeasy Mini Kit (Qiagen, Hilden, Germany) as per the kits instructions. From this kit, RLT buffer was added to disrupt the cell plasma

membrane to release the RNA. Ethanol was then added to promote selective binding of RNA to the spin column. RNA binding enables contaminants to be washed away efficiently in wash steps and also allows for high RNA quality. The binding, washing and elution steps were carried out in a centrifuge at 8000g.

2.10.2 RNA or DNA estimation

A Nanodrop 8000 spectrophotometer (Fisher Scientific) was used to quantify the amount of DNA or RNA and assess purity. The Nanodrop provides a 260/280nm ratio that allows the assessment of purity. Values close to 1.8 are generally accepted for 'pure' DNA and 2.0 for 'pure' RNA.

2.10.3cDNA (Complementary DNA) synthesis

For reverse transcription, 500ng/ml of random hexamers was incubated with 1µg of purified RNA. The hexamers randomly bind to the RNA nucleotide sequence at 70°C for 10mins followed by rapid cooling on ice for 5mins. A reaction containing either reverse transcriptase (RT) or no reverse transcriptase (nRT) in separate tubes was set up with the following components 940U/ml RNasin (to inhibit RNase degradation), (10mM) dNTPs and (5X) reverse transcriptase buffer. This mixture was incubated at 25°C for 15mins, 42°C for 50mins and 70°C for 15mins to generate cDNA from the RNA template in the RT tubes. The nRT mixtures acts as a negative control where no product will be amplified during PCR.

2.10.4 Primer design

Primers (Invitrogen) were designed using the Primer 3 software (<http://primer3.ut.ee/>). Specificity of primers was confirmed by performing a BLASTsearch (<https://blast.ncbi.nlm.nih.gov/Blast.cgi>).

2.11 Polymerase chain reaction (PCR)

PCR reactions were set up in PCR tubes containing 1µg cDNA template, forward, and reverse primers (25µm) and DreamTaq Green PCR Master Mix (2X). PCR was performed in a three step process in a thermal cycler (Life Technologies, California, USA) where the DNA was amplified in repeated cycles. The initial step included denaturation 95°C, 5min followed by 35cycles (or as required) consisting of 95°C, 1min denaturation step, 52°C 1min annealing (hybridisation) step and 72°C 1min elongation step). Finally, an extension time of 72°C 10min. The annealing temperature for each PCR was determined by the melting temperature (TM) of each primer.

PCR products were analysed qualitatively by agarose gel electrophoresis which separates DNA by size and charge. Samples were placed in 1% agarose gel (AGTC Biproducts Ltd, Hessle, UK) in TBE buffer containing GelRed™ (Biotium, California, USA). GelRed™ is a nucleic acid fluorescent dye (Huang et al., 2010). A DNA ladder with known sizes was used to determine the size of unknown bands. The gel was placed in a tank (Fisher scientific) filled with TBE and run at 120 V for 45mins or until the ladder had separated. After running, the gel was visualised and image was captured under a UV illumination (UVP GelMax Imager, Fisher scientific).

2.12 DNA sequencing

It is possible that during the PCR process, primers could anneal non-specifically to sequence of non-target DNA thereby giving misleading results. In order to avoid this, the amplicons were sent for sequencing to confirm the expected PCR product. Bands in agarose gels were excised with a scalpel blade already washed in 70% ethanol under a dark reader transilluminator (Labtech, East Sussex). DNA

fragments within the gel was extracted and purified using a QIA quick gel extraction Kit (Qiagen) according to the manufacture's protocol. The purified DNA was sent to Source bioscience, Nottingham (<http://www.sourcebioscience.com/>) where Sanger sequencing was used. The sequenced results returned as a chromatogram and were compared with the expected sequence using BLAST search <https://blast.ncbi.nlm.nih.gov/Blast.cgi> to confirm the identity of the amplicon.

2.13 RT-Real Time PCR

Differential expression of alternatively spliced isoforms of the human *CXADR* gene was evaluated using custom designed TaqMan primers and probes (Thermofisher) (Chapter 3, Table 3.2). For human isolated islets, 250ng of total RNA was retro-transcribed using Superscript III Reverse Transcriptase kit (Thermofisher) and 10ng of the resultant cDNA was loaded into (2X) TaqMan Universal Master Mix, (20X) TaqMan gene expression assay buffer and nuclease-free water in a final volume of 20 μ l. Data were normalised using the expression of β -Actin, GAPDH and β 2-microglobulin. Reactions were performed on a verity Thermal Cycler and ViiA7 Real Time PCR instruments (Thermofisher). Data was analysed and exported using Expression Suite software 1.1 (Thermofisher) and finally elaborated using the $2^{-\Delta Ct}$ method. *Courtesy of Prof. Francesco Dotta and Dr. Guido Sebastiani, University of Siena, Italy*

2.14 Laser capture microdissection of human islets

Laser capture microdissection (LCM) of human islets was performed on OCT frozen sections from pancreas of non-diabetic nPOD donors (6017, 6096; Table 3.4). Briefly, 5 μ m thick frozen sections were fixed in 70% (v/v) ethanol for 30

seconds and then dehydrated in 100% ethanol, xylene and then air dried for 5 minutes. An Arcturus Xt microdissection instrument (ThermoFisher, Waltham, MA, USA) was used to capture human islets based on beta-cell autofluorescence. Hs-Caps (ThermoFisher) were used to microdissect identified islets. Microdissected islets were then lysed in Arcturus Picopure kit Extraction Buffer for 30 minutes at 42°C and subjected to total RNA extraction using Arcturus Picopure RNA extraction kit following the manufacturer's instructions (ThermoFisher).

Total RNA from isolated human islets was extracted using miRNeasy mini kit (Qiagen,). Briefly, human isolated islets were lysed in Qiazol solution and chloroform was added to separate DNA, RNA and proteins. The aqueous phase was then loaded on to RNA binding columns and eluted in 30µl of nuclease-free water. RNA quality were evaluated using a 2100 Bioanalyzer RNA 6000 Pico kit (Agilent Technologies, Santa Clara, CA, USA) and only samples with RNA Integrity Number (RIN) >5.0 were used for further analyses.

1ng of total RNA was retro-transcribed using Superscript III Reverse Transcriptase kit (ThermoFisher). The resultant cDNA was pre-amplified using 0.2x Tris-EDTA diluted TaqMan assays pool (designed to amplify *CXADR* isoforms plus 3 housekeeping genes (β -Actin, GAPDH, β 2-microglobulin) and 2x Preamp Master Mix in a final volume of 50µl. The pre-amplification reaction was diluted in Tris-EDTA and 5µl of each pre-amplified cDNAs were used in a Real-Time PCR reaction in a final volume of 20µl. *Courtesy of Prof. Francesco Dotta and Dr. Guido Sebastiani, University of Siena, Italy*

2.15 RNAseq

RNA sequencing (RNAseq) was performed using islets obtained from 5 normoglycemic human islet donors or EndoC- β H1 cells as described (Eizirik et al., 2012). Genes and transcripts were assigned a relative coverage rate as measured in RPKM units (“reads per kilobase of exon model per million mapped reads”) and compared with 15 other normal human tissues, analysed by RNA sequencing and deposited at the Illumina Body Map 2.0:GSE30611.

RNAseq analysis was also examined from isolated human islets and EndoC- β H1 which were exposed to the following cytokines; (50U/ml) recombinant human IL- 1β (R & D Systems, Abingdon, UK) and (1000U/ml) human IFN- γ (PeproTech, London,UK) for 48hrs. *Courtesy of Prof. Decio L. Eizirik, Universite Libre de bruxelles, Belgium.*

2.16 Protein analysis by Western blotting

2.16.1 Sample preparation

Cell lines cultured to 70% confluency were washed with ice-cold PBS and lysed with an amount of lysis buffer depending on the growth area of culture flasks for 10mins on ice. 10 μ l/ml of both protease and phosphatase inhibitors (Sigma) were added to the lysis buffer (Table 2.1) to inhibit the degradation of proteins. Adherent cells were removed from flasks using cell scrapers (Sarstedt, Nmbrecht, Germany) and transferred to microfuge tubes. Tubes with cell lysate were vortexed for 15secs with 5sec on ice between each vortexing. Protein lysate (supernatant) was separated from the insoluble fraction by centrifugation for 10mins at 5000rpm at 4 $^{\circ}$ C. Lysates were either stored at -20 $^{\circ}$ C or protein concentration was determined using the BCA protein detection assay.

2.16.2 Protein estimation

The total protein concentration of unknown samples was quantified with the Pierce™ BCA Protein Assay (ThermoFisher Scientific). Bicinchoninic acid (BCA) uses a colorimetric approach whereby Cu^{2+} is reduced to Cu^{1+} by the interaction of protein bonds in an alkaline solution. A colour change from green to purple is observed when bicinchoninic acid molecules chelate with Cu^+ ion. The colour change is directly proportional to the amount of protein present in the sample.

In a 96 well plate, a standard curve of BSA (0, 200, 400, 600, 800, 1000 and 1200 $\mu\text{g}/\text{ml}$) was created with lysis buffer and protein samples mixed at a dilution of 1:5 and 1:10 in lysis buffer in duplicates were added. BCA reagents A and B were mixed at a ratio of 1:50; 200 μl of this solution was added to each well. The plate was left to incubate at room temperature for about 10-15mins while placed on a microplate shaker (Grant-bio, Cambridgeshire, UK) and absorbance was measured at 562nm with a PHERAstar (BMG Labtech Ltd, Aylesbury, England). The protein concentration was either estimated manually by comparing the absorbance of standards to those of the unknown samples with Microsoft excel or using the PHERAstar wizard software.

2.16.3 Electrophoresis and protein transfer

Initially proteins were denatured before subjected to electrophoresis, which involved protein separation based on their molecular size, shape and charge through the addition of an electric current. For protein denaturing, equal amount of protein (20-50 μg) were used and lysates were treated with (4X) LDS sample buffer (25%) and 10% β -mercaptoethanol (reducing agent that cleaves protein disulphide bonds) and heated for 10min at 70°C. Samples were loaded along with the prestained protein ladder (Geneflow) onto pre cast Bis-Tris4-12% poly-

acrylamide gels (Invitrogen) in a XCell Sure Lock system (Invitrogen, California, USA) set at 120volts in (20X) MOPS SDS running buffer) for 1hr. Samples were ran until the dye reached the bottom of the gel. The gel was removed from the tank and placed on blotting paper soaked in transfer buffer. PVDF (polyvinylidene difluoride) membrane cut at the appropriate size was first permeabilised in methanol before being placed on top of the gel. Additional blotting paper was placed on top of the membrane (blotting paper-gel-membrane), finally padded foams were placed on either side to form a sandwich. The sandwich was then placed in a cassette and transferred into aXCell II Blot Module (Invitrogen) containing transfer buffer (Table 2.1). The transfer was run at 30v for 2hrs to allow for protein transfer from the gel to the PVDF membrane

2.16.4 Antibody probing

After transfer, membranes were blocked in 5%(w/v) skimmed milk protein (Sigma) made in Tris buffered saline with Tween 20 (TBST) buffer (Table 2.1) for 1hr on a roller mixer (BioCote Ltd, Coventry, UK) to prevent non-specific binding of antibody to the membrane. After blocking, membranes were probed with primary antibody diluted in 5% (w/v) milk overnight at 4⁰C. Primary antibody was removed by washing thrice in TBST for 5mins. Secondary antibody (of the appropriate species) conjugated to alkaline phosphatase (AP) at 1:10,000 or goat anti-rabbit IgG (H+L) AlexaFluor680 (Table 2.6) was made in 1% (v/v) milk with TBST and added to the membrane for 1hr at room temperature. Membrane was washed three times in TBST for 15mins before detection with a chemiluminescent detection agent.

Table 2.6 List of secondary antibodies for Western blotting

Western blotting secondary antibodies	Company	Catalogue #
Anti-Mouse alkaline phosphatase	Sigma	A3562
Anti-Rabbit Alkaline phosphatase	Sigma	A3687
Goat anti-rabbit IgG(H+L) highly crossed absorbed, AlexaFluor plus 680	Thermofisher	A327-34

2.16.5 Detection of proteins

Proteins were detected using a CDP-star (Sigma) for AP conjugated antibodies and for streptavidin conjugated antibody, ECL substrate was utilised (Cell signalling, Massachusetts, United States). Membranes were incubated with chemiluminescent substrate for 5min after draining off the excess. Proteins were visualised using the C-Digit blot or Odyssey CLX scanner (Li-COR Biosciences, UK), to detect protein bands. Protein ladder was made visible by drawing lines on top of the membrane ladder and exposing to bright light for 30secs after which membrane was placed with protein facing downwards on the surface for scanning. Bands were developed on the scanner after 12mins

2.17 Flow cytometry

Flow cytometry measures the chemical and physical characteristics of the single cells through a beam of light while flowing in suspension. Properties measured include cell number, size, granularity as well as fluorescence intensity of cells (McSharry, 1994). In this study, cellular antigens were detected both, extracellularly and/or intracellularly.

2.17.1 Cell preparation

Cells were collected in culture media and pelleted by centrifugation at 1500RPM for 5mins. Cells were then re-suspended at a concentration of 2×10^5 cells/ml in a fluorescence activated cell sorting (FACS) wash buffer (Table 2.1) in FACS tubes (Sarstedt).

2.17.2 Extracellular staining of surface antigen

For extracellular staining, the cell pellet was re-suspended in FACS tube at a suitable antibody concentration made in FACS buffer and incubated for 45mins at room temperature. Cells were then washed once in FACS buffer to remove any non-specific binding and centrifuged at 1500rpm for 5mins. Secondary antibody was made up in FACS buffer and incubated with the cells for 30min at room temperature. Cells were washed in FACS buffer, then re-suspended in 500 μ l FACS buffer and analysed immediately on a flow cytometer (BD Accuri™ C6 Plus).

2.17.3 Intracellular staining of antigen

For intracellular staining after the cell preparation step, cells were fixed with 500 μ l of 4% paraformaldehyde for 10minutes and washed twice with FACS buffer at 1500rpm for 5mins. Primary antibody was made up in permeabilisation buffer (0.3% (v/w) saponin in FACS buffer). The fixation-permeabilisation step is necessary to retain the morphological structure of the cells while enabling antibody to gain access to the intracellular compartment. Cells were incubated in primary antibody on ice for 1hr, after this time point cells were washed twice with 500 μ l of 0.03% (v/v) saponin in FACS buffer with centrifugation at 5000rpm for 5minutes at 4°C. Secondary antibody was prepared in 0.3% saponin in FACS buffer, ratchet and incubated for 30mins in ice. Cells were then washed in 0.03%

(v/v) saponin in FACS buffer twice for 5mins, 4°C at 1500rpm and 3000rpm respectively. Finally cells were re-suspended in 500µl in FACS buffer and analysed on the BD Accuri™ C6 plus Flow cytometer.

2.18 Proximity ligation assay (PLA)

Proximity ligation assay was developed by the Fredriksson research group (Fredriksson et al., 2002) and can be used to visualise protein-protein interactions (provided that two proteins are within 30-40nm of one another) in fixed cells and tissue samples. DuoLink in situ detection reagent red (DUO92008) was purchased from Sigma-Aldrich, Dorset, United Kingdom. This experiment requires two primary CAR antibodies recognizing different epitopes, a pair of PLA probes (positive and negative) and a detection reagent.

Initially, samples were blocked in blocking solution followed by two primary antibodies (raised in rabbit or mouse) incubation at a suitable concentration overnight in cells or depending on antibody incubation time on tissues. Samples were then washed twice for 5mins in Wash buffer A (1X) and secondary antibody conjugated with a PLA oligonucleotides (5X) stock were added at 1:5 dilution in a pre-heated humidity chamber for 1hr at 37°C. Cells or tissues were washed in Buffer A twice for 5mins and ligation solution (5X) was mixed in high purity water (1:5 dilution) with the addition of 1U /µl Ligase (1:40 dilution) to create a ligation-ligase which was added to the sample and incubated in a pre-heated humidity chamber for 30mins at 37°C. Amplification (5X) solution was made in high purity water (1:5 dilution) with 10U/µl polymerase (1:80 dilution) which was incubated with samples in a pre-heated humidity chamber for 100mins at 37°C. Slides were then washed in 1X washbuffer B twice for 10mins and in 0.01X wash buffer B for

1min. Slides were then mounted in Duolink *insitu* mounting medium with DAPI. After 15mins samples were visualised with a fluorescence microscope.

2.19 Co-immunoprecipitation

2.19.1 Cell lysate preparation

Cells at 70% confluency were washed twice in ice cold PBS and lysed with co-immunoprecipitation lysis buffer (Table 2.1) for 30mins with occasional rocking. Cells were then scraped and gently transferred to a microfuge tube. Cells were further disrupted by vortexing (3 times) for 5secs. Cell lysates were centrifuged at 12000rpm for 10mins at 4°C and supernatant were transferred into fresh microfuge tubes. As an input control, 2%(v/v) of protein lysate was taken out of each sample, denatured at 70°C for 10min and stored at 4°C. Thereafter, protein lysates were incubated with (2-3µg) of antibodies or isotype control (mouse IgG and rabbit IgG antibodies) on a rotator (Bio-Cote, Staffordshire, UK) overnight at 4°C. The following day, protein G sepharose bead slurry (50%;w/v) supplemented with protease and phosphatase inhibitors was added to the protein lysate-antibody mix and incubated for 4hrs at 4°C. 50% (w/v) bead slurry was prepared by washing protein G sepharose bead (three times) with lysis buffer followed by adding equal volumes of beads and lysis buffer.

2.19.2 Precipitation of Immune complexes

The protein-bead mixture was centrifuged at 12000rpm for 20sec at 4°C. Supernatant was discarded and the resultant pellet was washed three times; 1, in lysis buffer, 2, TBS with 10% lysis buffer and 3, TBS with centrifugation at 12000rpm for 20sec in between. Protein was eluted from the beads by adding 25%(v/v) LDS buffer and 10%(v/v) β-mercaptoethanol and heating at 70°C for

10min. Samples were vortexed briefly and the protein was loaded on an SDS-PAGE gel and Western blotting was performed as described in section 2.16

2.20 DNA cloning

This is a molecular technique in which fragments of DNA (gene of interest) are inserted into a plasmid to produce a recombinant DNA vector which is then transformed *in vivo* into competent bacteria to be replicated (Vosberg, 1977). I utilised this technique to generate vectors containing the specific isoform of CAR (CAR-SIV) and a truncated form of this which were transfected into the human beta cell line 1.1B4.

2.20.1 Agar plates

Culture growth medium for agar plates was prepared with 35g/l of LB broth with agar (Sigma). LB broth (liquid growth medium) was also prepared with 20g/l of LB broth. Both solutions were autoclaved at 121°C, 15psi for 15min and stored at 4°C until required. To make agar plates, culture growth medium was melted in a microwave and allowed to cool. Antibiotics (25mg/ml Kanamycin and 100µg/ml Ampicillin) (Sigma) were added (to enable selection of bacteria containing the plasmid) and dispensed into multiple sterile petri dishes. Agar plates were then wrapped in parafilm and stored at 4°C for a maximum of 3 months.

2.20.2 Bacterial transformation and plasmid purification

The commercially available CAR plasmid (Origene, Rockville, USA) (Appendix, *Figure 8.1*) was used at low and high concentration (100ng or 1µg) with Competent *E. coli* (JM109 strain, Promega), which had a transformation efficiency of either $>1 \times 10^7$ or $>1 \times 10^8$ cfu/µgplasmid. Initially, plasmid was

added to 100µl of competent *E.coli* and gently 'flicked' to mix, then left on ice for 10mins, heat shocked at exactly 42°C for 50secs and immediately returned to ice for 2mins. Heat shocking is a critical step for optimal transformation because it makes the bacteria membrane more permeable for the plasmid to gain entry (Cramer et al., 1996). 900µl of liquid growth medium (LB broth) was added to each transformation reaction and incubated for 1hr at 37°C on an orbital shaker incubator (Grant-bio). 50µl of culture was spread onto kanamycin or Ampicillin containing agar plates. Kanamycin and Ampicillin were used because all plasmids in this study had the resistance gene to both antibiotics. The plates were then left to grow overnight in an incubator at 37°C. Single colonies were picked up from plates with sterile loops and inoculated into 5ml Kanamycin/ Ampicillin LB broth for 8hrs at 37°C on a shaker until turbid.

Purified plasmid DNA was then extracted according to the manufacturer's instruction by Mini-prep and Maxi-prep kit (Qiagen).

2.20.3 Glycerol storage

Transformed bacteria colonies not used regularly were stored for up to a year in glycerol. In a cryovial with 150µl of glycerol, 850µl of turbid bacteria suspension was added, vortexed and stored at -80°C. These colonies could then be easily used again by scraping the top of the glycerol stock with sterile microbial loop and streaking onto an agar plate with either Kanamycin or Ampicillin.

2.21 Transient transfection of purified plasmid

1.1B4 cells (5×10^4 cells/ml and 2×10^5 cells/ml) were seeded into a 24 well plate and 6 well plate respectively and left to adhere. Transfection mix was made by incubating DNA in Opti-MEM (Fisher Scientific) and transfection reagent

was incubated for 15mins at room temperature. Thereafter, cells were incubated with this mix for 6-24hrs.

2.21.1 Identification of a suitable transfection reagent for the human pancreatic beta cell line 1.1B4

In order to utilise the human beta cell line 1.1B4 for overexpression studies, a suitable transfection reagent had to be selected and optimised. A control pMax-GFP tag vector provided as a kind gift from Dr. John Chilton (Appendix, *Figure 8.2*), which makes transfected cells fluoresce green, was transiently transfected into the 1.1B4 cells utilising a variety of different transfection reagents which include Lipofectamine (Fisher Scientific), Attractene (Qiagen), Fugene (Promega) and Avalanche-Omni (EZ Biosystems)

To determine if the transfected pMax-GFP vector could be detected in the 1.1B4, cells in culture were transfected, PFA fixed and then visualised under an Upright fluorescence microscope. Representative images of pMax-GFP transfection in 1.1B4 cells are presented demonstrating no green fluorescent protein (GFP) positive cells with the Lipofectamine reagent (*Figure 2.3A*). With the Attractene reagent, GFP+ cells were observed but the staining pattern showed compromised nuclei either condensed or abnormal invaginations in some cells (white arrows), likely due to high toxicity. Only a few GFP+ cells were detected with the Fugene reagent. In contrast, many GFP+ cells were observed when the Avalanche-Omni reagent was utilised in 1.1B4 cells. There was also minimal evidence of toxicity (*Figure 2.3D*)

The Lipofectamine and Attractene reagent were discontinued from further experiments. This was due to the lack of GFP+ transfected cells by the

Lipofectamine reagent and the toxicity encountered in cells with Attractene. The transfection efficiency of Fugene and Avalanche-Omni transfection reagent were further optimised according to the manufacturers' instruction and quantified by flow cytometry.

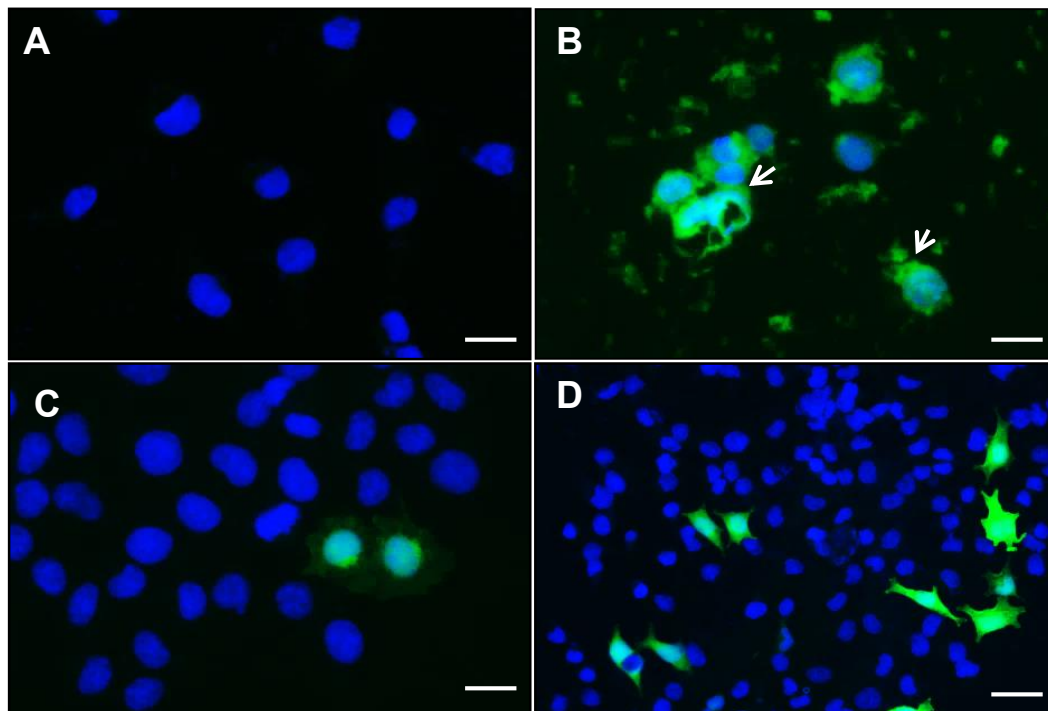


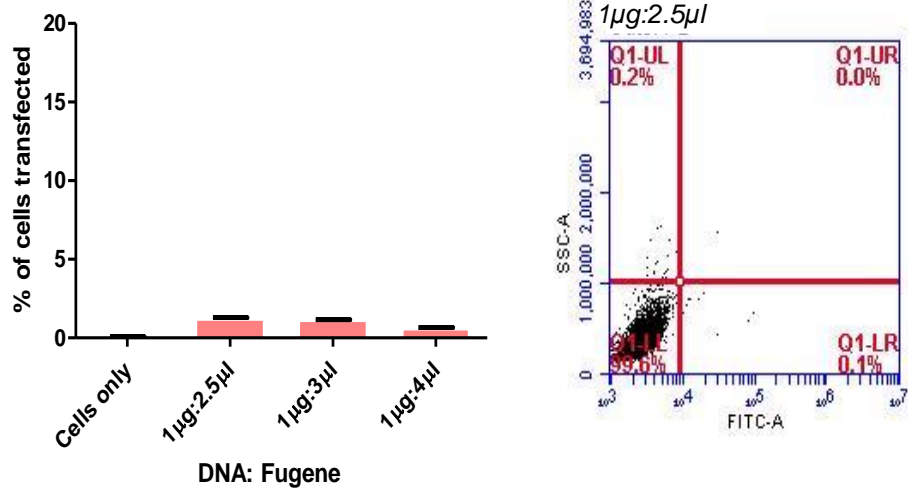
Figure 2.3 Immunocytochemical analysis showing pMax-GFP vector transfected into 1.1B4 cells utilising different transfection reagents

1.1B4 cells were seeded at 5×10^4 cells/ml and transfected with the different transfection reagents (lipofectamine, attractene, fugene and avalanche-omni) for 24hrs. The transfected pMax-GFP vector in 1.1B4 cells with the different transfection reagents are shown (green) in (A) lipofectamine (B) attractene with compromised nucleus due to toxicity (white arrows) (C) fugene and (D) avalanche-omni. Nucleic were stained using DAPI (blue). Data are representative of three independent replicates. Scale bar $25\mu\text{m}$

To further optimise the transfection efficiency, different DNA to transfection reagent ratios were chosen and the % of GFP+ cells was analysed by flow cytometry. The representative flow plots display the optimum DNA to transfection

reagent ratio selected for Fugene reagent yielding approximately 0.1%. Avalanche-Omni had a transfection efficiency of between 7-20%, dependent on the ratio of DNA to transfection reagent, the optimal ratio was 0.5µg DNA: 0.4µl Avalanche-Omni (*Figure 2.4*). Avalanche-Omni clearly had the best transfection efficiency (~20%) in 1.1B4 cells and was utilised in subsequent experiments.

A



B

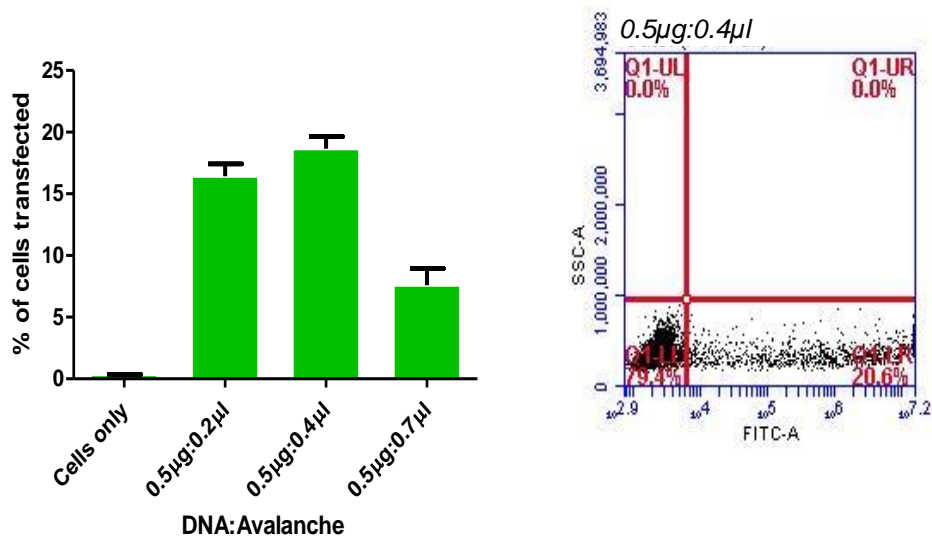


Figure 2.4 Avalanche-Omni reagent has a 20% transfection efficiency when compared to Fugene transfection reagent in the 1.1B4

1.1B4 cells were seeded at 5×10^4 cells/ml and pMax-GFP vector was transfected with either the avalanche-omni or fugene transfection reagents for 24hrs. Graph displays (A) DNA: Fugene reagent ratios and a flow plot with 0.1% transfection efficiency in quadrant 1, lower right (Q-1LR) (B) DNA: Avalanche ratios and a flow plot with 20% transfection efficiency in quadrant 1, lower right (Q-1LR). In the graphs, data represent mean values from three independent experiments (mean \pm SEM).

2.21.2 Transient transfection of CAR-SIV Myc construct into the human pancreatic beta cell line 1.1B4.

The presence of CAR-SIV in transiently transfected cells was initially analysed using RT-PCR and specific primers that selectively amplify either CAR-SIV or CAR-TVV. Only the CAR-SIV isoform was detected in transfected cells shown in Figure 2.5A.

Additionally, CAR-SIV protein levels was also detected by immunocytochemistry using anti-CAR CT, anti-Myc and anti-insulin. Myc positive cells were detected, however only very low levels of overexpressed CAR-SIV were detected in those same 1.1B4 cells that should in theory have Myc-tagged CAR-SIV (*Figure 2.6*). The result suggested that the Myc-tag located at the end of CAR-SIV C' terminus is interfering with anti-CAR CT binding.

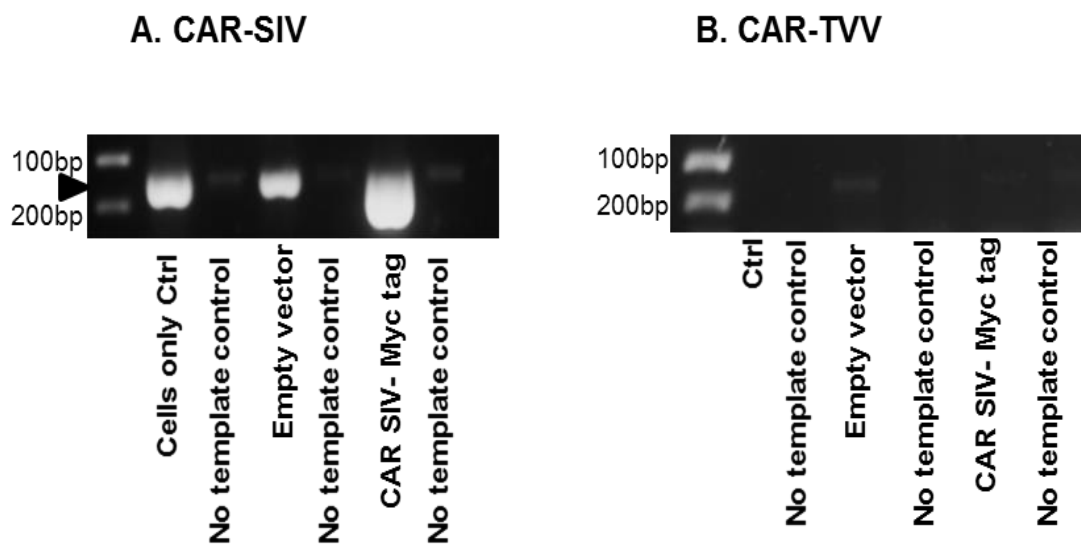


Figure 2.5 RT-PCR confirms the overexpression of CAR-SIV and not CAR-TVV in 1.1B4 cells transfected with CAR SIV-Myc.

1.1B4 cells were seeded at 5×10^4 cells/ml, CAR SIV-Myc and empty vector was transfected for 24hrs. Total RNA was isolated and normalised to contain $1\mu\text{g}$ of RNA before converting to cDNA. The cDNA was subsequently used in PCR reaction (35cycles) with specific primers designed to specifically amplify CAR-SIV and CAR-TVV (Table 3.2). (A) Overexpressed CAR-SIV is visualised at an intense band size of approximately 253bp (black arrow) in the CAR-SIV Myc tag and bands confirming the expression of endogeneous CAR-SIV are also present in the control and empty vectors in the 1.1B4 cells (B) No detection of CAR-TVV in the CAR SIV-Myc tag vector, empty vector or control 1.1B4 cells. Data are representative of three independent experiments.

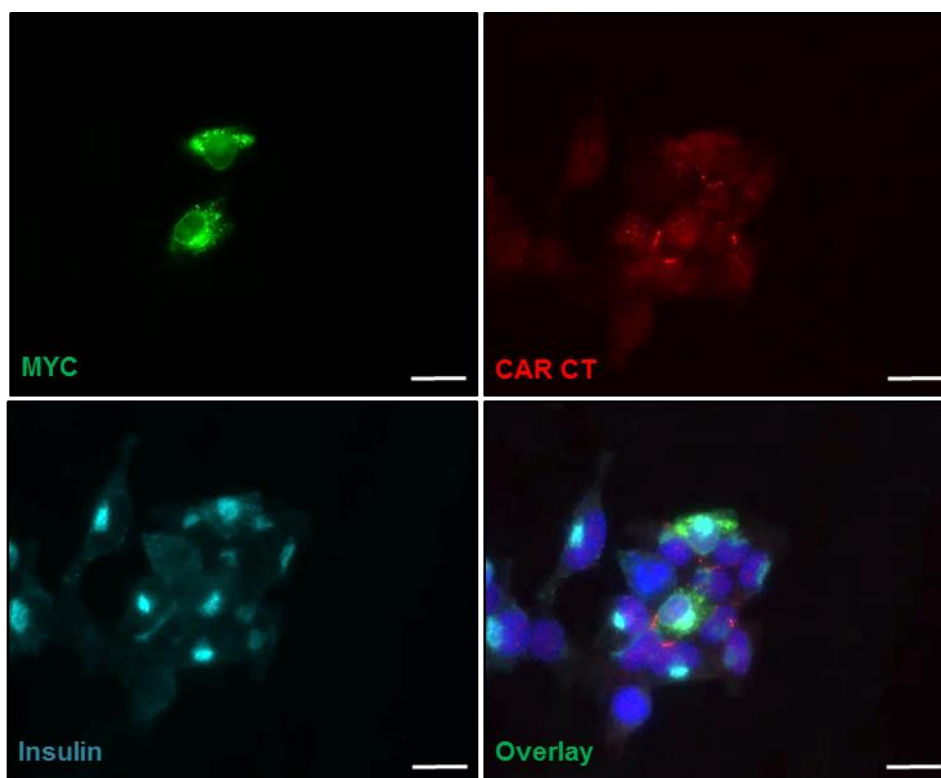


Figure 2.6 Immunocytochemical analysis demonstrates low expression of CAR-SIV in transfected CAR-SIV Myc 1.1B4 cells

1.1B4 cells were seeded at 5×10^4 cells/ml and transfected with CAR-SIV Myc vector in avalanche-omni transfection reagent for 24hrs. Cells were labelled with anti-Myc, anti-CAR CT and nuclei were stained with DAPI (dark blue). Immunocytochemical image confirms the expression of Myc-tag (anti-Myc;green) but very low expression of CAR-SIV (anti-CAR CT; red) in transfected CAR-SIV Myc tag vector, insulin (anti-insulin; light blue) is also detected in the 1.1B4 cells. Scale bar 25 μ m Data are representative of three replicates.

To assess if indeed the Myc-tag was preventing the visualisation of CAR-SIV overexpression in the cells, western blotting was utilised and blots were probed with the CAR CT or CAR ECD antisera. The results revealed that the CAR CT antibody (targeted towards the C-terminus epitope of CAR-SIV) did not obtain a band with increased intensity (estimated 40kDa) in CAR-SIV Myc-tag transfected

cells. The (positive) control, HEK cells transfected with CAR-SIV Myc, also show no dramatic increase in the band intensity when compared to the empty vector transfected cells (*Figure 2.7A*). However, the CAR ECD antiserum (which recognises the extracellular domain; located away from the Myc-tag) did detect an intense band with slightly increased molecular weight at around 50kDa in the CAR-SIV Myc-transfected cells when compared with the empty vector and control cells (*Figure 2.7B*). The increased molecular weight is likely due to the addition of the Myc-tag to CAR-SIV construct. HeLa cells which endogenously express high levels of CAR were utilised as a positive control (Polacek et al., 2005), where an intense band at the estimated size of 40kDa was observed. These results suggest that the Myc-tag could hinder the access of the CAR CT antiserum to the very C' terminus of CAR. This could also have an impact on the localisation of CAR and the binding of other cellular CAR interacting proteins (Shevtsova et al., 2006)

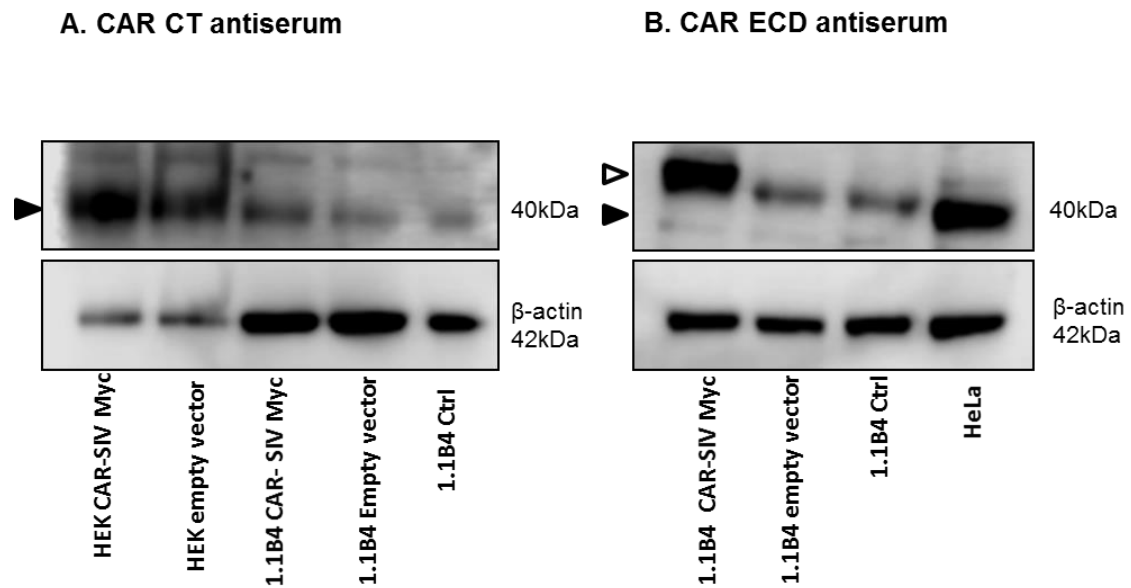


Figure 2.7 Western blot analysis confirms low expression of CAR-SIV in transfected CAR-SIV Myc-tag 1.1B4 cells

1.1B4 and HEK 293T cells were seeded at 5×10^4 cells/ml, CAR-SIV Myc and empty vector were transfected for 24hrs. Cells were lysed and total protein was isolated for western blot analysis utilising antisera against CAR CT or CAR ECD. β -actin was used as a loading control. (A) low CAR-SIV (anti-CAR CT) is detected at 40kDa in the CAR-SIV Myc vector as well as the empty and control vector in both 1.1B4 and HEK 293T cells (B) In contrast, there is an intense band size at a higher molecular weight detecting CAR (anti-CAR ECD) in CAR-SIV Myc compared to empty and control vector in 1.1B4 cells and positive control HeLa cells. Blot images are representative of three independent experiments

2.22 Site directed mutagenesis

To investigate whether the Myc-tag was interfering with CAR CT antiserum binding and potentially CAR-SIV localisation, we next employed a site-directed mutagenesis approach to remove the Myc-tag from the CAR-SIV Myc construct by introducing a mutation (a stop codon encoded in primers) at the end of the C' terminus of CAR-SIV before the beginning of the Myc tag in the nucleotide sequence (Appendix, *Figure 8.3*). A truncated version of CAR-SIV isoform was also created from the CAR-SIV Myc-tag (Appendix, *Figure 8.3*). Site directed mutagenesis was carried out according to the manufacturer's protocol (New England Biolabs) as shown in *Figure 2.8*.

Initially, an exponential amplification (PCR) was carried out using a SimpliAmp thermal cycler (Life technologies, California, USA). In a PCR tube the following reagents were assembled for a 25µl reaction; Q5 Hot Start High-Fidelity 2X Master Mix, 10µM forward primer, 10µM reverse primer, 10ng/µl of template DNA and nuclease-free water. Annealing temperatures and time were set according to the mutagenic primers designed from the NEB primer design software and final extension time was set at 72°C for 10 mins.

Kinase, Ligase and DpnI (KLD) reaction was set by treating the PCR products with (2X) KLD Reaction buffer, (10X) KLD Enzyme Mix (kinase, ligase and DpnI) to allow for proper ligation of the plasmid and nuclease free water. These components were mixed and then incubated at room temperature for 5mins.

Components were then transformed into NEB 5-alpha competent *E.coli* in the ratio of 1:10. SOC medium was added to the mixture and incubated at 37°C for 60mins on a shaker. Cells were plated on the Kanamycin-agar plate and

incubated overnight at 37°C. Colonies were grown further in culture tubes with SOC medium overnight, gently shaking at 37°C.

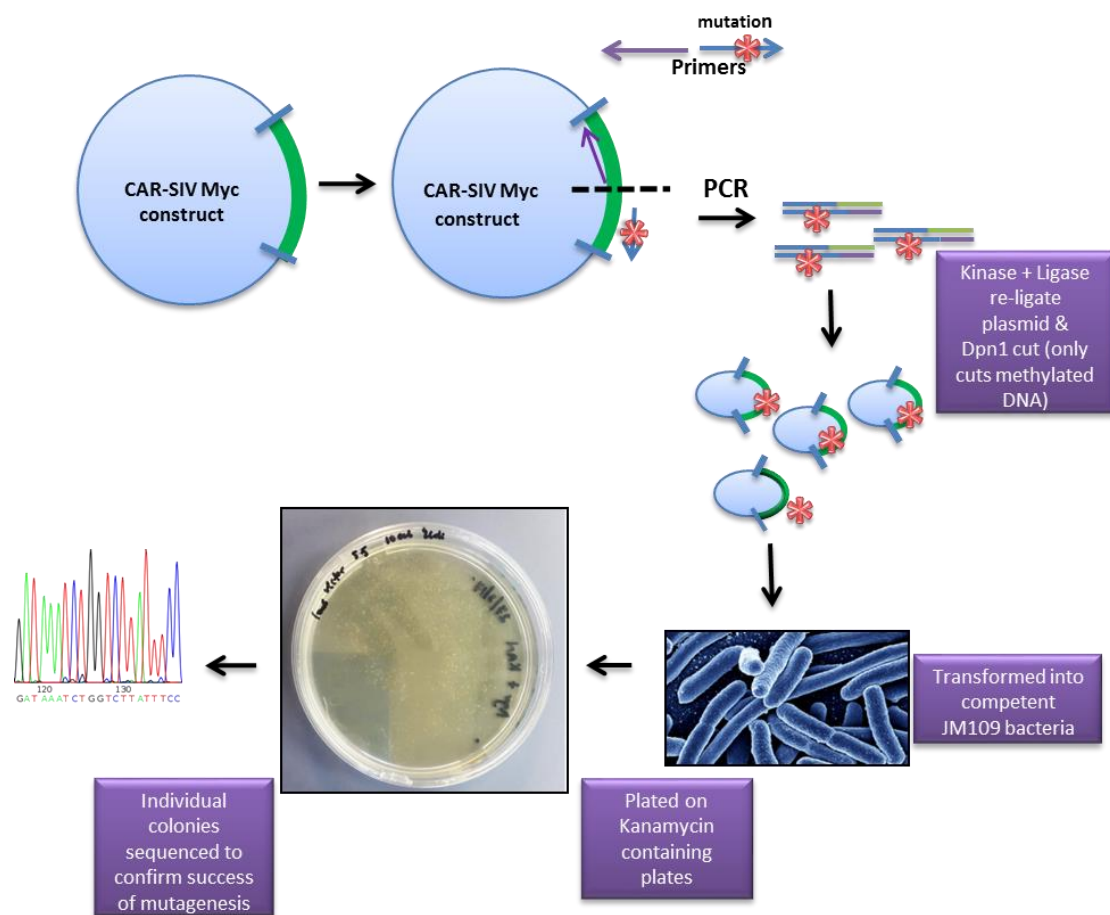


Figure 2.8 Pipeline of site directed mutagenesis

2.22.1 Restriction digest

The identity of the plasmid can be verified using enzymes to cleave specific DNA sequences and this was first demonstrated in an oncogenic virus SV40 (Nathans and Danna, 1972). Prior to digest, the circular DNA sequence was inputted in Ap.E, A plasmid Editor, version 1.11.0.0 software to determine what enzymes would cleave the sequence. Enzymes for single (one enzyme) or double digest (two enzymes) as well as 100% activity digestion buffers were chosen from Promega website <http://www.promega.com/a/apps/retool/>. For all digests, the following components were assembled together in a tube; 100µg/ml BSA, 5µl of (1X) digestion buffer, 2µg DNA, 1µl of 10U restriction enzyme, with reaction mix made up to 50µl with nuclease-free (nf)H₂O. Negative controls containing no enzymes will be 'uncut' providing a basis for comparison with cut DNA. The reaction mix was incubated in a water bath for 12hrs at 37⁰C or in a thermocycler with 2 cycles (37⁰C for 12hrs and then transferred to 10⁰C) to ensure complete digestion. The digested product was added to 10µl (1X) DNA loading dye and ran on an agarose gel electrophoresis with a 1kb DNA ladder on a separate lane. The restriction digest carried out on the wild-type CAR-SIV-Myc construct should cleave at particular sites by restriction endonucleases (EcoRI and MluI). It is important to note that due to the insertion of the stop codon to the nucleotide sequence the MluI site was destroyed, hence it is expected that only one cut with the EcoRI would be observed in constructs with the new stop codon. As expected, the DNA extracted from majority of the colonies were cleaved by EcoRI yielding an approximate band size fragment of 3858bp (*Figure 2.9*). This revealed the successful mutation of the CAR-SIV Myc-tag construct to remove the Myc tag



Figure 2.9 Restriction digest confirms the wild-type CAR-SIV vector. PCR image shows that the wild-type CAR-SIV vector was digested by EcoRI and MluI in only three colonies (green box) wild-type. Data are representative of three replicates.

2.22.2 Direct sequencing confirming successful site directed mutagenesis

Direct DNA sequencing confirmed the presence of the inserted mutation and truncation and the identity of the wild-type CAR-SIV and the truncated CAR-SIV mutant construct by alignment with sequences held in the NCBI database as shown in Figure 2.10.

A

```
SeqA 1036 AGGAAGTTCATCACGATATCAGGGAAGATGTGCCACCTCCAAAGAGCCGTACGTCCACTG
SeqB      AGGAAGTTCATCACGATATCAGGGAAGATGTGCCACCTCCAAAGAGCCGTACGTCCACTG

SeqA 1096 CCAGAAGCTACATCGGCAGTAATCATTATCCCTGGGGTCCATGTCTCCTTCCAACATGG
SeqB      CCAGAAGCTACATCGGCAGTAATCATTATCCCTGGGGTCCATGTCTCCTTCCAACATGG

SeqA 1156 AAGGATATTCOAAGACTCAGTATAACCAAGTACCAAGTGAAGACTTTGAACGCACTCCTC
SeqB      AAGGATATTCOAAGACTCAGTATAACCAAGTACCAAGTGAAGACTTTGAACGCACTCCTC

SeqA 1216 AGAGTCCGACTCTCCCACCTGCTAAGGTAGCTGCCCTAATCTAAGTCGAATGGGTGCGA
SeqB      AGAGTCCGACTCTCCCACCTGCTAAGGTAGCTGCCCTAATCTAAGTCGAATGGGTGCGA

SeqA 1276 TTCCTGTGATGATTCCAGCACAGAGCAAGGATGGGTCTATAGTAACG
SeqB      TTCCTGTGATGATTCCAGCACAGAGCAAGGATGGGTCTATAGTATAG
```

B

```
SeqA 1036 AGGAAGTTCATCACGATATCAGGGAAGATGTGCCACCTCCAAAGAGCCGTACGTCCACTG
SeqC      AGGAAGTTCATCACGATATCAGGGAAGATGTGCCACCTCCAAAGAGCCGTACGTCCACTG

SeqA 1096 CCAGAAGCTACATCGGCAGTAATCATTATCCCTGGGGTCCATGTCTCCTTCCAACATGG
SeqC      CCAGAAGCTACATCGGCAGTAATCATTATCCCTGGGGTCCATGTCTCCTTCCAACATGG

SeqA 1156 AAGGATATTCOAAGACTCAGTATAACCAAGTACCAAGTGAAGACTTTGAACGCACTCCTC
SeqC      AAGGATATTCOAAGACTCAGTATAACCAAGTACCAAGTGAAGACTTTGAACGCACTCCTC

SeqA 1216 AGAGTCCGACTCTCCCACCTGCTAAGGTAGCTGCCCTAATCTAAGTCGAATGGGTGCGA
SeqC      AGAGTCCGACTCTCCCACCTGCTAAGGTAGCTGCCCTAATCTAAGTCGAATGGGTGCGA

SeqA 1276 TTCCTGTGATGATTCCAGCACAGAGCAAGGATGGGTCTATAGTAACG
SeqC      TTCCTGTGATGATTCCAGCACAGAGCAAGGATAGTCTATAG-----
```

Figure 2.10 Direct sequencing confirmation of the generation of CAR-SIV wild type and truncated CAR-SIV constructs by insertion of mutation

The DNA from colonies were extracted, purified and sequenced. Purple squares indicate (A) SeqA (CAR-SIV sequence held in NCBI database) aligned to Seq B (wildtype CAR-SIV construct), generated mutant (B) SeqA (CAR-SIV sequence held in NCBI database) aligned to Seq B (truncated CAR-SIV mutant construct). Data is a representative image from three replicates

2.23 Human growth hormone assay (HGH)

The cell lines 1.1B4 or INS-1E cells were transfected with Avalanche reagent with several constructs; human growth hormone (HGH), wild-type CAR-SIV, truncated CAR-SIV mutant and empty vector between (6-13hrs). Thereafter, fresh cell media was added to cells and left for a further 48hrs. Cells were then washed with 500µl of pre-warmed Krebs buffer and then incubated with pre-warmed 500µl Krebs buffer supplemented with 0.1%(w/v) BSA and 0mM glucose for 90mins at 37°C. To stimulate cells to secrete growth hormone which is a surrogate of insulin secretion, 300µl Krebs buffer with 0.1%(w/v) BSA supplemented with 20mM glucose, 200µM IBMX, 10µM forskolin and 25mM KCl were incubated in cells for 1hour at 37°C. 200µl cell supernatant was collected and used for human Growth Hormone assay below or stored at -20°C for later use.

Growth Hormone Assay (Sigma-aldrich) is a quantitative colorimetric immunoassay which detects secreted human Growth Hormone (hGH) released into cell culture supernatants from cells transfected with a construct encoding hGH (da Silva Xavier et al., 2003). Growth hormone has been previously reported to monitor secretory activity and it was shown to be co-sorted and secreted with insulin (Iezzi et al., 1999). Therefore, it was used in this study to monitor the functional impact of CAR on insulin secretion in the 1.1B4 cells. The growth hormone assay is based on a sandwich ELISA principle with a microplate module already coated with anti-hGH antibodies to capture secreted human Growth Hormone which is then labelled with detection antibodies. To perform this assay, 100µg/ml of hGH stock (1:2 dilution) was used to prepare standard dilution series (0pg/ml, 400pg/ml, 200pg/ml, 100pg/ml, 50pg/ml, 25pg/ml and 12.5pg/ml). Standards and cell supernatants (200µl) were pipetted in each well, covered and

incubated for 1hr at 37°C. Wells were rinsed (5 times) with wash buffer (1X) and incubated with 200µl of 1µg/ml of anti-hGH-DIG for 1hr at 37°C. Following this, wells were washed (5 times) and incubated with 200µl of 200mU/ml anti-DIG-POD for 1hr at 37°C. For the substrate reaction, microplate modules were washed (5 times) and 200µl of POD substrate mixed with substrate enhancer (1ml of POD substrate per 1mg of substrate enhancer) was added to each well and incubated at room temperature between 10-30mins until colour developed. Absorbance of samples was then measured at 405nm with a reference wavelength at 490nm. The standard curve was then plotted with y-axis depicting the absorbance readings and the hGH concentration (pg/ml) on the x axis. Unknown samples were determined by inserting the absorbance reading into a linear equation. A pictorial diagram of the human Growth Hormone process is shown below in Figure 2.11

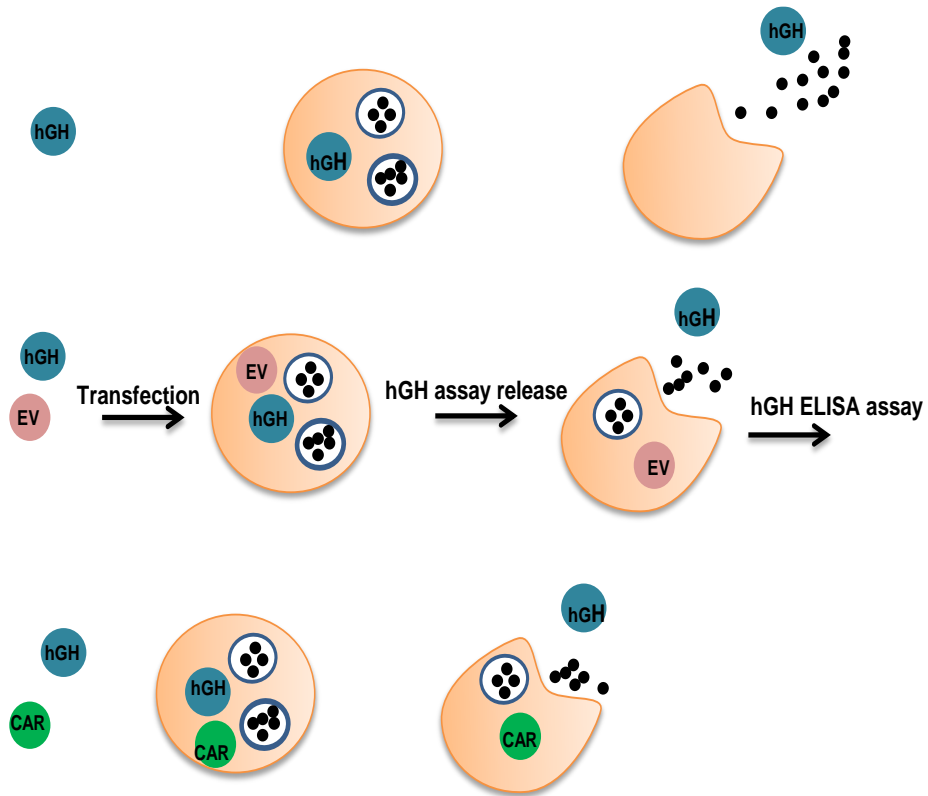


Figure 2.11 Pictorial diagram of human Growth Hormone secretion process.

Cells are transfected with either human growth hormone (hGH) vector only (upper panel), a combination of human growth hormone (hGH) vector and empty vector (EV; middle panel) or a combination of human growth hormone (hGH) vector and CAR-SIV Myc vector (CAR; lower panel). Following starvation, the cells are stimulated with glucose, IBMX, forskolin and KCl, to induce growth hormone release. The growth hormone secreted by the transfected cells in the supernatant is then collected and assessed by the hGH ELISA.

2.24 Statistical analysis

Immunofluorescence images of islets were selected randomly from stained pancreas sections. Pearson correlation coefficient (PCC) was used to estimate the colocalisation between proteins using the JACoP plugin from Image J. The PCC values range from 0 to no correlation to 1 for positive correlation. Graphpad PRISM 5.04 was employed for all statistical analysis and data were expressed as mean values \pm SEM. Statistical significance was calculated using student t-test and for multiple comparisons the Bonferroni multiple comparison test was used.

CHAPTER 3

Characterisation of CAR isoforms in the human beta cell and pancreas

3.1 Introduction

There is accumulating evidence that Coxsackie B viruses can trigger the development of autoimmunity and type 1 diabetes with the weight of evidence implying that such viruses may directly infect human pancreatic beta cells (Yeung et al., 2011, Morgan and Richardson, 2014). CAR is an important mediator of CVB infection (Bergelson et al., 1997) and there have been extensive studies documenting the importance of an interaction between Coxsackie B viruses or adenoviruses with CAR as a means to generate a productive infection (Excoffon et al., 2014). However, there are very few studies addressing the relative contribution of the various isoforms of CAR in different cells and tissues.

Most studies to date have assessed the effects of whole or partial CAR knockout in mice to confirm its importance in CVB infections. For example, a study in adult mice demonstrated that specific deletion of CAR in heart and pancreas prevented CVB3 infection in these tissues (Kallewaard et al., 2009, Shi et al., 2009). Shi *et al* (2009) demonstrated that deleting exon 1 of CAR in mice knocked-out both the transmembrane and soluble isoforms of CAR and that this prevented CVB3 entry and replication in the heart (Shi et al., 2009). Ylipaasto *et al* (2004) reported that a monoclonal antibody “CAR Rmcb” raised against human CAR (HCAR) prevented infection of CVB4 in human beta cells (Ylipaasto et al., 2004). Together, these studies demonstrate the importance of CAR in mediating CVB infection in mice and humans, but they do not elucidate the relative contributions of the different CAR isoforms.

In addition, it is important to note that CVBs show differential tissue tropism in mice compared to humans, with the exocrine tissue being the major target in mice, whereas the endocrine tissue is targeted in humans (Stone et al., 2018).

To better understand the specific endocrine cell targeting of CVBs in human it is important to study and characterise the precise CAR isoform expression profile in both human pancreatic islets and human beta cell lines at the mRNA and protein levels.

The objectives of this chapter are as follows;

- To examine the transmembrane and soluble CAR isoform expression profile at the RNA and protein level in *in situ* human pancreatic tissue and in cultured pancreatic beta (EndoC- β H1 and 1.1B4) and ductal cell lines (PANC-1).
- To examine the effect of cytokine treatment on the different CAR isoforms in isolated human islets and human pancreatic beta cell (EndoC- β H1)
- To evaluate CAR expression in autoantibody positive patients, type 1 diabetes and type 2 diabetes patients
- To assess if there is differential CAR isoform expression in human and mouse pancreas

3.2 Results

3.2.1 RT-PCR detection of mRNA encoding specific CAR isoforms in human pancreatic islets and human beta cell lines

To assess if isoforms of CAR having the transmembrane domains could be detected at the mRNA level in human pancreatic islets and human beta cell lines, RNA was extracted (Section 2.10) from isolated human islets and from the human pancreatic beta cell line, 1.1B4. cDNA was synthesised and the expression of CAR isoforms was assessed by PCR using primers (Table 3.1) designed to hybridise with sequences in exon 5 and exon 7. These primers are capable of amplifying both the transmembrane isoforms, CAR-SIV and CAR-TVV but are not able to distinguish between them. An amplicon of approximately 345bp was detected in isolated human islets and 1.1B4 cells (*Figure 3.1*).

Table 3.1 Primer sequence to target both CAR-SIV and CAR-TVV

Target Sequence	Primers
CAR-SIV/CAR-TVV (exon 5 Fd)	CAGTGCCTGTTGCGTCTAAA
CAR-SIV/CAR-TVV (exon 7 RV)	CTTAGCAGGTGGGAGAGTCCG

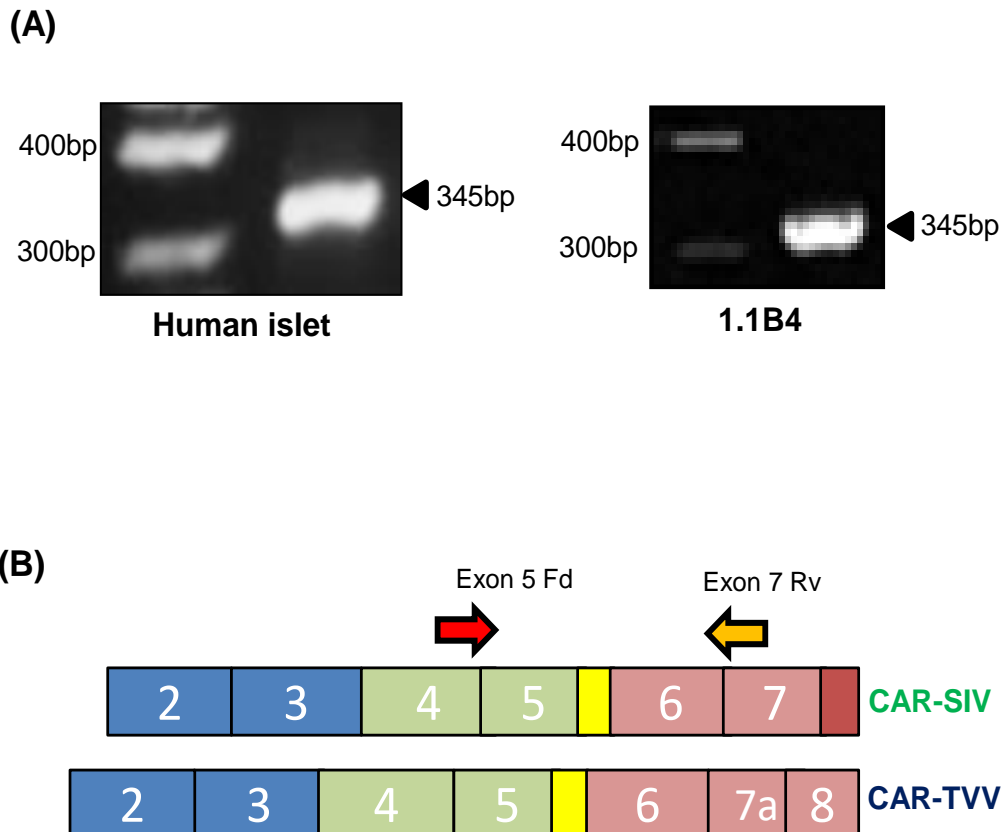


Figure 3.1 CAR-SIV or CAR-TVV transmembrane isoforms are amplified in isolated human islet and 1.1B4.

Total RNA was isolated from cell lysates of isolated human islets and 1.1B4 cells. Following quantification, 1 μ g of RNA was converted to cDNA. The cDNA was subsequently used in a PCR reaction (35cycles) with primers designed to amplify the transmembrane isoforms of CAR (Table 3.1). PCR products were then separated by electrophoresis (A) RT-PCR analysis display approximately 345bp band(black arrow head) for both transmembrane isoforms which cannot be discriminated in both isolated human islet and 1.1B4 cells (n=3) (B) Schematic diagram of primers annealing to exon 5 and exon 7 of both CAR-SIV and CAR-TVV isoform

To identify which of the transmembrane isoforms was specifically amplified in the human islet preparations; isoform specific primers (Table 3.2) were designed to selectively amplify either CAR-SIV or CAR-TVV. These would produce products of 253bp for CAR-SIV and 233bp for CAR-TVV. As shown (*Figure 3.2A*) the primer pair designed to amplify CAR-SIV, yielded a band at approximately 250bp and those against CAR-TVV generated a (faint) band at approximately 230bp. The differences in intensity of the products suggest that the CAR-SIV isoform could be more abundant. In support of this, when the amplification protocol was reduced from 35 to 30 cycles (*Figure 3.2B*), the CAR-TVV band was lost but the band corresponding to the CAR-SIV isoform was retained. These results were confirmed in two different isolated human islet preparations (obtained from Oxford and Worcester respectively) (*Figure 3.2C*). Controls in which no template DNA was added, yielded no bands thereby confirming the specificity of the RT-PCR analysis of human islet RNA. The amplified bands were excised and sequenced to confirm the successful amplification of sequences equivalent to those expected in CAR-SIV and CAR-TVV respectively. The amplified sequences were aligned with those held in the NCBI database (*Figure 3.3*) and it was confirmed that the two relevant isoforms of CAR are expressed at the RNA level in human beta cells and in human beta cell lines.

Table 3.2 Primer sequence specific for CAR-SIV and CAR-TVV isoform

Target Sequence	Primers
CAR-SIV (exon 6 Fd)	GGAAGTTCATCACGATATCAG
CAR-SIV (exon 7 Rv)	AATCATCACAGGAATCGCAC
CAR-TVV (exon 6 Fd)	GGAAGTTCATCACGATATCAG
CAR-TVV (exon 8 Rv)	TTCCATCAGTCTTGTAAGGG

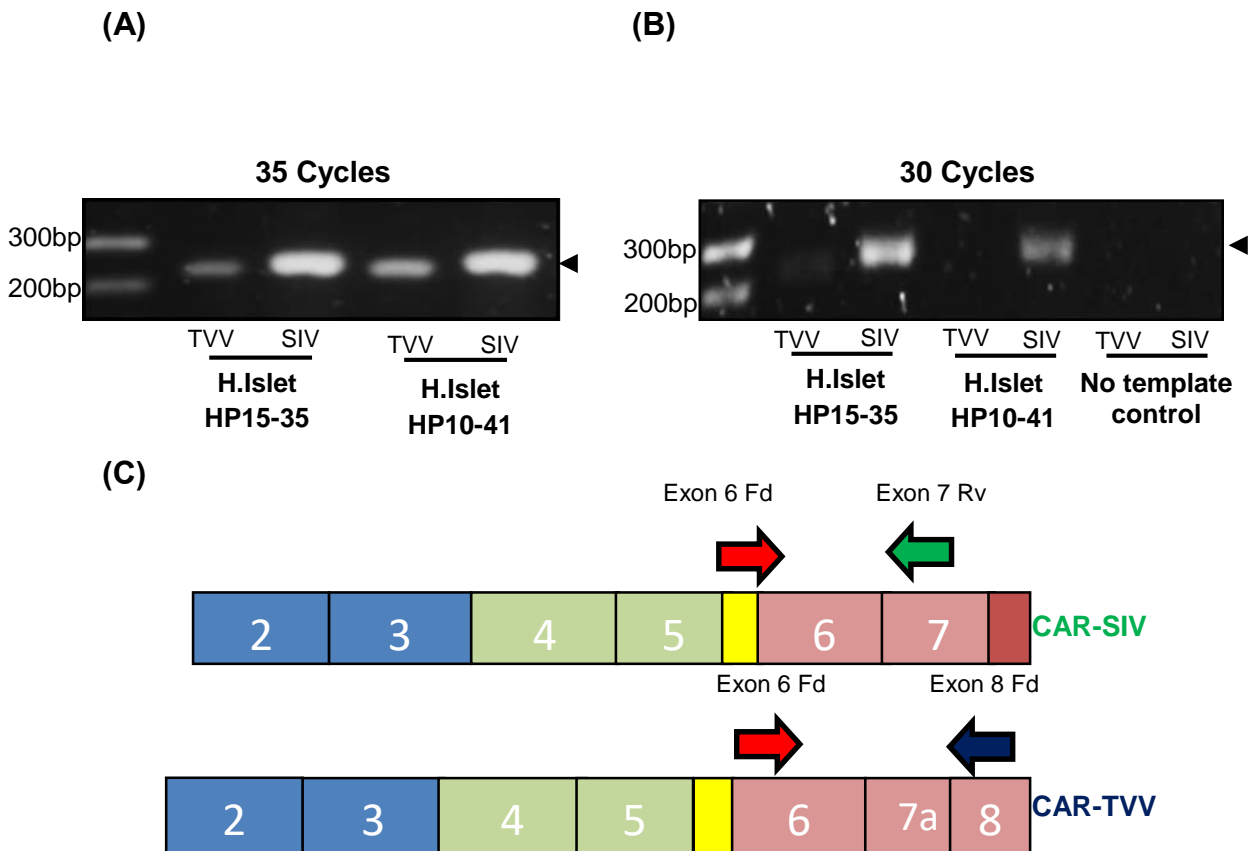
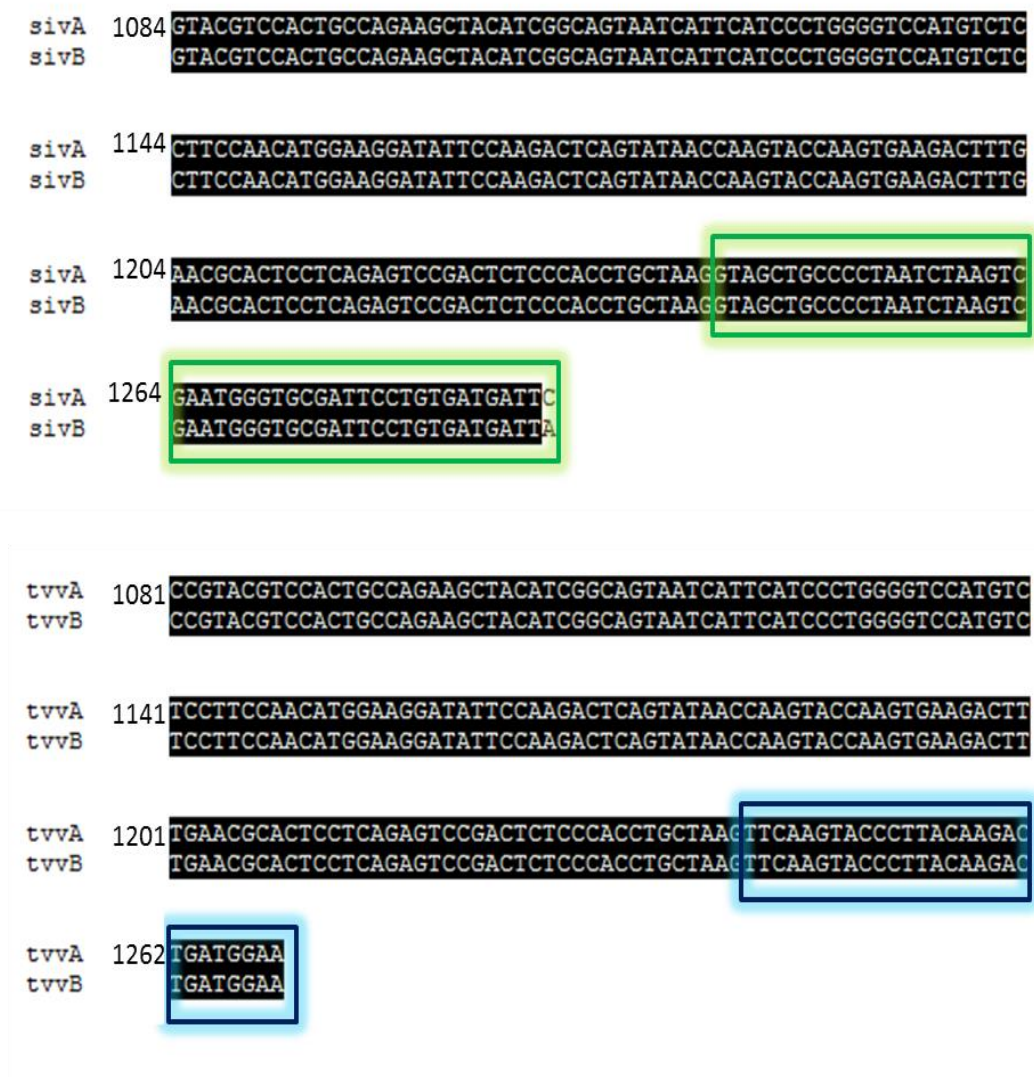


Figure 3.2 Isoform specific RT-PCR analysis revealed that CAR-SIV is more abundant than CAR-TVV from two independent isolated human islets.

Total RNA was isolated from cell lysates of isolated human islets. Following quantification, 1 μ g of RNA was converted to cDNA. The cDNA was subsequently used in a PCR reaction (35 and 30 cycles) with specific primers designed to amplify CAR-SIV and CAR-TVV isoforms of CAR (Table 3.2). PCR products were then separated by electrophoresis. RT-PCR at (A) 35 cycles revealed that a band at 253bp for CAR-SIV (black arrow) and a band at 233bp (black arrow) for CAR-TVV ($n=3$)(B) 30 cycles demonstrated that CAR-SIV is still retained (250bp) but the CAR-TVV band is lost ($n=3$) (C) Schematic diagram of specific primers annealing to (exon 6 and exon 7) for CAR-SIV and (exon 6 and exon 8) for CAR-TVV isoform.




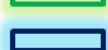
 Differences between CAR-SIV and CAR-TVV


Figure 3.3 CAR-SIV and CAR-TVV isoform is confirmed in isolated human islets.

DNA was extracted, purified and sequenced. Alignment of (A) CAR-SIV (sivA) from NCBI Accession NM_001338 to sequenced CAR-SIV (sivB) and (B) CAR-TVV (tvvA) from NCBI Accession NM_001207066 to sequenced CAR-TVV (tvvB). Data are representative of images from three replicates

3.2.2 TaqMan qRT-PCR detection of mRNA encoding specific CAR isoforms in isolated and laser captured micro-dissected human pancreatic islets

To enable the identification and quantification of all of the different CAR isoforms (including those with transmembrane domains, as well as the soluble forms) we next utilised an isoform specific qRT-PCR using the TaqMan platform. This was performed by our collaborators at the University of Siena, Italy (Dr Sebastiani and Prof. Dotta). Specific primers targeting the transmembrane isoforms CAR-SIV and CAR-TVV were designed in Exeter (*Table 3.2*) while the soluble isoforms CAR 4/7, CAR 3/7 and CAR 2/7 were designed by a commercial supplier (ThermoFisher) to span the exon-exon boundaries allowing for the selective amplification of specific CAR isoforms. TaqMan probes (*Table 3.3*) were also designed for each CAR isoform by ThermoFisher (*Figure 3.4*). RNA was extracted from isolated human islets from 5 non-diabetic control cases (University of Siena, Italy; *Table 3.4*) and from laser captured micro-dissected (LCM) islets from 2 non-diabetic control cases (*Table 3.4*)

Table 3.3 TaqMan probe sequence for the five CAR isoforms

Target sequence	Probe ID	TaqMan Probe Sequence
CAR 2/7 exon_2_7	AIKAMSZ	GGTGGATCAAGTGGGAAGAT
CAR 3/7 exon_3_7	AILIKY7	GTAGTTCTTGGGAAGATGTG
CAR 4/7 exon_4_7	AIMSI5F	CATGGTTAGCAGGGAAGATG
CAR-TVV exon_6_7	AIPAFHN	CCAACATGGAAGGATATTCC
CAR-SIV exon_6_7	AIN1HBN	CGATATCAGGGAAGATGTGC

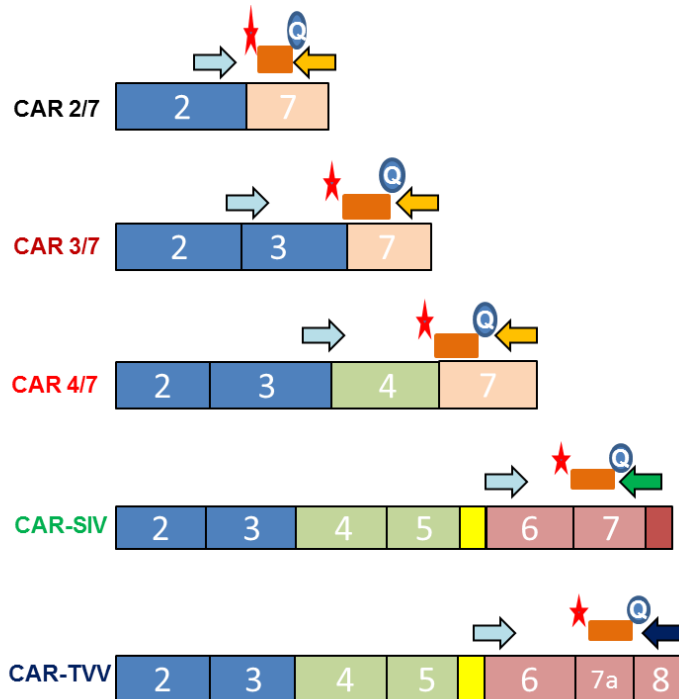


Figure 3.4 Schematic diagram displaying the location of TaqMan probes and primers for each of the five CAR isoforms

Table 3.4 Isolated human islet donors

Sample ID	Gender	Age	BMI (Kg/m ²)
Isolated islet donors			
1	M	52	34.2
2	M	50	27.4
3	M	55	28.0
4	F	79	23.9
5	M	59	26.7
LCM nPOD donors			
6017	F	59	24.8
6096	F	16	18.8

Results from the TaqMan qRT-PCR analysis clearly demonstrated differential CAR isoform expression in human islets (*Figure 3.5A*). The two transmembrane domain containing isoforms CAR-SIV and CAR-TVV were expressed at highest levels in both the isolated human islet extracts (*Figure 3.5A*) and in RNA obtained from LCM islets recovered from pancreas sections (*Figure 3.5B*). The soluble CAR 4/7 was also present in both isolated and LCM islets but at a lower abundance; while the smaller soluble, isoforms (CAR 3/7 and CAR 2/7) were present only minimally. Visualisation of islets by virtue of their intrinsic autofluorescence enabled the LCM analysis to be performed on frozen human pancreatic tissue (*Figure 3.6*). Attempts were also made to assess CAR isoform expression in LCM exocrine tissue however; the RNA integrity number (RIN) values were extremely low (2.8 and 2.6) and therefore the RNA was deemed to be of insufficient quality for use in qRT-PCR. In contrast, good quality RNA (RIN values of 5.1 and 7.2) was extracted from the islets (*Table 3.5*). Thus, we have been unable to assess the expression of the different CAR isoforms in human exocrine pancreas tissue.

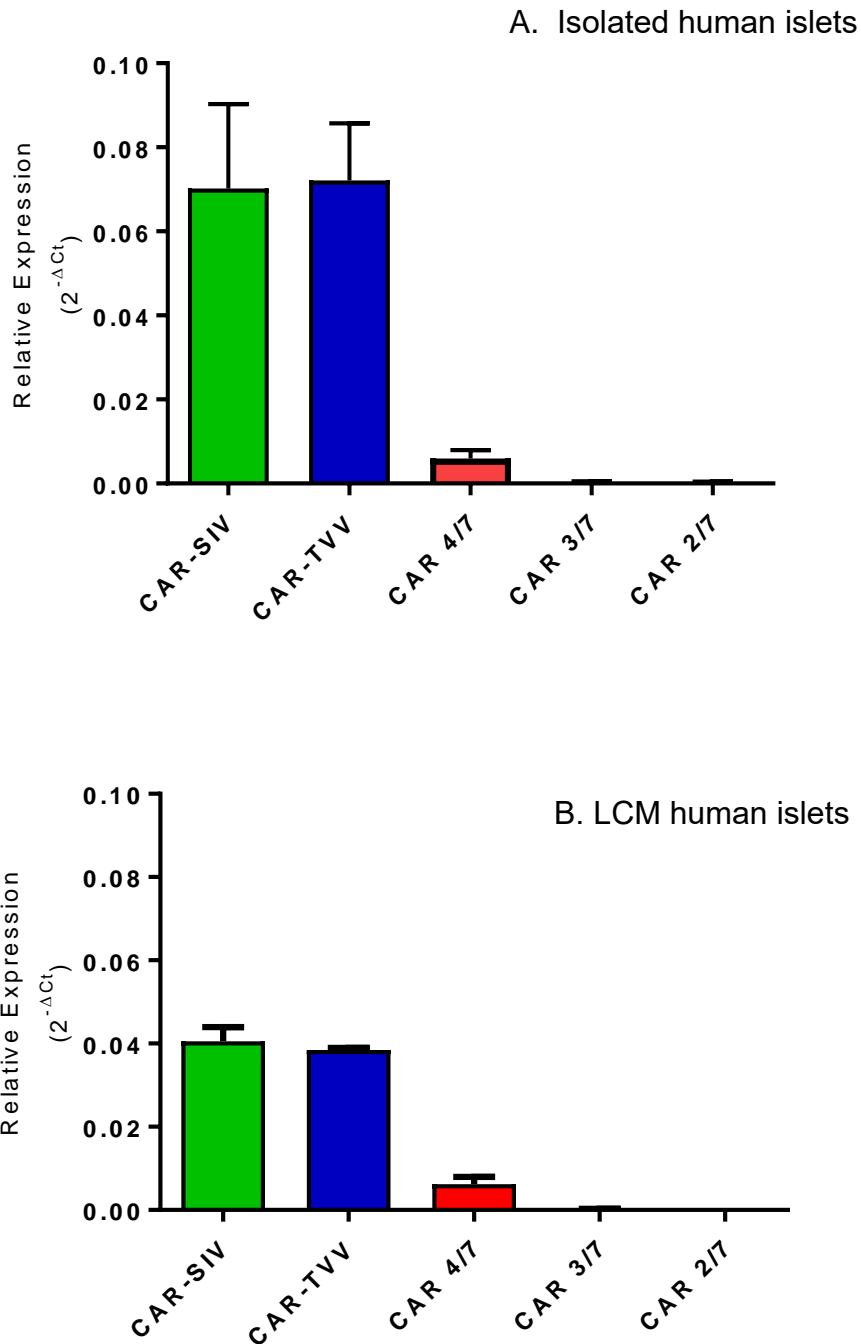


Figure 3.5 CAR-SIV and CAR-TVV is expressed in both isolated and LCM human islets. Total RNA was isolated from cell lysates of isolated and LCM human islets cells. Following quantification, 250ng of RNA was converted to cDNA. The cDNA was subsequently used in a qRT-PCR reaction with TaqMan probes and primers (Fig 3.4) designed to amplify both the transmembrane and soluble CAR isoforms. Analysis by qRT-PCR from A. isolated human islets (n= 5 individuals) and B. LCM human islets (n= 2 individuals) show that CAR-SIV and CAR-TVV are highly expressed, CAR4/7 is at low levels while CAR 3/7 and CAR 2/7 are barely detectable. Data were normalised to the relative expression of three housekeeping genes β -actin, GAPDH and B2M and relative expression is presented as mean \pm SEM. Courtesy of University of Siena

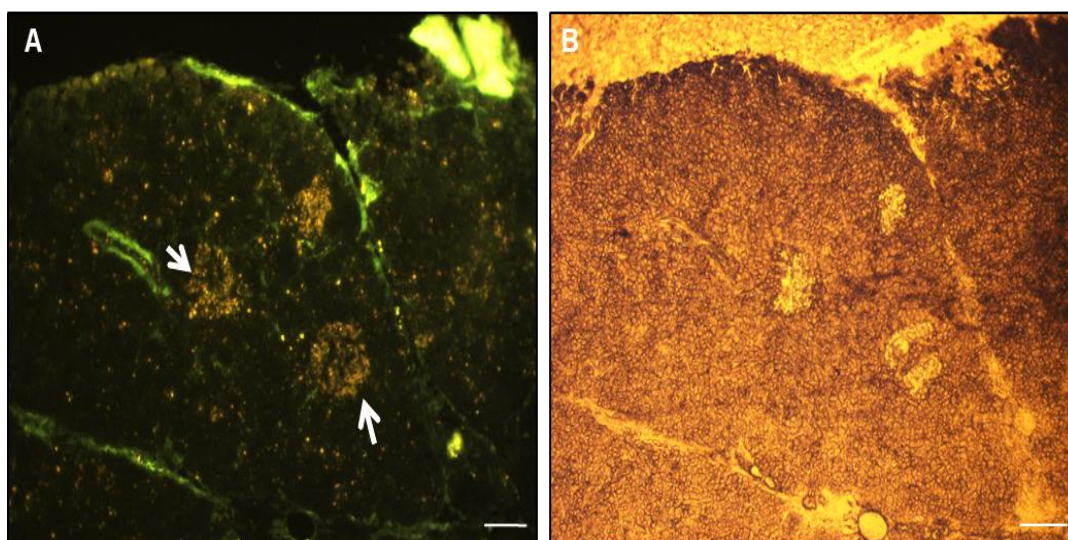


Figure 3.6 Visualisation of human islets for laser capture microdissection (LCM)
 (A)Autofluorescence images show intact human islets (white arrows) for LCM
 (B)Bright field images of human islets removed after laser capture microdissection, Scale bar 50µm, Courtesy of University of Siena

Table 3.5 RIN values of LCM human islets (nPOD) donor

Sample ID	Number of LCM islets	RIN value
6017	52	5.1
6096	39	7.2

3.2.3 RNAseq and RT-PCR detection of mRNA encoding specific CAR isoforms and effect on cytokine treatment in human pancreatic islets and human beta cell lines

Via further collaboration (with Prof. Decio Eizirik of the Universite Libre de Bruxelles, Belgium), we have also been able to quantify the alternatively spliced isoforms using RNAseq analysis in both isolated human islets and in the human pancreatic beta cell line, EndoC- β H1. The results confirmed that the various CAR isoforms were differentially expressed (*Figure 3.7*) in both islets and EndoC- β H1 cells. RNAseq obtains RNA content information by utilising high-throughput sequencing technologies to sequence cDNA (Morin et al., 2008) and provides data in the form of the total number of reads per kilobase per million mapped reads (RPKM) and this demonstrated a predominant expression of CAR-SIV. This agreed with the earlier PCR data where CAR-SIV had a higher intense band than CAR-TVV. CAR-SIV expression was three-fold higher than that of CAR-TVV in EndoC- β H1 cells, and was two-fold higher in human islets. The soluble isoform CAR 4/7 was less abundant than the two transmembrane isoforms, while CAR 3/7 and CAR 2/7 were barely detectable in either the human beta cell line or in human islet preparations. This again supported the earlier TaqMan PCR analyses (*Figure 3.5*)

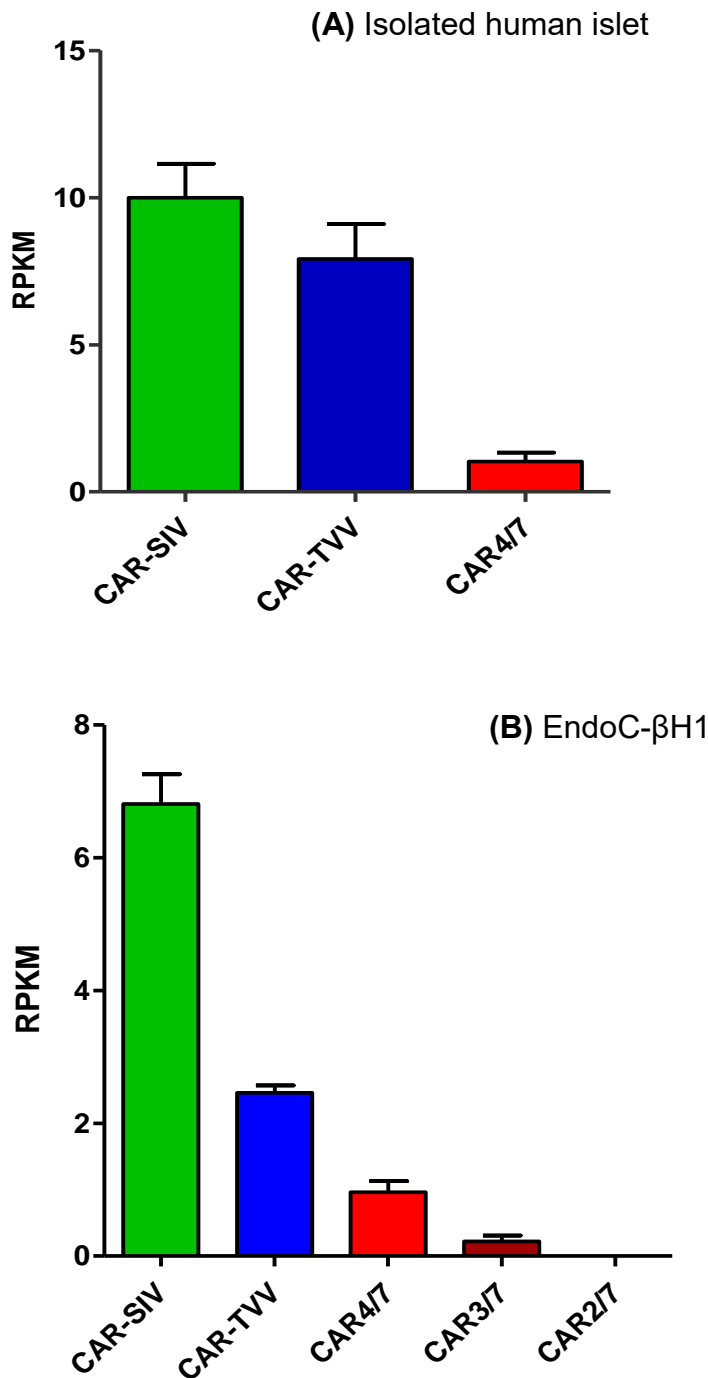


Figure 3.7 RNAseq analysis demonstrates higher expression of CAR-SIV compared to CAR-TVV and low expression of CAR4/7

Total RNA was isolated from cell lysates of isolated human islets cells and EndoC-βH1. Following quantification, 2µg of RNA was converted to cDNA. The cDNA was subsequently subjected to RNAseq analysis

(A) Isolated human islets obtained from 5 normoglycaemic human islets expressing CAR-SIV, CAR-TVV and CAR 4/7 (mean ± SEM) (B) EndoC-βH1 cells expresses the CAR-SIV, CAR-TVV, CAR 4/7, CAR3/7 and CAR 2/7, (n=3). Courtesy of Prof. Decio.L. Eizirik

Finally to confirm the presence of CAR4/7 isoform, a CAR4/7 isoform specific PCR was performed using specific primers (Table 3.6) on RNA extracted from isolated human islets and from the human pancreatic beta cell line 1.1B4. This confirmed the expression of the soluble CAR4/7 isoform shown in

Figure 3.8B. A lower band was also observed which may imply the presence of other soluble CAR isoforms. The identity of the transcript was subsequently verified by direct DNA sequencing of the relevant amplified product (*Figure 3.8C*).

Table 3.6 Primer sequence targeting the CAR soluble isoforms

Target Sequence	Primers
CAR4/7 (exon 4 Fd)	TAAGCCTTCAGGTGCGAGAT
CAR4/7 (exon 7 Rv)	GCGCTAGAGCAAGCAAAGTT

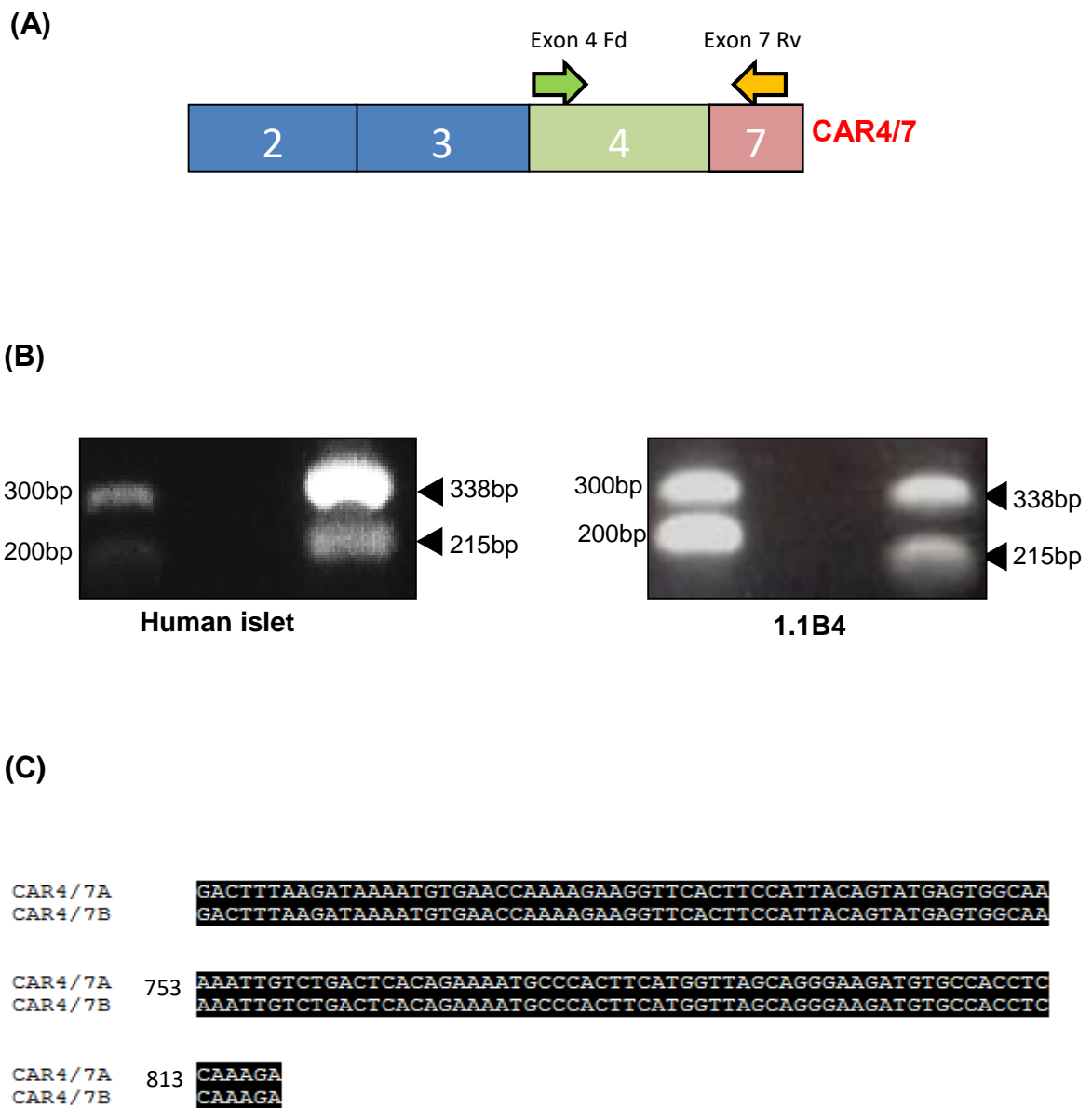


Figure 3.8 RT-PCR confirms the soluble CAR4/7 isoform expression in isolated human islets and 1.1B4 cell line

Total RNA was isolated from cell lysates of isolated human islets and 1.1B4 cells. Following quantification, 1µg of RNA was converted to cDNA. The cDNA was subsequently used in a PCR reaction (35 cycles) with primers designed to soluble CAR4/7 isoform (Table 3.6) (A) Diagram of primers annealing to exon 4 and exon 7 in CAR4/7 isoform (B) Soluble CAR4/7 produces a band at approximately 338bp (black arrow head) in isolated human islets and 1.1B4 (n=3) (C) CAR4/7 (CAR4/7A) sequence held in NCBI accession number NM_001207063 aligns perfectly with sequenced data (CAR4/7B) from human islets and 1.1B4

Several studies have demonstrated that isolated human islets infected with CVB strains can induce cytokines and chemokines that have a potential to trigger inflammatory responses contributing to autoimmune type 1 diabetes (Olsson et al., 2005, Anagandula et al., 2014a). The impact of these inflammatory signals on the expression of CAR isoforms has not been assessed. Utilising the RNAseq analysis performed by Prof. Decio Eizirik, we examined the effect of cytokine (human IL-1 β and human IFN- γ) treatment of isolated human islets and EndoC- β H1 cells on the transmembrane domain and soluble CAR isoforms. The results demonstrate that the cytokines did not alter expression of any of the different CAR isoforms (*Figure 3.9*), as these data were comparable to the RNAseq data from non-infected isolated human islets and EndoC- β H1 (*Figure 3.7*).

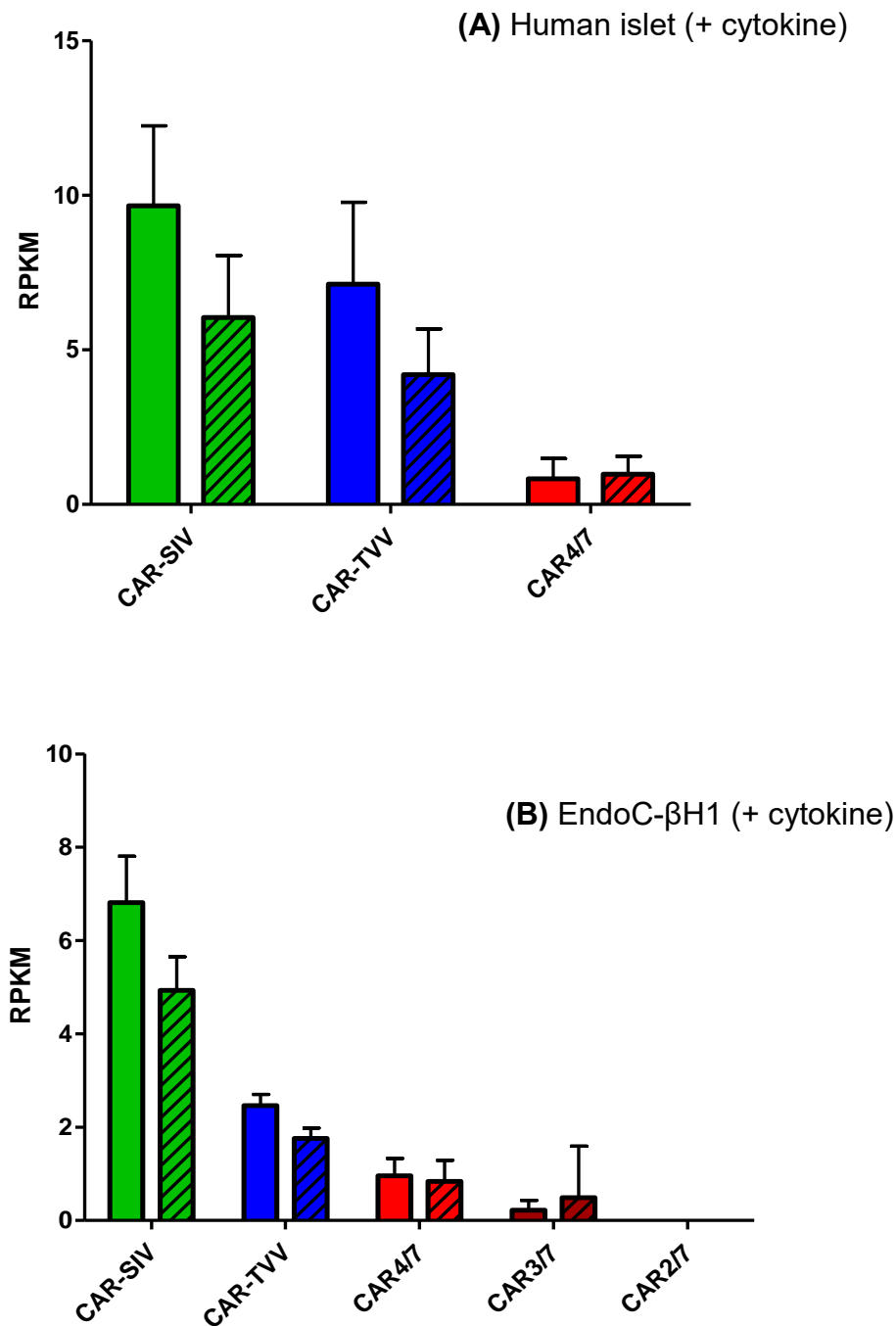


Figure 3.9 RNAseq analysis confirms no effect of cytokines on levels of mRNA of CAR isoforms

Isolated human islets and EndoC-βH1 cells were exposed to the following cytokines human IL-1β (50U/ml) and human IFN-γ (1000U/ml) for 48hrs.

Total RNA was then isolated from cell lysates of isolated human islets cells. Following quantification, 2µg of RNA was converted to cDNA. The cDNA was subsequently subjected to RNAseq analysis (A) Isolated human islets obtained from normoglycaemic human islets with no cytokine (plain bar) and cytokine treatment (shaded graph) (n=5 individuals)(mean ± SEM) (B) EndoC-βH1(n=3),(mean ± SEM). Courtesy of Prof. Decio. L. Eizirik

3.2.4 Detection of CAR isoform protein expression in human pancreatic tissue by immunohistochemistry

To determine the CAR isoform protein expression profile in human pancreatic tissue, three commercially available antisera were employed in parallel. These were directed, respectively against the N terminus (designated “CAR NT”), an unspecified region within the extracellular domain (“CAR ECD”) or the C’ terminus (“CAR CT”) of CAR. As such, use of these antisera enabled the multiple isoforms of CAR to be distinguished according to their predicated differences in immunoreactivity when probed with the various antisera (*Figure 3.10*)

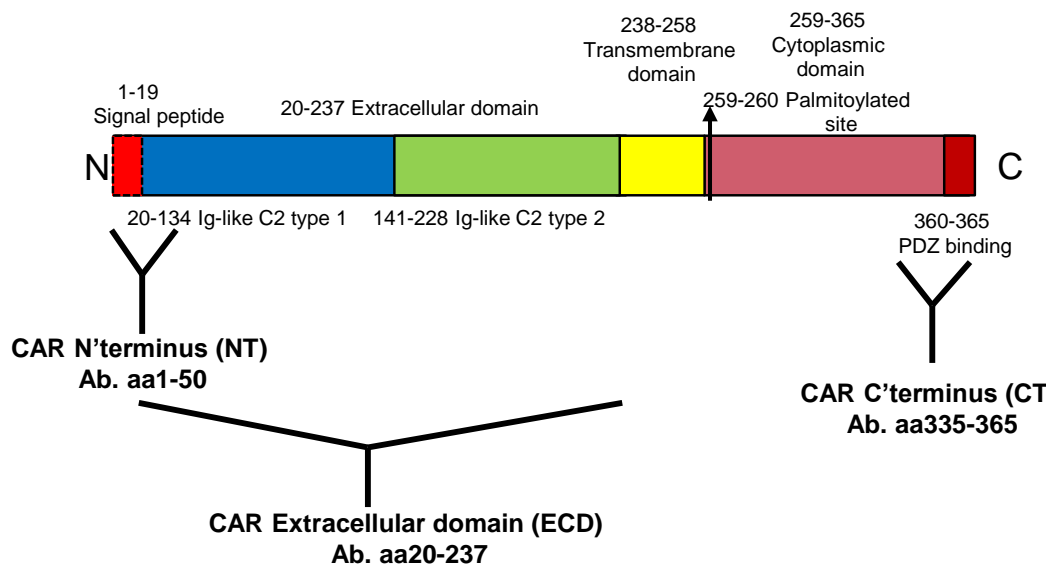


Figure 3.10 Schematic diagram of CAR antisera immunoreactivity against CAR protein

CAR antisera directed against the N terminus (CAR NT antiserum), extracellular domain (CAR ECD antiserum) and the C terminus (CAR CT antiserum) of CAR protein

An immunohistochemical approach was utilised to examine the protein expression profile in the human pancreas sections of non-diabetic adults (Appendix, Table 8.1) using the three different CAR antisera. The antiserum designated “CAR NT” was raised against the immediate N’ terminus of the CAR protein (*Figure 3.10*), therefore, this antiserum can be expected to detect the CAR-SIV, CAR-TVV, CAR 4/7, CAR 3/7 and CAR 2/7 isoforms. The image presented (*Figure 3.11; upper panels*) reveals that this antiserum diffusely labelled both the endocrine cells in the islets and the acinar cells within the exocrine tissue (as judged by the areas of brown immunostaining). The “CAR ECD” antiserum recognises epitopes present within a large region encompassing 217 amino acids of the extracellular domain of CAR (*Figure 3.10*), implying that it should recognise isoforms CAR-SIV, CAR-TVV, CAR 4/7 and potentially, CAR 3/7. In human pancreas sections, this antiserum stained the islets strongly (*Figure 3.11; lower panels*), whereas the acinar cells of the exocrine tissue were stained only weakly.

Finally, the CAR CT antiserum was tested. This was raised against an epitope within the C’ terminal 30 amino acids (335-365) of the CAR-SIV isoform; a region which harbours a unique PDZ binding domain. As such, this antiserum is highly specific for the CAR-SIV isoform. As shown in (*Figure 3.12*) CAR CT immunoreactivity was restricted only to the islets in human pancreas and no staining was detected in the exocrine tissue. Importantly, no staining was observed in either the islets or the exocrine tissue when a rabbit IgG isotype (negative) control was tested in the pancreatic tissue (*Figure 3.12*).

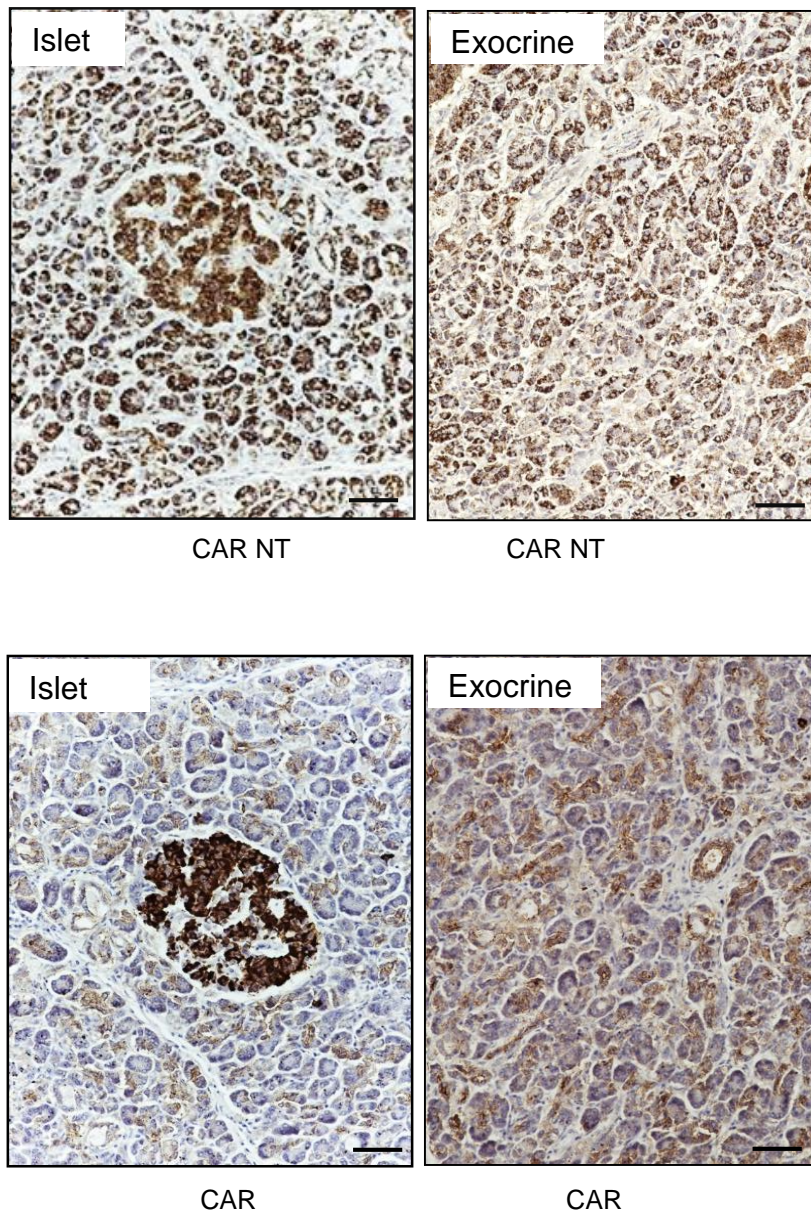


Figure 3.11 CAR isoforms are detected in the islet and exocrine pancreas utilising CAR (NT and ECD) antisera in NDA pancreas.

Immunohistochemical images revealed brown immunostaining with CAR NT antiserum (upper panels) detected in both islets (left hand side) and exocrine tissue (right hand side) and CAR ECD (lower panels) antiserum detected in islets but faintly in exocrine. Data are representative of at least three donors, Scale bar 20 μ m

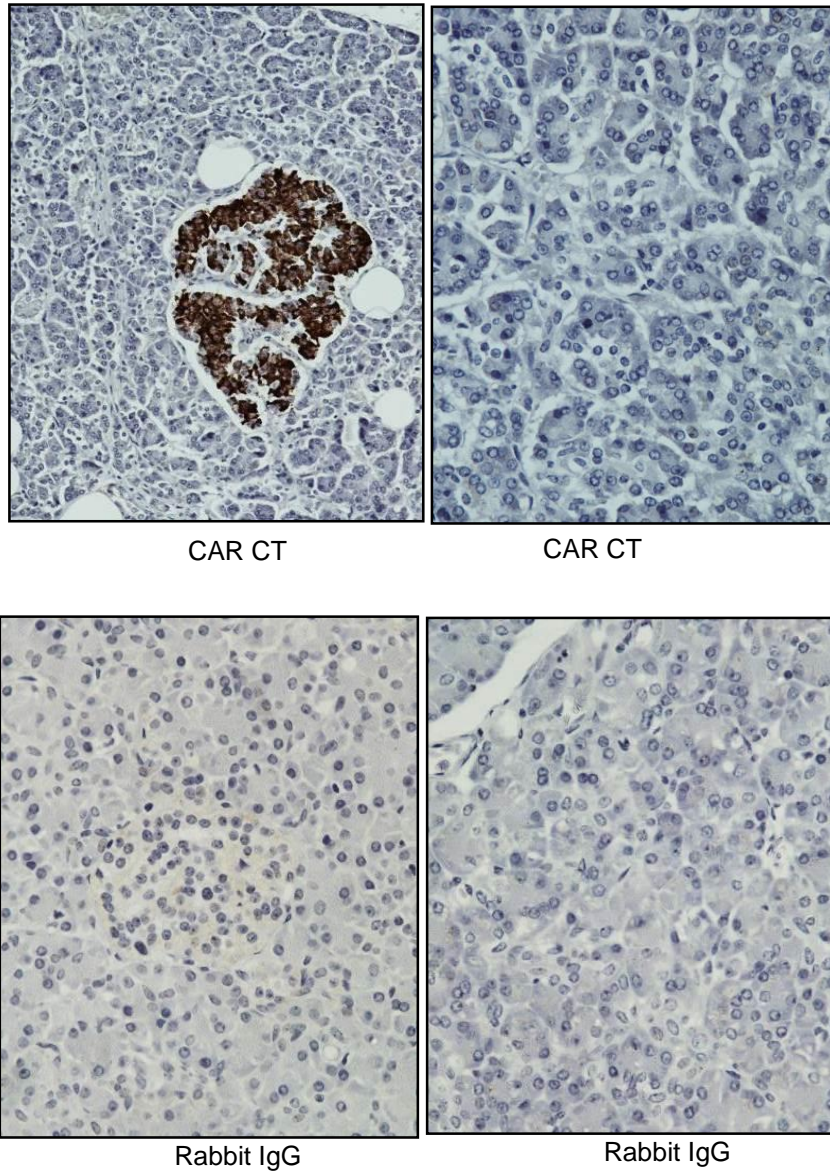


Figure 3.12 CAR isoform is detected in the islet and not in the exocrine tissue utilising CAR CT antiserum in NDA pancreas.

Immunohistochemical images revealed brown immunostaining with CAR CT antiserum (Upper panel) detected in only islets(left hand side) while rabbit IgG (Lower panel) negative control antiserum is negative in both the islet and exocrine pancreas. Data are representative of at least three donors, Scale bar 20µm

In order to begin to estimate the extent of expression of CAR isoforms in human pancreas, the chromogen detected under the bright field microscope was quantified using a method which measures the Reciprocal intensity (RI) of the brown stain (Nguyen et al., 2013). In this approach, standard colour images acquired by bright field microscopy are deemed to have a maximum intensity value of 250 (for white/unstained areas) as measured by a function in the Fiji software available within Image J. By contrast, the target chromogen and haematoxylin stained areas have lower intensity values which are inversely correlated with the amount of antigen present. RI is derived by subtracting the intensity of staining measured within a selected stained region of interest (ROI) from the maximum intensity (250). This then serves as a reference resulting in a value for RI that correlates with the amount of chromogen and/or haematoxylin present in that region of the sample (Nguyen et al., 2013), with the higher the value the more intense the stain. Using this method, it was revealed (*Figure 3.13A*) that all three CAR antisera labelled the islets to an equivalent extent while the rabbit isotype control yielded a much lower value (as expected). By contrast with the data obtained from islets, differential staining intensities (indicative of differential CAR expression) were detected in the exocrine pancreas (*Figure 3.13B*). Most significantly, the staining intensity measured after treatment with the CAR CT antiserum was equivalent to that measured with the isotype control, thereby implying that the epitope detected by this antiserum (i.e. the CAR-SIV isoform) is absent from the exocrine pancreas (*Figure 3.12*)

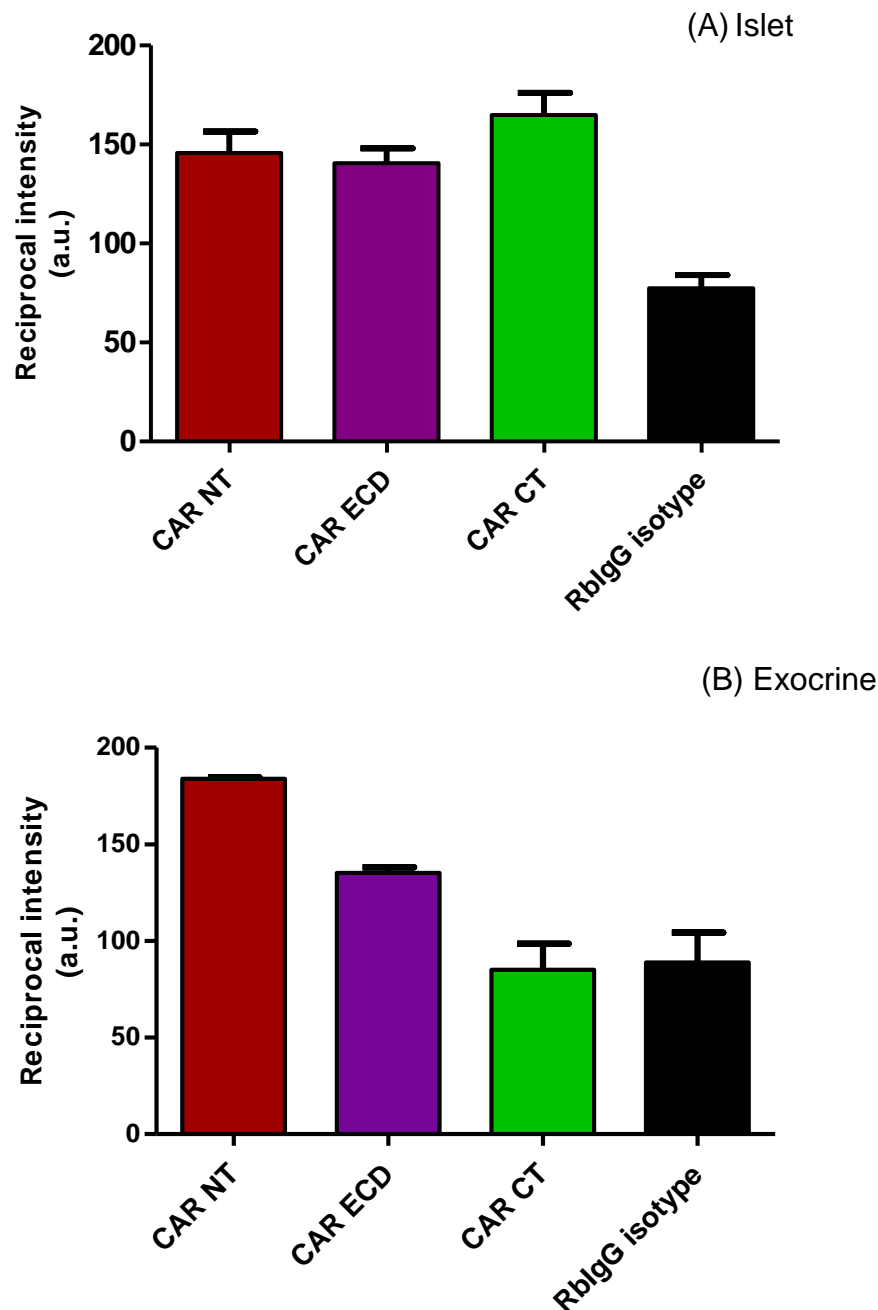


Figure 3.13 CAR isoform expression estimated by reciprocal intensity demonstrates that staining with CAR CT antisera detects high levels of CAR expression in the islets and not in the exocrine

The reciprocal intensity was utilised to quantify the extent of CAR isoform expression from the immunohistochemical images in (Fig.3.11 and Fig 3.12). The higher the values, the higher the staining with CAR antisera in the tissue. (A) Staining with CAR antisera (CAR CT, CAR ECD and CAR NT) detects high levels of CAR in the islets and no rabbit IgG staining in the islets while (B) staining with CAR antisera (CAR NT and CAR ECD) are present at high and moderate levels respectively in the exocrine tissue but staining with antisera (CAR CT and rabbit IgG) are negative. Each bar graph represents 6 images from tissue samples stained with the different CAR antisera and Rabbit IgG. Each dataset is represented as (mean \pm SEM). Arbitrary unit (a.u)

3.2.5 Detection of CAR isoform protein expression by immunofluorescence analysis in human pancreatic tissue

Immunohistochemical analysis of human pancreas sections has revealed that the islets express high levels of the CAR-SIV isoform of CAR and that this isoform is absent from the exocrine pancreas. However, examination of staining pattern suggests that, although a large number of hormone expressing cells are immunopositive, not all islet cells express this isoform. Examples of islets cells which are immunonegative for CAR-SIV are indicated by the yellow arrows (Figure 3.14)

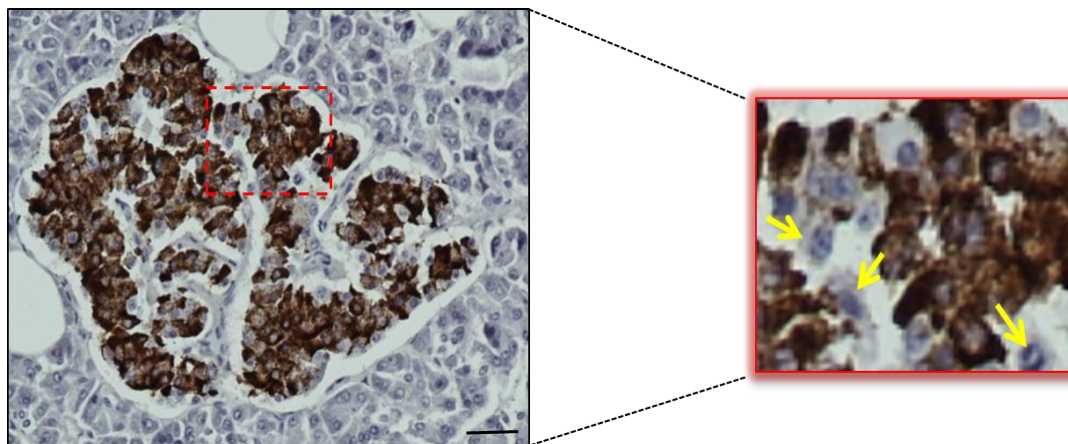


Figure 3.14 The CAR-SIV isoform is absent in some endocrine cells of the islets. The magnified image (red box) revealed that CAR-SIV (anti-CAR CT; brown stain) is not detected in some endocrine cells of the islets (yellow arrows), data are representative of three independent donors. Scale bar 20 μ m

Therefore, to determine which of the islet cell subtypes may preferentially express the different CAR isoforms, “combined immunofluorescence microscopy” was employed. This method enables the direct visualisation and localisation of antigens within a given cell or tissue. By employing the CAR CT antiserum in combination with anti-insulin (to label beta cells) and anti-glucagon (alpha cells), this allowed the subsets of endocrine cells expressing this particular isoform to be determined. Intriguingly, the CAR CT staining was present only within the insulin producing beta cells (*Figure 3.15A*), suggesting that the CAR-SIV isoform was expressed solely in these cells. Non-beta cells in the islets were immunonegative for the CAR-SIV isoform. Staining with anti-glucagon antibody to identify alpha cells confirmed these findings (*Figure 3.15B*). In summary, these results demonstrate that the CAR-SIV isoform is expressed exclusively in human beta cells in the pancreas tissue.

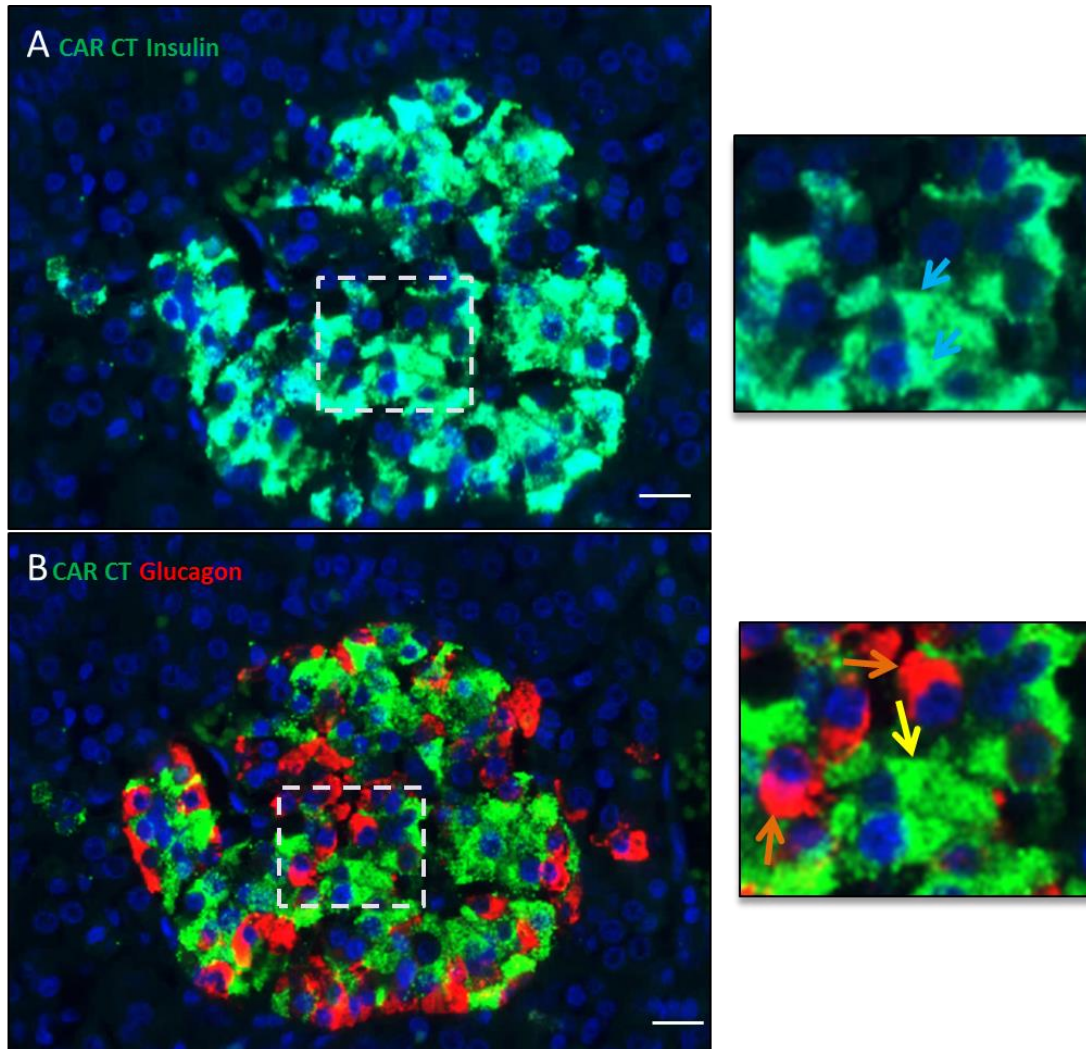


Figure 3.15 Immunofluorescence images demonstrate that CAR-SIV is present in the beta cells

(A) CAR-SIV (anti-CAR CT; green) is detected in insulin (anti-insulin; light blue) containing beta cells; magnified images (light blue) show insulin and CAR-SIV (B) CAR-SIV is not detected in glucagon positive (anti-glucagon; red) alpha cells, magnified images of CAR-SIV (yellow arrows), glucagon (orange arrows). Nuclei was stained with DAPI (dark blue). Data are representative of three independent donors, Scale bar 25 μ m

3.2.6 Detection of other CAR isoforms by immunofluorescence analysis in human pancreatic tissue

To ascertain if, in addition to CAR-SIV, other CAR isoforms are also expressed at the protein level in human pancreas, a comparison was made between the staining obtained with the CAR CT antiserum (detects CAR-SIV only) and that seen with antiserum that recognises the extracellular domain of CAR (CAR ECD) and can label multiple isoforms (CAR NT)

Table 3.7 CAR antisera and their predicted CAR isoforms

Antisera	Predicted isoforms based on epitope recognised
CAR CT	CAR-SIV
CAR ECD	CAR-SIV CAR-TVV CAR 4/7 & CAR 3/7
CAR NT	CAR-SIV CAR-TVV CAR4/7 CAR 3/7 & CAR 2/7

It was revealed that positive immunostaining with CARNT was detectable (albeit weakly) in some endocrine and exocrine cells (*Figure 3.16*) compared to the immunohistochemistry analysis in (*Figure 3.11*). Based on the inconsistencies obtained in the IHC and IF staining with the CAR NT antiserum, it was deemed unsuitable and therefore discontinued in this study. CAR ECD staining was detected in the beta cells of most islets, where it co-localised with insulin. Positive staining was not observed in alpha cells as assessed by co-labelling with anti-glucagon (*Figure 3.16*). Unlike the earlier immunohistochemistry experiments where the Envision HRP system was utilised to visualise the immunostaining of CAR by deposition of a precipitated chromogen (*Figure 3.11*), there was limited/

no labelling in the exocrine regions when immunofluorescence methods were employed (*Figure 3.16*). One potential reason for this could be that the protein expression of the relevant CAR isoforms in the exocrine tissue is low and this leads to loss of sensitivity when employing immunofluorescence approaches. The IHC protocol utilises a secondary antiserum having a dextran backbone containing multiple HRP molecules and as such, it acts to amplify the HRP signal. In contrast, in immunofluorescence the primary antiserum is recognised by a fluorescently-conjugated secondary antibody, which contains a single fluorophore, so no signal amplification is achieved. This means that weakly expressed proteins may not be detected efficiently using these reagents.

Summing up the data generated by the immunostaining patterns; the expression profiles of CAR isoforms using the semi-quantitative method could be deduced as follows; the CAR-SIV isoform of CAR is expressed strongly and exclusively in the beta cells of the islets. The CAR-TVV isoform may be present at moderate levels in the beta cells as well as in the exocrine tissue. The soluble CAR 4/7 isoform may also be present in the beta cells and exocrine cells, but at relatively low levels (Table 3.8).

To independently validate the CAR CT antiserum staining of the “CAR-SIV” isoform, Laura Nigi from the University of Siena (Professor Dotta’s Lab), performed combined immunofluorescence staining of CAR CT, insulin and glucagon in selected nPOD cases (*Figure 3.17*). The staining achieved was directly comparable to our results using samples from the Exeter Archival Diabetes Biobank (*Figure 3.16*)

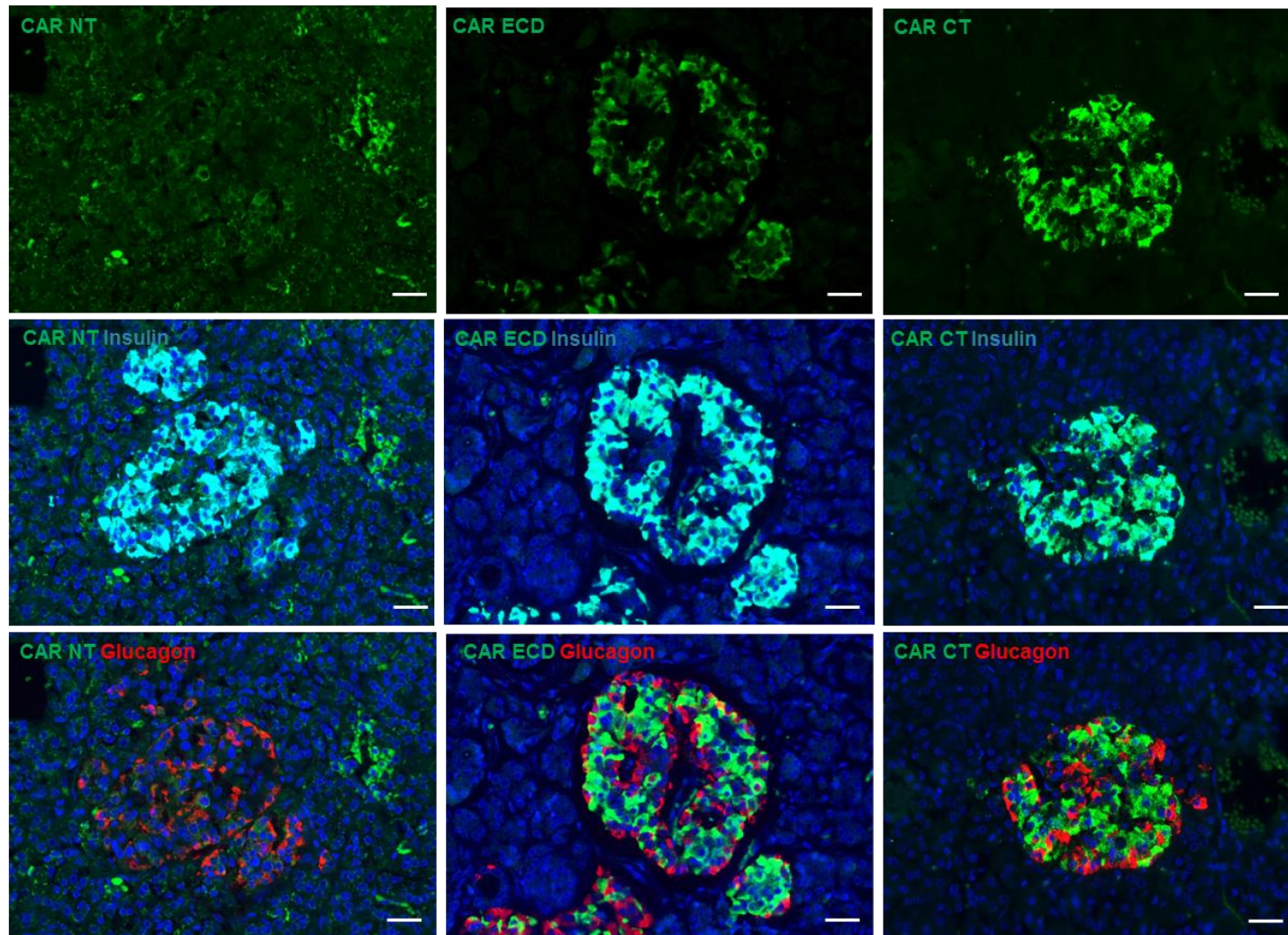


Figure 3.16 Representative immunofluorescence microscopy images of CAR isoforms in the islet. Endocrine cells and exocrine cells of a normal human pancreas detected by CAR antisera. CAR NT, CAR ECD and CAR CT antisera (green), insulin (anti-insulin; light blue) and glucagon (anti-glucagon; red), DAPI (nuclei stain, dark blue). Data are representative of three independent donors. Scale bar 25µm

Table 3.8 Summary of CAR antisera staining pattern using the semi-quantitative method

Antisera	Isoform recognised	Endocrine (β cell) expression	Exocrine expression
CAR CT	CAR-SIV	+++ (Strong)	- (Negative)
CAR ECD	CAR-SIV CAR-TVV CAR4/7 CAR3/7	+++ (Strong)	+ (Weak)
CAR NT	CAR-SIV CAR-TVV CAR4/7 CAR3/7 CAR2/7	++ (Moderate)	++(Moderate)

Table 3.9 Autoantibody positive, type1 diabetes and normal cases

Case ID	Case Type	Cohort	Age	Sex	Duration of disease
6098	Diabetes	nPOD	17.8	M	-
6153	No diabetes	nPOD	15.2	M	-
6027	AAb+	nPOD	18.8	M	-
6167	AAb+	nPOD	37	M	-

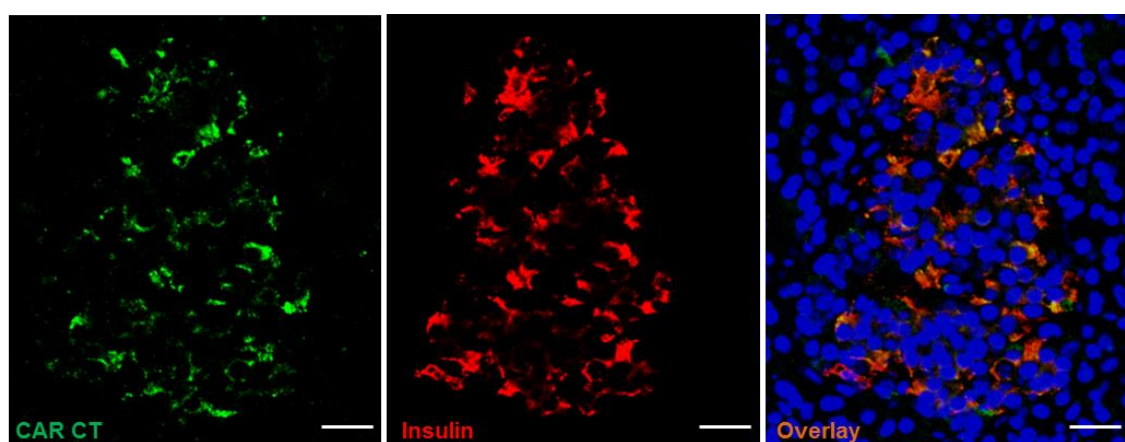


Figure 3.17 Immunofluorescence images provide independent confirmation of CAR-SIV isoform in the beta cells from an autoantibody positive non-diabetic case

Representative images displaying CAR-SIV (anti-CAR CT ; green) in insulin containing beta cells (anti-insulin; red), DAPI (dark blue; nuclei) in the human pancreatic tissue. Data are representative of two independent donors. Scale bar 25 μ m. Courtesy of University of Siena.

3.2.7 CAR isoform expression by Western blotting

In addition to the antisera utility for immunohistochemical studies, the CAR CT and CAR ECD antisera are also both approved for use in Western blotting. Therefore, to further confirm the presence of CAR isoforms in the human pancreas, proteins were extracted from isolated human islets, two human beta cell lines (EndoC- β H1, 1.1B4) and a human pancreatic ductal cell line (PANC-1). Cell lysates were electrophoresed on poly-acrylamide gels then transferred onto a PVDF membrane. Following a blocking step, the membranes were probed with either CAR ECD or CAR CT antisera. Probing with the CAR CT antiserum revealed a band running approximately 40kDa (equivalent to the calculated molecular weight) in isolated human islets. A similar (but less intense) band was also seen in the human beta (EndoC- β H1, 1.1B4) and ductal (PANC-1) cell line models (*Figure 3.18A*). A lower 20kDa band was also observed which has been demonstrated in previous study to be a cleavage product by γ -secretase (Houry et al 2013). The CAR ECD antiserum labelled an appropriately 40kDa band (corresponding to the expected size) which was more intense in isolated human islets compared to EndoC- β H1, 1.1B4 and PANC-1 cells (*Figure 3.18B*). With the CAR ECD, the results also show an intense band at a lower molecular weight estimated to be ~32kDa in 1.1B4 cells which was present, but much weaker in extracts of EndoC- β H1 cells. This observed lower fragment may be due to the shedding of CAR extracellular domain into the extracellular space by Metalloproteases such as A Disintegrin and metalloprotease (ADAM10) known to cleave cell surface protein receptors (Huovila et al., 2005).

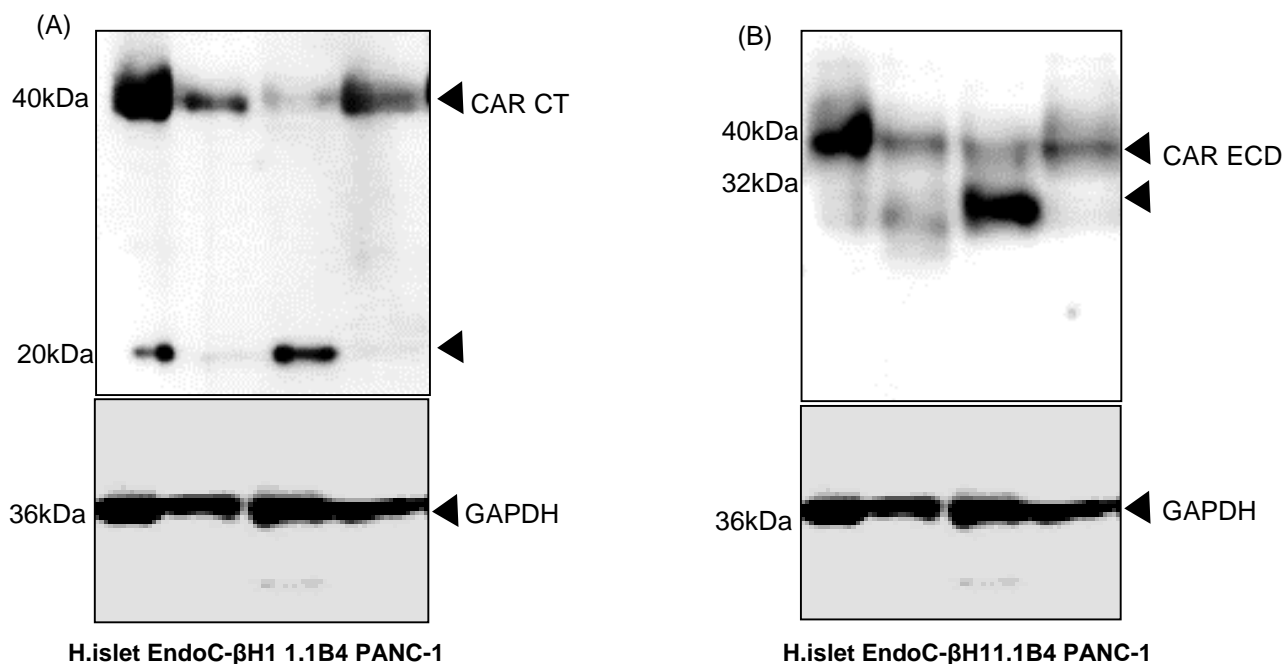


Figure 3.18 Western blot analysis utilising the CAR CT and CAR ECD antisera detects CAR-SIV in isolated human islets, 1.1B4, EndoC-βH1 and PANC-1 cell lines

EndoC-βH1, 1.1B4, PANC-1 cells and isolated human islets were lysed and total protein was isolated for western blotting to detect CAR CT and CAR ECD. β-actin was used as a loading control. (A) Detection of band size estimated at (40kDa) for CAR-SIV isoform (anti-CAR CT), lower 20kDa molecular weight bands are cleavage product by γ-secretase observed in isolated human islets, EndoC-βH1 and 1.1B4 cells. (B) CAR ECD antiserum detects a band at approximately (40kDa) implying detection of the CAR-SIV isoform and the lower fragments are cleavage products by ADAM10 present in EndoC-βH1 and 1.1B4 cells. Loading control GAPDH at 36kDa. Blot images are representative of three independent experiments

Overexpression of ADAM10 in the human glioma U251N cell line stably expressing CAR and murine embryonic hippocampal neurons endogenously expressing CAR led to shedding and increased shedding of CAR respectively, as detected by a band on a Western blot of approximately 32kDa (Houri et al., 2013). Accordingly, ADAM10 expression in the human pancreatic tissue and human pancreatic beta cell lines was assessed in the next section 3.2.8. With the CAR CT, there were smaller CAR fragments visualised by lower bands observed at an estimated size of 20kDa in isolated human islets, weaker in EndoC- β H1 and more intense in 1.1B4. It has been reported previously that cell surface protein such as CAR that can undergo extracellular domain shedding could also undergo regulated intramembrane proteolysis (RIP) cleavage by γ -secretase complex leading to the release of their intracellular domains into the cytosol. A study by Houry *et al* (2013) also demonstrated that apart from the full length CAR observed in U87 CAR cell lysates, two lower C terminal fragments of approximately 20kDa (CTF1) and 14kDa (CTF2) were also detected (Houry et al., 2013). It was further observed that inhibition of the γ -secretase led to a decrease in CTF2 and CTF1 levels. This could represent the lower molecular weight band detected by the CAR CT antisera, particularly in the 1.1B4 cells (*Figure 3.18A*). Together, these data imply that the CAR-SIV isoform is highly expressed in isolated human islets and is also expressed in EndoC- β H1, 1.1B4 and PANC-1 cells. The data also show that CAR can be cleaved in both human islets and human pancreatic beta cell lines. The CAR ECD antiserum could potentially detect CAR extracellular domain shedding and the CAR CT antiserum could detect intramembrane proteolysis (RIP) cleavage of the C terminal in isolated human islets and the pancreatic beta cell line EndoC- β H1 and 1.1B4.

3.2.8 Detection of ADAM10 expression in isolated human islets, human pancreatic tissue and beta cell line EndoC-βH1

To assess the expression of ADAM10, Prof. Decio Eizirik performed RNAseq analysis in isolated human islets and EndoC-βH1 cells. RNAseq data revealed that ADAM10 was expressed at high levels in isolated human islets and EndoC-βH1 (*Figure 3.19A*). Immunohistochemistry data also revealed that ADAM10 was expressed at high levels in the islets compared to the exocrine tissue of the pancreas (*Figure 3.19B*). Immunofluorescence analysis revealed that ADAM10 was detected in both alpha cells (detected by anti-glucagon) and the insulin containing beta cells (detected by anti-insulin) as shown in *Figure 3.19C*.

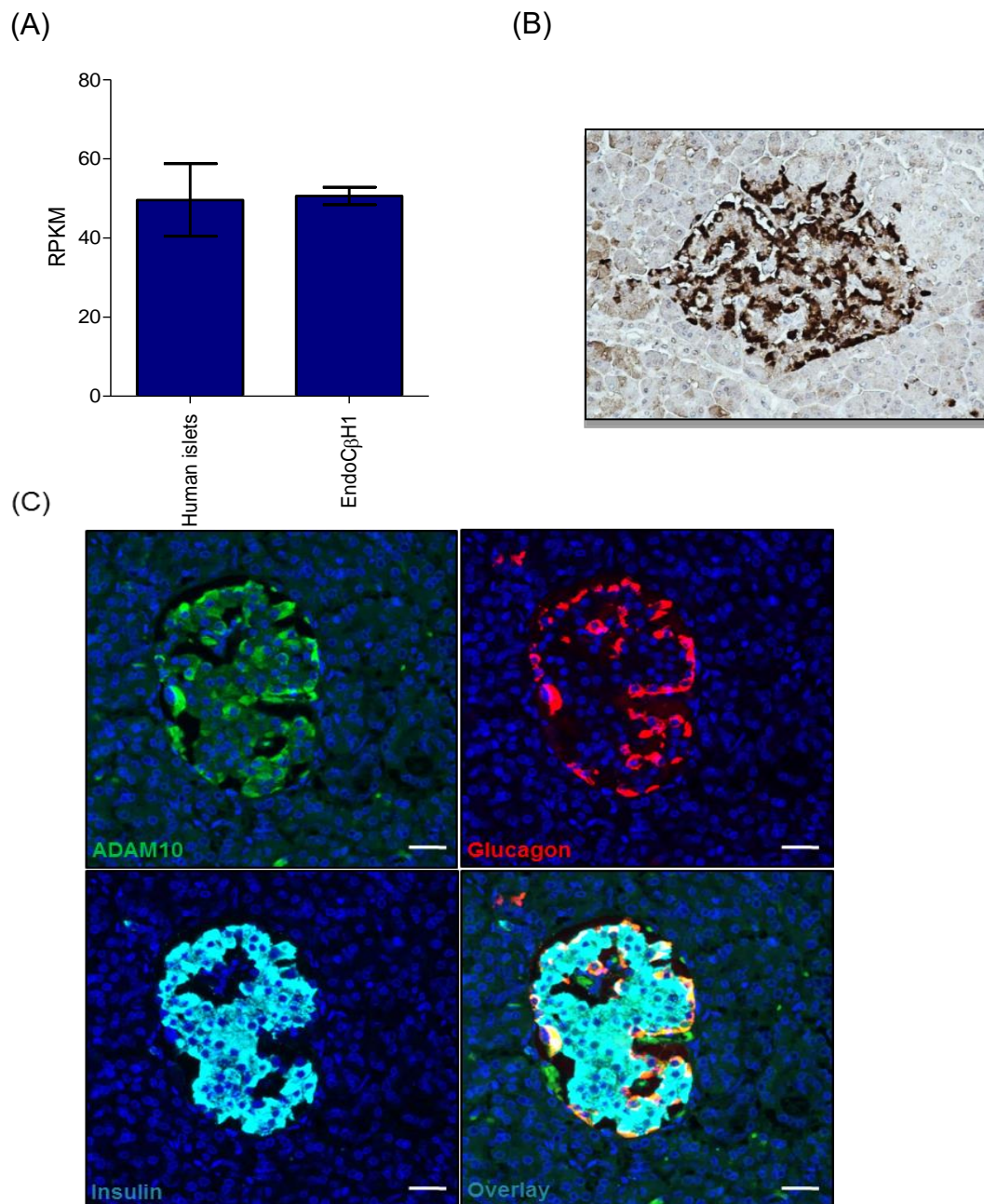


Figure 3.19 ADAM10 is expressed in isolated human islets and EndoC-βH1

Total RNA was isolated from human islets and EndoC-βH1 cells. Following quantification, 2μg of RNA was converted to cDNA. The cDNA was subsequently subjected to RNAseq analysis. ADAM10 expression was examined by IHC and IF by staining human pancreas tissue.

(A) RNAseq indicate high levels of ADAM10 in EndoC-βH1 and isolated human islets from 5 normoglycaemic islets (mean ± SEM), courtesy of Prof. Decio Eizirik (B) ADAM10 (brown stain) is expressed in the endocrine cells of the islet and (C) ADAM10 (anti-ADAM10; green) is expressed in alpha cells (anti-glucagon; red) and some beta cells (anti-insulin; light blue). Nuclei were stained using DAPI (blue) in human pancreatic tissue. Data are representative of three independent donors. Scale bar (B) 20μm (C) 25μm

3.2.9 Comparison of CAR CT and CAR RmcB antisera in human pancreatic tissue and the human pancreatic beta cell line 1.1B4

A study by Hodik *et al* (2016) demonstrated that by using an antiserum designated “CAR RmcB” that CAR was significantly higher in type 1 diabetes pancreas and autoantibody positive cases compared with normal diabetes control cases (Hodik *et al.*, 2016a). The CAR RmcB antiserum will recognise an unspecified region within the extracellular domain of CAR (*Figure 3.20*). We decided to acquire this CAR RmcB antiserum to test sequentially with CAR CT in the human pancreatic tissue and human pancreatic beta cell line 1.1B4 by immunohistochemistry and Western blotting. The results revealed that CAR CT was detected in the islet as expected but CAR RmcB was not detected in the islet or exocrine tissue of the human pancreatic tissue (*Figure 3.21A*). Also, by Western blotting CAR CT was detected but not the CAR RmcB in the human beta cell line 1.1B4 (*Figure 3.21B*)

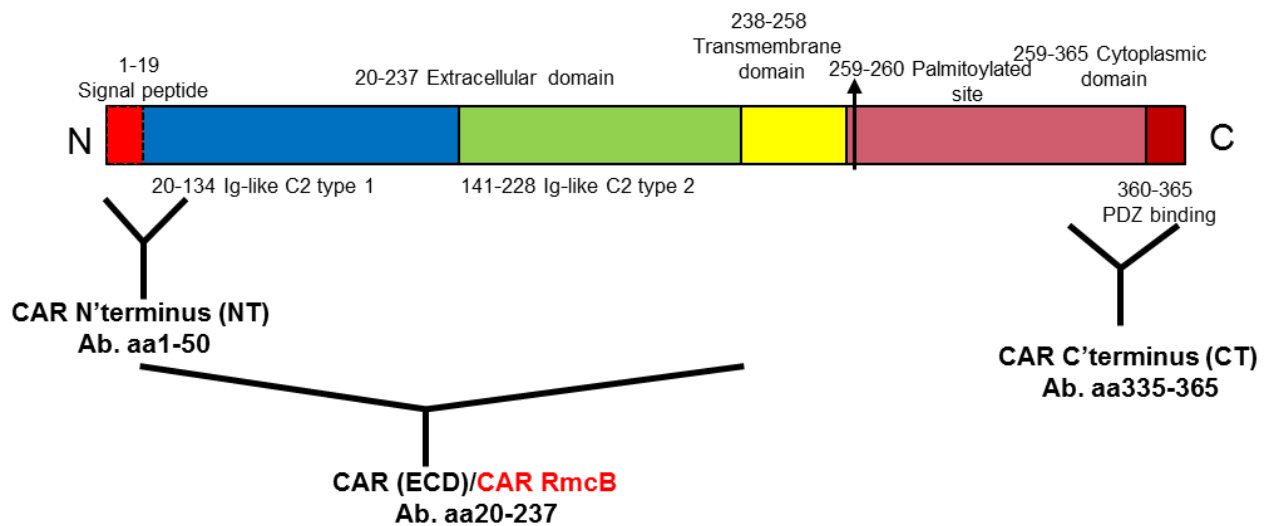
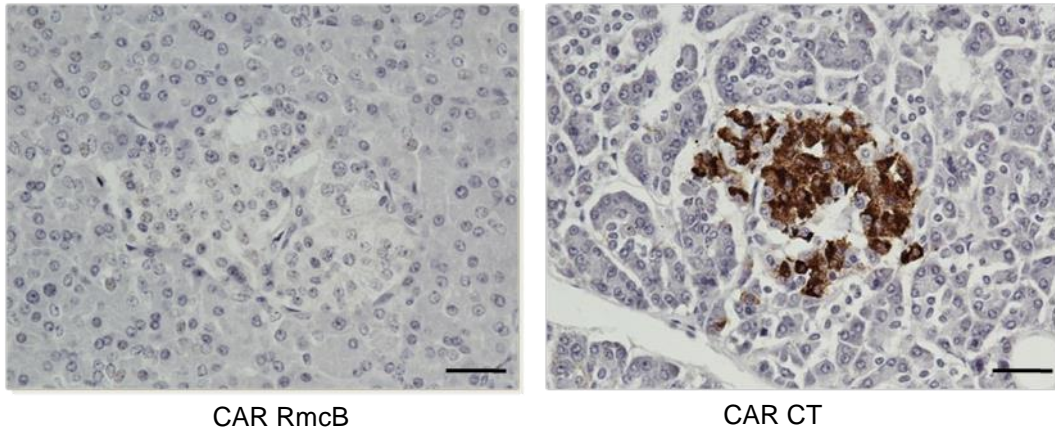


Figure 3.20 CAR RmcB antiserum epitope recognises the extracellular domain of CAR protein

(A) Pancreatic tissue



(B) 1.1B4 cells

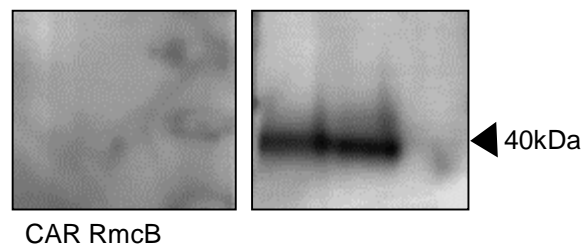


Figure 3.21 Comparison of the CAR CT and CAR RmcB antisera in the human pancreatic tissue and in the human pancreatic beta cell line 1.1B4

FFPE human pancreas tissue were subjected to IHC to detect antisera against CAR RmcB or CAR CT. 1.1B4 cells were also lysed and total protein was isolated, for western blotting to detect antisera against CAR RmcB or CAR CT. β -actin was used as a loading control (A) Staining with CAR RmcB antiserum is not detected in human pancreas tissue but staining with CAR CT antiserum is detected by IHC. Scale bar 20 μ m (B) CAR RmcB antiserum is not detected by western blotting in each lane of 1.1B4 cells but CAR CT antiserum is detected in each lane of 1.1B4 cells at an approximate size of 40kDa (black arrow head). IHC data are representative of three independent donors and western blots are representative of three independent experiments.

3.2.10 CAR-SIV isoform expression in the human pancreas

CAR expression has been reported in embryonic mice with high levels found in the brain (Honda et al., 2000b) and heart (Ito et al., 2000). Interestingly, immediately after birth CAR was shown to be rapidly downregulated at both the mRNA and protein level with no detection in adult brains (Honda et al., 2000b). To address whether CAR-SIV expression changes in the human pancreas at different times of life, we examined its expression in pancreases from non-diabetic control individuals collected across different age groups (22 cases; age range 4 weeks (neonate) to 59yrs). The pancreatic samples studied were from the Exeter Archival Diabetes Biobank (EADB) cohort. The samples were co-stained with CAR CT, anti-insulin and anti-glucagon. No differences in the CAR-SIV isoform protein expression were observed across the different spectrum of ages (*Figure 3.22*). In all of these cases, CAR-SIV was expressed exclusively in insulin positive beta cells (*Figure 3.23*) in agreement with the previous findings.

As stated above the initial staining was performed on EADB samples, which are mainly samples collected from autopsies conducted as long as 50 years ago and in which the fixation types and times were variable. To confirm that the pattern of staining was the same in pancreas material collected more recently and under standardised conditions, the CAR-SIV isoform expression was also confirmed in two further cohorts; the DiViD and nPOD collections. In complete agreement with the findings from the EADB cohort, CAR-SIV was expressed exclusively in the beta cells.

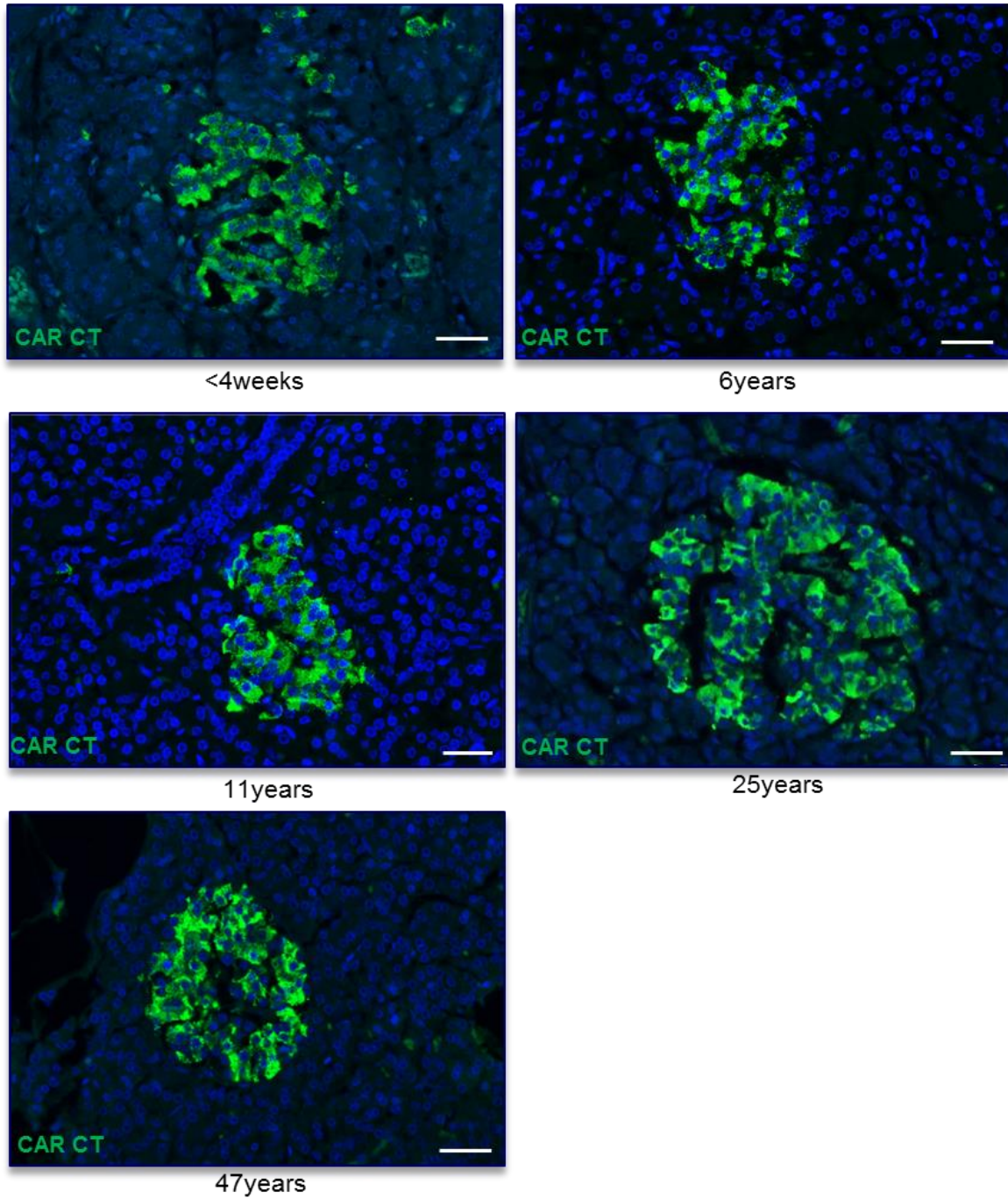


Figure 3.22 Consistent expression of CAR-SIV isoform in the islets of non-diabetes cases from neonates to adulthood.

Representative images examined by immunofluorescence analysis. This revealed that CAR-SIV (anti-CAR CT; green) expression is consistent in the islets from neonates (<4weeks) to adulthood (47years). Nuclei were stained using DAPI (blue). Data are representative of images from five donors. Scale bar 25 μ m

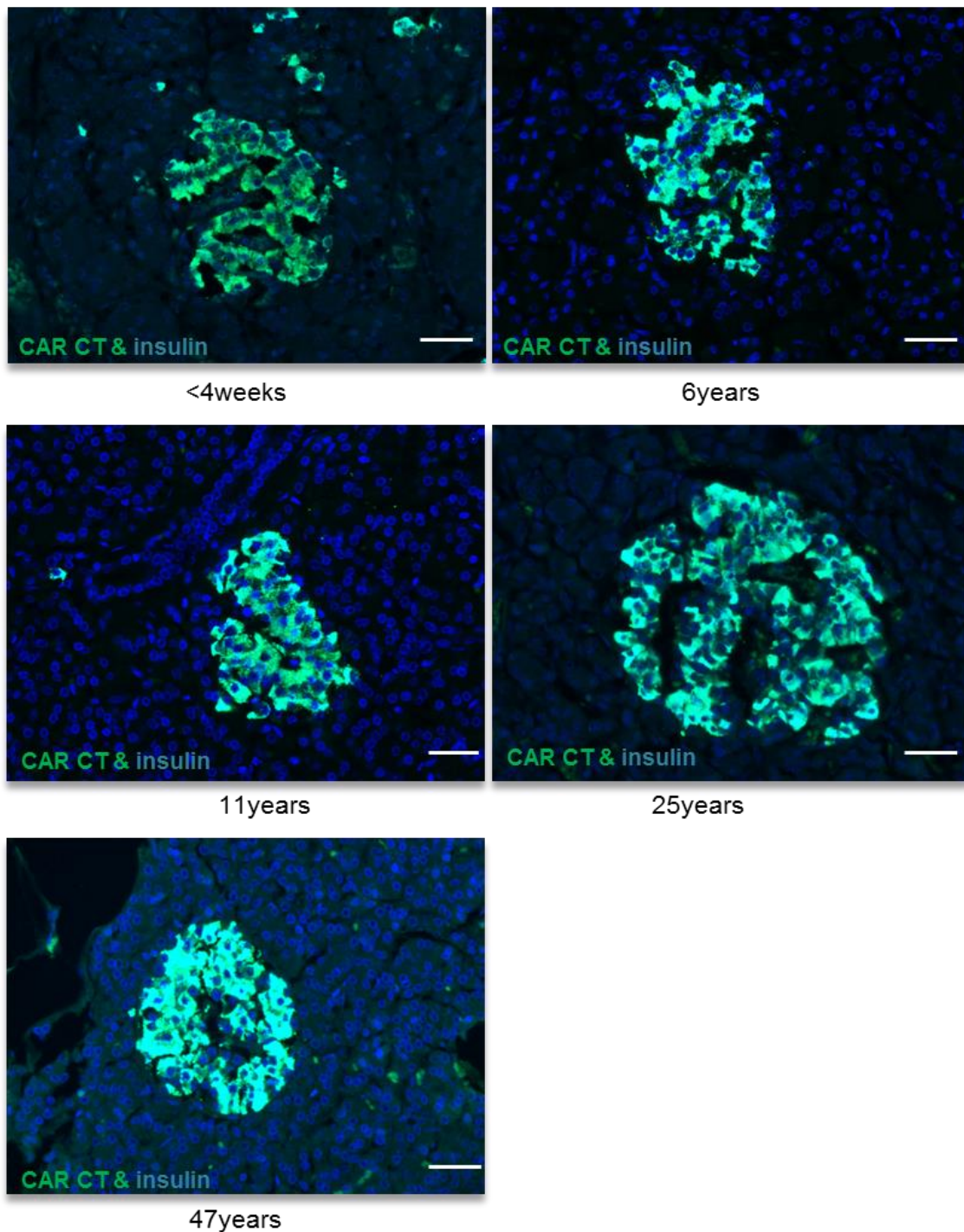
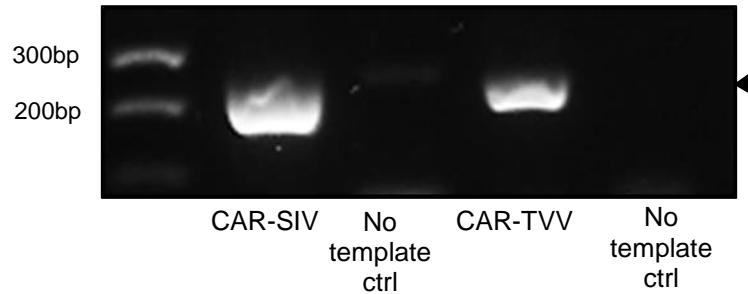


Figure 3.23 Consistent expression of CAR-SIV isoform and insulin in beta cells in non diabetic pancreas.

Representative images examined by immunofluorescence analysis. This revealed that CAR-SIV (anti-CAR CT; green) is expressed exclusively in the insulin (anti-insulin; light blue) containing beta cells in normal non-diabetes cases from neonates (<4weeks) to adulthood (47years). Nuclei were stained using DAPI (blue). Data are representative of images from five donors. Scale bar 25µm

Careful analysis of the normal pancreas tissues in the EADB samples also revealed that CAR CT and CAR ECD immunostaining was faintly detected in the ductal cells of the normal pancreas which appeared to be expressed on the surface (*Figure 3.24*). This result suggests that CAR-SIV and other CAR isoforms (CAR-TVV, CAR4/7, or CAR3/7) recognised by CAR ECD antiserum may be expressed at low levels in the ductal cells of the pancreas. To confirm at the RNA level, if the transmembrane CAR isoforms are both expressed in the ductal cells, RT-PCR analysis on the ductal cell line, PANC1, with the isoform specific primers to specifically amplify CAR-SIV and CAR-TVV was employed. As shown in *Figure 3.24*, the primer pair designed to amplify CAR-SIV yielded an intense band size at approximately 250bp and those against CAR-TVV generated a smaller band at approximately 230bp. This implies that both the CAR-SIV and CAR-TVV are both expressed in the ductal cells

(A) PCR



(B) IHC

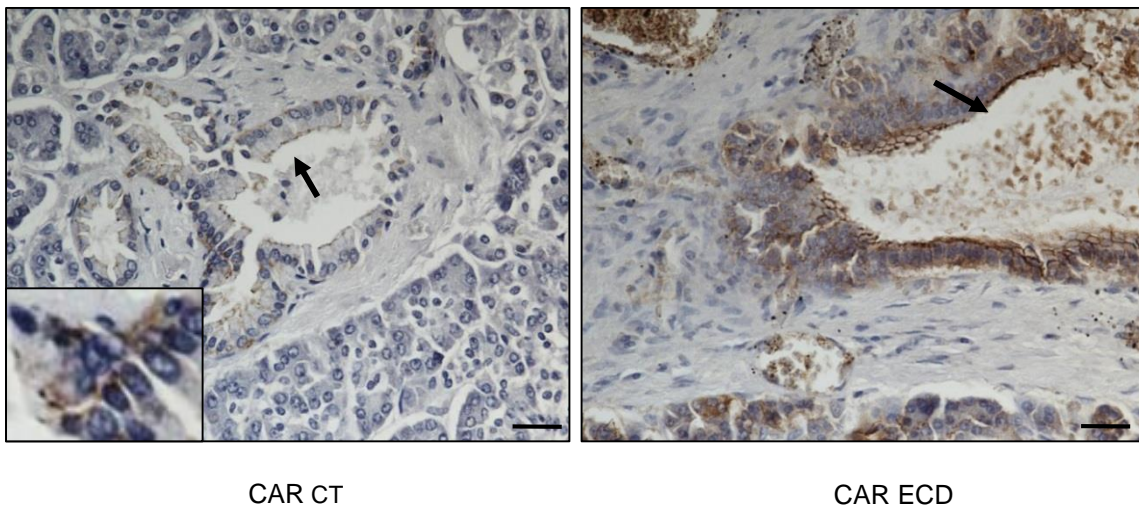


Figure 3.24 CAR isoforms expression in the ductal cells of the human pancreas.

Total RNA was isolated from cell lysates of PANC-1 cells. Following quantification, 1µg of RNA was converted to cDNA. The cDNA was subsequently used in a PCR reaction with specific primers designed to amplify CAR-SIV and CAR-TVV isoforms of CAR (Table 3.2). FFPE human pancreas tissue were subjected to either anti-CAR CT or anti-CAR ECD for IHC analysis. (A) RT-PCR revealed bands at 250bp for CAR-SIV and a band at 230bp for CAR-TVV in the human ductal PANC-1 cell line (B) Left panel show magnified image of immunostaining with anti-CAR CT detecting faint CAR-SIV (black arrow) on the surface of ductal cells and right panel show CAR ECD (black arrow) which detects CAR-SIV, CAR-TVV, CAR 4/7 and CAR3/7 on the surface of ductal cells. RT-PCR data are representative of three independent experiments while IHC data are representative images from at least three donors. Scale bar 20µm

3.2.11 CAR-SIV isoform expression in the pancreas of Type 1 diabetes patients

As previously noted, there is circumstantial evidence for a role of enteroviruses in the development of type 1 diabetes and a viral capsid protein (VP1) can be found in the beta cells of patients with this disease (Richardson et al., 2014). The two transmembrane isoforms, CAR-SIV and CAR-TVV are known to be capable of propagating a productive infection and we decided to investigate whether the expression of these proteins changes in the pancreases of people with type 1 diabetes (Appendix, Table 8.1). Strikingly, it was observed that the CAR-SIV isoform was labelled only in residual insulin-containing islets (ICI). In these islets CAR-SIV expression was similar to healthy controls. In contrast, CAR-SIV was not expressed in insulin deficient islet (IDI) where the beta cells have been destroyed (*Figure 3.25 & Figure 3.26*)

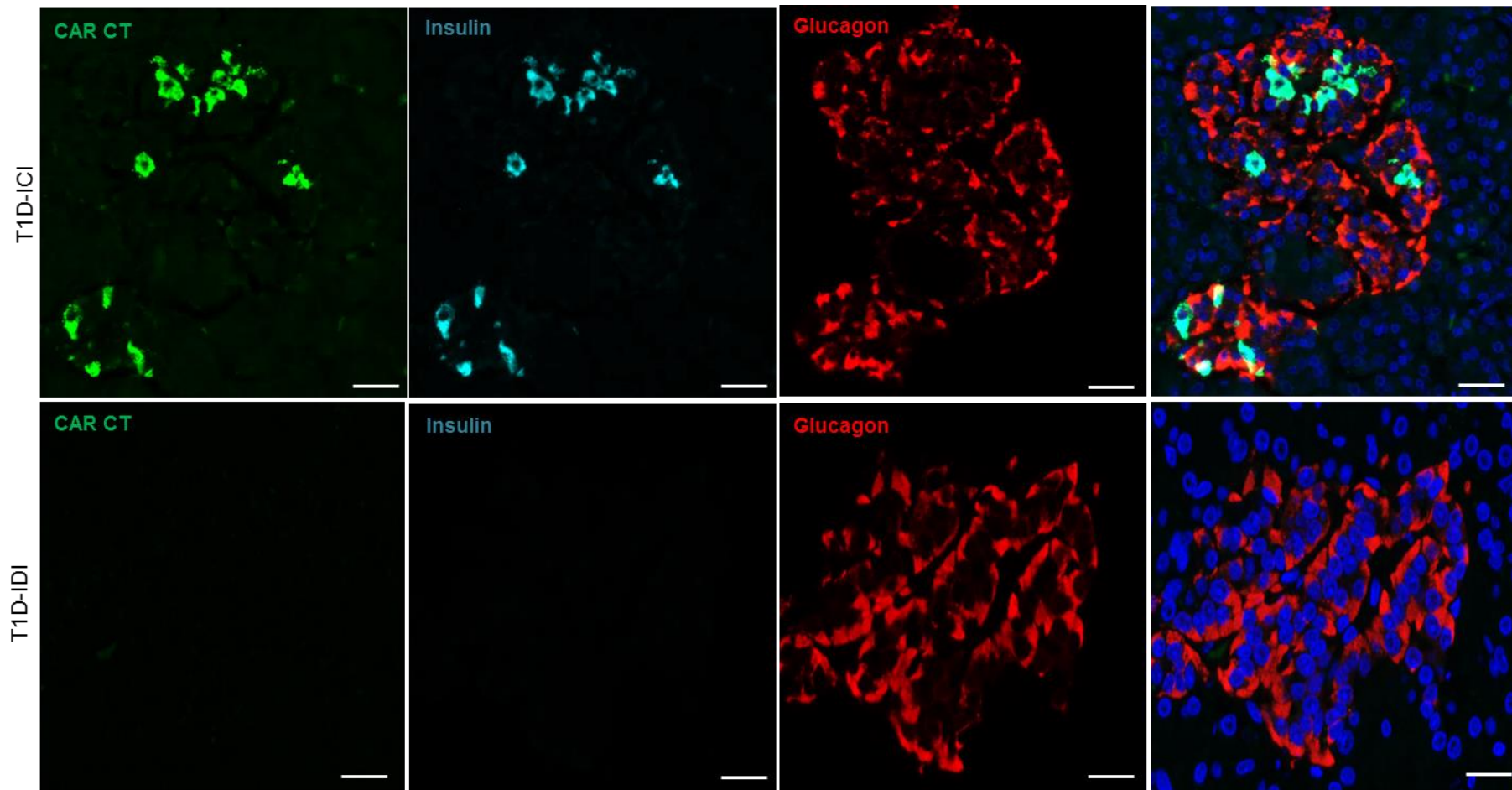


Figure 3.25 CAR-SIV is expressed in only the insulin containing islets of Type 1 diabetes cases and not in insulin deficient islets.

Representative immunofluorescence images of the CAR-SIV isoform (anti-CAR CT; green), insulin (anti-insulin; light blue), glucagon (anti-glucagon; red) and DAPI (nuclei; dark blue) in an insulin containing islet (ICI; upper panel) and insulin deficient islet (IDI); lower panel) of a type 1 diabetes case. Data are representative of images from ten independent donors, Scale bar 25 μ m

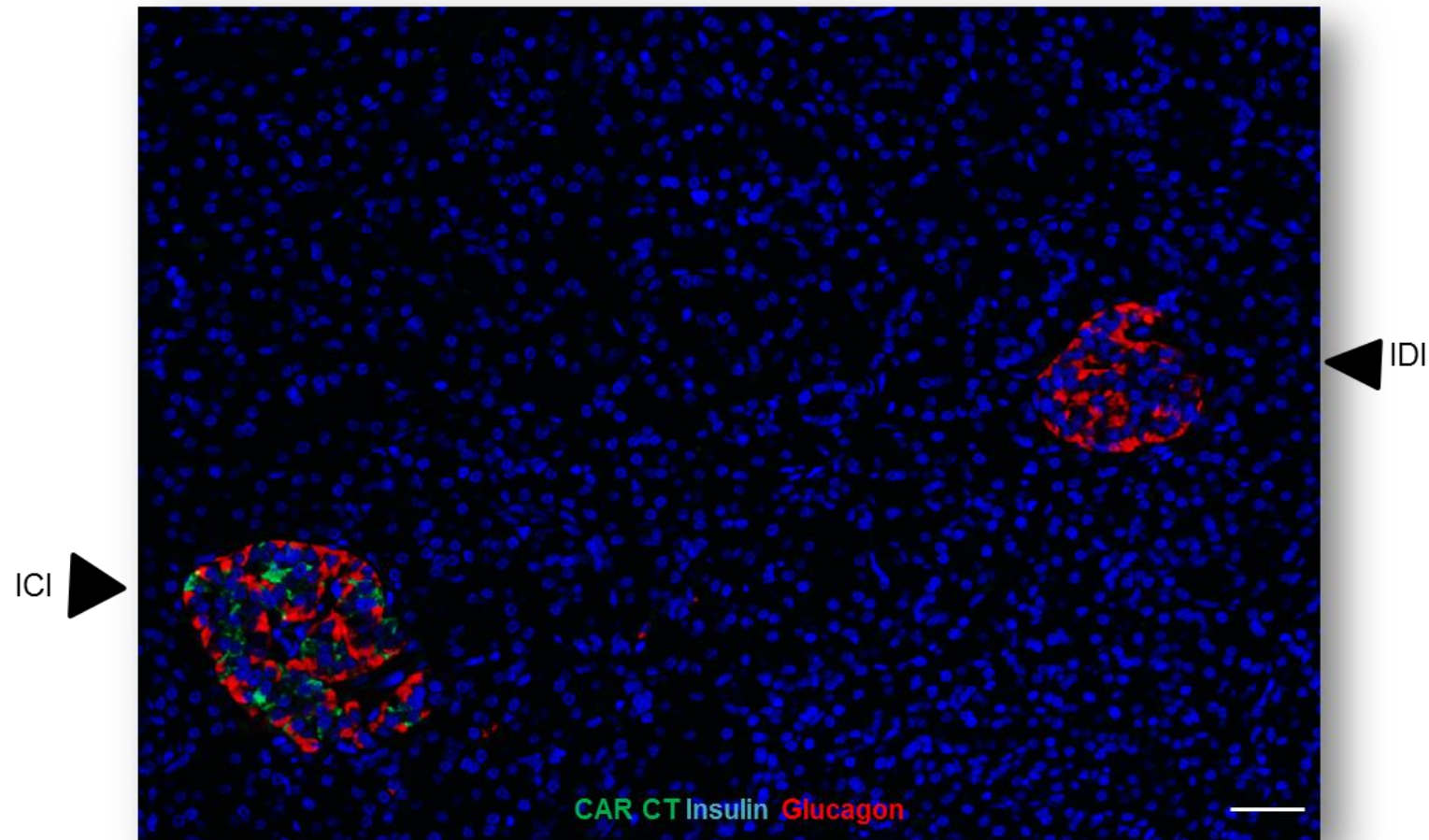


Figure 3.26 CAR-SIV is present only in insulin containing islets (ICI) and absent in insulin deficient islets (IDI)

Immunofluorescence image shows CAR-SIV (anti-CAR CT; green) in insulin containing islets (ICI) of beta cells (anti-insulin; light blue, black arrow head) and not in alpha cells (anti-glucagon; red). In contrast, the neighbouring insulin deficient islet (IDI), is negative for CAR-SIV but positive for glucagon. Nuclei were stained using DAPI (blue). Data are representative of images from ten independent donors, Scale bar 50µm

3.2.12 CAR-SIV isoform expression in the pancreas of Type 2 diabetes patients

Type 1 and Type 2 diabetes are clearly different diseases although they share certain similarities and both are defined according to the inability of affected people to regulate blood glucose levels effectively. Type 1 diabetes is characterised by the increasing loss of beta cells while in Type 2 diabetes, the pancreas tissue retains beta cells but these become progressively more dysfunctional (Lillioja et al., 1993). The aim here, was to monitor the expression of the CAR-SIV isoform in the pancreases of people with type 2 diabetes (T2D, 3 cases; 46-56years). The presence of CAR-SIV in pancreatic beta cells within the islets was confirmed and its expression did not appear to be altered when compared with normal pancreas (*Figure 3.27*)

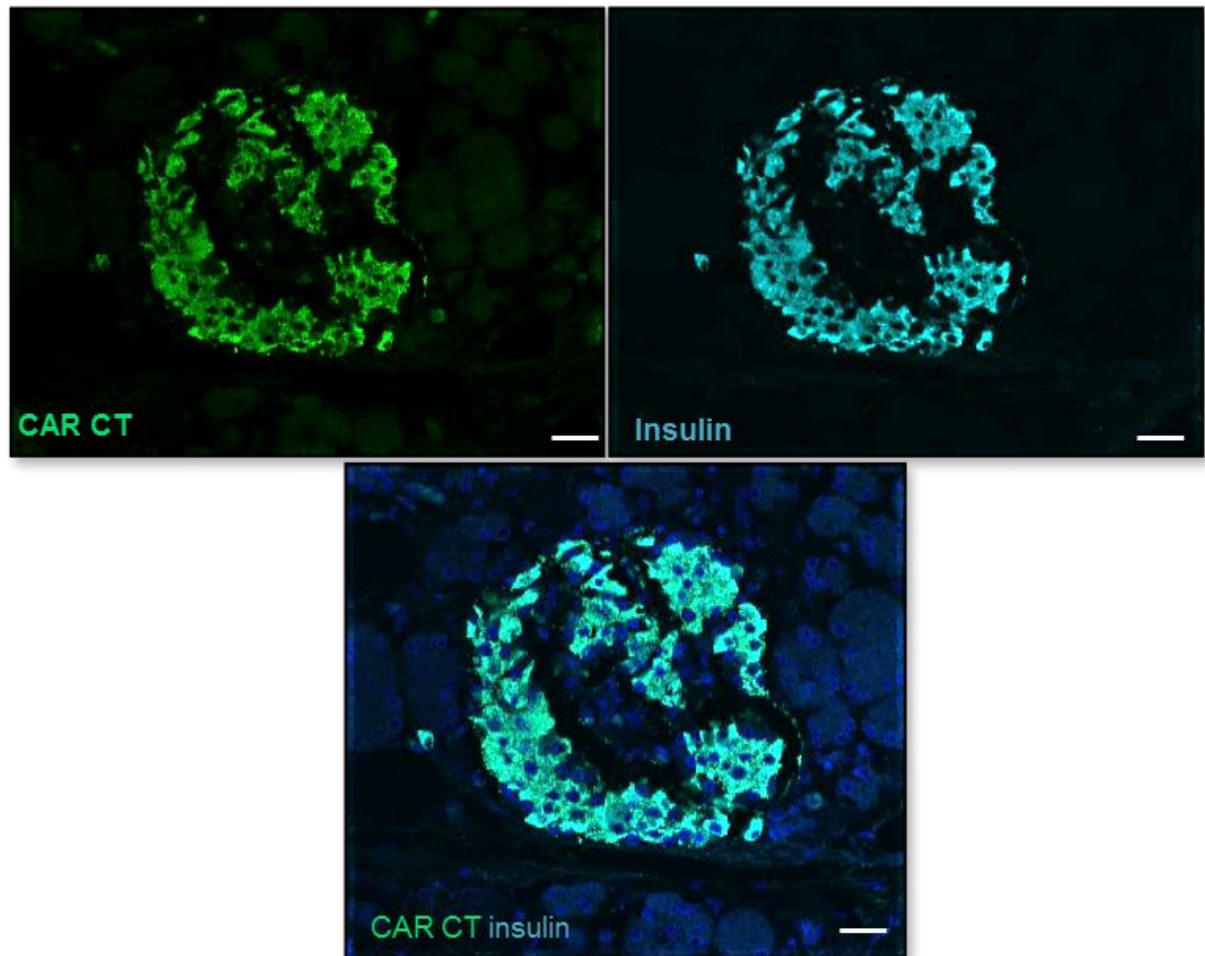


Figure 3.27 Expression of CAR-SIV is not altered in a pancreas from a Type 2 diabetes case

Representative immunofluorescence images of consistent expression of CAR-SIV (anti-CAR CT; green) in insulin containing islets (anti-insulin; light blue) and DAPI (nucleic; blue). Data are representative of images from three donors, Scale bar 25 μ m.

3.2.13 Differential staining of CAR-SIV isoform in mouse and human pancreas tissue

In acute enteroviral infection of the human pancreas, only the beta cells are infected (Berinstein et al., 1995, Roivainen et al., 2000). By contrast, when mice are inoculated with CVB viruses, the exocrine tissue is heavily infected while the islets are largely spared (Arola et al., 1995, Klingel et al., 1996, Szopa et al., 1989). Immunostaining of CVB-infected human neonatal pancreas tissue and

CVB-infected mouse pancreas tissue with an antiserum that recognises the enteroviral VP1 protein confirmed these previous observations shown in Figure 3.28, in that, VP1 expression is observed only in the islets of the human tissue (upper panel) and in the exocrine tissue of the mouse pancreas (lower panel).

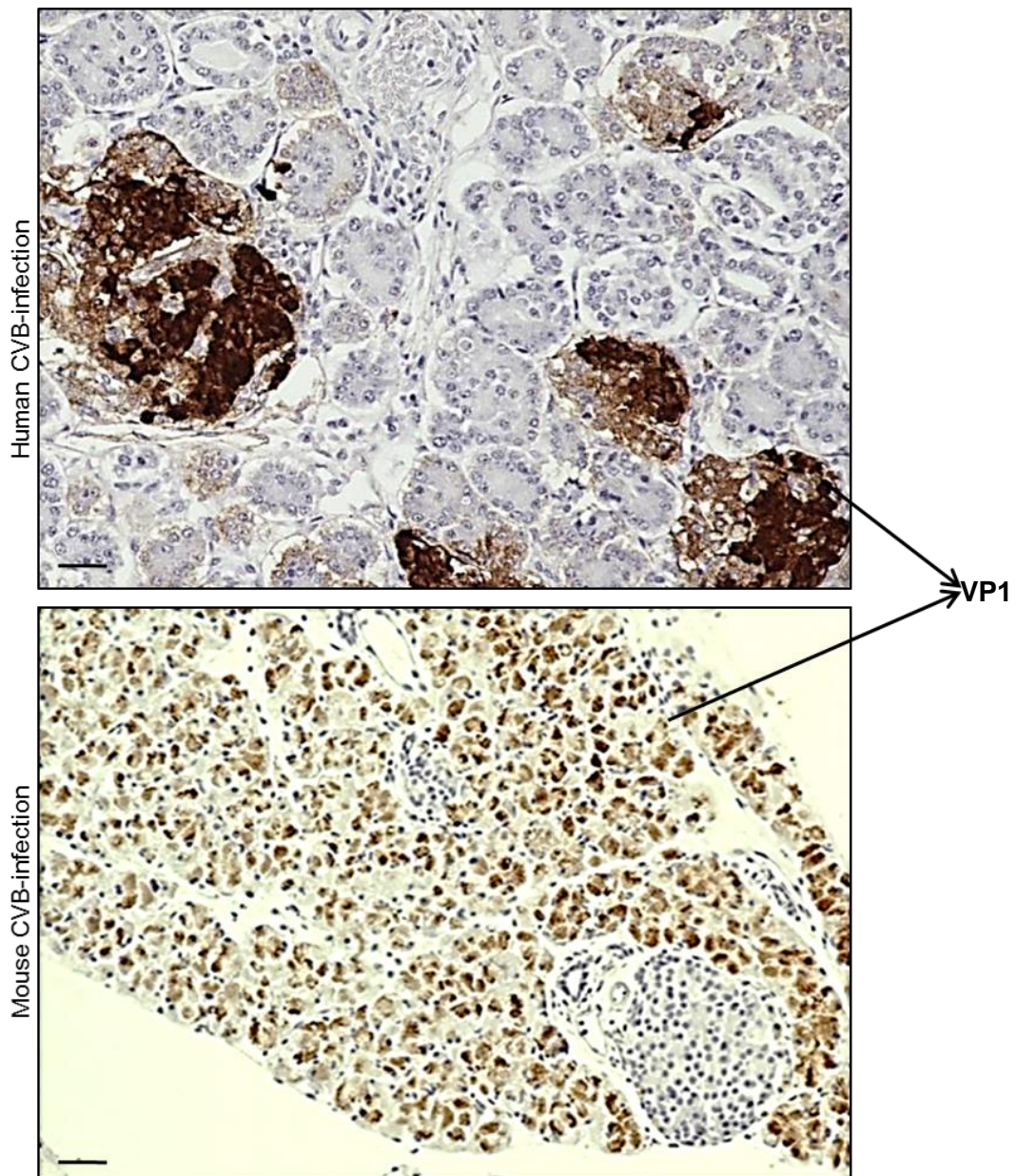


Figure 3.28 Differential enteroviral VP1 protein expression in CVB infected human and mouse pancreatic tissue

Immunohistochemical images displaying expression of enteroviral protein VP1 (black arrow) specifically in the islets of human pancreas, however, the exocrine tissue is negative (upper panel). In contrast, the exocrine tissue of the mouse pancreas is strongly VP1 positive (black arrow) whereas the islets are negative, lower panel. Data are representative of images from three donors and from three independent mice. Scale bar 50µm

To examine whether this reflects a difference in the expression of CAR in mouse and human pancreas, we utilised the CAR CT and CAR ECD antisera, both of which are capable of recognising murine CAR. Intriguingly, the CAR CT antiserum failed to label CAR-SIV in either the islets or exocrine tissue of mouse and rat pancreas (*Figure 3.29*). However, the CAR ECD antiserum, which purportedly reacts with both mouse and human CAR (according to the manufacturer) detected CAR protein in the exocrine tissue. In contrast to the cytoplasmic localisation seen in human islets, the CAR ECD staining was distributed on the surface of the exocrine cells (*Figure 3.29*). This antiserum cannot differentiate between the CAR-SIV and CAR-TVV isoforms and is capable of recognising both. Alignment of the human and mouse CAR show 93% similarity in the protein sequence for the epitope recognised by CAR CT (*Figure 3.30*) and given that specific binding epitope of the CAR CT (detects CAR-SIV isoform) was not detected in the mouse pancreas, the combined results suggest that the CAR-TVV isoform is expressed on the surface of the pancreatic exocrine cells in mouse. In stark contrast to humans, very little CAR isoform staining is observed in the islet cells. Importantly though, this distribution of expression fits with the tropism of the CVB virus in human and mouse pancreas tissue.

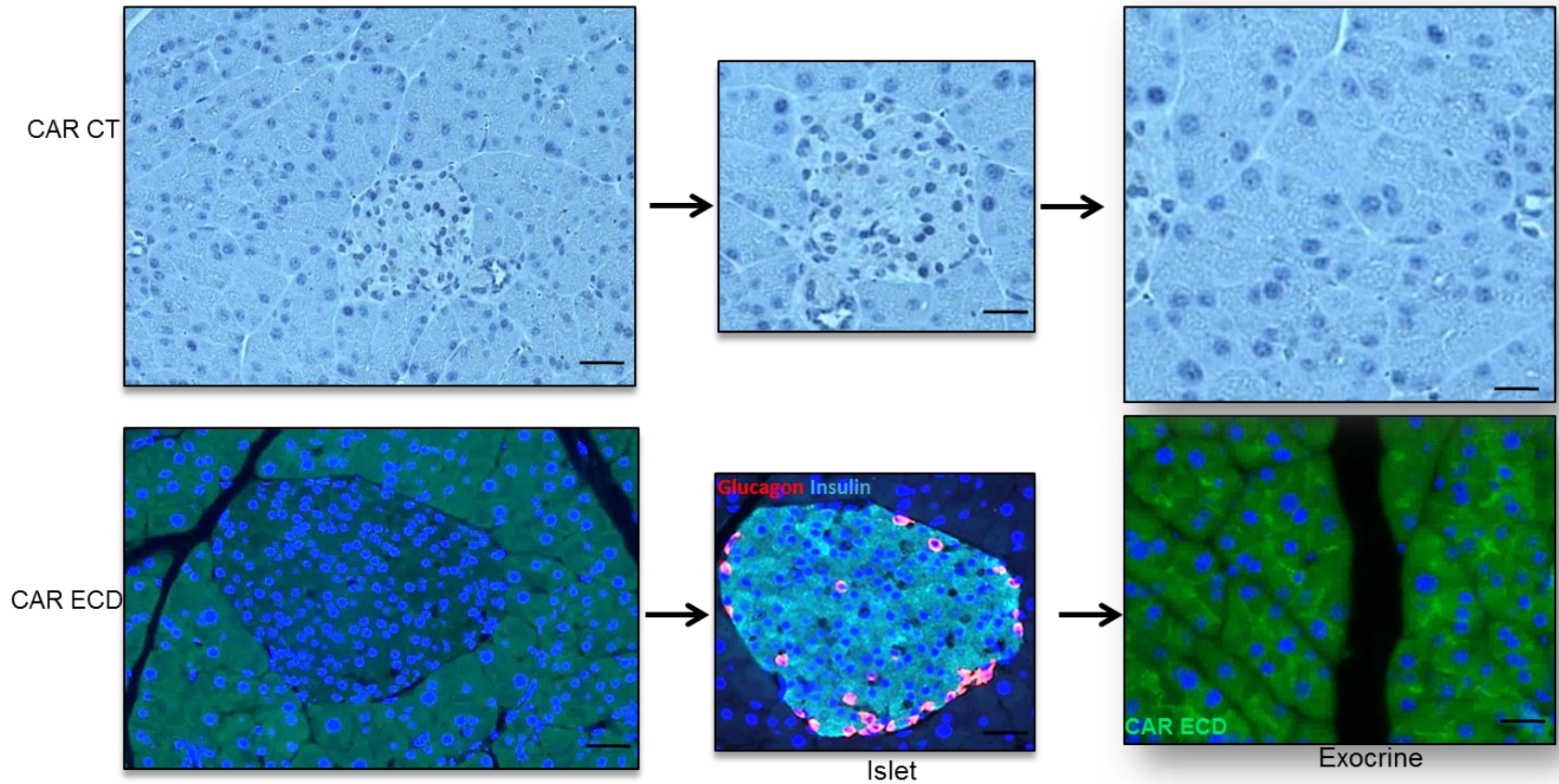


Figure 3.29 Differential immunostaining with CAR CT and CAR ECD antisera in mouse pancreas tissue.

Upper panel show that staining with anti-CAR CT (CAR-SIV) is not detected in the islet or exocrine of mouse pancreas. Lower panel revealed that staining with CAR ECD is detected in the exocrine but negative in the islet (anti-insulin; light blue and anti-glucagon; red) in mouse pancreas. Nuclei were stained using DAPI (dark blue). Data are representative of images from three independent mice, Scale bar 25 μ m.

3.3 Discussion

3.3.1 Expression of transmembrane CAR isoform in isolated human islets and beta cell lines

This current study used a range of RNA detection techniques, including RT-PCR, TaqMan qRT-PCR and RNASeq to demonstrate collectively that three CAR isoforms, which include the two transmembrane domain containing isoforms CAR-SIV and CAR-TVV, and the soluble CAR4/7 isoform are expressed in isolated human islets, laser capture microdissected (LCM) human islets and in the human pancreatic beta cell lines EndoC- β H1 and 1.1B4. The RT-PCR and RNAseq data imply that CAR-SIV is predominant. The other transmembrane domain isoform, CAR-TVV, is more moderately expressed and CAR 4/7 is expressed at only a low level in isolated human islets and in the human pancreatic beta cell line EndoC- β H1. Conversely, qRT-PCR analysis showed that in both isolated and LCM islets the two transmembrane isoforms CAR-SIV and CAR-TVV maybe expressed in equivalent amounts. It is important to note that this technique utilises high specificity TaqMan qRT-PCR with fluorescently labelled probes that will only hybridize to specific sequences (Tajadini et al., 2014). Therefore, the discrepancy in the data obtained from the qRT-PCR may be attributed to the contamination of isolated human islet cells with exocrine cells during islet isolation thereby enriching CAR-TVV expression. Unfortunately, we could not assess CAR isoform expression in the exocrine tissue, despite efforts to do so via LCM of exocrine material, due to low RNA integrity. This would have enabled further discrimination of CAR isoforms in the exocrine compartment. Hence, one limitation of this study was the inability to assess the isoforms present at the RNA level in the exocrine pancreas. A recent *in vitro* study by Hodik *et al*

(2016) utilised SYBR green based Real time PCR to demonstrate that CAR mRNA expression levels decreased linearly over a period of 12 days in isolated cultured human islets and that CAR mRNA levels were significantly reduced in isolated human islets infected with three different strains of CVB-1, compared to uninfected control islets (Hodik et al., 2016a). The relative CAR mRNA expression levels measured in that study utilised SYBR green based Real time PCR while in this thesis we employed the TaqMan qRT-PCR making it difficult to compare CAR mRNA expression in both studies. A drawback of the Hodik (2016) study is that the alternatively spliced CAR isoforms were indistinguishable because the sequences of the primers were not designed to identify the different isoforms. In conclusion, these findings are in agreement with our data in that they identify robust CAR expression in isolated human islets. Their finding that CAR levels reduce following infection is also interesting and implies that the direct infection and destruction of beta cells, could consequentially then result in a reduction of CAR expression over time.

3.3.2 Expression of soluble CAR isoform in isolated human islets and pancreatic beta cell lines

This present study also demonstrated at the RNA level that soluble CAR_{4/7} was expressed in modest amounts, while the other soluble isoforms, CAR_{3/7} and CAR_{2/7}, were barely detectable in isolated human islets or in the human pancreatic beta cell lines, EndoC- β H1 and 1.1B4. Taken together, the different RNA approaches concur that the soluble CAR_{4/7} isoform is expressed in isolated human islets, EndoC- β H1 and 1.1B4 cells. The CAR_{4/7} isoform may also be expressed in the acinar cells of the exocrine tissue and /or at low levels in the beta cell although, there was no antisera available in this present study to

specifically recognize the CAR4/7. The structure of the CAR 4/7 isoform contains a complete extracellular D1 domain and a partial D2 domain that are known to be important for CVB binding, since mutations leading to deletion of the extracellular domain in Chinese hamster ovary (CHO) cells resulted in lack of virus binding (Excoffon et al., 2005). As CAR 4/7 lacks the transmembrane domain (*Figure 3.8*) the protein is soluble and secreted from the cell and is unable to mediate infection (Dörner et al., 2004) unless, perhaps, it is internalized by an endocytic mechanism. Studies by Yanagawa *et al* (2004) and Dorner *et al* (2006) show that if mice are infected with CVB3 strains in the presence of CAR4/7 that the level of infection in myocardium and pancreas are reduced when compared to mice infected with CVB3 strains alone (Yanagawa et al., 2004, Dörner et al., 2006). The same was also seen in an *in vitro* model where HeLa cells were less susceptible to infection with CVB in the presence of CAR4/7 (Goodfellow et al., 2005). In addition, Excoffon *et al* (2014) have highlighted the possibility that CAR soluble isoforms secreted from the cells could directly interact with both Coxsackieviruses and Adenoviruses thereby acting as a decoy viral receptor reducing viral infectivity (Excoffon et al., 2014).

3.3.3 Cytokine treatment has no effect in CAR isoform expression in the isolated human islets and EndoC- β H1 cells

Study by Eizirik *et al* (2012) showed that pro-inflammatory cytokines could alter the splicing and expression of about 20% of genes present in the human islet (Eizirik et al., 2012). In the present study, RNAseq analysis of cytokine treated isolated human islets and EndoC- β H1 showed no significant changes in the various CAR mRNA isoforms (*Figure 3.9*), suggesting that there is no alteration in splicing of CAR under these conditions. qPCR analysis of isolated human islets

that had been incubated with the chemokine CXCL10 also failed to show a change in CAR expression (Hodik et al., 2016a). It is possible though that there may be other factors regulating CAR expression during a viral infection that have not been identified as Hodik *et al* (2016) also demonstrated that UV-treated culture supernatants of CVB infected human islets increased CAR mRNA expression even after 4 days of culture compared to control culture medium (Hodik et al., 2016a).

3.3.4 CAR isoform expression in the human pancreatic tissue

CAR isoform expression at the protein level was assessed using a range of different technologies (immunohistochemistry, immunofluorescence microscopy and Western blotting) with these antisera (CAR CT, CAR ECD and CAR NT).

The antibody epitopes were carefully assessed to map the different CAR antisera to the different CAR isoforms. The results demonstrate that CAR CT would recognise only the CAR-SIV isoform. In contrast, the CAR ECD could recognise CAR-SIV, CAR-TVV, CAR 4/7 and potentially also the CAR3/7 isoforms. Finally, CAR NT should recognise all of the CAR isoforms. The CAR CT antisera proved to be specific in recognising the CAR-SIV isoform in the human beta cells utilising the different approaches immunohistochemistry, immunofluorescence microscopy and Western blotting (the specificity of this antisera is investigated further in Chapter 6). However, when utilising the CAR ECD and CAR NT antisera, other CAR isoforms such as the CAR-TVV and CAR4/7, seen at the RNA level, are likely to be detected. The data presented here suggest that these isoforms could be present in the pancreatic beta cell or in the exocrine compartment as additional staining, on top of that observed with the CAR CT antisera was seen in these compartments.

The pancreatic ductal cells have also been shown to be infected by enterovirus (Ylipaasto et al., 2004, Alidjinou et al., 2017), interestingly, both staining with CAR CT and CAR ECD antisera were detected on the surface of the ductal cells in the pancreas implying the presence of CAR isoforms in these cells (Alidjinou et al., 2017). The CAR-TVV isoform may also be expressed in the other endocrine cells as well as in the beta cells, acinar and ductal cells of the exocrine pancreas but there was no specific CAR-TVV antiserum commercially available to directly test its expression in the human pancreatic tissue. Hence, another limitation in this present study was the lack of a CAR-TVV antiserum. In conclusion, the results of the antisera staining (Table 3.8) in combination with the RNA expression data, imply that CAR-SIV is the predominant isoform present in the human pancreas and that it is specifically expressed within human pancreatic beta cells.

3.3.5 CAR isoform protein expression in the isolated human islets and pancreatic beta cell lines

The Western blot analysis in this study revealed that labelling with the CAR ECD antisera recognised a molecular weight band at approximately 40kDa in isolated human islets, EndoC- β H1, 1.1B4 and PANC-1 cells. Interestingly, there were some lower band fragments in the EndoC- β H1 and 1.1B4 which have been reported in previous studies to be the cleavage products of metalloproteases such as ADAM10 (Houri et al., 2013). Indeed, our results (*Figure 3.19*) by RNAseq and immunohistochemistry revealed that ADAM10 is highly expressed in isolated human islets, EndoC- β H1, and also in the beta and alpha cells of the human pancreatic tissue. It is possible that since ADAM10 is present in the islet cells that it can access CAR-SIV and cleave the extracellular domain. One could also speculate that the lower fragments detected by the CAR antisera could be

other isoforms of CAR because the CAR ECD antiserum will be able to detect CAR-TVV and CAR 4/7. However, this is unlikely because the molecular weight of CAR-SIV and CAR-TVV cannot be distinguishable (40kDa and 39kDa respectively) and the soluble CAR4/7 has a predicted molecular weight of 28kDa which is much lower than the 32kDa band observed. Importantly, the CAR CT antiserum which only recognises the CAR-SIV isoform, produced a band of ~40kDa in isolated human islets, the human pancreatic beta and ductal cell lines. The size of the band seen with the CAR CT antiserum is comparable to that observed with the CAR ECD antiserum. If the cells were expressing high levels of the CAR-TVV isoforms, one would expect the band to be bigger in the CAR ECD probed samples, as it can recognise both CAR-SIV and CAR-TVV. This suggests that although CAR-TVV may be expressed it is unlikely to be at very high levels. The lower fragments (approx. 20kDa) detected were also seen in previous work by Houri *et al* (2013) demonstrating that after cleavage by ADAM10, CAR could undergo regulated intramembrane proteolysis (RIP) cleavage by a γ -secretase complex leading to the release of the intracellular domains into the cytosol (Houri et al., 2013). The CAR CT antiserum will be able to detect these intracellular fragments and the smaller fragment sizes observed in this present study would fit with this hypothesis. Houri *et al* (2013) posited that the extracellular domain shedding and regulated intramembrane proteolysis (RIP) may be a mechanism for CAR degradation and protein turnover. The Western blotting results confirm the microscopy findings and suggest that CAR-SIV is the predominant CAR isoform in human islets.

3.3.6 CAR isoform expression in autoantibody positive individuals without diabetes and individuals with Type 2 Diabetes

Whilst investigating CAR in the human pancreas tissue Hodik *et al* (2016) suggested that CAR expression was increased in the endocrine cells of autoantibody-positive non-diabetic donors and type 1 diabetes patients when compared to non-diabetic controls (Hodik et al., 2016a). Their study utilised the CAR RmcB antiserum which is predicted to recognise an unspecified region in CAR extracellular domain and as such these isoforms; CAR-SIV, CAR-TVV, CAR 4/7 and CAR 3/7. The data presented in this thesis (*Figure 3.21*) were not able to reproduce their findings with this particular antiserum. The CAR CT and CAR RmcB antisera were used simultaneously in several different techniques, but the anti-CAR RmcB was negative in the pancreatic tissue, as opposed to the positive staining observed with CAR CT antiserum. The CAR RmcB antiserum was also shown to not be appropriate for use in Western blotting. In Chapter 4 of this thesis, this antiserum is shown to be suitable in flow cytometry and immunocytochemistry, but not for Western blotting and IHC-paraffin protocol (IHC-P). This suggests that this antibody recognises the native form of CAR, which is further, supported by its ability to act as a blocking antibody (binds CAR in live cells) and as such can prevent CVB-infection (Ylipaasto et al., 2004). An additional limitation of the Hodik study was that they did not address which endocrine cells are expressing CAR. Having shown that the CAR RmcB antiserum was not suitable for IHC-P sections, we utilised the CAR CT antiserum in combination with anti-insulin and anti-glucagon antisera in the human pancreatic tissue from normal pancreas donors, autoantibody positive non-

diabetic donor and type 1 diabetes patients. Contrary to the data by Hodik *et al* (2016) there were no observed changes in CAR-SIV expression pattern in the human pancreatic beta cells in any of the type 1 diabetes pancreas cases (*Figure 3.25*) and there was no age related changes in the normal diabetes cases (*Figure 3.22*). Our collaborator, Dr Laura Nigi (University of Sienna) provided an independent confirmation of a similar CAR-SIV expression pattern in the human pancreatic tissues which were in agreement with what we observed (*Figure 3.23*). However, one interesting finding emerged from the study of the type 1 diabetes pancreas cases was that when the beta cells had been destroyed (insulin-deficient islets); CAR-SIV expression was completely lost. Importantly, this supports our observation that the CAR-SIV isoform is selectively expressed in the beta cells.

3.3.7 Differential CAR isoform expression in mouse and human pancreatic tissue

Experimental studies in mice have reported that Coxsackie B viruses preferentially infect the pancreatic acinar cells and not the islets (Ross *et al.*, 1974, Szopa *et al.*, 1989, Arola *et al.*, 1995, Bopegamage *et al.*, 2005a). In support of this, our findings, demonstrate that we fail to detect CAR-SIV in mouse islets at the protein level. In agreement, studies utilizing *in situ* hybridization assay in pancreatic tissue from mice failed to show any expression of CAR mRNA in the islets (Mena *et al.*, 2000, Bopegamage *et al.*, 2005b), together this may explain why mouse islets are normally spared during CBV infection. Another study using purified CAR-TVV antiserum indicated via Western blotting that mCAR1 (CAR-TVV) is highly expressed in whole mice pancreases when compared to mCAR2 (CAR-SIV) (Raschperger *et al.*, 2006). As described above,

CAR mRNA levels in mice have been observed at much higher levels in acinar cells of the exocrine tissue than in islets (Mena et al., 2000). The study by Mena *et al* (2000) did not discriminate between the different CAR isoforms present, but one could speculate that it is the CAR-TVV that is present in the exocrine cells. This is in accord with our results where staining within the pancreas was only observed with the CAR ECD antisera (detects both CAR-SIV and CAR-TVV) in the acinar cells and not with the CAR CT antisera (detects only CAR-SIV).

3.3.8 Summary:

Our data provides compelling evidence that CAR-SIV is the predominant transmembrane domain CAR isoform confined to the human beta cell and that CAR-TVV and CAR 4/7 may also be present at lower amounts in the human beta cell and/or acinar cells of the exocrine pancreas. Importantly, CAR-SIV presence in the pancreatic beta cells supports the susceptibility of these cells towards CVB replication and infection. In contrast, failure to observe the CAR-SIV expression in the islets of mice may explain why their islets are normally spared during infection.

This chapter has been able to identify a specific isoform of CAR (CAR-SIV) that is distributed in the human beta cell and also acknowledges that other CAR isoforms (CAR-TVV and CAR 4/7) may also be present in the beta and acinar cells of the human pancreas.

CHAPTER 4

Characterisation of CAR antisera using human pancreas tissue, beta and ductal cell lines

4.1 Introduction

In Chapter 3, it was demonstrated that the CAR antisera (CAR CT and CAR ECD) were both suitable for immunohistochemistry, immunofluorescence microscopy and Western blotting while the CAR RmcB antiserum was not suitable for any of these assays (Table 4.1).

Table 4.1 Summary of the utility of CAR antisera in different assays (+ suitable, -not suitable)

Antisera	CAR isoforms recognised	IHC-P/IF (FFPE)	Western blotting
CAR CT	CAR-SIV	+	+
CAR ECD	CAR-SIV CAR-TVV CAR4/7 CAR3/7	+	+
CAR RmcB	CAR-SIV CAR-TVV CAR4/7 CAR3/7	–	–

To characterise the CAR antisera (CAR CT, CAR ECD and CAR RmcB) further in this study, human pancreatic beta and ductal cell lines were employed. The “CAR RmcB” antiserum was also chosen because it had previously been utilised in immunocytochemistry (ICC) and flow cytometry to demonstrate CAR surface expression on a range of different cell lines; for example HeLa, A549, HCT, HRT18 (McDonald et al., 1999). The CAR RmcB antiserum is also predicted to be directed against an unspecified region within the extracellular domain (*Figure 4.1*) and therefore might be expected to detect CAR-SIV, CAR-TVV, CAR4/7 and CAR3/7.

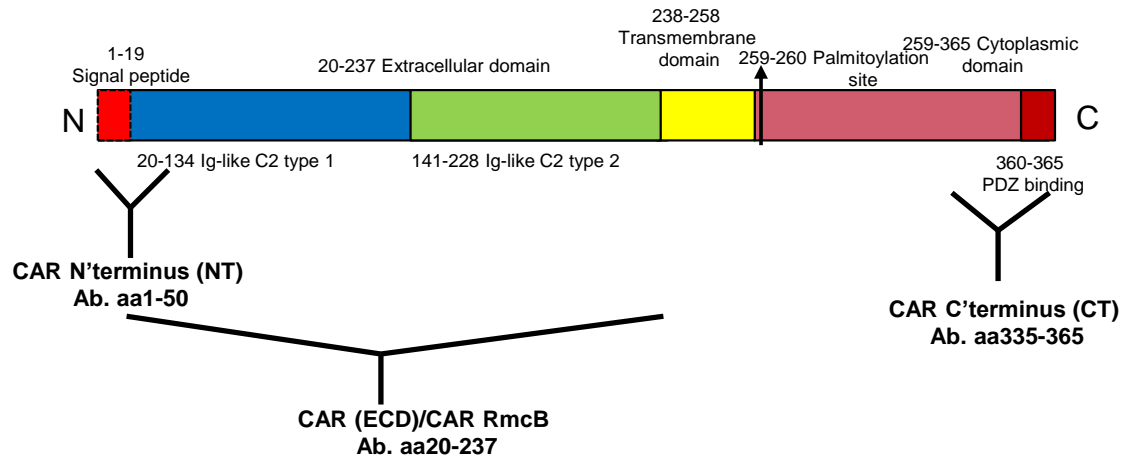


Figure 4.1 Schematic diagram of CAR antisera (CAR NT, CAR ECD, CAR RmcB and CAR CT) immunoreactivity against CAR protein

The objectives of this chapter are therefore as follows;

- To characterise CAR isoform antisera specificity and evaluate their utility in different assays utilising human pancreatic beta and ductal cell lines (EndoC- β H1, 1.1B4 and PANC-1)
- To determine CAR-SIV orientation in the human beta cell line utilising the different CAR antisera
- To explore CAR-SIV differential expression further in a variety of normal and cancerous tissues

4.2 Results

4.2.1 Trial of CAR antisera in human pancreatic ductal cell line

In order to further characterise the three CAR antisera (CAR CT, CAR ECD and CAR RmcB), PANC-1 cells (which have been shown to express CAR in Chapter 3, section 3.2.10 and in a recent study (Alidjinou et al., 2017) were employed to determine their suitability for ICC and flow cytometry.

In this analysis, the three CAR antisera (CAR CT, CAR ECD and CAR RmcB) were delivered to permeabilised PANC-1 cells and unbound antiserum was removed by washing. This was followed by staining with goat anti-rabbit or anti-mouse AlexaFluor555 secondary antisera; cells were mounted with Dako mounting medium and viewed under a fluorescence microscope. Trial of these antisera on PANC-1 cells revealed that anti-CAR CT and anti-CAR RmcB could be detected by ICC, as indicated by the yellow arrows, while the CAR ECD antiserum could not be detected (*Figure 4.2A*)

To assess the three CAR antisera by flow cytometry, surface analysis was performed with the CAR ECD and CAR RmcB antisera, both of which recognise the extracellular domain of CAR on the outer surface of the cells, while an intracellular approach was undertaken for CAR CT antiserum because of its ability to recognise CAR's cytoplasmic tail (Wang and Bergelson, 1999). Intact, PANC-1 cells were incubated with CAR antisera (CAR ECD and CAR RmcB) to detect CAR on the cell surface, while in the case of anti-CAR CT, immunolabelling was carried out on permeabilised cells where the antiserum could gain access to intracellular epitopes. A rabbit/mouse IgG isotype control (negative) was also included. Unbound antisera were removed by washing and a secondary goat anti-rabbit or anti-mouse AlexaFluor488 detection antiserum was used to visualise

staining. This was then analysed on a flow cytometer. In accord with the ICC results, the CAR CT and CAR RmcB antisera were both detected as clearly seen by the displacement of the peak (in red) to the right compared with isotype controls (black)(*Figure 4.2B*). In contrast, CAR ECD antiserum was not detected as clearly seen by the lack of peak shift when compared to the isotype control (*Figure 4.2B*). This is despite the fact that CAR protein of the appropriate molecular weight was observed in PANC1 cells by Western blotting with this antiserum (Chapter 3, section 3.2.7).

The above results imply that anti-CAR CT and anti-CAR RmcB are both suitable for use in ICC and flow cytometry, while anti-CAR ECD is not appropriate for utilisation in these assays.

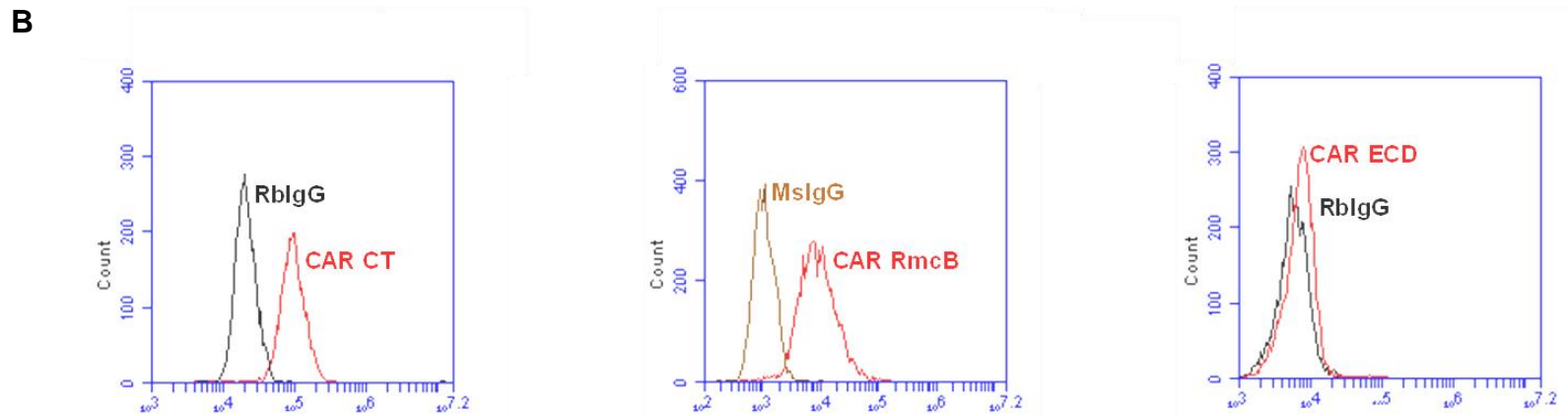
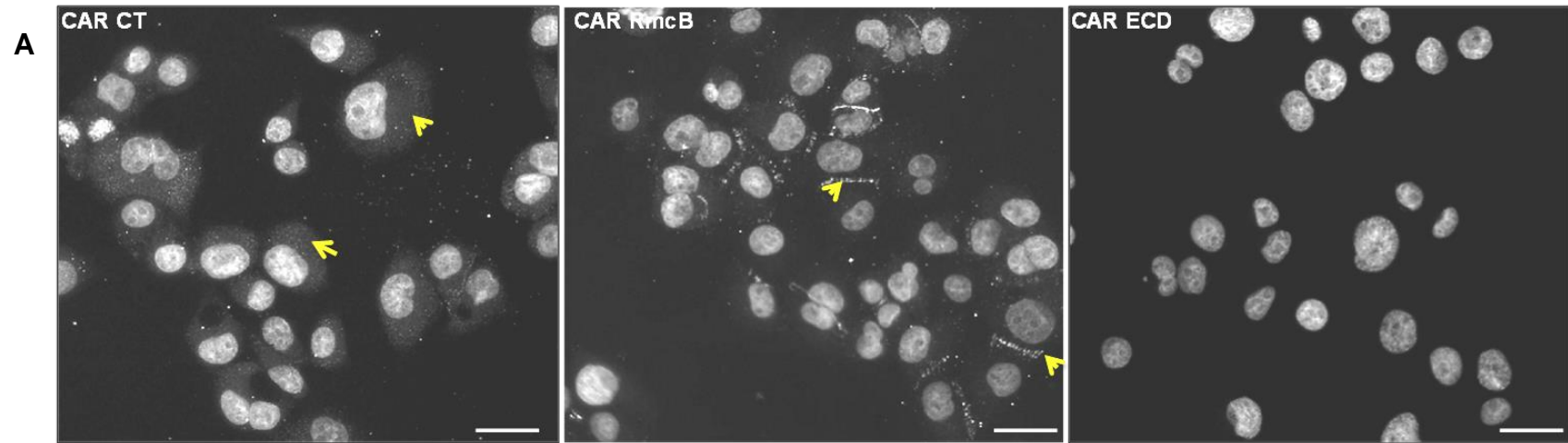


Figure 4.2 Staining with CAR RmcB and CAR CT antisera, but not CAR ECD, in PANC-1 cell line

(A) Immunocytochemical analysis detected staining with anti-CAR CT, anti-CAR RmcB as shown by the pale white signal (yellow arrows), Nuclei were stained with DAPI (white spherical shape), anti-CAR ECD was not detected. Scale Bar 25 μ m (B) Representative flow cytometry plots showing positive staining with anti-CAR CT and anti-CAR RmcB immunolabelling compared to negative controls (Rabbit IgG (RbIgG) and Mouse IgG (MslgG) while anti-CAR ECD staining was not detected as observed by the lack of shift from the negative control (Rabbit IgG) (n=3).

4.2.2 Detection of CAR surface expression in the human pancreatic beta and ductal cell line model

Having confirmed that the CAR RmcB antiserum is suitable for flow cytometry, it was utilised to determine if CAR is expressed on the surface of the human pancreatic beta cell lines, EndoC- β H1 and 1.1B4. The PANC-1 cell was utilised as a positive control. Cells in routine culture were harvested and incubated with either anti-CAR RmcB directly conjugated to a phycoerythrin (PE) or mouse IgG PE isotype (negative) control. The representative histogram plot of the surface expression demonstrates that CAR is expressed on the surface of both EndoC- β H1 and PANC-1 cells (*Figure 4.3A*). The flow cytometric analysis clearly shows a displacement of the peak (in red) to the right with anti-CAR RmcB labelled cells, compared with mouse IgG isotype control (black). Importantly, this also confirms that the extracellular domain of CAR is presented on the outer surface of the cells. In contrast, 1.1B4 cells exhibited only very weak expression of CAR on the cell surface when compared to the isotype control (*Figure 4.3A*)

To support these data, cells grown on coverslips were PFA fixed, followed by immunolabelling with CAR RmcB antiserum. The staining was detected with a goat anti-mouse AlexaFluor555 secondary antiserum; cells were mounted with Dako mounting medium and viewed under a high resolution confocal microscope. The results demonstrate anti-CAR RmcB labelling on the surface of EndoC- β H1 and PANC-1 cells (*Figure 4.3B*). Punctate CAR surface expression was observed in both cell lines with occasional areas of enriched CAR localised to junctions between neighbouring cells (yellow arrow heads). This is indicative of cell surface tight junction formation between cells (Cohen et al., 2001b). The 1.1B4 cells

revealed very low expression of anti-CAR RmcB on the surface of 1.1B4 cells which correlates with the flow cytometry data (*Figure 4.3A*).

The flow cytometry and confocal immunocytochemistry analysis revealed that anti-CAR RmcB (which is expected to recognise the three known CAR isoforms present in the human pancreas CAR-SIV, CAR-TVV and CAR4/7 (as demonstrated in Chapter 3 RNA and proteomics analysis) can recognise CAR expressed on the surface of EndoC- β H1 and PANC-1 cells. CAR was found to be only weakly expressed on the surface of 1.1B4 cells.

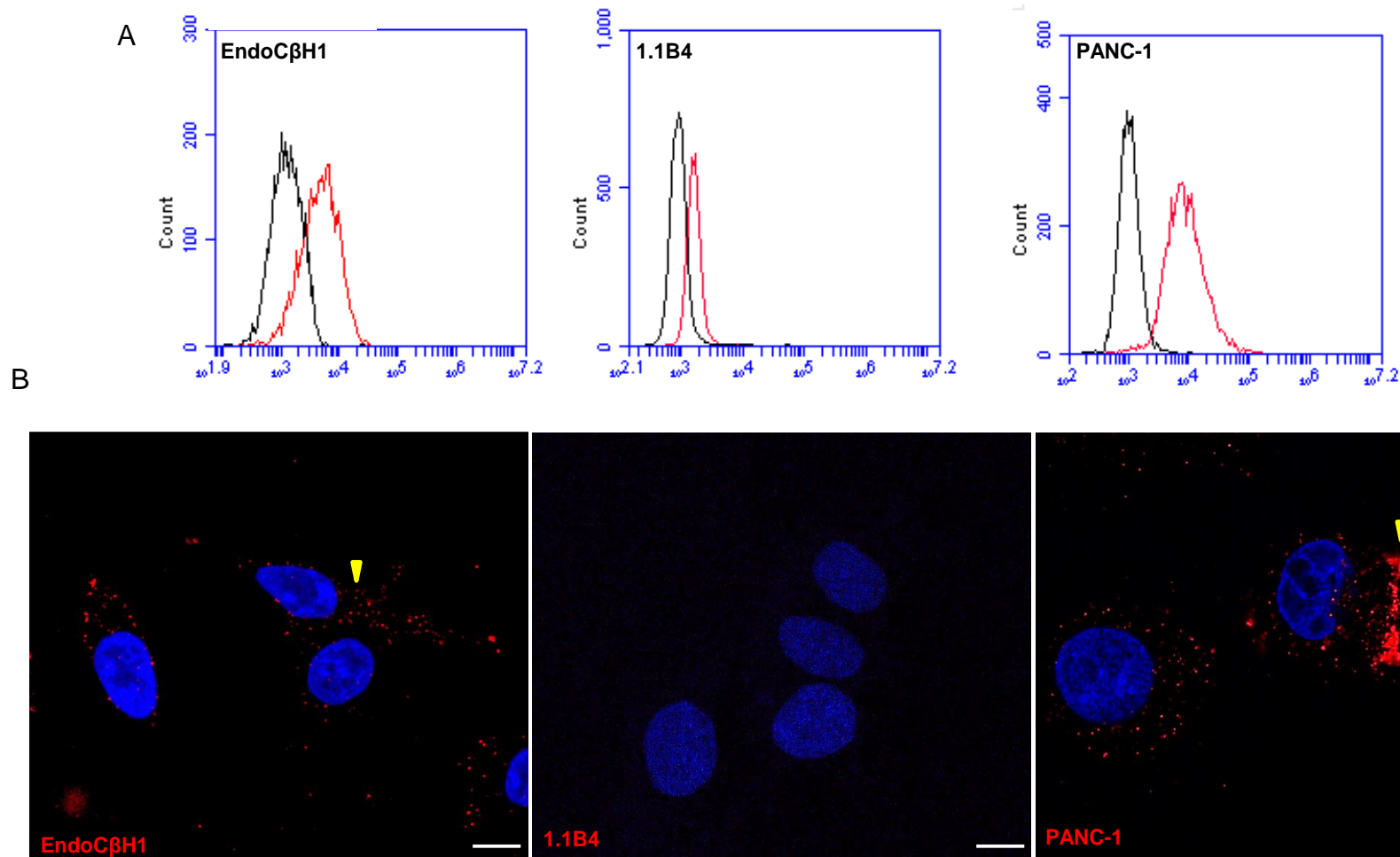


Figure 4.3 CAR expression is detected on the surface of cells by staining with CAR RmcB antisera

CAR RmcB antisera labelling demonstrates that CAR is strongly expressed on the surface of EndoC- β H1, PANC-1 but weakly on 1.1B4 cells. (A) Representative flow cytometry plots showing staining with anti-CAR RmcB revealed surface expression (red) in EndoC- β H1, 1.1B4 and PANC-1 cells, Isotype control (black) (B) Immunocytochemical images of anti-CAR RmcB (red) and nuclei (blue) in EndoC- β H1 (yellow arrows), PANC-1(yellow arrows) and no labelling in 1.1B4. Scale bar 7.5 μ m (n=3)

4.2.3 Detection of intracellular CAR expression in the human pancreatic beta and ductal cell line models

In order to detect intracellular CAR expression in the human pancreatic beta and ductal cell line models, EndoC- β H1, 1.1B4 and PANC-1 cells were collected and subjected to PFA fixation. Cells were then incubated with anti-CAR CT or rabbit IgG isotype control (negative) diluted in a permeabilisation buffer containing 0.3% saponin, to allow each antiserum to gain access to the intracellular cell compartment. Unbound antiserum was removed by washing and a secondary goat anti-rabbit AlexaFluor488 detection antiserum was used to visualise staining. This was then analysed on a flow cytometer. Intracellular CAR-SIV expression (red) was detected in all three cell lines (*Figure 4.4A*) when compared to the rabbit IgG isotype control (black).

To further confirm the flow analysis, ICC staining of each of the cell lines was performed. PFA fixed cells were permeabilised with 0.5% Triton X-100 and labelled with anti-CAR CT followed by a goat anti-rabbit AlexaFluor488 secondary antiserum. Comparison of the staining pattern of anti-CAR CT in the cell lines confirmed that intracellular CAR is clearly visible in the EndoC- β H1 and PANC-1 cells but that it is only weakly expressed in 1.1B4 cells (*Figure 4.4*). Interestingly, there tended to be differential pattern of localisation between the cell lines. Although, the staining pattern was predominantly cytoplasmic in all three cell lines, the expression appeared more punctate in the EndoC- β H1 and PANC-1 cell lines. The ICC analysis therefore concurs with the flow cytometry data and suggests that the C terminus of CAR-SIV can be detected in the intracellular compartment of all the three cell models, albeit at higher levels in the EndoC- β H1 and PANC-1 cells compared to the 1.1B4 cells.

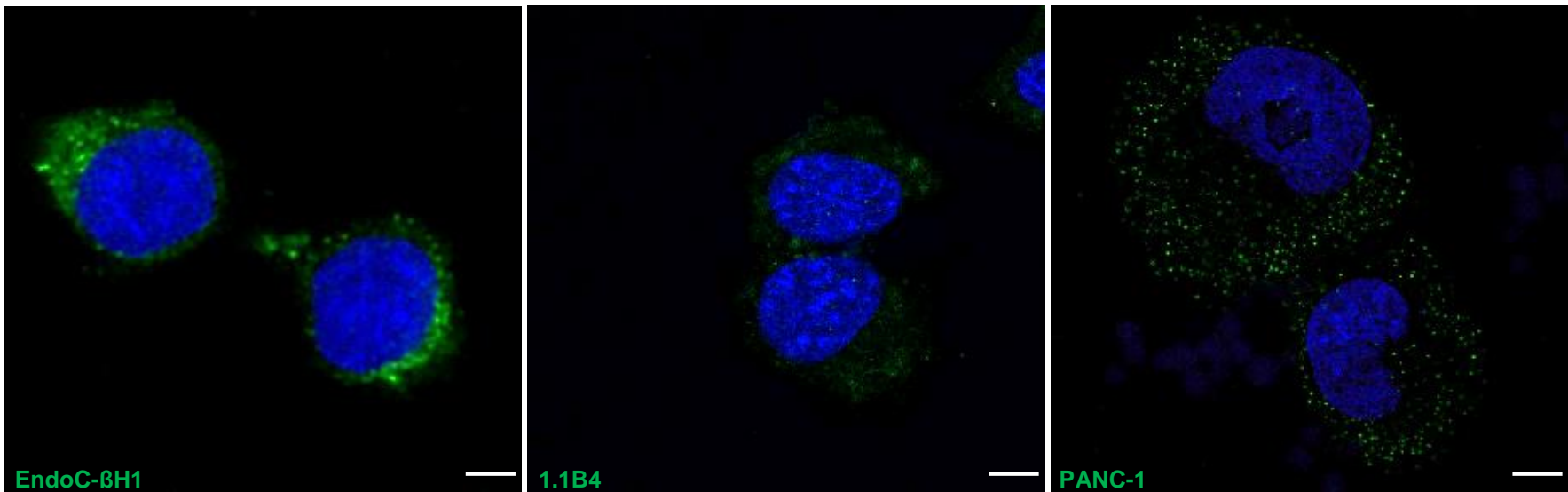
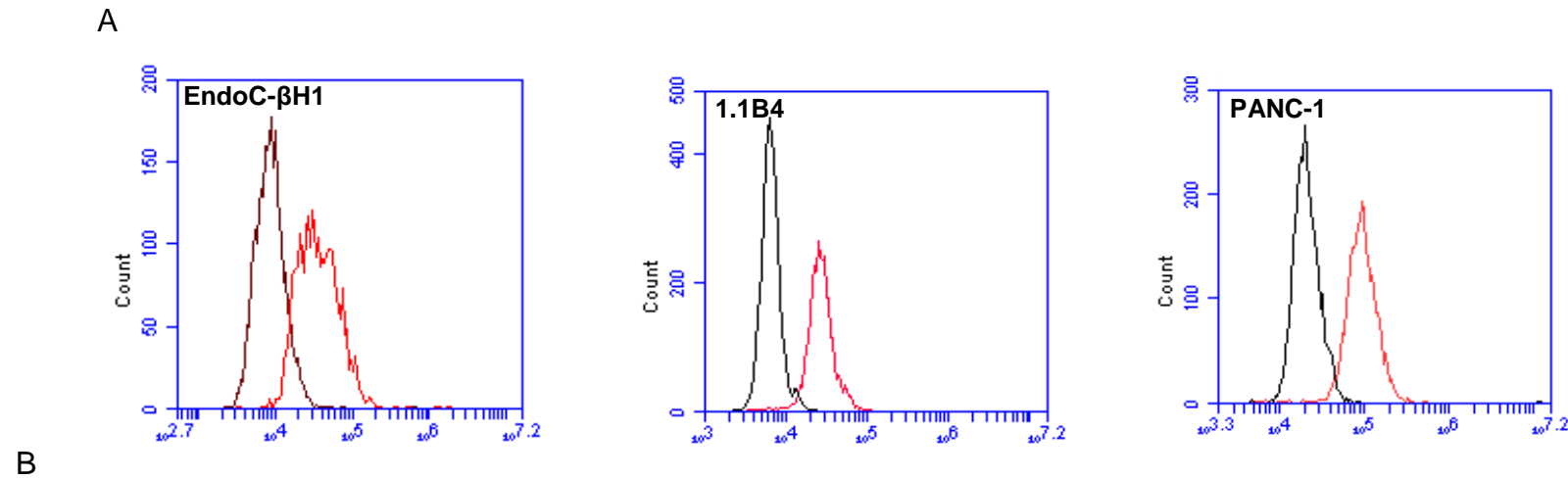


Figure 4.4 CAR-SIV isoform is detected intracellularly by staining with the CAR CT antisera in EndoC-βH1, 1.1B4 and PANC-1 cells. (A) Representative flow cytometric plot detecting intracellular CAR-SIV isoform (red) in EndoC-βH1, 1.1B4 and PANC-1. (B) Clear cytoplasmic and punctate localisation of anti-CAR CT (green) in EndoC-βH1 and PANC-1 and nuclei were stained with DAPI (blue). Cytoplasmic CAR-SIV expression is lower in 1.1B4 cells. Scale Bar 2.5µm (n=3)

4.2.4 Bioinformatics prediction of CAR-SIV isoform structural orientation within a cell

Taking into account the flow cytometry and ICC data in section 4.2.2 and 4.2.3 one would predict that CAR-SIV is orientated with the extracellular domain (ECD) exposed on the outside surface of the cell whereas the C terminus (CT) faces the cytoplasm. By inserting the protein sequence (FASTA format) from UniProt database into a proteomic bioinformatic tool “Protter” (<http://wlab.ethz.ch/protter/start/>) (Omasits et al., 2014), one can bioinformatically predict the orientation of the CAR-SIV isoform. The proposed orientation of CAR-SIV is illustrated (*Figure 4.5*) such that the region corresponding to the sequence beyond the signal peptide to the end of the extracellular domain is in the extracellular space/on the surface of cells and region beneath the transmembrane domain harbouring the C terminus (CT) is intracellular. The orientation of CAR-SIV was examined in more detail in the subsequent experiments detailed below.

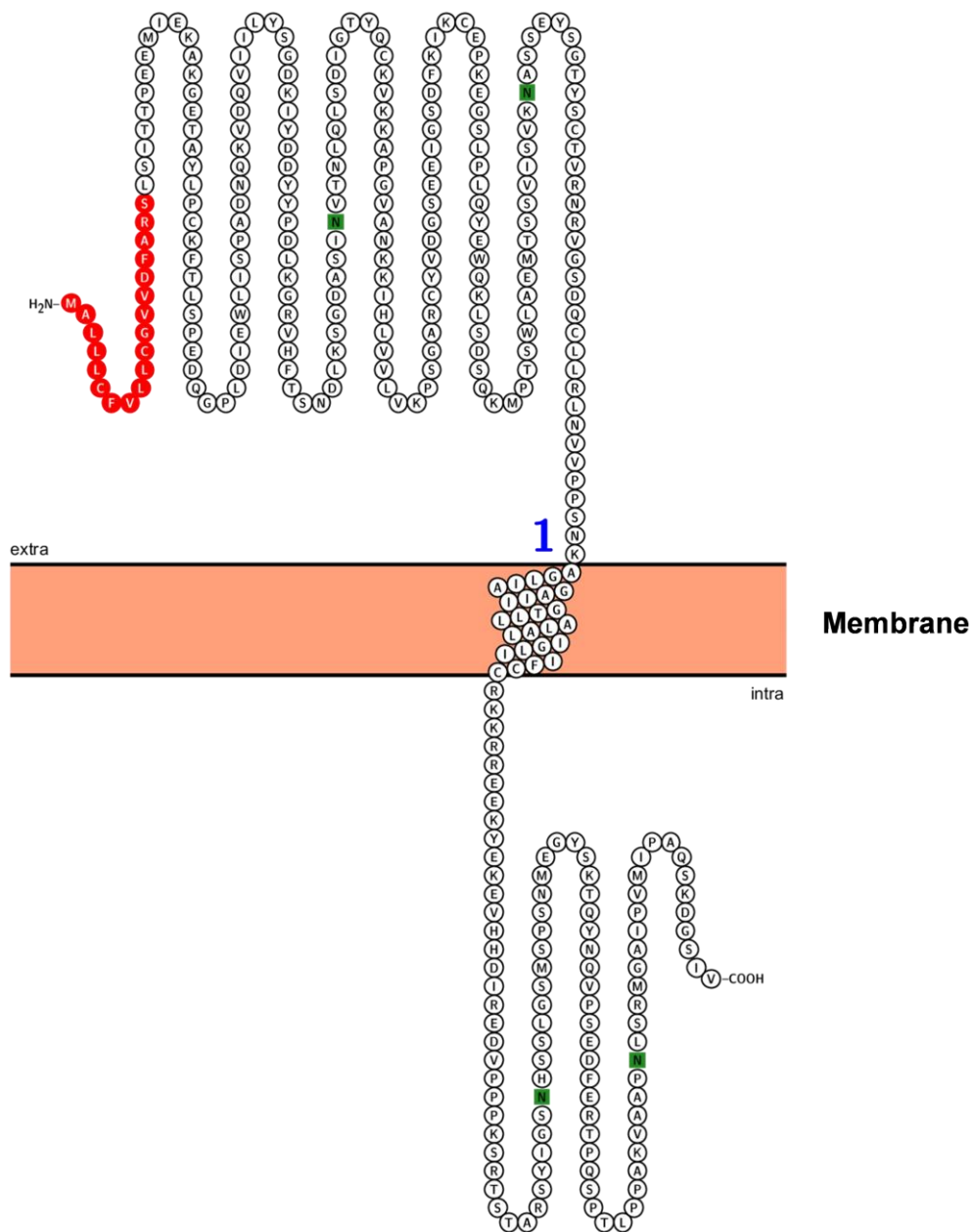


Figure 4.5 Bioinformatics prediction of the orientation of the CAR-SIV isoform with bioinformatic tool (Protter).

The region initiating from the signal peptide (red) to the end of the extracellular domain (1) is in the extracellular space or on the surface of the cell while the region beyond the transmembrane domain harbouring the C'terminus is intracellular

4.2.5. Flow cytometry detection of CAR orientation in the human pancreatic beta cell model (EndoC- β H1)

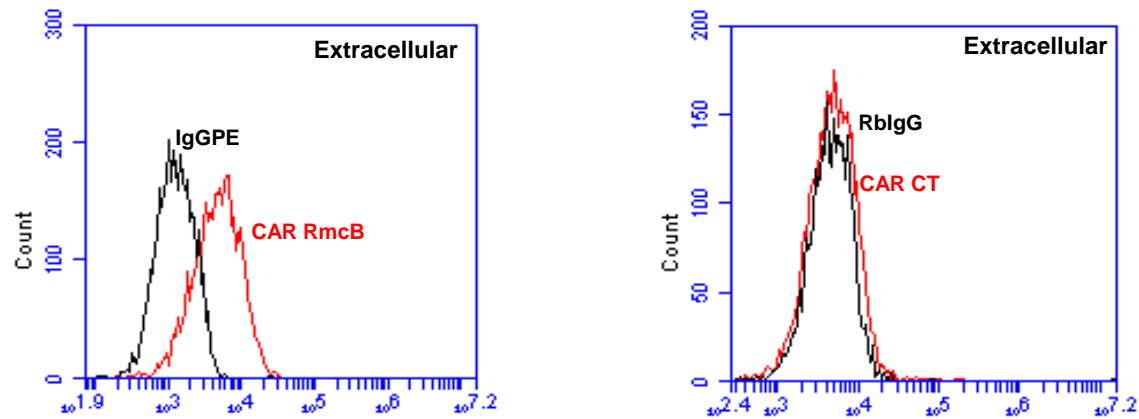
In order to confirm the orientation of CAR across the plasma membrane in human beta cells, the human pancreatic beta cell line EndoC- β H1 (shown to express high levels of the CAR-SIV isoform (*Figure 4.4*) was selected. The two CAR antisera that had previously been shown to be suitable for flow cytometry were utilised. The CAR RmcB antiserum, which binds to the ECD, and the CAR CT antiserum which binds to the CT of CAR-SIV were both tested in EndoC- β H1 cells. Cells were stained with both antisera immediately (without permeabilisation) to assess which epitope was expressed on the outer surface of the cell. Alternatively, the cells were fixed and permeabilised and then stained, to assess the intracellular epitopes. Isotype (controls) mouse IgG-PE or rabbit IgG were also included. In keeping with the previous results, the surface analysis demonstrates that anti-CAR RmcB was detectable on the extracellular surface of EndoC- β H1 cells (*Figure 4.6A*). There is a clear shift to the right in the histogram plot (red) labelled with anti-CAR RmcB compared to the mouse IgG-PE isotype (black) control. In contrast, no surface expression was observed with the anti-CAR CT on the EndoC- β H1 cells, as evidenced by the lack of a shift on the histogram plot when compared to the rabbit IgG (negative) control (*Figure 4.6A*).

Assessment of permeabilised cells with the anti-CAR RmcB revealed weak intracellular expression when compared to the mouse isotype control antiserum (*Figure 4.6B*). With anti-CAR CT there was a significant shift in expression observed when compared with its appropriate isotype control (*Figure 4.6B*). However, the punctate granular staining observed with the CAR RmcB antiserum (detecting majorly CAR-SIV and CAR-TVV) in permeabilised cells suggests that

a proportion of CAR expressed in these cells resides on/in a cytoplasmic organelle (*Figure 4.7; lower panel*)

These results confirmed that in the human pancreatic beta cell EndoC- β H1, the orientation of CAR-SIV is such that the extracellular domain is located on the surface/outside of the cell, while the C terminus harbouring the PDZ binding domain is located inside the cytoplasm. This fits nicely with the bioinformatics predicted orientation (*Figure 4.5*) and several other studies (Matthäus et al., 2017, Raschperger et al., 2006, Excoffon et al., 2014). The three CAR antisera (CAR CT, CAR ECD and CAR RmcB) have been successfully tested and characterised in the human pancreatic beta and ductal cell lines and this is summarised in Table 4.2.

A. Surface Expression



B. Intracellular Expression

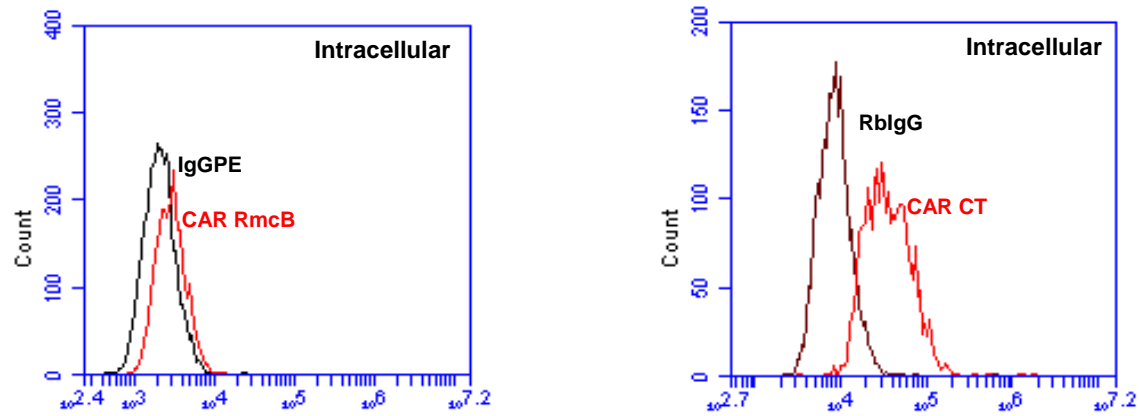


Figure 4.6 CAR orientation is detected utilising staining with anti-CAR RmcB and anti-CAR CT in the human pancreatic beta cell EndoC- β H1.

(A) Surface epitope labelling of anti-CAR RmcB (red) left plot and no surface labelling of anti-CAR CT (red) right plot in comparison to the negative controls (Rabbit IgG (RblgG) and IgGPE (Black) (B) Intracellular epitope labelling of anti-CAR CT (red) right plot and no intracellular labelling of anti-CAR RmcB (red) left plot in comparison to the negative control Rabbit IgG (RblgG) and IgGPE (black)(n=3)

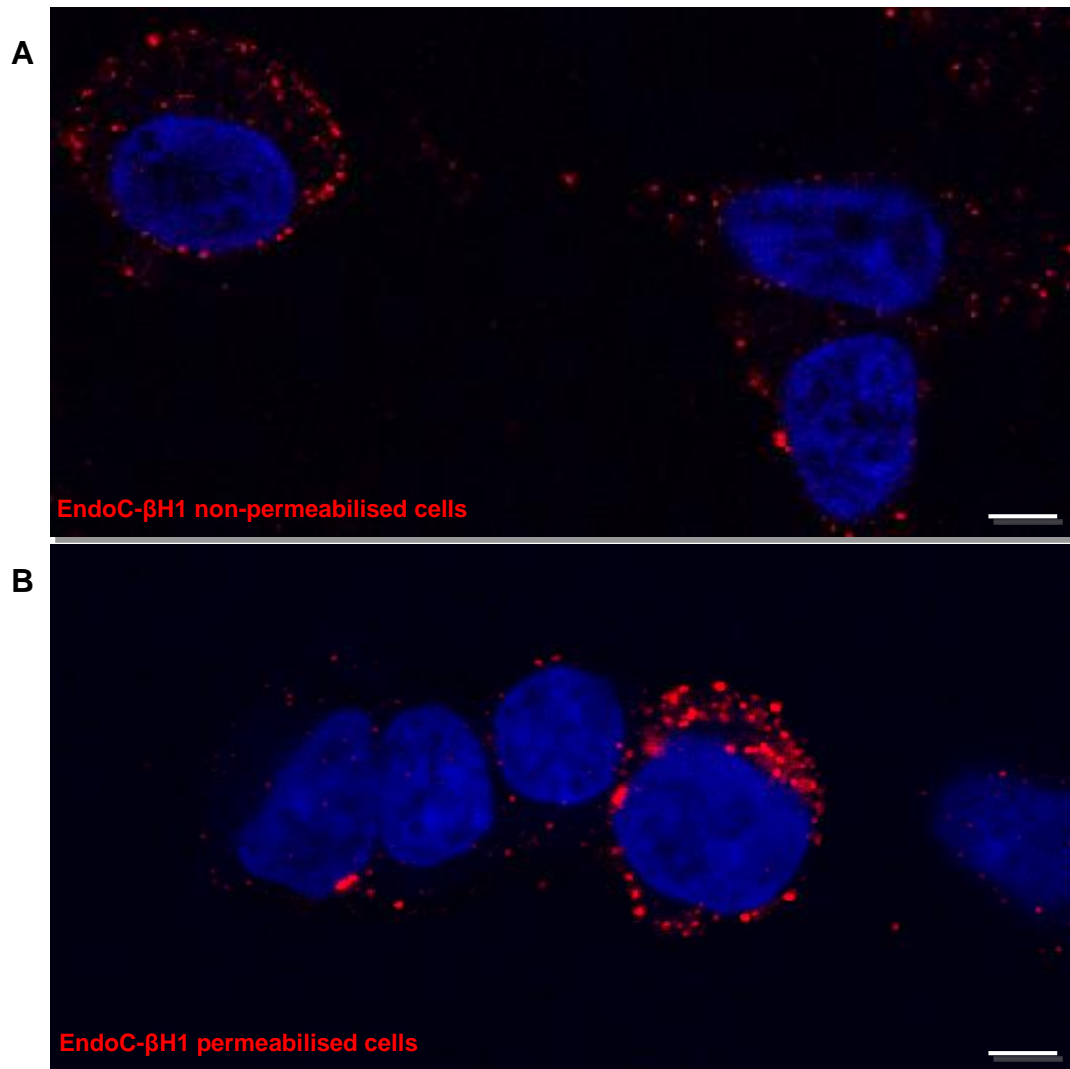


Figure 4.7 Staining with CAR RmcB suggests that the CAR-SIV isoform is present both on the surface of the cells and in an intracellular compartment

Immunocytochemical analysis (upper panel) show that staining with CAR RmcB (red) (A) revealed surface staining in non-permeabilised cells, (lower panel) but (B) in permeabilised cells there is some intracellular staining with CAR RmcB (red). Nuclei were stained in blue (DAPI). Data are representative of images from three replicates, Scale 7.5µm

Table 4.2 Validation of CAR antisera with different assays

Antisera	CAR isoforms recognised	IHC/IF FFPE	ICC Coverslips	Western blotting	Flow cytometry	CAR-form recognised
CAR CT	CAR-SIV	+	+	+	+	Native & denatured
CAR ECD	CAR-SIV CAR-TVV CAR4/7 CAR3/7	+	–	+	–	Non-native
CAR RmcB	CAR-SIV CAR-TVV CAR4/7 CAR3/7	–	+	–	+	Native

4.2.6 CAR-SIV isoform immunolabelling in normal and cancerous human tissues

The differential anti-CAR CT staining pattern in the human pancreatic beta and ductal cells shown in (*Figure 4.4*) prompted an investigation of CAR-SIV expression in a variety of tissues to assess its distribution and subcellular localisation profile.

Standard immunohistochemical staining was employed on a normal and cancerous human tissue microarray (TMA; Kind gift from Prof. Alan Foulis, Glasgow). The TMA was labelled with CAR CT antiserum using the conditions optimised in Chapter 3, section 3.2.4. The staining of the TMA demonstrates that CAR-SIV is highly expressed in the brain, pancreatic islets, testis, kidney (transitional cell carcinoma), bladder small cell carcinoma, stomach, heart and liver parenchyma (*Figure 4.8*). Expression was also observed in other normal and cancerous tissues, but not in normal nerve, normal vasculature, normal omentum and smooth muscle (*Figure 4.9*)

Careful examination of the TMA revealed that the pattern of CAR-SIV staining was not uniform in all cell types. Certain tissues/cancers exhibited clear surface expression (e.g. bladder, testis, kidney (transitional cell carcinoma)); (*Figure 4.8*) In contrast, other tissues/cancers exhibited a more granular cytoplasmic expression of CAR-SIV (e.g. the stomach, brain, heart, pancreatic islet, liver parenchyma; *Figure 4.8*). Interestingly, many of the normal and cancerous tissues/cell types in which this granular expression was observed have secretory functions.

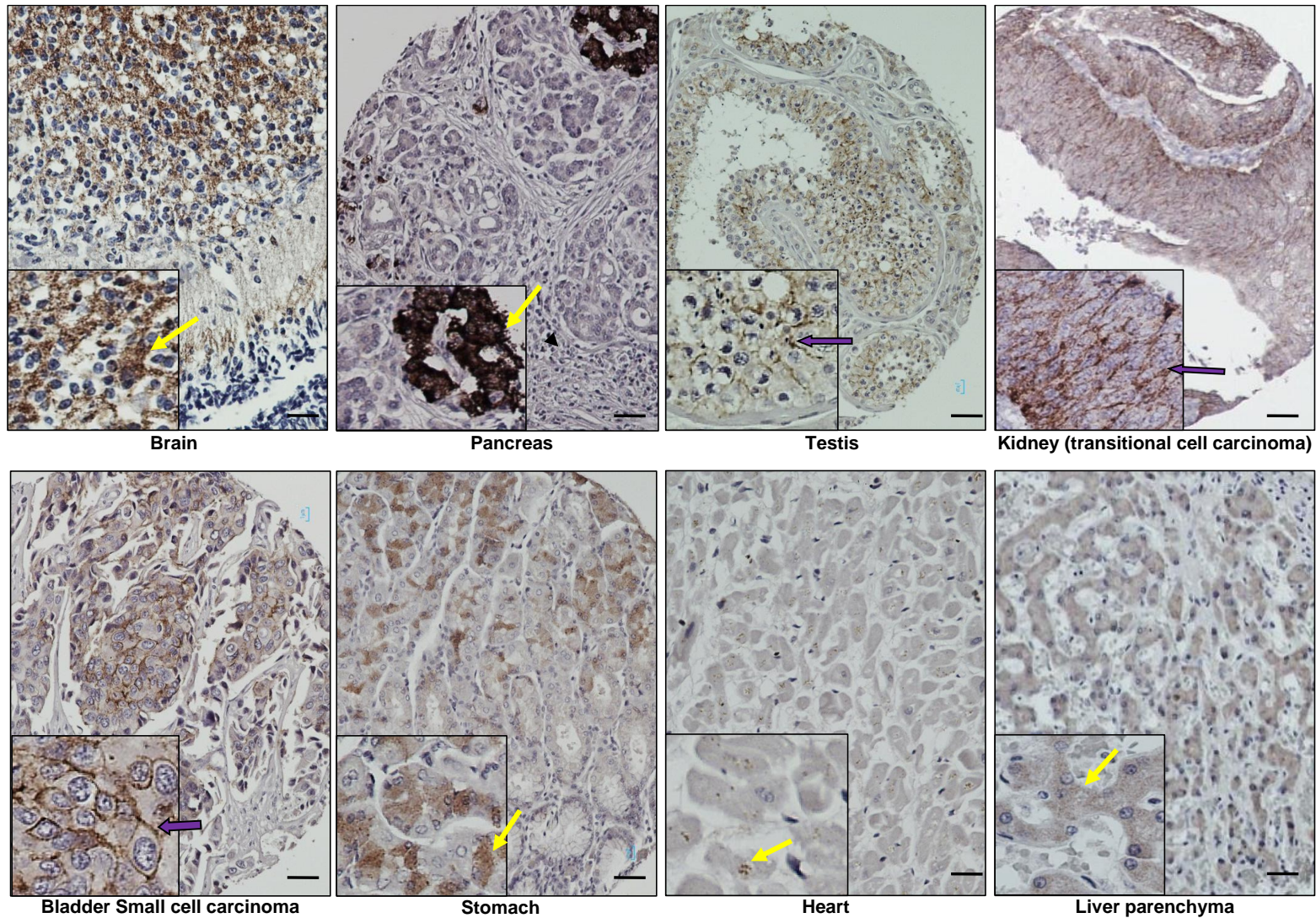


Figure 4.8 CAR-SIV isoform distribution and cellular localisation in normal and cancerous human tissues.

Staining with CAR CT antisera showed more cytoplasmic, granular expression in brain, islets, stomach, heart and liver (yellow arrow). In contrast, surface expression was observed in testis, kidney (transitional cell carcinoma), and bladder parenchyma (purple arrow). Scale bar 20 μ m

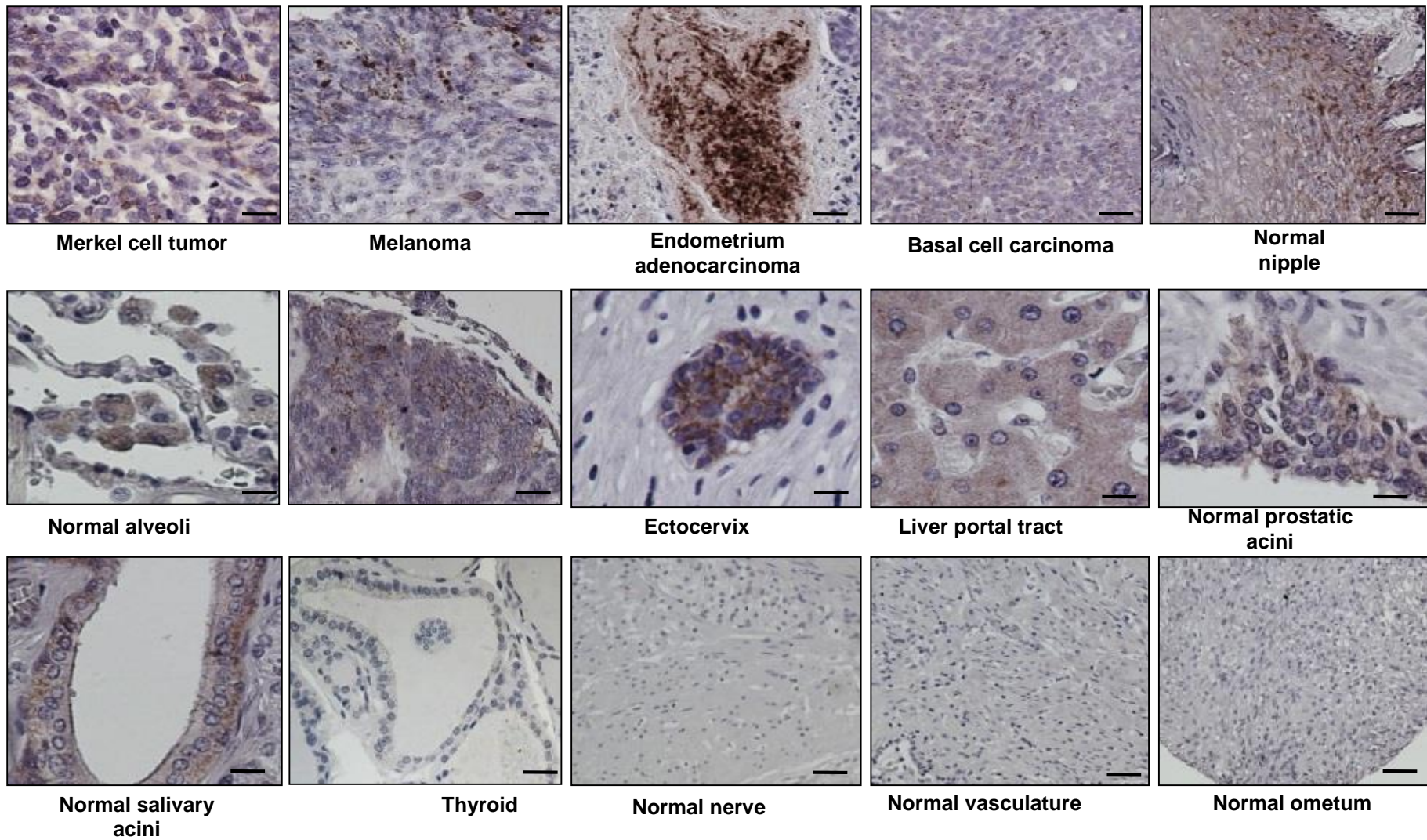


Figure 4.9 CAR-SIV isoform expression in normal and cancerous human tissues.

Staining with CAR CT antisera demonstrates that CAR-SIV is positive in merkel cell tumor, melanoma, endometrium adenocarcinoma, basal cell carcinoma, normal nipple, normal alveoli, squamous cell carcinoma, ectocervix, liver portal tract, normal prostatic acini, normal salivary acini and negative in normal nerve, vasculature, omentum and smooth muscle. Scale bar 20 μ m

An independent confirmation of these results was achieved by utilising RNAseq data kindly provided by Prof. Decio Eizirik (Brussels). Quantitative RNAseq measurements of the three CAR isoforms (CAR-SIV, CAR-TVV and CAR4/7) were performed in a variety of normal human tissues (*Figure 4.10*). CAR-SIV and CAR-TVV were both detected in 13 of 16 (81%) of normal tissues but were both negative in adipose, skeletal muscle and white blood cells. The soluble CAR 4/7 isoform was detectable at very low levels in 5 of 13 (38%) of the tissues. CAR-SIV was expressed at a higher level than CAR-TVV in 12 of 16 (75%) tissues including the brain, breast, lymph node, ovary, prostate, heart, kidney, testes, thyroid, liver, lungs and in isolated dispersed islets. CAR-SIV expression was highest in dispersed islet, brain, kidney, prostate, testis, and thyroid all of which contain secretory cells. Encouragingly, the CAR-SIV RNAseq data aligned closely with the protein expression data previously presented (*Figure 4.8 & Figure 4.9*). Furthermore, this RNAseq analysis supports the hypothesis that CAR-SIV is highly expressed in cells with secretory functions.

Together, the immunohistochemical and RNAseq results demonstrate that the CAR-SIV isoform is differentially localised depending on the cell type and that CAR-SIV is highly expressed at both the RNA and protein level in many cell types with a biological secretory function.

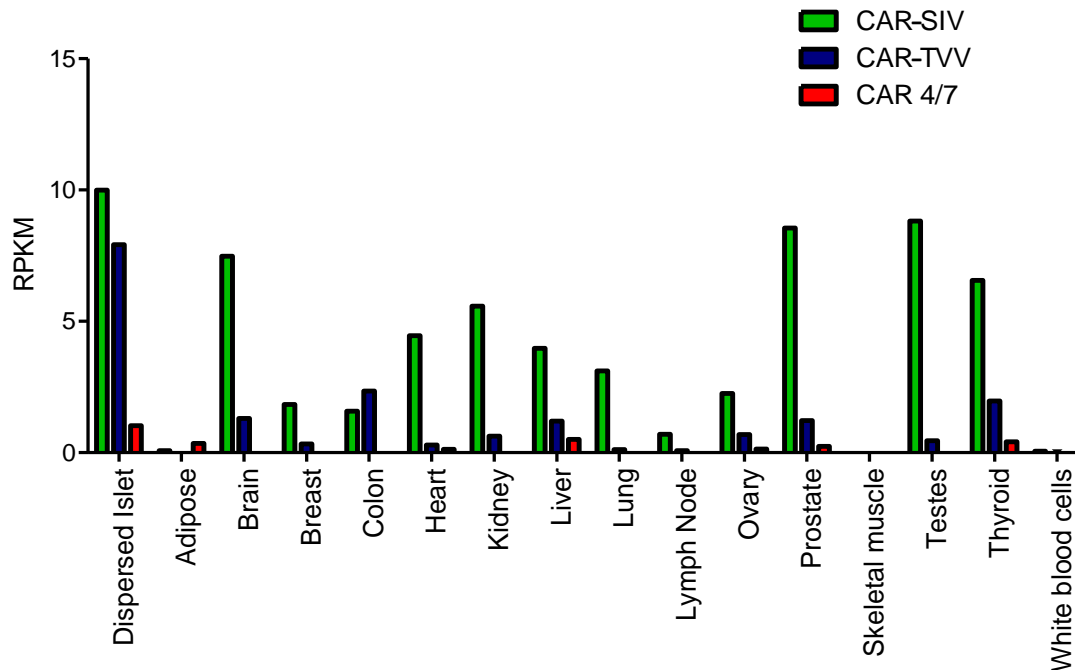


Figure 4.10 RNAseq analysis confirming the expression profile of CAR-SIV, CAR-TVV and CAR4/7.

Total RNA was isolated from cell lysates in different cells and tissues. Following quantification, 2µg of RNA was converted to cDNA. The cDNA was subsequently subjected to RNAseq analysis

CAR-SIV is expressed at higher levels than CAR-TVV and CAR 4/7 in most tissues. In particular, CAR-SIV is highly expressed compared to CAR-TVV in dispersed islets, brain, kidney, prostate, testes and thyroid, while CAR4/7 is least expressed in all tissues (mean RPKM). Courtesy of Prof. Decio. L. Eizirik

4.3 Discussion

4.3.1 CAR CT, CAR ECD and CAR RmcB antisera differentially label the human pancreatic ductal cell (PANC-1)

In characterising the three different CAR antisera (CARCT, CAR ECD and CAR RmcB) on the PANC-1 cells, it was resolved that the CAR CT antiserum recognises both the native and denatured form of CAR, while CAR RmcB recognises only the native form. This fits well with studies that have utilised CAR RmcB as a blocking antibody (Ylipaasto et al., 2004). In contrast, the CAR ECD antiserum only recognises CAR in a non-native form, produced following heating (IHC – Chapter 3, section 3.2.4) or upon treatment with reducing agents (Western blotting – Chapter 3, section 3.2.7) and is unable to recognise the native form (in flow cytometry and ICC). The utilisation of flow cytometry and ICC in the PANC-1 cells demonstrated that the anti-CAR CT detects intracellular CAR and the anti-CAR RmcB could detect CAR on the surface of the PANC-1 cells (see *Figure 4.2*).

4.3.2 The extracellular domain of CAR is present on the surface of human pancreatic beta and ductal cell lines

This present study revealed high levels of CAR surface expression on EndoC- β H1 and PANC-1 cells with a distinct pattern of localisation that was concentrated at points between adjacent cells. This pattern of localisation is a feature of cell-cell junctions and has been previously reported by a group utilising the CAR RmcB antiserum, which recognises the ECD (Excoffon et al., 2005). The significance of the CAR ECD for the cell-cell interaction was demonstrated through the generation of deletion mutants of the CAR ECD expressed in Chinese hamster ovary (CHO) cells. These mutants showed diffuse staining and

completely lacked any junctional surface localisation between the cells (Excoffon et al., 2005).

The importance of the ECD of CAR to drive CAR localisation to these cell-cell junctions was further demonstrated in CHO cells in which a glycosylphosphatidylinositol linked CAR ECD, which lacked the cytoplasmic and transmembrane domain, was shown to still accumulate at the cell-cell junction (Cohen et al., 2001b). Finally, mutations of the D2 domain (see Chapter 3 *Figure 3.8*) within the ECD also led to a lack of junctional localisation (Excoffon et al., 2005). Since CAR4/7 lacks the complete D2 domain and the transmembrane domain, this suggests that the distinct surface cell-cell staining observed in the EndoC- β H1 and PANC-1 cells is mediated by CAR-SIV and/or CAR-TVV isoform expression. This fits with the CAR-SIV and CAR-TVV isoform specific RNA expression in EndoC- β H1 and PANC-1 cells previously shown (Chapter 3, *Figure 3.7B*, & *3.25A*).

One unanticipated finding was the very low/weak surface expression of anti-CAR RmcB on 1.1B4 cells, which was supported by flow cytometry and ICC data. An explanation for this could be that 1.1B4 cells have very low levels of CAR protein and/or could have high levels of ADAM10, which has been demonstrated to cleave the CAR extracellular domain (Houry et al., 2013). The ADAM10 mediated cleavage products of CAR are approximately 32kDa (contains ECD) and 20kDa (contains the CT of CAR). A further cleavage of the 20kDa fragment by a γ -secretase, releases a 14kDa fragment of the CT CAR lacking any transmembrane sequence (*Figure 4.11*). Importantly, intense lower ~35kDa and 14kDa bands, which maybe these cleavage products (Chapter 3, *Figure 3.19*)

were detected in 1.1B4 cells, when probed with CAR ECD and CAR CT antisera respectively.

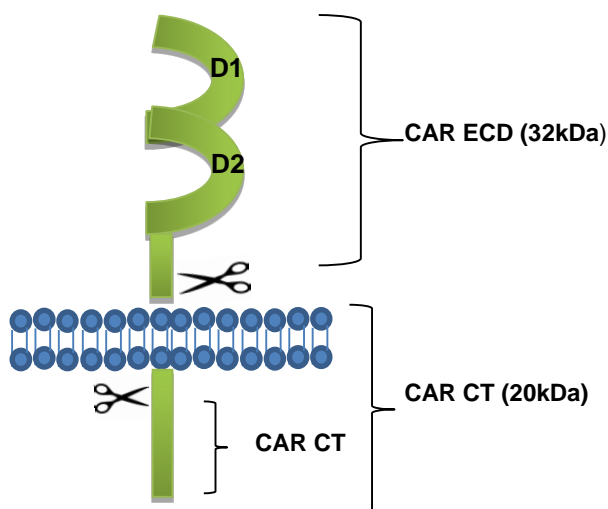


Figure 4.11 A model of CAR proteolysis, with molecular weights of the resulting fragments indicated.

Cleavage of CAR by ADAM10 (represented by the top pair of scissors) releases a 32 kDa fragment (CAR ECD) into the extracellular environment. The remaining 20 kDa fragment (CTF1) is processed by the γ -secretase complex (represented by the lower pair of scissors), generating a 14 kDa fragment (CTF2), adapted from (Hourii et al., 2013)

Together these results suggest that CAR is expressed in 1.1B4 cells, but that the levels of CAR on the surface may be lower (as suggested by the CAR RmcB results) than the other cell lines tested, potentially due to cleavage by ADAM10. In the future, it would be interesting to confirm this by using a specific inhibitor of ADAM10, such as G1254023X (Li et al., 2017)

In summary, these data suggest that both the CAR-SIV and CAR-TVV isoform (recognisable by CAR RmcB) can be localised to the surface of the pancreatic beta and ductal cells.

4.3.3 CAR CT antiserum staining suggests that CAR-SIV is present in intracellular compartments in human pancreatic beta and ductal cells

The CAR CT antiserum will detect the C terminus of only the CAR-SIV isoform and intracellular CAR-SIV expression was found in EndoC- β H1, 1.1B4 and PANC-1 cell lines.

Interestingly, with anti-CAR CT a predominantly cytoplasmic pattern was observed which was more punctate in EndoC- β H1 and PANC-1 than in 1.1B4. The result suggests that the CAR-SIV isoform may reside in a distinct intracellular membrane-bound compartment within the cytoplasm in the EndoC- β H1, PANC-1 and 1.1B4 cells (*Figure 4.4*). The 20kDa cleavage product observed in the 1.1B4 cells when probed with anti-CAR CT in Chapter 3, *Figure 3.19* and the low level of expression observed in 1.1B4 cells imply that the EndoC- β H1 cells model would be more appropriate for further study.

4.3.4 CAR orientation in EndoC- β H1 cell line

In this thesis, the orientation of CAR was confirmed in the human beta cell EndoC- β H1. The extracellular domain of CAR was demonstrated to face the outside of the cell, while the C terminus was present solely inside the cell. This is consistent with the predicted CAR orientation (Excoffon et al., 2010, Matthäus et al., 2017, Raschperger et al., 2006) and studies that have utilised mammalian cell expression system to show that CAR's N terminus (He et al., 2001) and extracellular domains interact with Coxsackie B viruses when presented outside the cell (Wang and Bergelson, 1999, Pinkert et al., 2016). Significantly, the level of the CAR-SIV isoform expression is high in these cells, as assessed by RNAseq (Chapter 3, *Figure 3.7*), Western blotting (Chapter 3, *Figure 3.19*) and intracellular

flow cytometry (*Figure 4.4A*) with the CAR CT antiserum and is likely to represent the major isoform in these cells. This is also supported by the observation that Western blotting with the CAR ECD antiserum (which recognises both CAR-SIV and CAR-TVV) did not reveal a larger or differently sized band when compared to the CAR CT antiserum (*Chapter 3, Figure 3.19B*). Importantly though, distinct intracellular membrane-bound compartments were also positive for CAR-SIV (as assessed by CAR CT staining), suggesting that this isoform can localise both at the surface and within distinct organelles within the EndoC- β H1 cells.

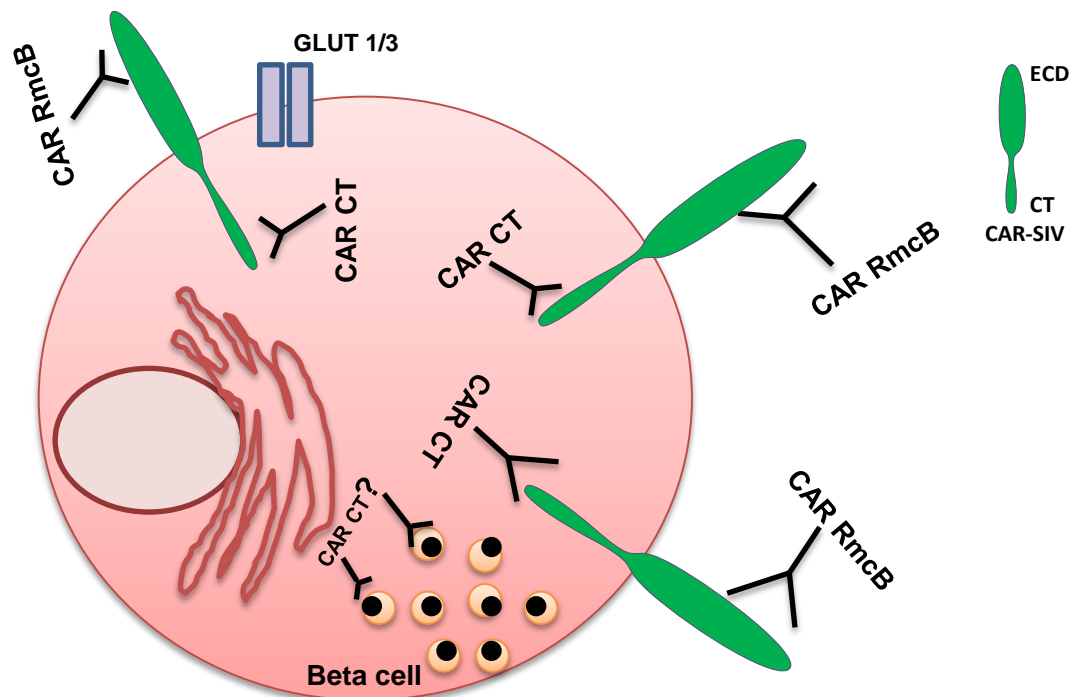


Figure 4.12 CAR-SIV orientation in the beta cell.

The C terminus (CT) harbouring the PDZ domain is located inside the cell (detected by anti-CAR CT) while the extracellular domain (ECD) is located on the surface of the cell (detected by anti-CAR RmcB). Could CAR CT be in an intracellular compartment such as the insulin granule?

4.3.5 CAR-SIV is differentially expressed in normal and cancerous human tissues

Interestingly, IHC analysis with anti-CAR CT in normal and cancerous tissues demonstrated that CAR-SIV was expressed in a large number of the tested tissues. The staining pattern, however, revealed differential localisation with the exhibition of surface staining in some tissues (for example bladder and kidney) which is consistent with its role in cell adhesion and tight junctions. In contrast, other cells (for example the stomach, islets and the brain) had a more granular cytoplasmic pattern. Interestingly, when assessing the functions of many of these tissues with this distinct CAR-SIV localisation, they were found to be involved in the secretion of various factors such as hormones, neurotransmitters and enzymes. The cytoplasmic granular or surface staining pattern in these tissues suggests that CAR-SIV may have distinct functions in these cell types.

Although, this present study was not focused on cancer progression, differential expression was observed in cancerous tissues. It has been proposed by many that CAR may act as a tumour-suppressor because several studies have shown that loss of CAR impacts on proliferation, migration, invasion and the metastatic potential of several cancer types and also leads to a decline in cell adhesion (Okegawa et al., 2001, Okegawa et al., 2000, Huang et al., 2005, Anders et al., 2009, Stecker et al., 2011, Matsumoto et al., 2005).

4.3.6 Differential CAR-SIV and CAR-TVV expression in normal and cancerous human tissues by RNAseq

The RNAseq analysis provided good confirmation of the IHC data by demonstrating that CAR-SIV RNA expression was detected in many of the cells/tissues shown to be positive for the CAR-SIV protein. Importantly, it

demonstrated that expression levels were high in many of the tissues involved in secretion. This provides further support for the hypothesis that CAR-SIV may have a distinct biological role in secretory cells. Importantly, CAR-SIV tended to be expressed at higher levels compared to CAR-TVV in these tissues. So although CAR-SIV and CAR-TVV may be present in similar tissues, their differential localisation suggests that they have different roles within these cells. Unfortunately, as mentioned previously, I have been unable to source CAR-TVV antiserum commercially or via authors of publications describing such an antiserum, which has made studying the localisation of this isoform in detail impossible within these studies. However, the localisation of the two transmembrane domain isoforms, CAR-SIV and CAR-TVV, in primary human epithelial cells has been assessed by Excoffon *et al* (2010). Initially, they generated adenovirus vectors expressing both of these two distinct forms. These were then utilised to generate isoform specific antisera from rabbits immunised with peptides directed against the last 13 C terminal amino acid of each, which differ between the two as described previously in (Chapter 1, *Figure 1.9*). Utilising these antisera in polarised human epithelial cells, which have distinct apical and basolateral membrane domains separated by tight and adherens junctions, the authors were able to demonstrate that CAR-SIV specifically localised to the basolateral membrane in these cells, mediating tight junction integrity via its colocalisation with ZO-1, a tight junction protein. In contrast, CAR-TVV was present at the apical membrane and did not colocalise with ZO-1 (Excoffon *et al.*, 2010). In a different study on murine tissue, utilising mCAR-2(CAR-SIV) and mCAR-1(CAR-TVV) specific antisera with immunofluorescence and Western blotting approaches, CAR-SIV was shown to be expressed at high levels at cell-cell contacts in hepatocytes in the liver and kidney. In contrast, only very

low/weak expression of CAR-TVV was observed (Raschperger et al., 2006). This is in accord with the RNAseq data presented in this thesis.

These differences in abundance and localisation have also been studied in human lung tissue and polarised airway epithelial cells (Excoffon et al., 2010). In terms of abundance, quantitative RT-PCR analysis revealed that CAR-SIV was expressed at higher levels than CAR-TVV in both human lung tissue and polarised airway epithelial cells (Excoffon et al., 2010) indicating that the CAR-SIV isoform is predominant. This finding agrees with the RNAseq data in the lung, presented in this study. In that same study, Excoffon *et al* (2010), confirmed the importance of CAR subcellular localisation for infection by utilising dissociated human polarised airway epithelial cells, that were transduced with adenovirus vectors expressing either CAR-SIV (which will localise to the basolateral face) or CAR-TVV (which will localise to the apical face). After culturing these cells for 1 week, to allow the cells to polarise and form a continuous epithelium, the cells were then infected with an adenovirus containing the LacZ gene. This demonstrated that cells transduced with the CAR-TVV (localised to the apical face) had a 5-fold increase in LacZ gene transfer compared to cells transduced with a GFP control and double the level compared to the CAR-SIV transduced cells. Therefore both CAR-TVV and CAR-SIV can mediate infection, but the localisation of the proteins could determine the initial entry route (Excoffon et al., 2010). In another study, the human colonic cell line (T-84) was allowed to form polarised monolayers by culturing cells to confluency in transwells for 1 week. Analysis of CAR localisation, assessed by CAR antisera that recognise both CAR-SIV and CAR-TVV, confirmed that CAR was localised to tight junctions between cells (Cohen et al., 2001b). These cells were then infected with CVB3 or adenovirus GFP (AdGFP) from either the apical region or the basolateral

region (performed by inverting the transwell insert and applying the virus). Immunocytochemical staining revealed little or no infection with CVB3 or AdGFP in cells exposed to virus on either the apical or basolateral surfaces. However, when the tight junctions were disrupted by EDTA before infection in these cells, there was a significant increase in infection by CVB3 and AdGFP in the cells (Cohen et al., 2001b). Moreover, to determine if this infection was mediated by CAR, EDTA treatment was followed by incubation with pre-immune serum or CAR antiserum raised against the extracellular domain (capable of recognising both CAR-SIV and CAR-TVV isoforms) before infection with CVB3 and AdGFP (Cohen et al., 2001b). The results demonstrate that both CVB3 and AdGFP infection were inhibited by CAR antiserum, but not by the pre-immune serum, signifying that disrupting the tight junctions makes CAR localisation accessible for virus attachment and infection. Thus, this implies that the localisation of both CAR-SIV and CAR-TVV in cells is critical for viral entry and successful virus production. All of these studies suggest that CAR expression at the cell surface is required to mediate entry of viruses. Our present study demonstrates that CAR-SIV is expressed in beta cells, with at least a proportion of it on the cell surface, and concurs with the sensitivity of beta cells to infection by enteroviral serotypes that utilise this receptor for entry.

In summary this chapter has characterised the use of CAR antisera in human pancreatic beta and ductal cell lines, revealing the orientation of CAR on the beta cell. It has also provided important evidence that the CAR-SIV isoform is enriched in several human cell type/ tissues that have a secretory function.

CHAPTER 5

Subcellular localisation of CAR-SIV in the human beta cell of the pancreas

5.1 Introduction

Several studies have investigated the subcellular localisation of CAR-SIV in various tissues, cells and cell lines and as such have provided some insights into CAR's biological role which include;

- Role in structural integrity in human and mouse cardiac muscle (Shaw et al., 2004)
- Role in cell-cell adhesion (Cohen et al., 2001b)
- A role in regulating paracellular transport of ions and molecules (Cohen et al., 2001b)
- Mediates the retention and trafficking of innate immune cells between different body compartments (Kotha et al., 2015)

As a result of the unexpected cytosolic localisation of CAR-SIV isoform in the human beta cells (revealed in chapter 3), it was important to further investigate its subcellular localisation which could provide more insights into its physiological role in human beta cell.

The objectives of this chapter are as follows;

- To examine the subcellular localisation of CAR-SIV in *insitu* human pancreatic tissue, isolated human islets and human pancreatic beta cell (EndoC- β H1, & 1.1B4).
- To examine CAR-SIV colocalisation with other insulin secretory granule proteins
- To explore CAR-SIV interaction with other protein partners in the human beta cell

5.2 Results

5.2.1 Cellular localisation of CAR-SIV in the human pancreatic beta cell

To determine where CAR-SIV is localised in the beta cells, formalin fixed paraffin embedded (FFPE) isolated human islets and *in situ* pancreas tissue, were subjected to co-immunofluorescence staining with anti-CAR CT and anti-insulin. This revealed that CAR-SIV was expressed in the insulin positive beta cells (as observed in Chapter 3, section 3.2.10) in both isolated human islets and in *in situ* pancreas sections. In isolated human islets all other cell types (DAPI positive, insulin negative) were negative for CAR-SIV expression (*Figure 5.1*). Strikingly, high resolution confocal microscopy revealed a punctate localisation of CAR-SIV within the beta cells and the apparent co-localisation with insulin (*Figure 5.2*). This implies a possible association between CAR-SIV and insulin secretory granule in beta cells in the human pancreas

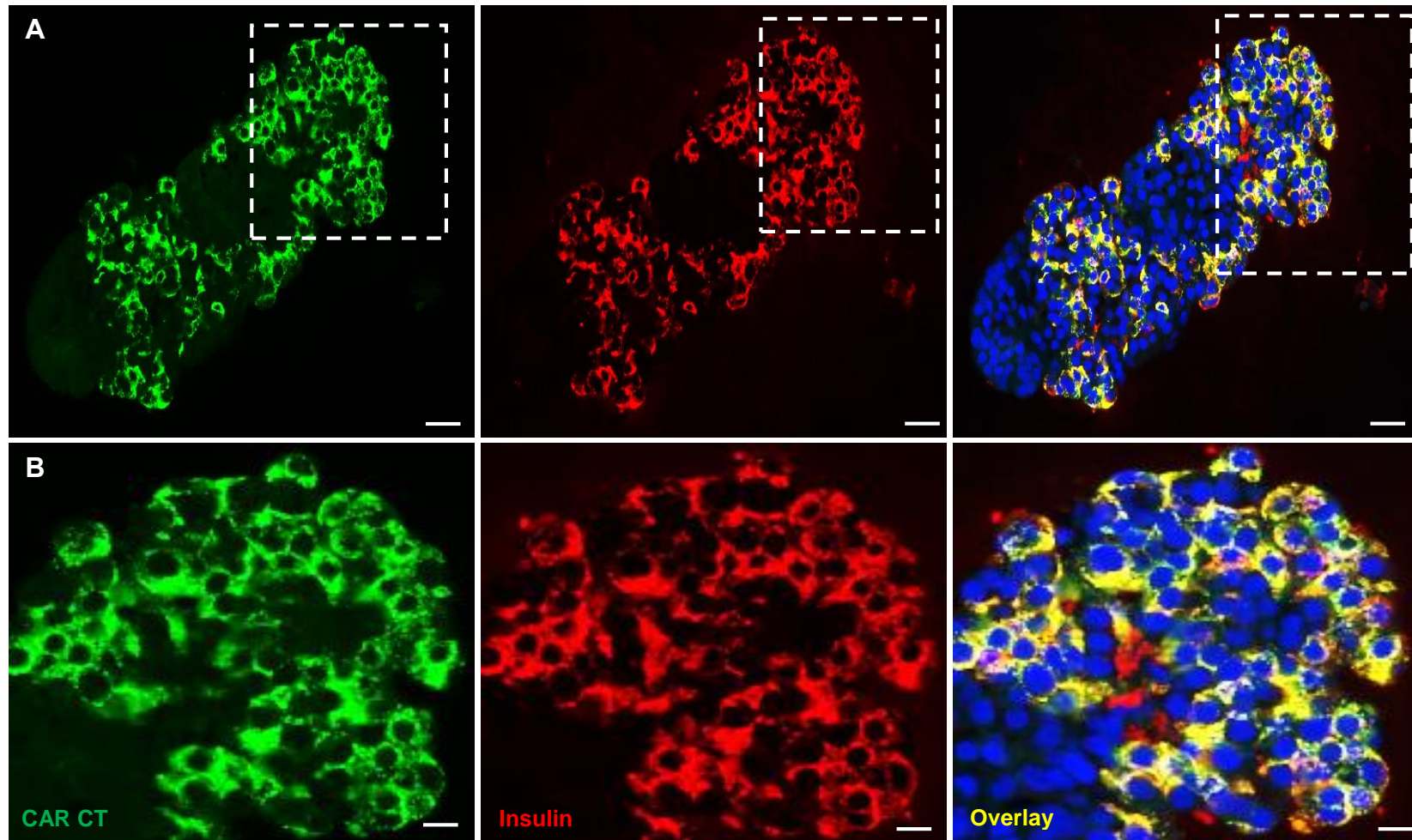


Figure 5.1 CAR-SIV colocalises with insulin in FFPE isolated human islets

(A) Representative immunofluorescence staining with CAR CT antisera revealed that CAR-SIV isoform (anti-CAR CT; green) and insulin (anti-insulin; red) colocalises (yellow) in isolated human islets. (B) Magnified images from (white broken box) demonstrates that CAR-SIV (anti-CAR CT; green) and insulin (anti-insulin; red) colocalises (yellow) in the human beta cell. Nuclei were stained with DAPI (blue). Data are representative of images from three donors. Scale bar 10µm

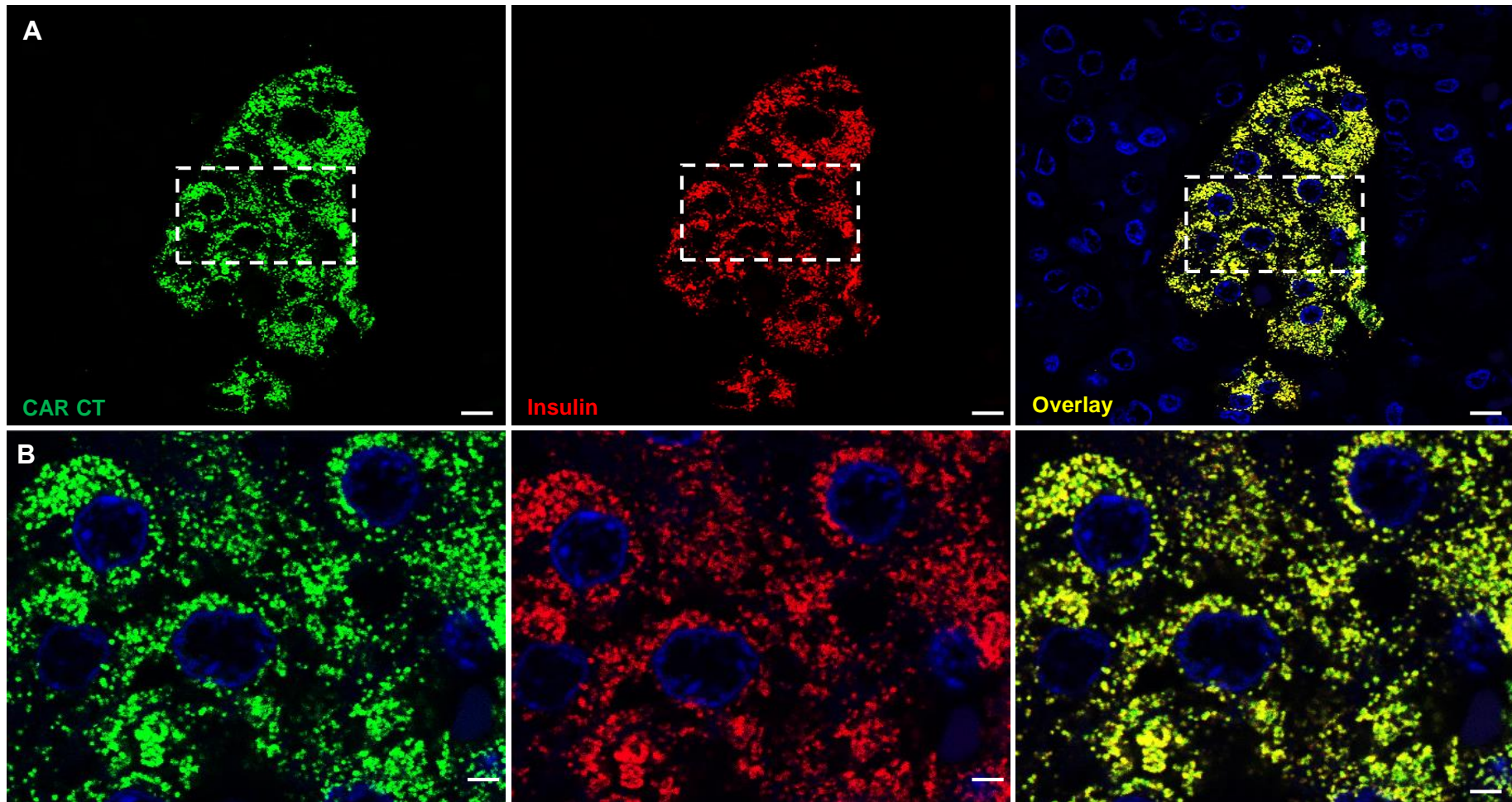


Figure 5.2 CAR-SIV colocalises with insulin in insitu human pancreas

(A) Confocal immunofluorescence staining with anti-CAR CT (green) show that CAR-SIV isoform colocalises (yellow, punctuate distribution) with insulin (anti-insulin; red) in the islet of normal control pancreas. Nuclei were stained with DAPI (blue). (B) Magnified images (white broken box) demonstrating immunofluorescence staining showing CAR-SIV (anti-CAR CT; green) colocalisation with insulin. Data are representative of images from three donors, Scale bar 5 μ m

5.2.2 Co-localisation of CAR-SIV with insulin secretory granule (ISG) proteins in the beta cell

Based on the interesting result that CAR-SIV co-localises with insulin in the beta cells, it was important to confirm whether CAR-SIV also co-localises with other insulin secretory granule proteins expressed in beta cells (Table 5.1). Initially, two ISG (insulin secretory granule) proteins were selected; the Zinc Transporter protein 8 (ZnT8), a granule membrane marker which mediates Zn ion transport, essential for the crystallisation of insulin, and prohormone convertase 1/3 (PC1/3), necessary for the conversion of proinsulin to insulin. The staining confirmed that both ZnT8 and PC1/3 were expressed (as expected) within the islets and that they were localised to the beta cells. Importantly, these two granule protein markers co-localised with the CAR-SIV isoform in the beta cells (Figure 5.3)

Table 5.1 Secretory granule proteins and their localisation in endocrine cells

Secretory granule protein	Endocrine cell localisation
ZnT8	Beta cells (Mature granule)
PC1/3 (Prohormone convertase)	Beta cells (Mature granule)
Proinsulin	Beta cell (immature granule/Golgi)
Glucagon	Alpha cells (granules; utilised as a negative control)

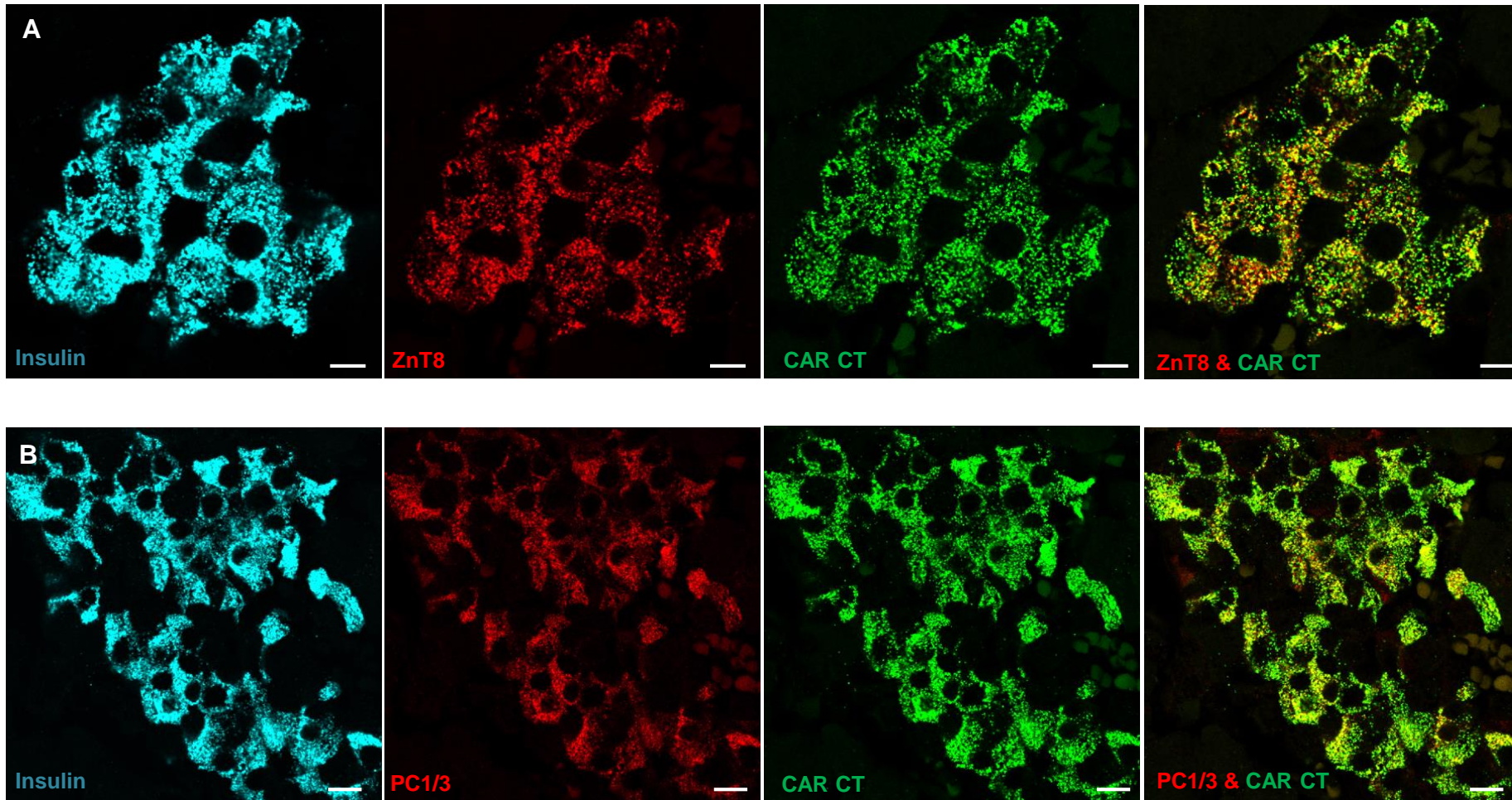


Figure 5.3 CAR-SIV colocalises with insulin secretory granule proteins in the beta cell.

Representative confocal immunofluorescence images shows the colocalisation (yellow) of CAR-SIV (anti-CAR CT; green) and insulin (anti-insulin; light blue) in relation to insulin secretory granule proteins (red) (A) ZnT8 (anti-ZnT8; red); (B) PC1/3(anti-PC1/3; red) in the islet of normal pancreas. Data are representative of images from at least three donors, Scale bar 10µm

Another beta cell marker, proinsulin, a precursor of mature insulin, is known to be localised mainly within the trans-Golgi and the immature insulin secretory granules (Liu et al., 2014). Co-staining of proinsulin and CAR-SIV revealed only partial colocalisation of these proteins in the beta cell (*Figure 5.4A*). An alpha cell granule marker “glucagon” was employed as a control (negative) to verify CAR-SIV colocalisation within the beta cell. The results demonstrate that anti-glucagon staining was detected in alpha cells (as expected) and that CAR-SIV did not colocalise with glucagon (*Figure 5.4B*). Indeed, these results suggest that CAR-SIV isoform is preferentially concentrated in the human beta cell mainly within the mature insulin secretory granules.

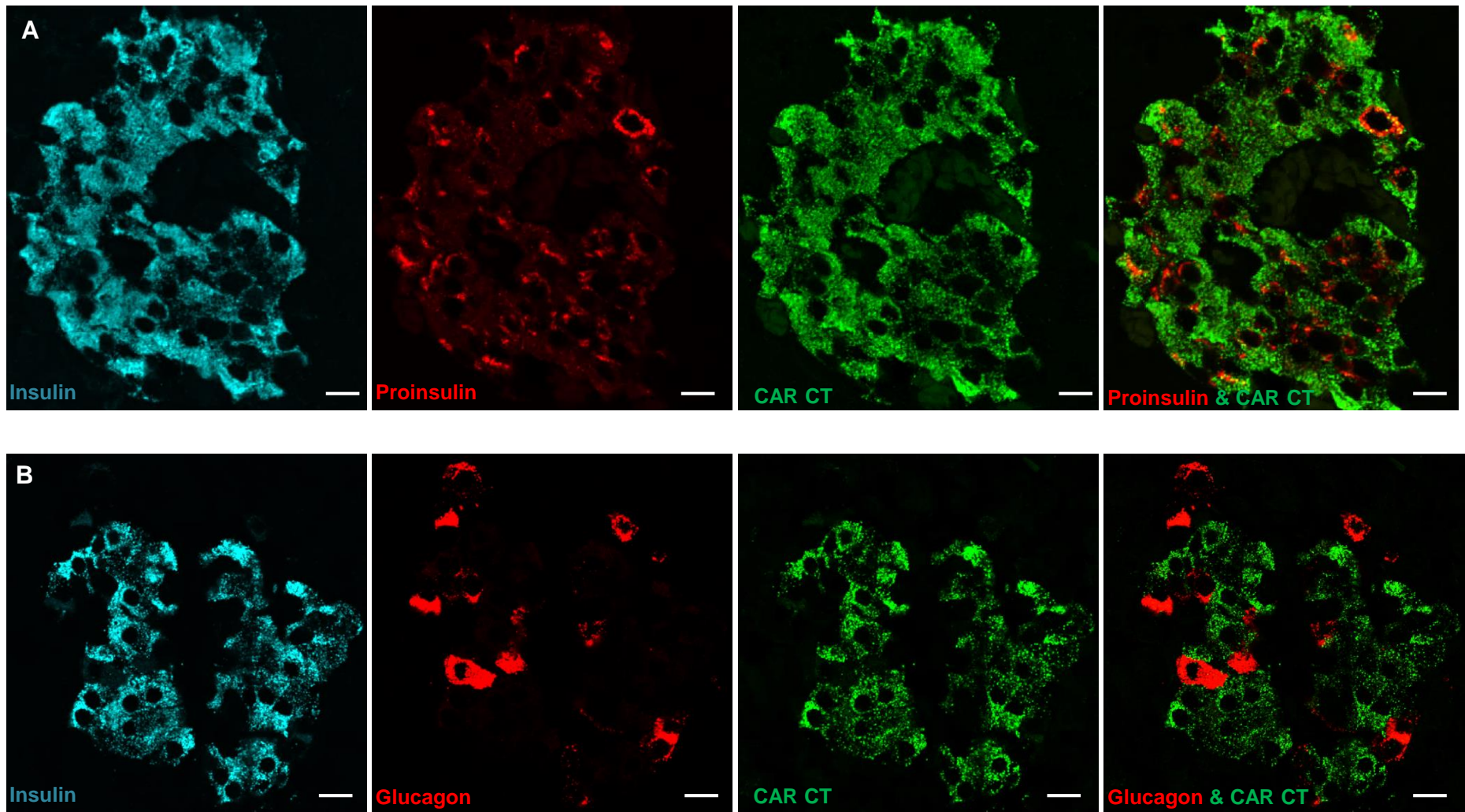


Figure 5.4 CAR-SIV shows a partial colocalisation with proinsulin and no colocalisation with glucagon secretory granule proteins in the human islet.

Representative confocal immunofluorescence images of CAR-SIV isoform (anti CAR CT; green) and insulin (anti-insulin; light blue) in relation to secretory granule proteins (red). Staining with CAR CT antisera reveals CAR-SIV partial colocalisation with (A) Pro-insulin (anti-proinsulin; red); and no colocalisation with (B) Glucagon (anti-glucagon; red) in the islet of normal pancreas. Data are representative of images from at least three donors. Scale bar 10µm

5.2.3 Pearson's correlation coefficient (PCC) quantifies the colocalisation between CAR-SIV and the secretory granule proteins

To quantitatively evaluate the colocalisation of CAR-SIV with secretory granule markers, labelled co-immunofluorescence images obtained from the confocal microscope were assessed using colocalisation software JACoP plugin from Image J version 1.48 Java 1.6.0 _20; (<https://imagej.nih.gov/ij/plugins/track/jacop2.html>). This allowed the generation of a Pearson's correlation coefficient (PCC) which estimates the degree of colocalisation/ association between any two labelled proteins in human pancreas tissue. The PCC values range from (0 – which indicates no colocalisation, to 1 for complete colocalisation).

The PCC provided a confirmation that insulin strongly colocalises with ZnT8 (0.94 ± 0.01) as would be expected from their well-known distribution in beta cells. Importantly, CAR-SIV strongly colocalises with insulin (0.95 ± 0.02), ZnT8 (0.84 ± 0.01) and PC1/3 (0.81 ± 0.02) (*Figure 5.5B&C*, Table 5.2).

In contrast, CAR-SIV weakly associates with proinsulin (0.55 ± 0.04) and does not associate with glucagon (0.05 ± 0.02) (*Figure 5.5*, Table 5.2) which is consistent with the representative high resolution images (*Figure 5.4D&E* and *Figure 5.5B*). These data provide further evidence that CAR-SIV is concentrated more within the mature insulin granule in comparison to the immature granule and that it is unique to the beta cell granules in the islet.

A

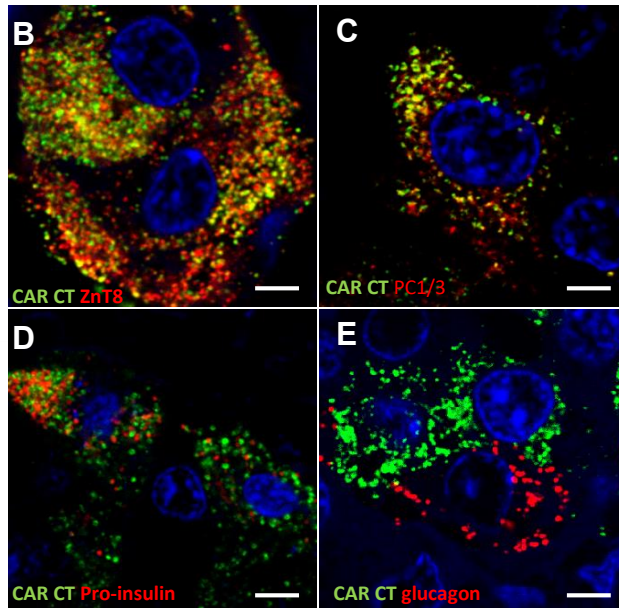
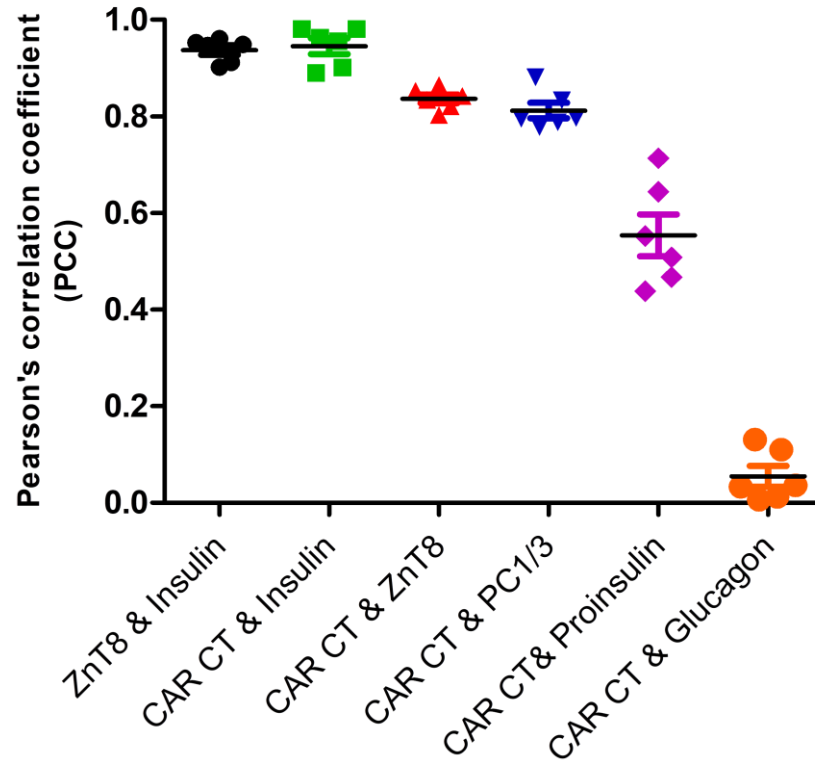


Figure 5.5 Pearson's correlation coefficient (PCC) demonstrating an association between CAR-SIV and insulin secretory granule protein

In the PCC graph (A) each data point represents an islet and from the combination of insulin secretory granule proteins assessed, 2 islets were examined from 3 independent cases. Zoomed in, higher magnification images of CAR-SIV isoform (anti-CAR CT; green) co-localises with secretory granule protein (red) (B)ZnT8; (C) PC1/3; partial co-localisation with (D)proinsulin and no co-localisation was observed with (E) glucagon, (DAPI) is shown in dark blue. Nuclei were stained with DAPI (blue). Immunofluorescence image are representative of images from three donors. Scale bar 10 μ m

Table 5.2 PCC analysis of CAR-SIV and secretory granule proteins

Granule Markers	PCC (Mean \pm SEM)
ZnT8 & insulin	0.94 \pm 0.01
CAR CT & insulin	0.95 \pm 0.02
CAR CT & ZnT8	0.84 \pm 0.01
CAR CT & PC1/3	0.81 \pm 0.02
CAR CT & proinsulin	0.55 \pm 0.04
CAR CT & glucagon	0.05 \pm 0.02

5.2.4 Manders correlation coefficient (MCC) quantifies the colocalisation between CAR-SIV and the secretory granule proteins

By means of an extension of the PCC analysis, the Manders correlation coefficient (MCC) was utilised to quantify the extent/proportion of one protein that overlaps/co-localises with a second protein and vice versa in the human pancreas. For example, it can be used to ask what proportion of the total CAR-SIV protein overlaps with proinsulin and in reverse, what proportion of proinsulin overlaps with CAR-SIV.

The MCC estimate of the co-localisation between CAR-SIV and other secretory granule proteins demonstrates that the majority of ZnT8 co-localises with insulin (0.93 \pm 0.02) and the same was true in the reverse for insulin (insulin co-localises with ZnT8; 0.88 \pm 0.02). Importantly, a high proportion of CAR-SIV co-localises with insulin (0.91 \pm 0.02), ZnT8 (0.87 \pm 0.01) and PC1/3 (0.87 \pm 0.02). This was also similar in reverse where the majority of ZnT8, insulin and PC1/3 also co-localise with CAR-SIV (0.73 \pm 0.04), (0.91 \pm 0.02) and (0.70 \pm 0.02) respectively

(Figure 5.6). This is consistent with these granule proteins all being present in mature insulin secretory granules.

In contrast, no co-localisation of CAR-SIV was found in either direction between CAR-SIV (0.03 ± 0.01) and glucagon (0.03 ± 0.01), (Figure 5.6). Importantly, there was a weak overlap between proinsulin and CAR-SIV (Figure 5.6).

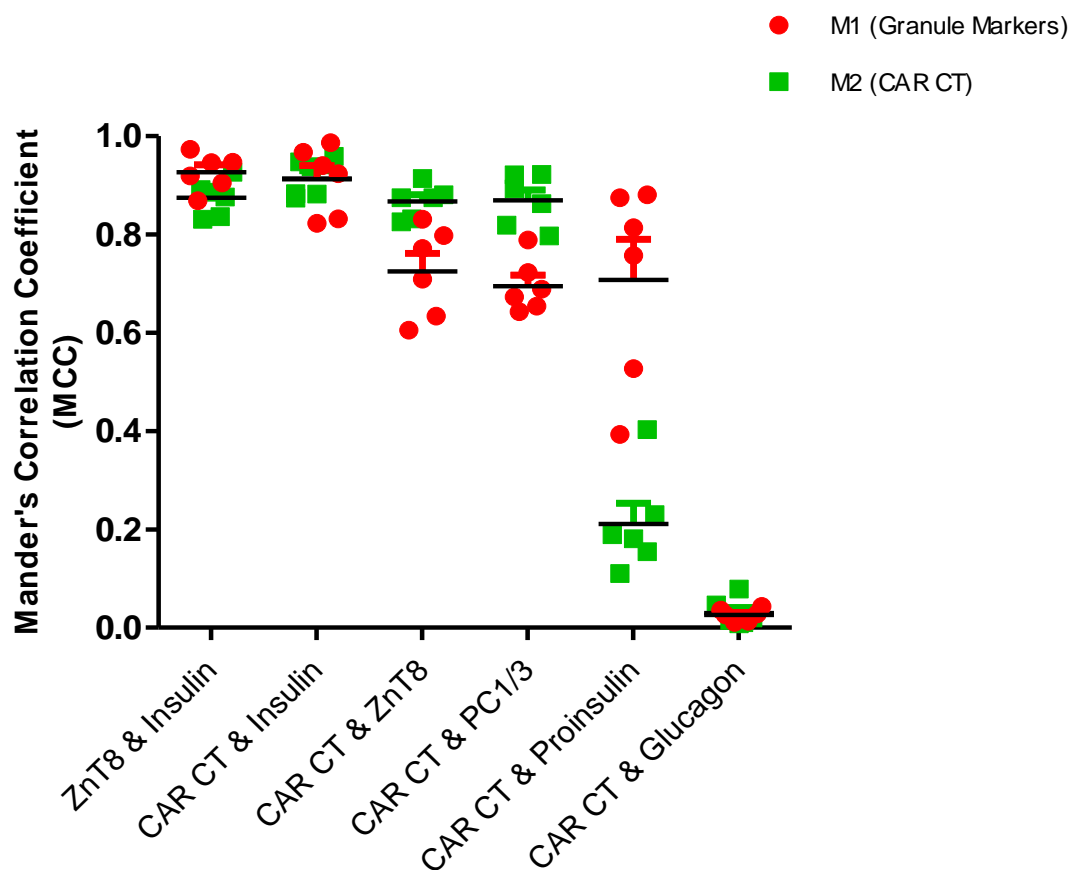


Figure 5.6 Mander's correlation coefficient (MCC) demonstrating the proportion of CAR-SIV that associates with insulin secretory granule proteins

In MCC graph, M1 (red) is the proportion of granule proteins that overlaps with CAR-SIV while M2 (green) is the proportion of CAR-SIV that overlaps with the granule proteins. Each data point represents an islet and from the combination of insulin secretory granule proteins assessed, 2 islets were examined from 3 independent cases

Careful examination of the MCC analysis for CAR-SIV and proinsulin revealed that a large proportion of total proinsulin colocalises with CAR-SIV (0.71 ± 0.082), this is likely to represent both CAR-SIV and proinsulin in the immature granules, as these emerge from the trans-Golgi. In contrast, CAR-SIV does not co-localise to the same extent with proinsulin (MCC: 0.21 ± 0.042), presumably because the majority of CAR-SIV is in the mature granules (shown below in *Figure 5.7*, Table 5.3).

Together, the Pearson's and Manders correlation coefficient reiterate the previous findings and provide supporting evidence that the majority of CAR-SIV is localised to the mature insulin secretory granule. A smaller fraction of CAR-SIV is also observed in the immature insulin granule. The proinsulin that colocalises with CAR-SIV may represent CAR-SIV and proinsulin present in the immature granule soon after emergence from trans-Golgi network

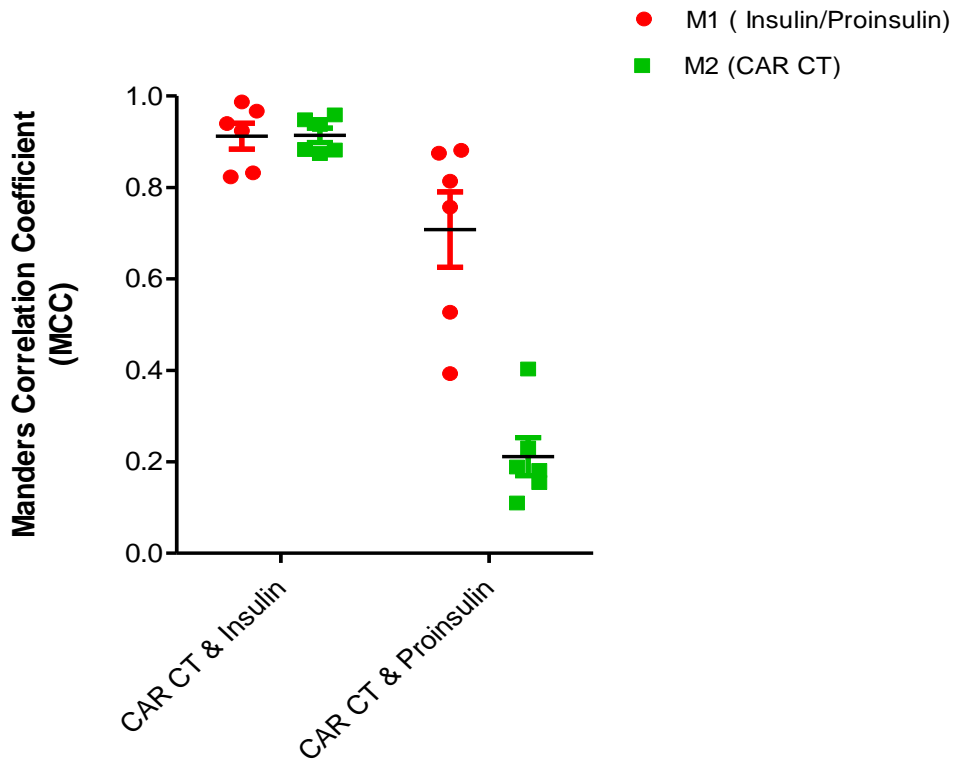


Figure 5.7 Mander's correlation coefficient (MCC) demonstrates that CAR-SIV associates more with insulin but less with proinsulin

M1 (red) is the proportion of insulin or proinsulin granule proteins that overlaps with CAR-SIV while M2 (green) is the proportion of CAR-SIV that overlaps with insulin or proinsulin proteins. In the MCC graph each data point represents an islet and from the combination of (CAR CT & insulin) and CAR CT & proinsulin) granule proteins assessed, 2 islets were examined from 3 independent cases

Table 5.3 MCC analysis of CAR-SIV, insulin and proinsulin proteins

	M1 ± SEM		M2 ± SEM	
Insulin	0.912 ± 0.028		CAR CT	0.914 ± 0.016
Proinsulin	0.708 ± 0.082		CAR CT	0.211 ± 0.042

5.2.5 Cryo-immunogold electron microscopy (Cryo-EM) of CAR-SIV and ZnT8 in the insulin granule

To directly examine the subcellular localisation of CAR-SIV in the beta cells and confirm whether or not it is located within the insulin secretory granule, Dr Varpu Marjomaki (University of Jyväskylä, Finland), performed cryo-immunogold electron microscopy with the CAR CT and ZnT8 antisera.

Immunogold labelling was performed on thin frozen non-diabetic human pancreas (nPOD) sections using the post-embedding Tokuyasu method (Slot and Geuze, 2007) with the antisera CAR CT (labelled with 10nm gold particles) and ZnT8 (labelled with 5nm gold particles). The micrograph images revealed no labelling in the exocrine granules (*Figure 5.8A&B*). Importantly, both the anti-CAR CT and anti-ZnT8 were localised to the dense core insulin secretory granules in human pancreas sections (*Figure 5.8C*). Higher magnification images confirmed the different sizes of gold labelling for anti-CAR CT (10nm) and anti-ZnT8 (5nm) (indicated by black arrows and arrowheads respectively) preferentially at the periphery of the insulin granule (*Figure 5.9*). The characteristic electron dense core structure of the secretory granule observed implies that they contain insulin (Hou et al., 2009). Immunostaining of the pancreas section with anti-insulin antiserum also verified that these were insulin granules (data not shown). It is important to note that the Cryo-EM technique used in this study employs uranyl acetate which yields "negative contrast" for organelle membranes in the staining method employed and as a consequence the appearance of the secretory granules differs from that seen using more conventional osmium labelled cells.

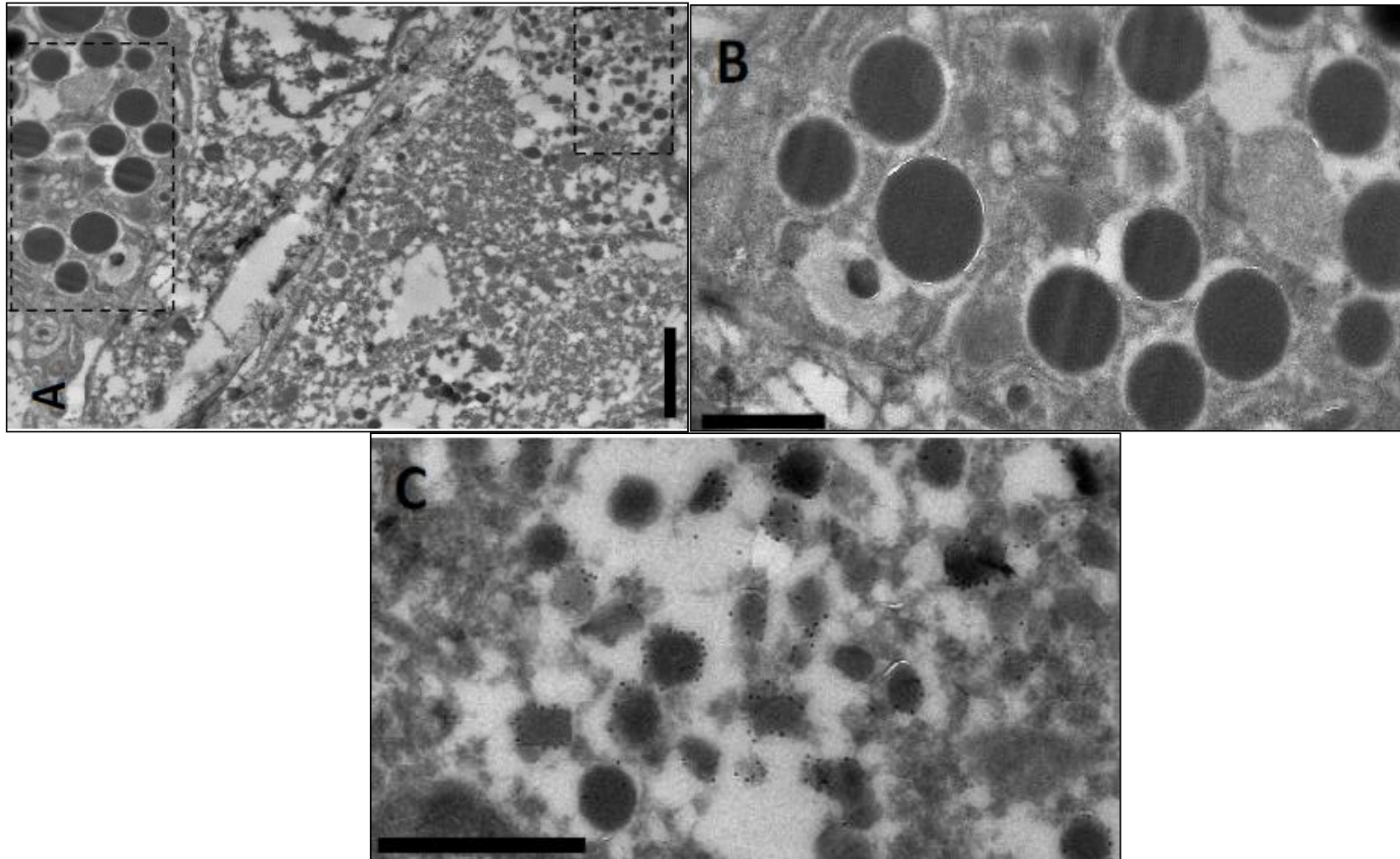


Figure 5.8 Cryo-immunogold electron microscopy revealed that CAR-SIV and ZnT8 is localised to the insulin granule

(A) Low magnification image demonstrates the presence of granules in both the acinar cells and islet cells (Black, broken lines) (B) Higher magnification image revealed lack of CAR-SIV labelling in acinar cell granules (C) Higher magnification image confirms immunogold labelling of CAR-SIV (anti-CAR CT; 10nm) and ZnT8 (ant-ZnT8; 5nm) in thin frozen sections of human pancreas tissue, Scale Bar: 2 μ m(A), 1 μ m(B,C). Courtesy of Dr. Varpu Marjomaki

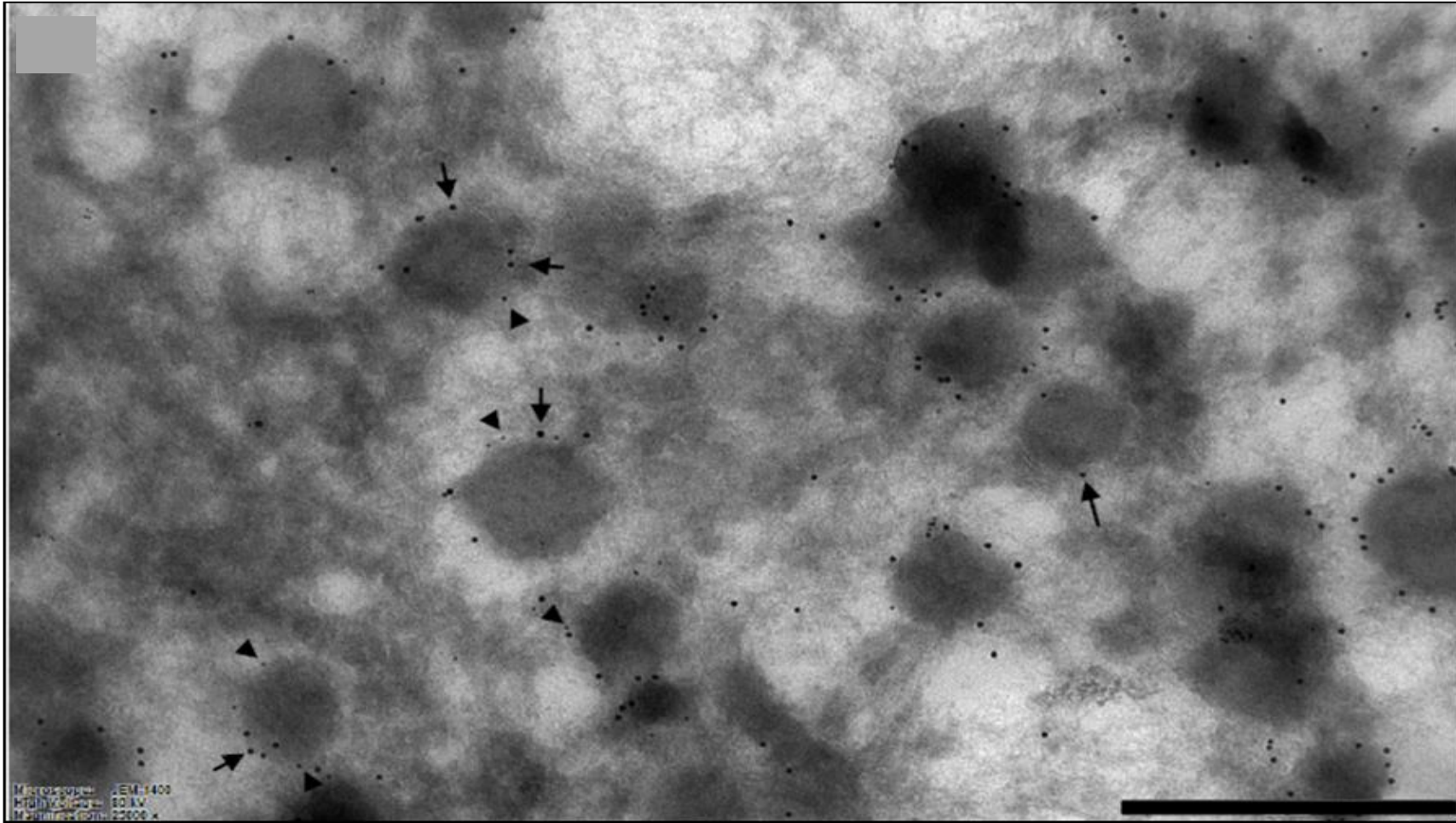


Figure 5.9 Cryo-immunogold electron microscopy.

Higher magnification image showing immunogold labelling of CAR-SIV (anti-CAR CT; 10nm; black arrows) and ZnT8 (anti-ZnT8; 5nm; black arrow heads) in thin frozen sections of human pancreas tissue. Scale bar 500nm. Courtesy of Dr. Varpu Marjomaki

5.2.6 Morphometric quantification of CAR-SIV labelling density

A morphometric analysis of CAR-SIV labelling density was quantified on non-diabetic (nPOD) control pancreas. CAR CT antiserum gold particle labelling in the different compartments of the beta cells, were calculated from 21 different micrographs across 1291 different membrane intersections utilising 841 CAR-SIV immunogold particles. This revealed that 79% of CAR-SIV gold particles were localised to the mature insulin secretory granule and only 14.4% in the immature insulin granule (*Figure 5.10*). Very minimal labelling of CAR-SIV gold particles were found in other intracellular vesicles (1%), endoplasmic reticulum (1.1%), mitochondria (1%), nucleus (1%) and the plasma membrane (2.5%) (*Figure 5.10*). These data provide firm confirmation that CAR-SIV is mainly found in the insulin secretory granule in comparison to other internal subcellular compartments.

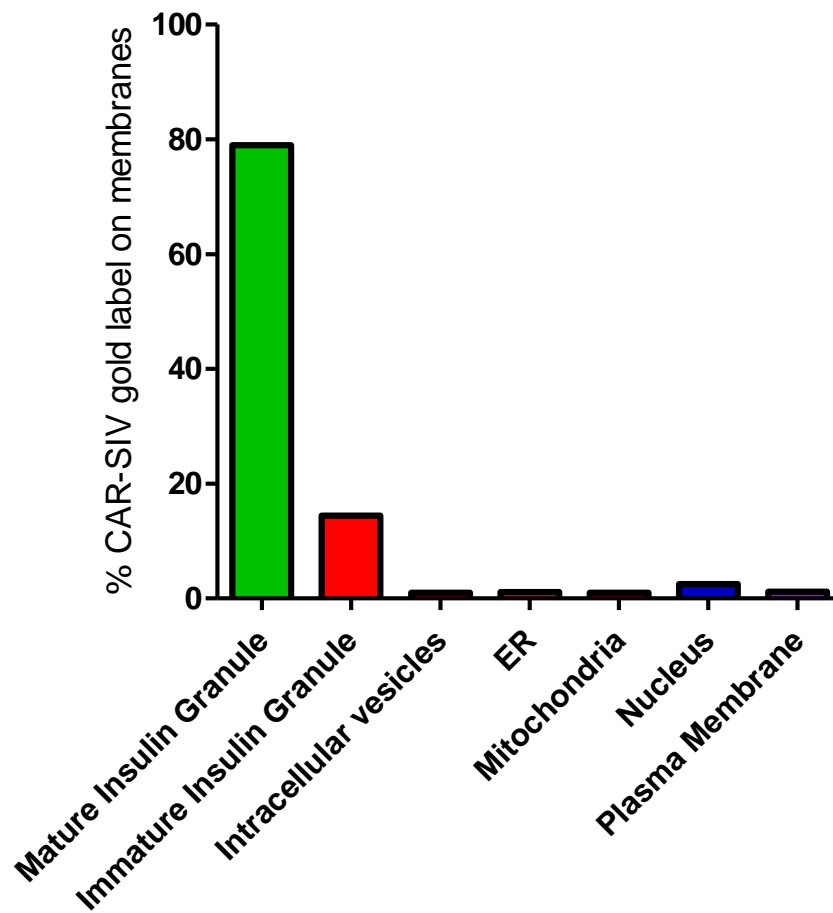


Figure 5.10 Cryo-immunogold electron microscopy quantification.

Graph showing the distribution of CAR-SIV in organelles in thin frozen human pancreatic sections based on quantification utilizing intersection counting. Courtesy of Dr. Varpu Marjomaki

5.2.7 CAR-SIV immunogold labelling at different stages of insulin granule maturation

Further confirmation of CAR-SIV localisation at different stages of insulin granule maturation was also provided by performing immunogold labelling on normal human pancreatic tissue with the following antisera: proinsulin (labelled with

20nm gold particles), CAR-SIV (10nm gold particles) and insulin (5nm gold particles).The data demonstrate that CAR-SIV was localised to granules in the beta cell (*Figure 5.11A&B*) which included; immature granules shown by the presence of proinsulin and CAR-SIV (*Figure 5.11C*); CAR-SIV was also localised to the maturing granules shown by the simultaneous presence of proinsulin, insulin and CAR-SIV (*Figure 5.11D*); and finally CAR-SIV was localised to the mature granule shown by the presence of insulin and CAR-SIV (*Figure 5.11E*).Assessment of 122 granules containing CAR-SIV revealed that 6 (4.9%) were positive for proinsulin (immature granules); 30 (24.6%) were positive for proinsulin and insulin (maturing granules) while the majority of CAR-SIV(86 (70.5%)) immunogold labelled granules were positive for insulin (mature granules).In addition, we show that unconjugated gold particles not bound to serum did not label the pancreatic tissue (*Figure 5.12*)

Collectively, these results suggest that CAR-SIV is present at all stages of granule maturation.

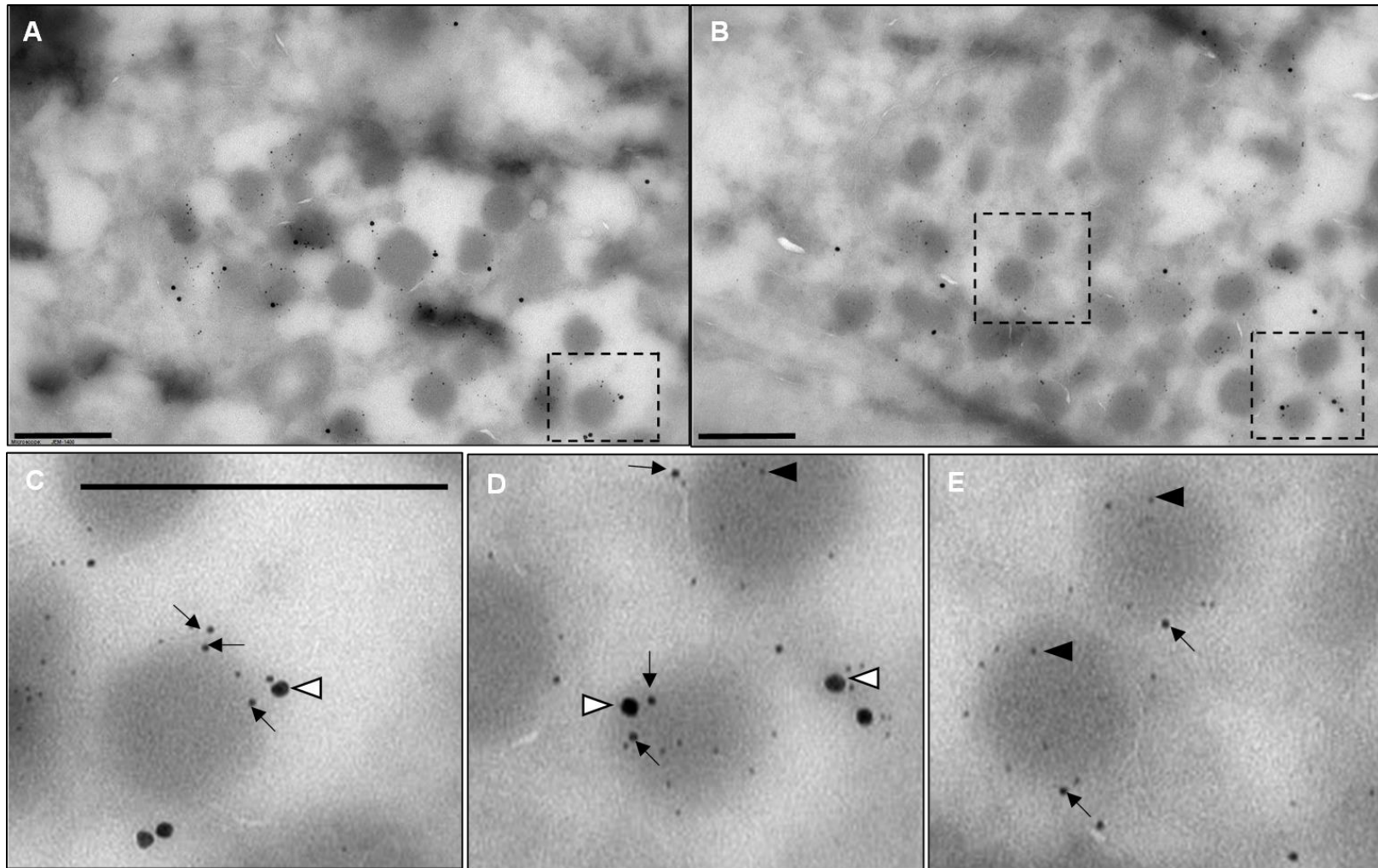


Figure 5.11 Cryo-immune EM analysis of insulin granules at different stages of maturation. Low magnification image (a-b) demonstrates immunogold labelling of insulin (5nm gold; black triangle); CAR-SIV (10nm gold; black arrow) and proinsulin (20nm gold; white triangle) in thin frozen sections of human pancreas tissue. High magnification image reveal (c) immature granules positive for proinsulin and CAR-SIV (d) maturing granules positive for proinsulin, insulin and CAR-SIV and mature granules positive for insulin and CAR-SIV, Scale bar 500nm. Courtesy of Dr. Varpu Marjomaki

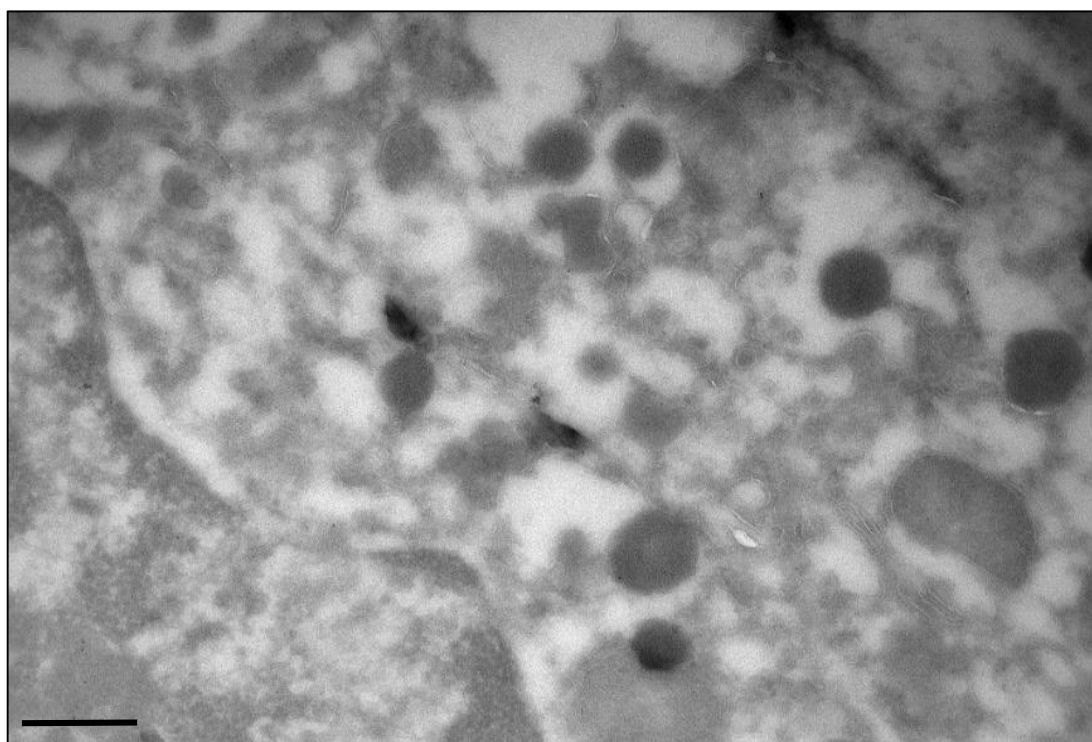


Figure 5.12 Cryo-EM analysis of pancreatic tissue with unconjugated gold particles. Pancreatic tissue when exposed to unconjugated gold particles display no labelling in the granules in the beta cell, Scale bar 500nm. Courtesy of Dr. Varpu Marjomaki

5.2.8 Detection of PICK1 protein expression in human pancreatic tissue by immunohistochemistry

There is cumulative evidence that a peripheral membrane protein PICK1 (Protein interacting with Ckinase 1), plays a crucial role in vesicle trafficking and is highly expressed in tissues characterised by secretory vesicles such as the brain, testis, kidney, stomach, and pancreas where extensive vesicle secretion occurs (Dev et al., 1999, Cao et al., 2007, Xia et al., 1999). Importantly, it has recently been shown that PICK1 plays a crucial role in insulin granule budding and maturation (Cao et al., 2013). PICK1 is a unique protein that contains both a PDZ domain

and a BAR domain (Xu and Xia, 2006). The BAR domain mediates its interaction with ICA69 and is important in sensing membrane curvature and facilitating vesicle formation (Jin et al., 2006, Madsen et al., 2008). Strikingly, the PDZ domain of PICK1 specifically interacts with the PDZ binding domain of CAR-SIV (Excoffon et al., 2004), but not the PDZ binding domain of CAR-TVV. Due to the localisation of CAR-SIV to the insulin secretory granule it is possible that the CAR-SIV PDZ binding domain may interact with PICK1 and play a fundamental role in the beta cell.

To assess if PICK1 is expressed in the human pancreas, a commercially available antiserum designated "PICK1 SC" with the capability of recognising the epitope belonging to the PDZ binding and BAR domain (22-105aa) was employed. Immunohistochemical studies revealed that PICK1 was detected in the islet cells and not in the exocrine compartment of *insitu* human pancreas (Figure 5.13)

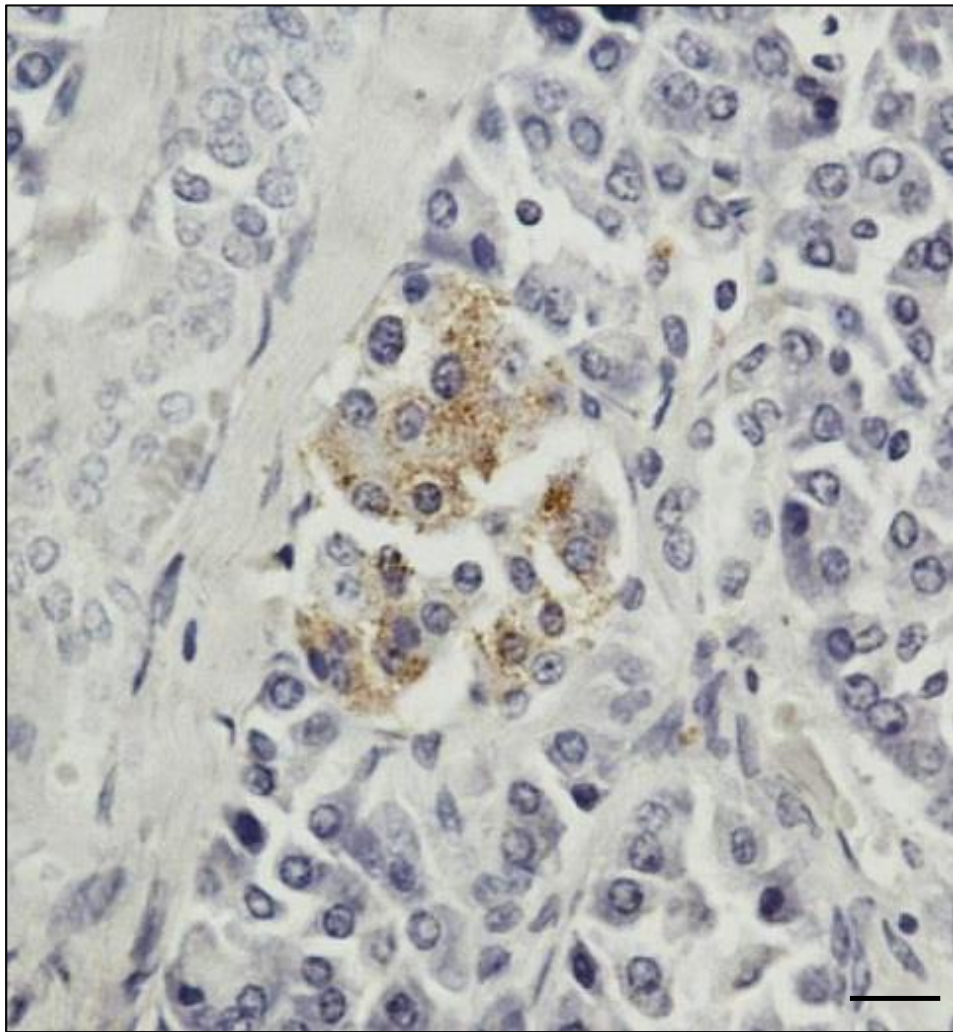


Figure 5.13 PICK 1 is expressed in the islet of normal human pancreatic tissue. Immunohistochemical analysis detecting PICK1 (anti-PICK1 SC; brown stain) in the endocrine cells of the islets and negative (no brown stain) in the exocrine tissue. Data are representative of images from three donors, Scale bar 20 μ m

5.2.9 PICK1 detection by immunofluorescence and confocal immunofluorescence microscopy

In order to determine if PICK1 is present in the beta cells, combined immunofluorescence staining was utilised with anti-PICK1 SC in combination with anti-CAR CT and anti-insulin in normal pancreatic tissue. PICK1 was present in the beta cells as detected by the colocalisation with anti-insulin and anti-CAR CT (*Figure 5.14A*) PICK1 was not however limited to the beta cells because non-beta cells were also PICK1 positive indicated by yellow arrows (*Figure 5.14B*).

To assess the extent of colocalisation of PICK1, CAR-SIV and insulin in the beta cell, confocal microscopy coupled with a hyvolution software which provides improved resolution upon deconvolution was utilised. The result demonstrates that both PICK1 and CAR-SIV were colocalised with insulin as indicated by the brown arrows in *Figure 5.15*.

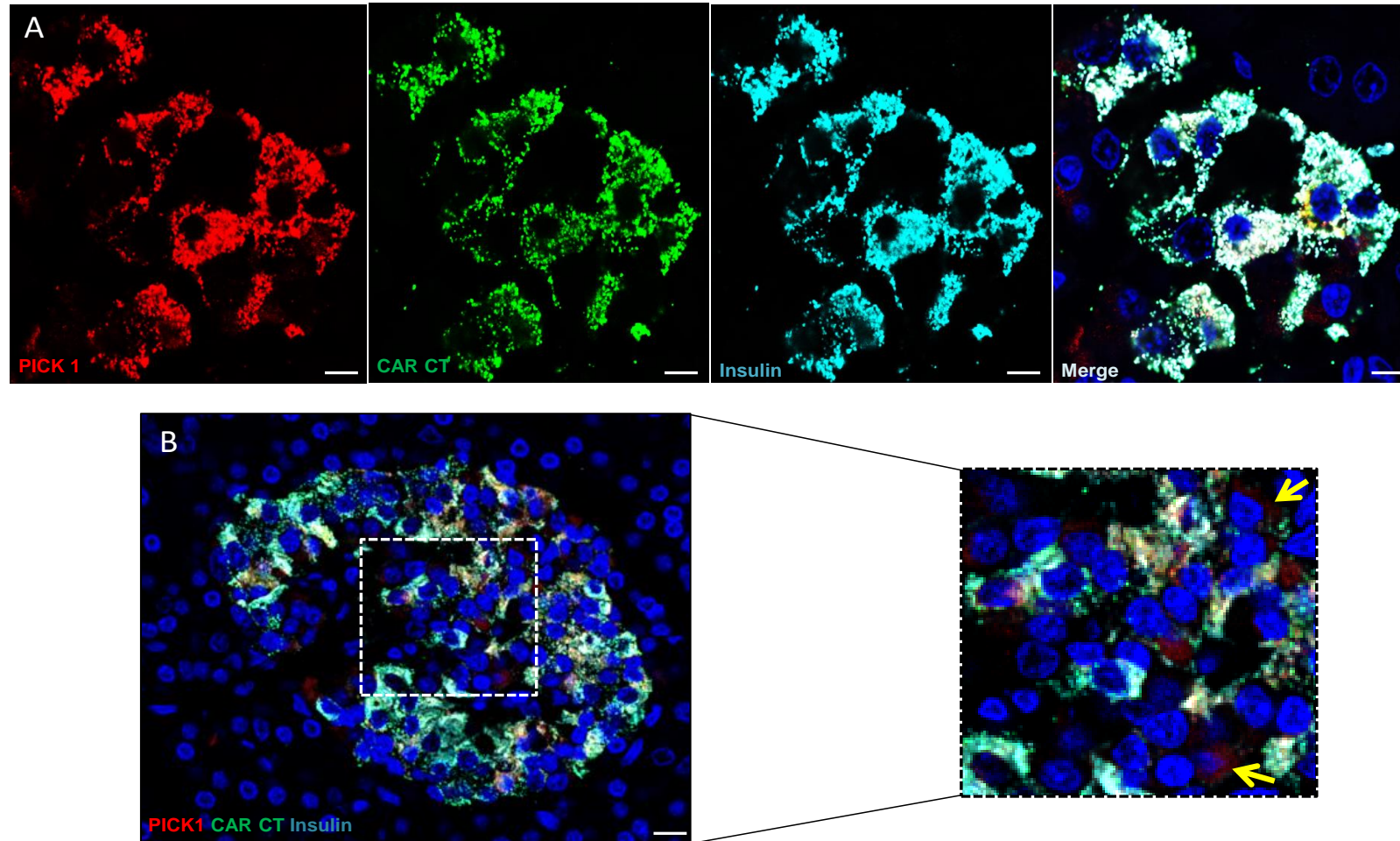


Figure 5.14 CAR-SIV colocalises with PICK1 and insulin in the beta cell in normal pancreas tissues.

(A) Representative confocal immunofluorescence images of CAR-SIV (anti-CAR CT; green) and PICK1 (anti-PICK1; red) colocalising (light blue) with insulin (anti-insulin; blue). (B) Magnified images of PICK1 (red; yellow arrows) show positivity in non-beta cells that are insulin and CAR-SIV negative. Nuclei were stained with DAPI (blue). Data are representative of images from three donors, Scale bar (A) 5um (B) 25um

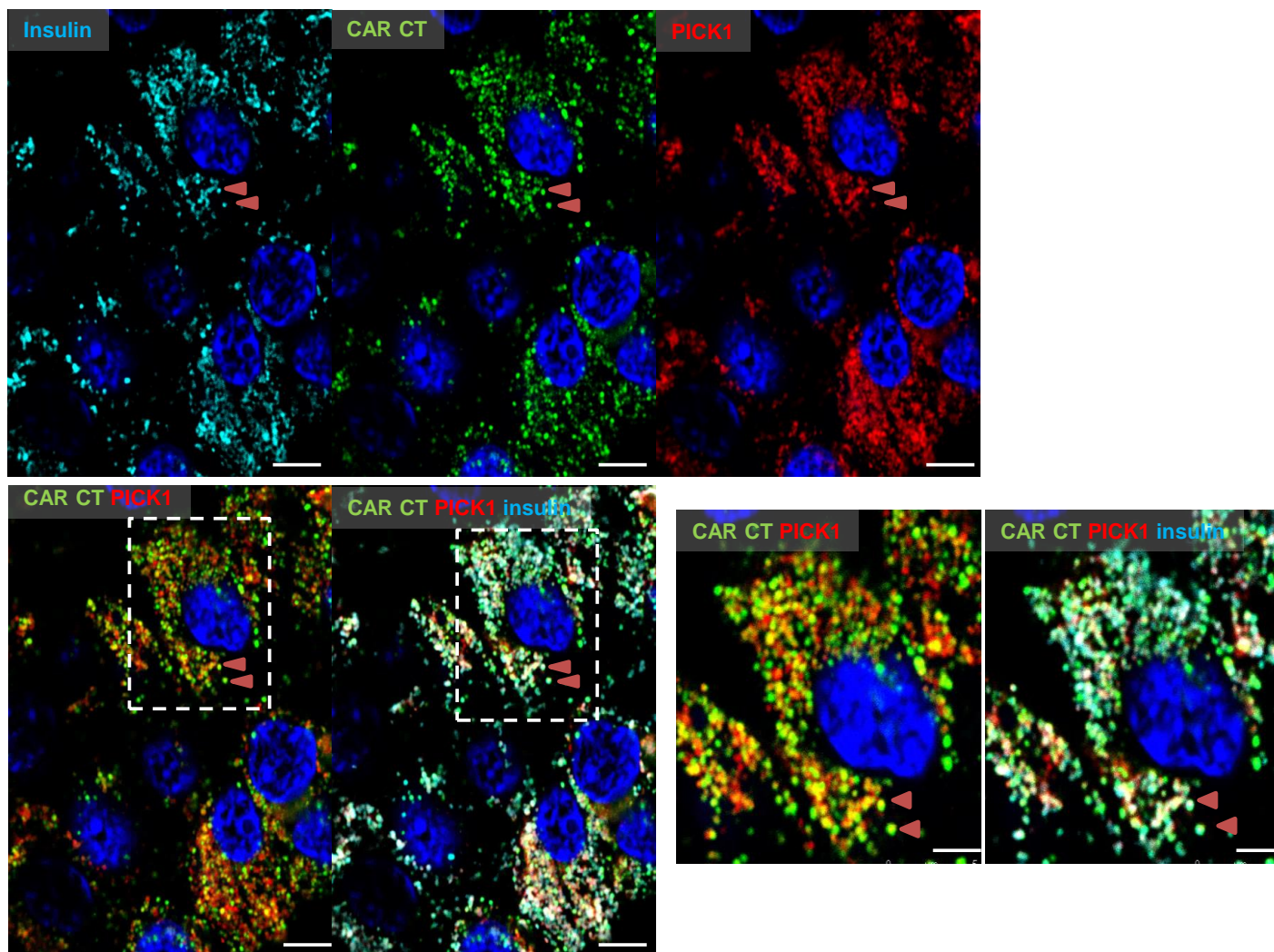


Figure 5.15 Confocal microscopy coupled with hyvolution imaging demonstrates a close association of CAR-SIV and PICK1 in insulin granule of normal human pancreas.

Magnified images with brown arrows indicate granules positive for CAR-SIV (anti-CAR CT; green), PICK1 (anti-PICK1 SC; red) and insulin (anti-insulin; light blue) in the beta cell, Nuclei were stained with DAPI (blue). Data are representative of images from three donors, Scale bar 5µm

5.2.10 Pearson's correlation coefficient and Mander's correlation coefficient quantifies the colocalisation of PICK1, CAR-SIV and Insulin

To quantify the extent of colocalisation between PICK1, CAR-SIV and insulin, the Pearson's correlation coefficient and Manders correlation coefficient were employed. PCC exhibited a strong association between CAR-SIV and insulin as expected (0.95 ± 0.02), CAR-SIV showed a strong association with PICK1 (0.73 ± 0.02) while PICK1 also strongly associated with insulin (0.84 ± 0.04) (*Figure 5.16A*, Table 5.4)

For MCC analysis, there was a strong overlap (as expected) between insulin and CAR-SIV (0.91 ± 0.03) and CAR-SIV and insulin (0.91 ± 0.02). The majority of CAR-SIV (0.84 ± 0.03) colocalises with PICK1, but not all PICK1 (0.55 ± 0.05) colocalises with CAR-SIV. A strong overlap was also observed with PICK1 and insulin (0.80 ± 0.06) and, insulin and PICK1 (0.85 ± 0.02) (*Figure 5.16B*, Table 5.4). One explanation for the lower MCC value of the PICK1 (0.55 ± 0.05) colocalisation with CAR-SIV could be due to the fact that PICK1 is expressed in non-beta cells (*as shown previously in Figure 5.14*) as well as beta cells.

Collectively, these data imply that PICK1 associates with CAR-SIV and insulin in the beta cell and based on PICK1's role we can postulate that CAR-SIV association with PICK1 may synergistically play a role in insulin granule maturation and trafficking of insulin vesicle granules

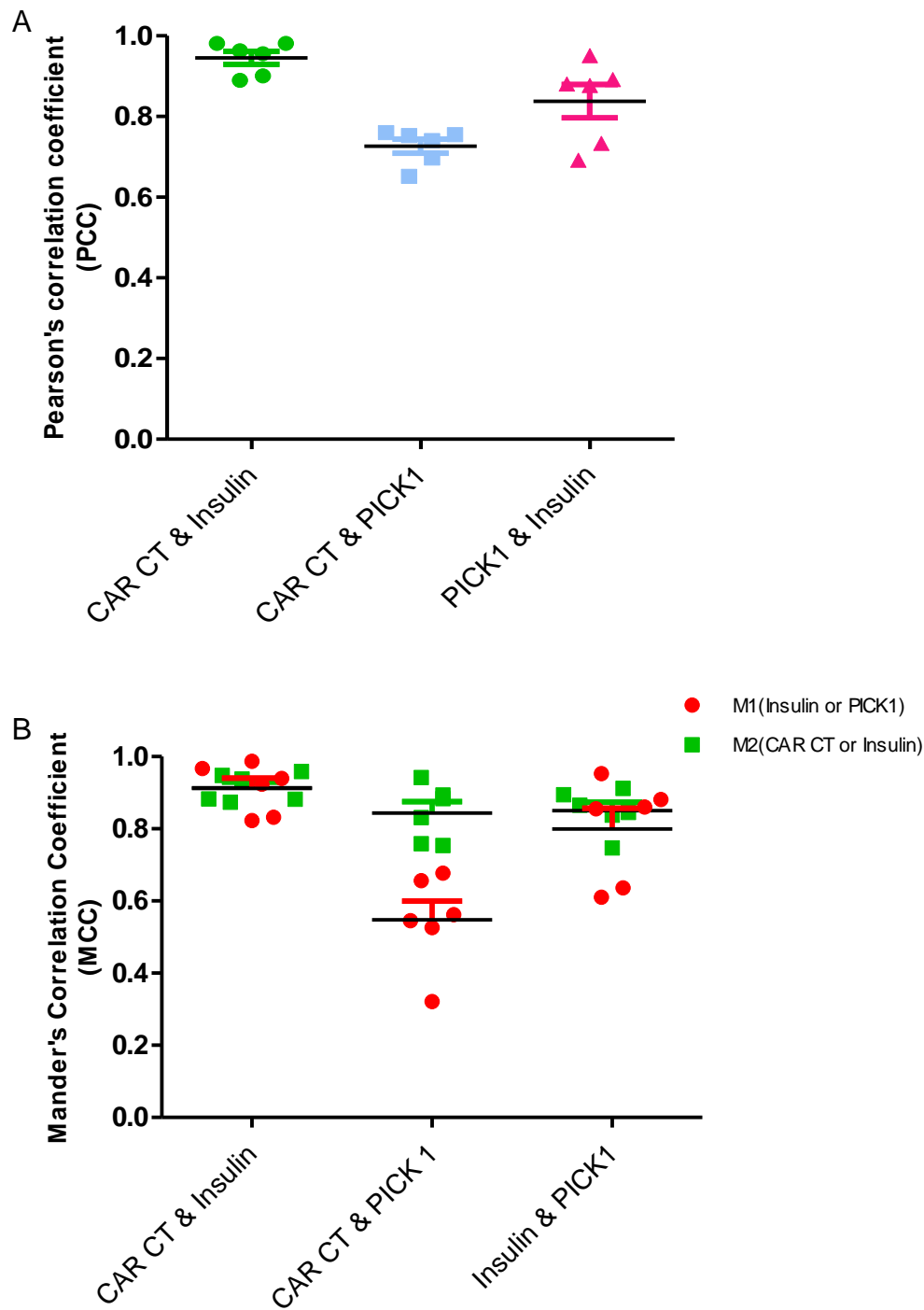


Figure 5.16 Pearson correlation coefficient and Manders correlation coefficient demonstrating the extent of CAR-SIV colocalisation with PICK1 and insulin.

(A) PCC and (B) MCC shows where M1 (red) is the proportion of insulin or PICK1 granule proteins that overlaps with CAR-SIV while M2 (green) is the proportion of CAR-SIV or insulin that overlaps with PICK1. In the graph, each data point represents an islet and from the combination of (CAR CT & insulin), (CAR CT & PICK1) and (insulin & PICK1) granule proteins assessed, 2 islets were examined from 3 independent cases

Table 5.4 Pearson and Manders correlation coefficient of CAR-SIV association with PICK1 and insulin. M1 – the proportion of the first protein that colocalises with the second; M2 – the proportion of the second protein that colocalises with the first.

Granule Markers	PCC (Mean \pm SEM)	M1	M2
Insulin (M1) & CAR CT (M2)	0.95 \pm 0.02	0.91 \pm 0.03	0.91 \pm 0.02
PICK1 (M1) & CAR CT (M2)	0.73 \pm 0.02	0.55 \pm 0.05	0.84 \pm 0.03
PICK1 (M1) & Insulin (M2)	0.84 \pm 0.04	0.80 \pm 0.06	0.85 \pm 0.02

5.2.11 PICK1 expression by Western blotting analysis

To validate PICK1 expression shown previously by immunohistochemical and immunofluorescence approach, three further commercially available antisera (suitable for Western blotting) designated “PICK1 ab133773”, “PICK1 ab3420” and “PICK1 L20/8” whose epitope recognition sites are displayed in Figure 5.17 were purchased.

Protein lysates extracted from human islets and pancreatic beta cell lines EndoC- β H1 and 1.1B4 were electrophoresed on poly-acrylamide gels and then transferred onto a PVDF membrane. Following a blocking step, membranes were probed with either “PICK1 ab133773” or “PICK1 L20/8”. Probing with PICK1 ab133773 antiserum revealed an estimated band at around 50kDa (equivalent to the estimated molecular weight) in isolated human islets. A similar sized but less intense band was also observed in EndoC- β H1 cells (*Figure 5.18A*). The PICK1 L20/8 antiserum also revealed a band estimated at 50kDa in the isolated human islets, again at a higher intensity when compared to EndoC- β H1 and 1.1B4 cells (*Figure 5.18B*). Together these results demonstrate that PICK1 is highly

expressed in isolated human islets and is also present in EndoC- β H1 and 1.1B4 cells albeit at lower levels.

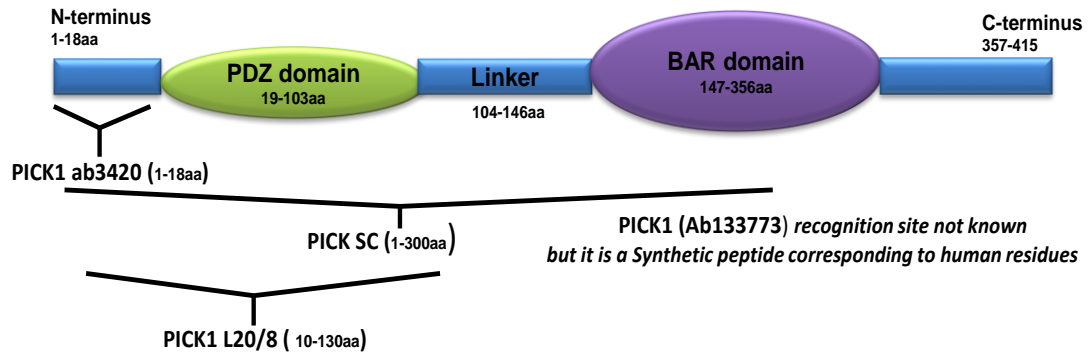


Figure 5.17 Schematic diagram of PICK1 antisera with epitope recognition sites against the PICK1 protein. Adapted from (Xu and Xia, 2006)

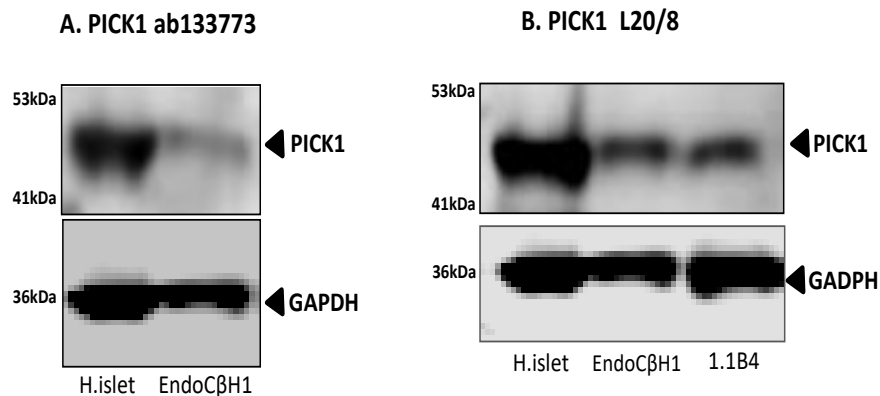


Figure 5.18 Confirmation of PICK1 expression in isolated human islets and pancreatic beta cell lines EndoC- β H1 and 1.1B4.

EndoC- β H1, 1.1B4 cells and isolated human islets were lysed and total protein was isolated for western blotting to detect PICK1 with both antisera; PICK1 ab133773 and PICK1 L20/8. Western blotting analysis detecting an approximate band size of 50kDa with two different PICK1 antisera (A) PICK1 ab133773 (B) PICK1 L20/8 and loading control GAPDH. Data are representative of 3 independent experiments.

5.2.12 Do PICK1 and CAR-SIV interact in the human pancreatic beta cell?

The study by Excoffon *et al* (2004) utilised co-immunoprecipitation experiments in overexpression studies to demonstrate that CAR-SIV and PICK1 interact with one another via the PDZ domain in human airway epithelial cells (Excoffon *et al.*, 2004)

To investigate if PICK1 could interact with CAR-SIV endogenously in the human pancreatic beta cells, we initially examined if these proteins could be individually immunoprecipitated from EndoC- β H1 cells. Protein lysates under non-denaturing conditions (Chapter 2, section 2.19) were collected from EndoC- β H1 cells and incubated with either CAR RmcB or PICK1 L20/8 antisera. Beads were added to bind to the antibody-lysate complex; unbound antibody/proteins were then removed by washing. Protein was then extracted from the beads using standard denaturing lysis buffer and examined by Western blotting.

PICK1 was successfully pulled down from using the PICK1 L20/8 antiserum, with an approximate band size of 50kDa which was also present in the total lysates input (positive) control (*Figure 5.19A*). Utilising other antisera, PICK1 pull down was also confirmed by precipitating lysates incubated with PICK1 ab3420 antiserum (*Figure 5.19B*). CAR-SIV was also successfully pulled down with the CAR RmcB antiserum, with a band size of 40kDa which was present in the total lysates input (positive) control (*Figure 5.19C*). CAR ECD antiserum was also capable of immunoprecipitating CAR (*Figure 5.19D*).

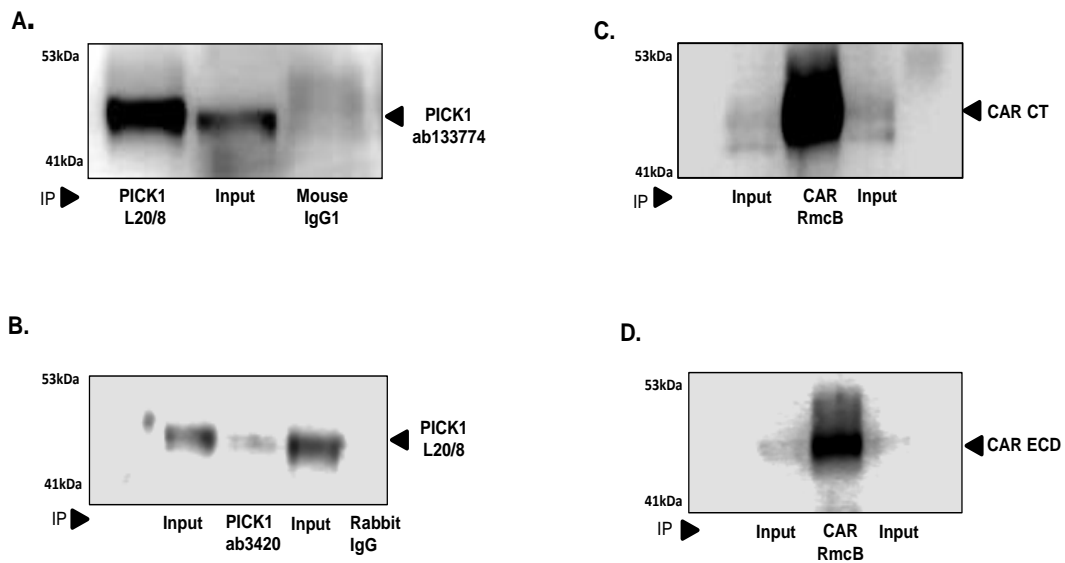


Figure 5.19 Immunoprecipitation of PICK1 and CAR-SIV independently from EndoC- β H1 with different antisera.

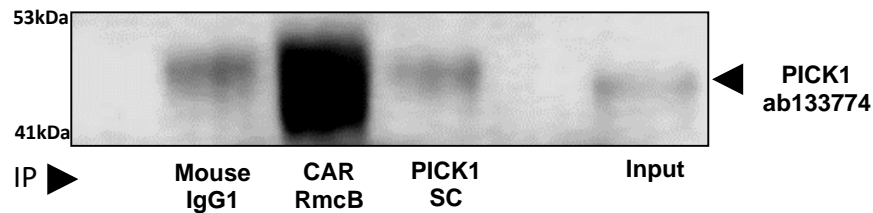
EndoC- β H1 cells were lysed and total protein was isolated for immunoprecipitation followed by western blotting. Immunoprecipitation of PICK1 with (A) PICK1 L20/8 antiserum pulls down PICK1 (anti-PICK1 ab133774) (B) PICK1 ab3420 antiserum pulls down PICK1 (anti-PICK1 IL/20). Immunoprecipitation of CAR-SIV with (C) CAR RmcB antiserum pulls down CAR-SIV (anti-CAR CT) (D) CAR RmcB antiserum pulls down CAR (anti-CAR ECD). Anti-mouse IgG and Rabbit IgG (controls) were all negative and all input (positive controls) were 2%. Data are representative of 3 independent experiments.

To directly confirm if PICK1 and CAR-SIV do interact, a co-immunoprecipitation (Co-IP) assay was utilised in lysates extracted from isolated human islets and EndoC- β H1 cells. The result shows that PICK1 was successfully pulled down along with CAR when immunoprecipitated with the CAR RmcB antiserum. A band for PICK1 (50kDa) was clearly observed in the CAR Co-IP lane, when

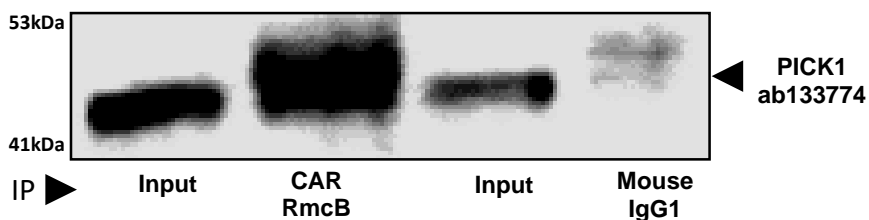
probed with the PICK1 SC antiserum. A PICK1 band was also present in total lysates input (positive) control lane (*Figure 5.20A*). These results were further confirmed in the EndoC- β H1 cells (*Figure 5.20B*) and when probed with the CAR CT antiserum a band for CAR-SIV at the appropriate molecular weight (40kDa) was observed confirming that the CAR-SIV isoform was part of this complex (*Figure 5.20C*).

In the other direction, utilising the PICK1 SC antiserum to Co-IP the complex in isolated human islets, CAR was pulled down, albeit weakly, from precipitated PICK1, revealed by a band of approximately 46kDa (*Figure 5.21A*). Similarly, in EndoC- β H1, utilising the PICK1 ab3420 to Co-IP, CAR was also pulled down. This band was however marginally higher in molecular weight when compared to the total lysates input (positive) controls (*Figure 5.21B*).

A. Human islets



B. EndoC-βH1



C. EndoC-βH1

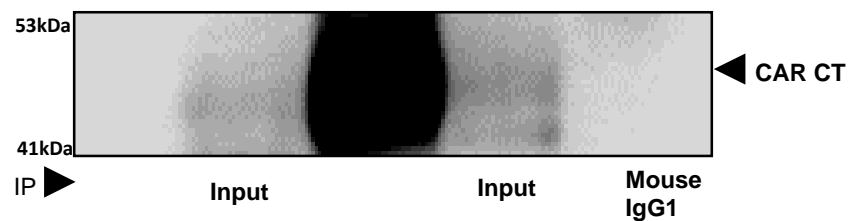
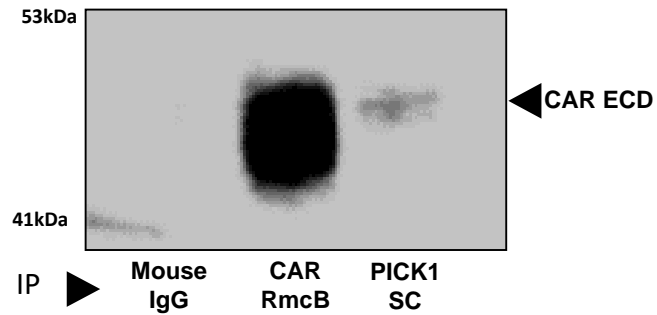


Figure 5.20 Co-immunoprecipitation of CAR pulls down PICK1.

Human islets and EndoC-βH1 cells were lysed and total protein was isolated for immunoprecipitation followed by western blotting. Co-Immunoprecipitation with CAR (anti- CAR RmcB) and PICK1(anti-PICK1 SC) pulls down PICK1(anti-PICK1 ab133774) from (A) isolated human islets and (B) EndoC-βH1 (C) CAR-SIV isoform complex is confirmed after probing with CAR CT antiserum, anti-mouse IgG and anti-Rabbit IgG were all negative and all input (positive) controls were 2%. Data are representative of 3 independent experiments.

A. Human islets



B. EndoC-βH1

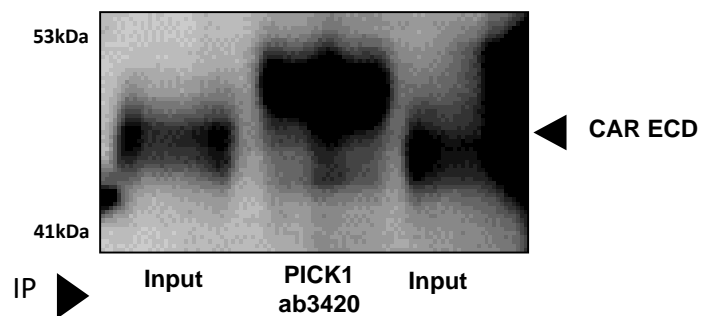


Figure 5.21 Co-immunoprecipitation of PICK1 weakly pulls down CAR.

Human islets and EndoC-βH1 cells were lysed and total protein was isolated for immunoprecipitation followed by western blotting. Co-immunoprecipitation with PICK1 (anti-PICK1 SC/anti-PICK1 ab3420) pulls down CAR (anti-CAR ECD) (A) from isolated human islets and (B) EndoC-βH1. Anti-mouse IgG was used as negative control and all input (positive control) were 2%. Data are representative of 3 independent experiments.

5.3 Discussion

The data obtained from examining the subcellular localisation of CAR-SIV isoform in the human pancreatic beta cell has provoked some fundamental findings which are discussed in this section below.

5.3.1 CAR-SIV colocalises with insulin in human pancreatic beta cells

In this study, high resolution confocal microscopy analysis observed a punctate cytoplasmic granular localisation of CAR-SIV in the beta cells of isolated human islets and human pancreatic tissue. This is consistent with CAR-SIV being distributed in a distinct intracellular organelle compartment. Analysis of the colocalisation of CAR-SIV and insulin demonstrated a strong association, suggesting that CAR-SIV is localised to the insulin granule within beta cells *in vivo*. Similarly, as shown previously in chapter 3 (*Figure 3.17*) two different CAR antisera, “CAR CT” antiserum which recognises the C terminus (CT) of CAR and the less selective “CAR ECD” antiserum which recognises the extracellular domain of CAR were shown to colocalise with insulin in isolated human islets and human pancreatic sections. These two independent CAR antisera directed against different regions of CAR protein provides strong supporting evidence of CAR-SIV localisation in the insulin granule.

5.3.2 CAR-SIV is present in both immature and mature insulin secretory granule proteins

This intriguing discovery that CAR-SIV was predominantly localised within the cytoplasm and that it closely associates with insulin in the beta cells,

encouraged additional study of four secretory granule proteins PC1/3, ZnT8, proinsulin and glucagon to investigate this further.

As described in Chapter 1 (section 1.3.3), during the biogenesis of insulin, the initial immature proinsulin secretory granules bud from the trans-Golgi network to undergo further processing. Acidification of the granule lumen then facilitates the cleavage activity of endoproteases PC1/3 (which cleaves the B-C junction of the proinsulin peptide sequence) and PC2 (which cleaves the A-C junction of the proinsulin peptide sequence) (Goodge and Hutton, 2000). Subsequently, carboxypeptidase (CPE) trims the C terminal two-basic amino acids yielding mature insulin and C peptide (Hutton, 1994, Tokarz et al., 2018)

Labelling of normal pancreatic tissue with PC1/3 antiserum, revealed its expected localisation within the insulin granule. Importantly, PC1/3 expression was shown to be strongly associated with CAR-SIV in the beta cells, providing yet further evidence of the localisation of CAR-SIV to the insulin granules.

The insulin secretory granule marker, ZnT8 may enable further maturation by facilitating the transport of two Zinc ions for insulin granule crystallisation to form dense core insulin structures (Dunn, 2005)

We show with Manders correlation coefficient (MCC) colocalisation analysis, the extent of association between CAR-SIV, ZnT8 and PC1/3. This revealed that a high proportion of CAR-SIV colocalised with ZnT8 (0.87 ± 0.01) and PC1/3 (0.87 ± 0.02). This was very similar in the reverse with ZnT8 colocalising with CAR-SIV (0.73 ± 0.04) and PC1/3 colocalising with CAR-SIV (0.70 ± 0.02) confirming strong association with CAR-SIV and ZnT8/PC1/3 in the human pancreatic beta cell.

The finding that CAR-SIV colocalises with multiple proteins within the insulin secretory granule such as insulin, ZnT8 and PC1/3 (Arias et al., 2000, Chimienti

et al., 2006) provides strong supporting evidence that CAR-SIV is located on the membrane of the insulin granule.

We also show no association between CAR-SIV and glucagon which further emphasises the fact that CAR-SIV is not present in alpha cells and is restricted to the insulin producing beta cells.

Importantly, assessment of the colocalisation of CAR-SIV and proinsulin using the Pearson's correlation coefficient (PCC) which estimates the degree of colocalisation between two proteins, demonstrates that CAR-SIV associates to a lesser extent with proinsulin. To understand this in more detail, we utilised an additional analysis to generate the MCC, which defines the extent of colocalisation between CAR-SIV and proinsulin. This revealed that the majority of proinsulin colocalised with CAR-SIV implying that both are contained in the trans-Golgi and in the immature granules as they bud from the trans-Golgi network. In reverse, however, the MCC analysis show that a lower proportion of CAR-SIV colocalised with proinsulin suggesting that the majority of CAR-SIV is in the mature granules.

Together these findings imply that CAR-SIV associates more with the mature insulin secretory granule than with the immature granule.

Additional strong confirmation of CAR-SIV localisation in the dense core mature insulin granules in the beta cell was made with Cryo-immuno EM studies, where the CAR-SIV was clearly shown to localise to the edge of the dense granule cores in beta cells. Morphometric quantitative analysis, demonstrated that 79% of the CAR-SIV bound 10nm gold particles were localised to the mature insulin granule. The insulin granule was distinguished based on the characteristic electron dense appearance of the granule cores. A further 14.4% of the labelled gold particles

were observed on immature secretory insulin granules. These results are in full accord with the MCC colocalisation analysis of CAR-SIV associating more with insulin than with proinsulin. There was also minimal evidence of CAR-SIV in the nucleus (2.5%), plasma membrane (1.2%), endoplasmic reticulum (1.1%) and mitochondria (1%).

To confirm further CAR-SIV localisation at different stages of insulin granule maturation, immunogold labelling of proinsulin, CAR-SIV and insulin was examined. This revealed that CAR-SIV was present in the immature granules, observed by the presence of proinsulin and CAR-SIV (*Figure 5.11C*); in the maturing granule observed by the presence of proinsulin, insulin and CAR-SIV (*Figure 5.11D*); and mature granules observed by the presence of insulin and CAR-SIV (*Figure 5.11E*). The assessment of 122 granules containing CAR-SIV also demonstrates that 4.9% were positive for proinsulin (immature granules); 24.6% were positive for proinsulin and insulin (maturing granules) and 70.5% were positive for insulin (mature granules). Together these results suggest that CAR-SIV is present within the granule membrane at all stages of granule maturation.

Importantly, in the pancreatic tissue no labelling was found when exposed to unconjugated gold particles and CAR-SIV was not labelled on adjacent acinar cells secretory granules, implying that CAR-SIV is not required for secretory granule biogenesis in all cell types.

Both the colocalisation analysis and the Cryo-EM studies are in concordance with the confinement of CAR-SIV to the insulin secretory granule.

5.3.3 CAR-SIV colocalises and interacts with PICK1 in the insulin secretory granule

In the previous sections multiple lines of evidence demonstrated that CAR-SIV is present in the insulin granule but the role of CAR-SIV in the insulin granule remains unclear. To address this, I examined which proteins can specifically interact with CAR-SIV, their roles in cells and identified the following proteins; ZO-1, Ligand of Numb-X2, MAGI-1b, PSD-95 and PICK1 summarised in Table 5.5

Table 5.5 Proteins interacting with CAR-SIV

Proteins interacting with CAR-SIV and possible roles
Interacts and associates with tight junction protein ZO-1 at tight junctions where it assists in the transport of ions and molecules (Cohen et al., 2001b, Excoffon et al., 2010)
Interacts with Ligand of Numb protein X2 which plays a role in Notch signalling in human embryonic kidney cells (Mirza et al., 2005)
Interacts with and permits the trafficking of MAGI-1b to cell-cell junction in human airway epithelial cells (Excoffon et al., 2010). MAGI-1b has been shown to interact with adenovirus viral proteins (Glaunsinger et al., 2000)
Interacts with PSD-95 through the PDZ binding domain and immunocytochemistry revealed that CAR-SIV can pull the protein from the cytoplasm to cell-cell junction in human airway epithelial cells (Excoffon et al., 2010, Excoffon et al., 2004)
PICK1 Interacts with CAR-SIV through the PDZ binding domain (Excoffon et al., 2004) and PICK1 was previously shown to play a role in the maturation and trafficking of insulin granules (Cao et al., 2013)

It is possible that knowledge of CAR-SIV association and interaction with other cellular proteins may give insights into its biological role in the beta cell. Interestingly, from published studies, a candidate protein PICK1 with a unique PDZ domain and BAR domain was shown to interact specifically with the PDZ binding domain of CAR-SIV and not CAR-TVV. This was demonstrated by co-immunoprecipitation (Co-IP) assay when co-transfected CAR-SIV and PICK1 COS-7 cells, pulled down PICK1 (Excoffon et al., 2004). In contrast, co-transfected CAR-TVV and PICK1 did not pull down PICK1 (Excoffon et al., 2010). Moreover, immunocytochemical (ICC) analysis of co-transfected CAR-SIV and PICK1 in COS-7 cells resulted in the colocalisation of CAR-SIV and PICK1 at the perinuclear region and cell-cell junction (Excoffon et al., 2004). In contrast, there was no colocalisation between CAR-TVV and PICK1 at cell-cell junction and limited perinuclear colocalisation was observed (Excoffon et al., 2010). These studies therefore affirm that CAR-SIV is a selective binding partner of PICK1 in polarised epithelial cells.

In mouse pancreas, Cao *et al* (2013) found via immunocytochemical (ICC) and Cryo-EM studies that PICK1 is localised to insulin granules (Cao et al., 2013). PICK1 has also been found to play a fundamental role in insulin secretory granule trafficking and maturation for example, very recently a study with beta cell specific PICK1 knockout mice revealed that plasma insulin levels were significantly reduced when compared to age-matched WT mice (Li et al., 2018). Also, *in vitro* tests in isolated islets from these knock-out mice demonstrated a reduction in glucose stimulated insulin secretion (Li et al., 2018). Additionally, it was revealed that PICK1 knockout mice had elevated circulating proinsulin levels. In addition, Cryo-EM analysis confirmed the presence of more immature proinsulin granules than mature insulin granules when compared to the wildtype-mice (Cao et al.,

2013), implying that PICK1 is not only involved in insulin secretory granule trafficking but also in the maturation of these insulin granules.

Since, PICK1 is localised to the insulin granule and plays a role in maturation and trafficking of insulin secretory granule, it may therefore be a potential cytosolic protein which binds to the PDZ binding domain of CAR-SIV in the insulin granule. As such, we propose that the orientation of CAR-SIV in the insulin secretory granule is such that the “extracellular domain” would face the lumen of the insulin granule, with the transmembrane domain region securing the protein in the membrane surrounding the granule while the C terminus of CAR with the PDZ binding domain faces towards the cytoplasm area for possible interaction with other cytoplasmic PDZ domain proteins such as PICK1 (*Figure 5.22*).

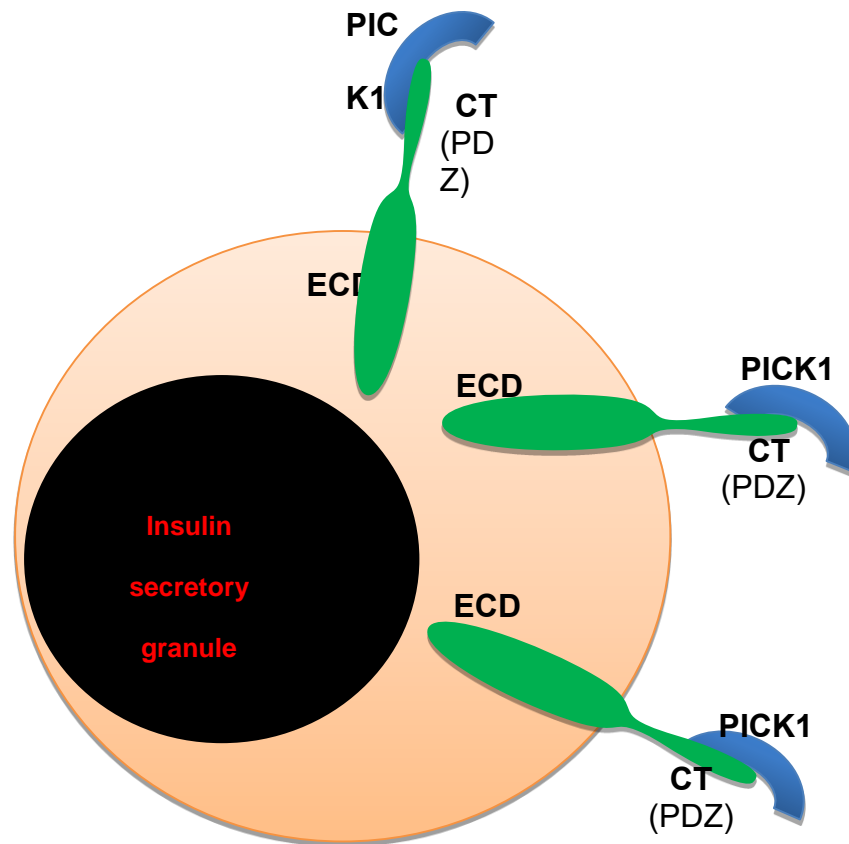


Figure 5.22 Proposed CAR-SIV orientation in the insulin secretory granule.

The “extracellular domain” faces the lumen of the insulin granule with the transmembrane domain anchoring the protein in the membrane surrounding the granule while the C terminus faces the extra-granular environment for possible interaction with other PDZ proteins such as PICK1

We found via immunolabelling analysis that PICK1 is expressed in the human beta cell and western blotting analysis detected PICK1 in isolated human islets, EndoC-βH1 and 1.1B4 cells. Additionally, we show with hyvolution confocal microscopy that CAR-SIV colocalises with PICK1 in the human beta cells and that they both strongly associate with insulin.

Furthermore, we tested to observe if there was any interaction between endogenous CAR-SIV and PICK1 in isolated human islets and EndoC- β H1. Indeed, PICK1 was robustly pulled down along with CAR immunoprecipitate. This indicates that CAR-SIV and PICK1 do interact endogenously in the human beta cell. We observed in the other direction that CAR was pulled down alongside immunoprecipitated PICK1 in EndoC- β H1 but at a marginally higher molecular weight when compared to the total lysates input (positive) controls (*Figure 5.21B*). A possible reason for this could be that PICK1 may preferentially bind to CAR that has undergone post-translational modification (phosphorylation or glycosylation), thereby impacting on its size.

In isolated human islets there was a lower efficiency of CAR pull down with the PICK1 antisera. One potential reason for this could be that the PICK1 antisera utilised is targeted to the region of PICK1 that includes the PDZ domain. As such, if CAR is strongly interacting with PICK1, access to this epitope might be restricted. The PICK1 antisera, under these circumstances will preferentially recognise unbound PICK1 and not the PICK1 bound to CAR (pictorial diagram is displayed in Figure 5.23). Nevertheless, in all of the above experiments neither CAR, CAR-SIV nor PICK1 was pulled down in both directions by the control antisera (rabbit IgG or mouse IgG) confirming the specificity of the co-immunoprecipitation assay.

Collectively, these findings provide compelling evidence that CAR-SIV colocalises, interacts and associates with PICK1 in the human pancreatic beta cell.

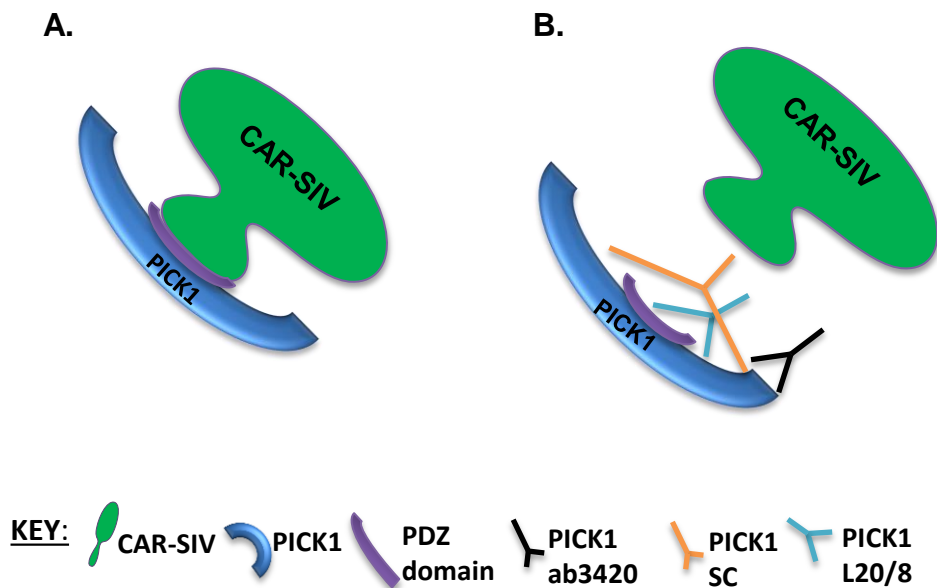


Figure 5.23 Pictorial diagram of CAR-SIV and PICK1 binding

(A) CAR and PICK1 interaction via the PDZ binding domain (B) low efficiency of CAR pull down may be due to the inability of the available PICK1 antisera to successfully gain access to the epitopes of the PDZ binding domain interaction of CAR-SIV and PICK1 complex or that PICK1 may only bind to unbound PICK1.

Importantly, the role of PICK1 in insulin granule budding, maturation and trafficking had been investigated in several studies. As previously mentioned PICK1 also has a BAR domain, which has been shown to form tight heteromeric BAR domain complex with the BAR domain of an islet autoantigen ICA69 in the brain and in rodent beta cells (Cao et al., 2007, Cao et al., 2013). PICK1 and ICA69 interaction functions in sensing membrane curvature and facilitating vesicle formation (Jin et al., 2006, Madsen et al., 2008). It was further demonstrated that PICK 1 knockout mice lacked ICA69 and that ICA69 knockout

mice exhibited lower insulin and high proinsulin levels, the same phenotype observed in the PICK1 knockout mice (Cao et al., 2013) supporting the evidence that both proteins are involved in the maturation and trafficking of insulin granules.

I therefore propose the following model (see Figure 5.24). PICK1 associates through its BAR domain with ICA69 to form a heteromeric complex (PICK1-ICA69) to induce the curvature of the membrane of an immature granule vesicle (containing proinsulin) and encourages the budding of the vesicle from the trans-Golgi network. CAR-SIV is also localised to the immature granule vesicle and could interact with PICK1 via its PDZ binding domain. As the granule begins to mature, ICA69 is lost and it is thought that this enables PICK1 to form homomeric complexes (PICK1-PICK1) and also increases the PDZ domain binding slots (Cao et al., 2013) possibly for the enrichment of CAR-SIV to continue the process of maturation and trafficking of the insulin secretory granule. This therefore suggests a possibility that PICK1 and CAR-SIV interaction in the beta cell may play a role in the maturation and trafficking of the insulin secretory granules.

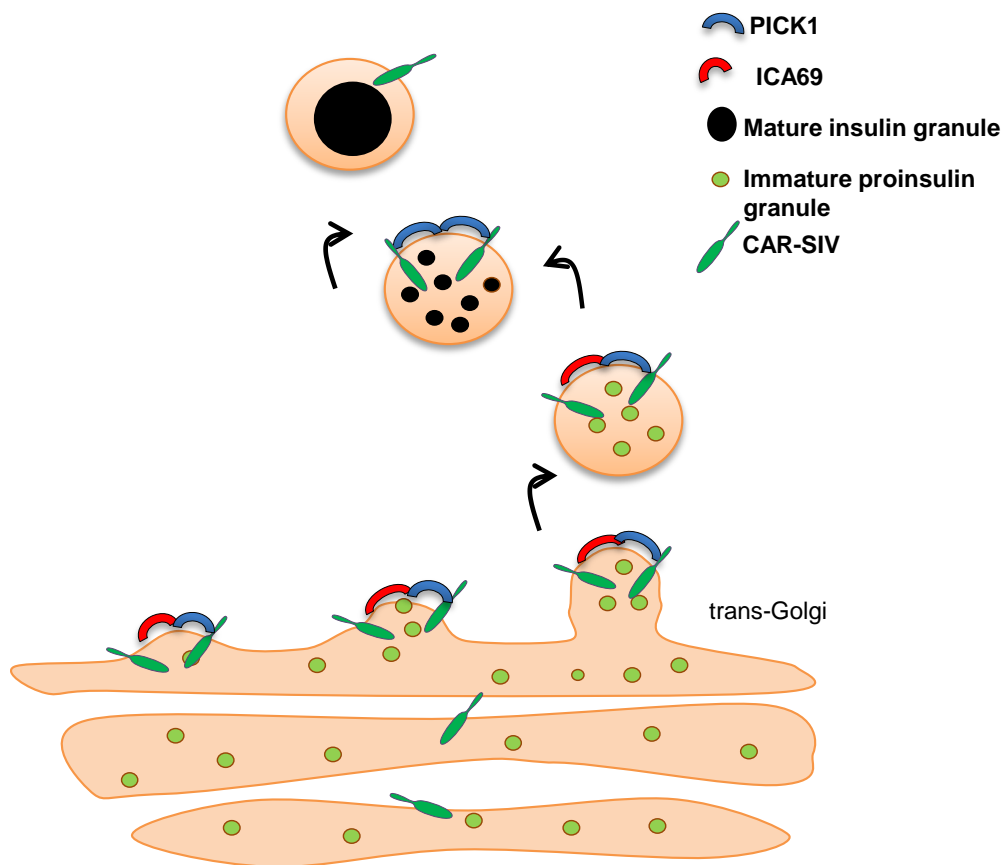


Figure 5.24 Model for CAR-SIV, PICK1 and ICA69 insulin granule maturation and trafficking.

PICK1 and ICA69 form a heteromeric BAR complex structure that assists in imposing curvature on membranes, to facilitate the budding of the immature granule from the trans-Golgi network. CAR-SIV also localises to the immature granule vesicle and interacts with PICK1 via its PDZ binding domain. As the granule begin to mature, ICA69 is lost from the maturing granule enabling CAR-SIV and PICK1 interaction to continue the process of maturation and trafficking of the insulin granules. Adapted from (Holst et al., 2013)

Possibilities for CAR-SIV involvement in trafficking of insulin granules is further strengthened through its interaction with other proteins that have been revealed to be expressed in the beta cell. Recently, Gan *et al* (2017) utilising imaging analysis (3D confocal and electron microscopy) showed that human and mice beta cells can be polarised. It was further revealed that *in situ* pancreatic beta cells had 3 distinct domains consisting of an apical domain identified by the enrichment with PAR-3 and ZO-1 proteins, a lateral region enriched by E-cadherin and GLUT-2 proteins and a distinct basal domain enriched with synaptic scaffold protein Liprin oriented towards the vasculature (Gan et al., 2017). One hypothesis that would require more research is that CAR-SIV may be able to direct insulin granules to distinct membrane localisations within beta cells, depending on which protein it interacts with. At the apical domain CAR-SIV can interact with ZO-1 (Excoffon et al., 2010); the lateral region where CAR interacts with E-cadherin (Morton et al., 2013) or the basal domain where it was shown that high K^+ stimulated insulin exocytosis from the basal region into the bloodstream detected by two photon live cell imaging in stimulated isolated mice islets (Low et al., 2014).

This chapter has therefore revealed a punctate localisation of CAR-SIV within the beta cells and further demonstrated that it was specifically localised to the insulin secretory granule. I also found that CAR-SIV colocalises and interacts with the cytosolic protein PICK1 in the beta cell. The CAR-SIV and PICK1 interaction may be important for the maturation and trafficking of insulin secretory granules.

CHAPTER 6
Investigation of the role of CAR-SIV
in the human pancreatic beta cell
line

6.1 Introduction

The novel findings presented in chapter 5 that the CAR-SIV isoform is localised to insulin secretory granules and that it co-localises and interacts with PICK1 imply a synergistic role for CAR-SIV in the trafficking and maturation of the insulin secretory granules. On this basis, it was appropriate to undertake functional studies in a human pancreatic beta cell model to investigate the role of CAR-SIV in insulin secretion.

The objectives of this chapter are as follows;

- To confirm the generation of wildtype and truncated CAR-SIV vectors
- To develop a human growth hormone model to explore CAR-SIV physiological role in the human pancreatic beta cell

6.2 Results

6.2.1 Confirming the generated wildtype CAR-SIV and truncated CAR-SIV mutant constructs

To understand the functional role of CAR-SIV in human pancreatic beta cells, overexpression studies were employed in the 1.1B4 cell line. Two CAR-SIV constructs; one encoding the wild-type (full length) protein and a second encoding a truncated mutant (in which the three C-terminal amino acids “SIV” were deleted) were generated by site-directed mutagenesis (Chapter 2, section 2.22). Each was transiently transfected into 1.1B4 cells which were then immunolabelled with anti-CAR CT and anti-CAR RmcB. The results revealed that CAR-SIV was overexpressed successfully in the transfected cells and a similar staining pattern

was observed with CAR CT and CAR RmcB antisera (*Figure 6.1A*). In contrast, no immunolabelling was achieved with the CAR CT antiserum when the truncated CAR-SIV mutant was transfected into the cells which is consistent with the absolute requirement for the terminal three amino acid motif “SIV” for CAR CT antiserum binding. However, as expected, the CAR RmcB antiserum still detected the truncated CAR-SIV mutant (*Figure 6.1B*).

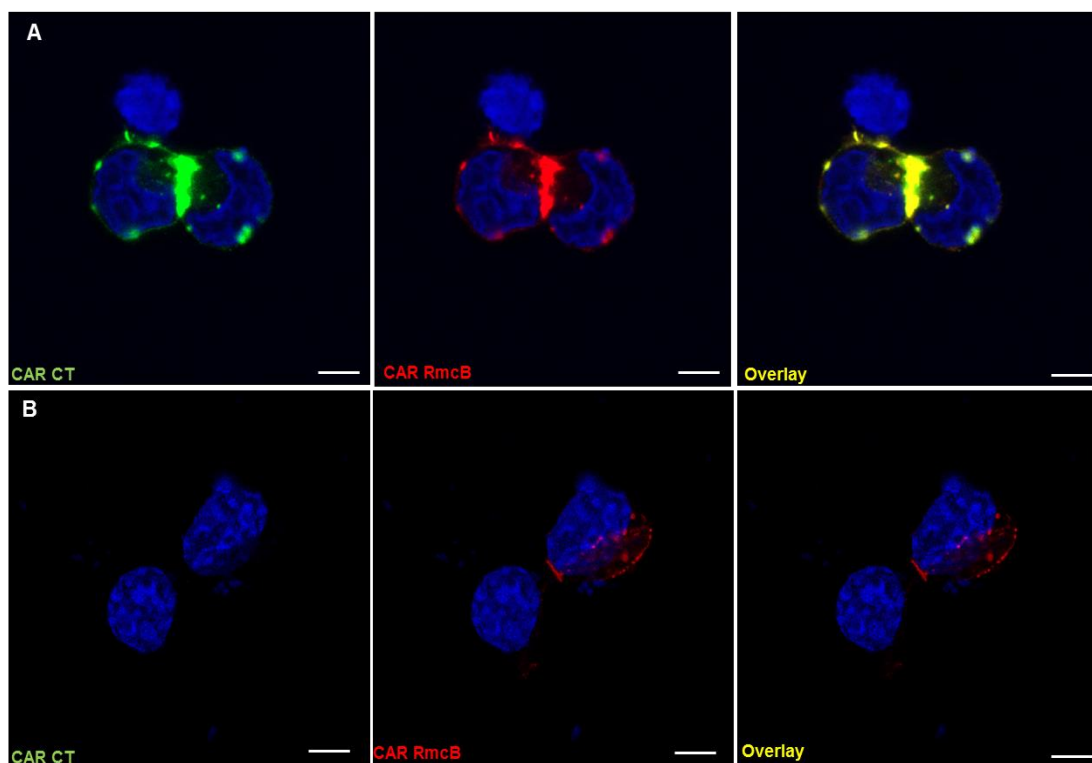


Figure 6.1 Full length CAR-SIV isoform is overexpressed in wild-type CAR-SIV and not in truncated CAR-SIV mutant constructs in 1.1B4 cell line

(A). CAR-SIV (anti-CAR CT; green) and staining with anti-CAR RmcB (anti-CAR RmcB; red) is detected in wild-type CAR-SIV constructs (B) CAR-SIV (anti-CAR CT; green) is not detected but staining with CAR RmcB antiserum (anti-CAR RmcB ;red) is detected in truncated CAR-SIV mutant construct. Nuclei were stained with DAPI (blue). Data are representative of three replicates. Scale bar 2.5 μ m

To further validate that CAR-SIV overexpression had been achieved, western blotting was employed. 1.1B4 cells were transfected with the following plasmids;

empty vector, truncated CAR-SIV mutant, CAR-SIV Myc tag (where a Myc-tag was placed at the C' terminal end of CAR-SIV) and wild-type CAR-SIV construct. The western blot analysis confirmed that wild type CAR-SIV isoform is detectable by the CAR CT antiserum in the 1.1B4 cells; as indicated by a single band (expected molecular weight of 40kDa) in the relevant lane (*Figure 6.2*). In contrast, this antiserum did not detect the truncated CAR-SIV mutant and it also failed to label the Myc-tagged variant, presumably because the Myc-tag physically hindered the antibody access. The anti-CAR ECD detected all variants of CAR as shown in *Figure 6.2*.

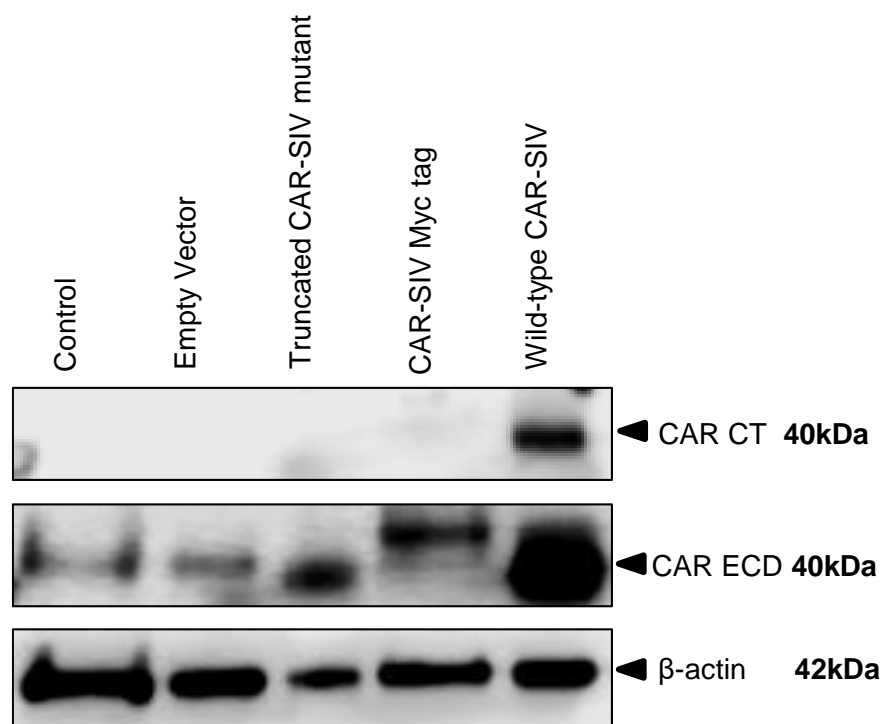


Figure 6.2 Confirmation of the CAR CT antiserum detecting only the full length CAR-SIV isoform.

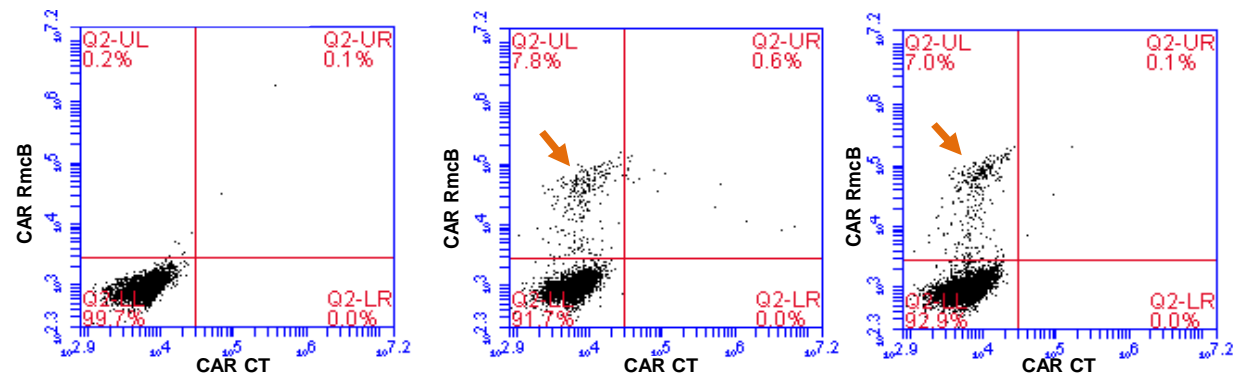
1.1B4 cells were seeded at 5×10^4 cells/ml and transfected with empty vector, truncated CAR-SIV mutant, CAR-SIV Myc tag and Wild-type CAR-SIV in avalanche-omni transfection reagent for 24hrs. 1.1B4 cells were then lysed and total protein was isolated for western blotting. Western blot analysis detects an estimated (40kDa) of CAR-SIV (anti-CAR CT) in only the wild-type CAR-SIV construct. In contrast, CAR ECD antiserum detects a band at approximately (40kDa) in control, empty vector, truncated CAR-SIV mutant, CAR-SIV Myc tag and in wild-type CAR-SIV construct. Loading control β -actin (42kDa), Data are representative of three independent experiments.

To support these data, flow cytometry analysis (previously optimised as described in Chapter 4, section 4.2.2 and 4.2.3) was performed, utilising the CAR RmcB and CAR CT antisera. These were used to label both surface and intracellular CAR in non-permeabilised and permeabilised 1.1B4 cells transfected with the empty vector, wild-type CAR-SIV or truncated CAR-SIV mutant constructs, respectively.

The results revealed that CAR RmcB antiserum labelled the surface of cells transfected with either wild-type or truncated CAR-SIV constructs (as expected) indicated by the orange arrows in the scatter plot (*Figure 6.3A*). However, little or no labelling was achieved in the cells transfected with empty vector. This is in agreement with the data obtained in Chapter 4 where 1.1B4 cells were shown to have very weak surface expression of endogenous CAR. As shown previously (Chapter 4) the CAR CT antiserum can label intracellular CAR-SIV in permeabilised pancreatic beta cells. As expected, CAR CT did not label the surface of cells transfected with any of the constructs tested (*Figure 6.3A*).

When assessing the patterns of intracellular staining in permeabilised 1.1B4 cells, using anti-CAR CT, it was evident that intracellular CAR-SIV was present endogenously and that it was expressed at higher levels (indicated by purple arrows) in cells transfected with the wild-type CAR-SIV construct (*Figure 6.3B*). In contrast, no labelling was seen in cells expressing the truncated CAR-SIV mutant construct (*Figure 6.3B*) supporting previous conclusions about the antibody specificity.

A. Extracellular staining



B. Intracellular staining

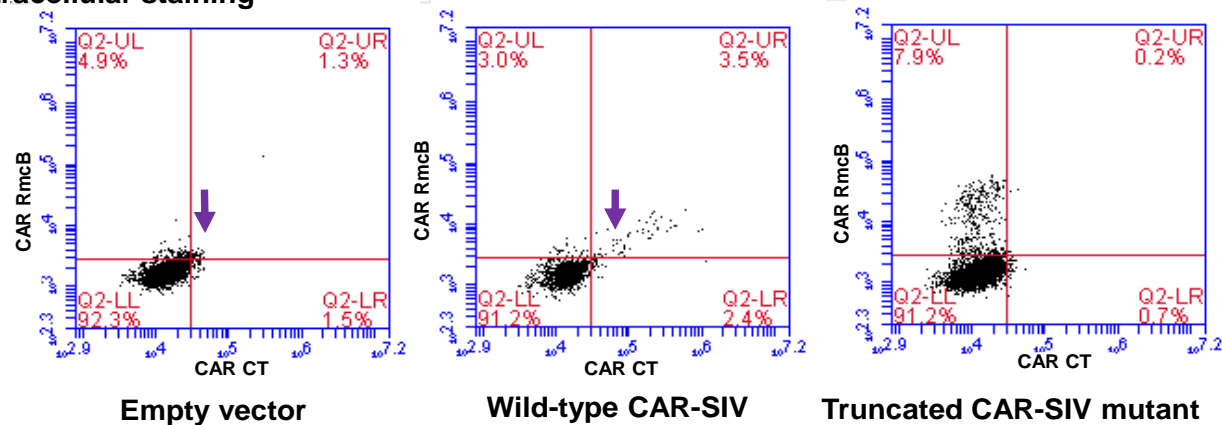


Figure 6.3 Representative flow scatter plot confirming labelling with CAR RmcB and CAR CT antisera in CAR-SIV transfected 1.1B4 cells.

(A) Surface CAR (anti-CAR RmcB; orange arrow) is expressed in wild-type CAR-SIV, truncated CAR-SIV mutant but not in empty construct 1.1B4 cells. (B) Intracellular CAR-SIV (anti-CAR CT; purple arrows) is expressed in the empty and in the wild-type CAR-SIV construct but not in the truncated CAR-SIV construct. Data are representative of three replicates

6.2.2 Detection of CAR CT and CAR RmcB antisera binding in transfected cells using a proximity ligation assay

To assess the binding of CAR CT and CAR RmcB antisera in transfected cells, a proximity ligation assay (PLA) was employed. PLA requires the close proximity of two antisera (within a maximum distance of 30-40nm) to yield a positive signal (Chapter 2, section 2.18).

Briefly, INS-1E cells were transiently transfected with wild-type CAR-SIV or the truncated CAR-SIV mutant and immunolabelled with CAR CT and CAR RmcB antisera before being subjected to PLA. The cells were also co-stained with anti-insulin after completion of the proximity ligation assay. Labelling with anti-CAR CT and anti-CAR RmcB was detected in cells expressing the wild-type CAR-SIV construct (*Figure 6.4A*). In contrast, no signal was obtained in cells transfected with the truncated CAR-SIV mutant construct (*Figure 6.4B*). Thus, these data are consistent with the concept that the C terminal motif "SIV" is essential for anti-CAR CT binding. In summary, the results obtained using full length wild-type CAR-SIV and truncated CAR-SIV mutant constructs have validated the specificity of the CAR CT antiserum in a range of different assays (*Figure 6.5*, Table 6.1).

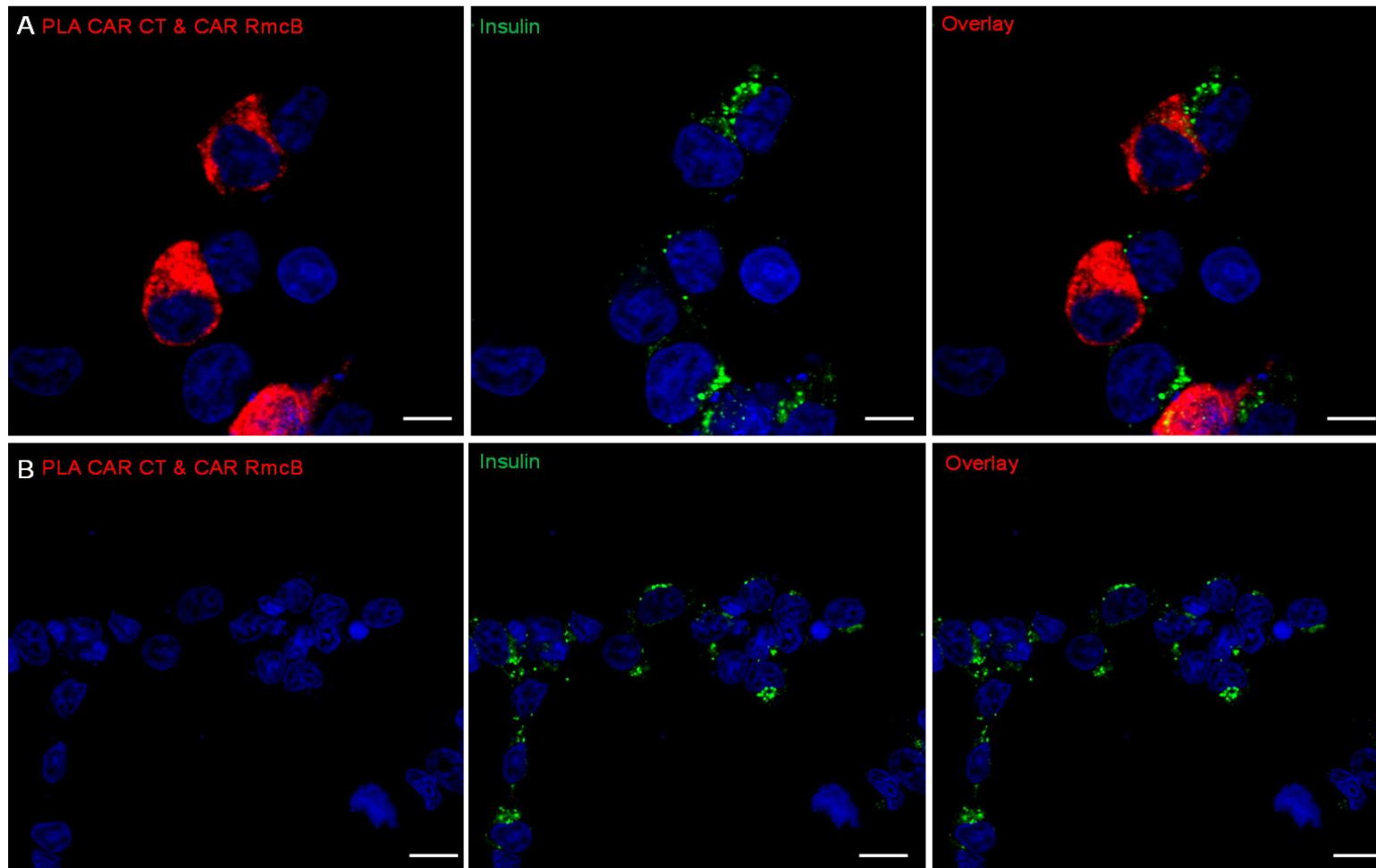


Figure 6.4 Proximity ligation assay demonstrates the binding of CAR CT and CAR RmcB in the different CAR-SIV constructs

(A) Close proximity binding of CAR RmcB and CAR CT antisera was detected in select INS-1E cells transfected the wild-type CAR-SIV construct (red),insulin (green). In contrast, no proximity binding for (B) CAR RmcB and CAR CT antisera binding was detected in cells transfected with the truncated CAR-SIV mutant. Nuclei were stained with DAPI (blue). Data are representative of three replicates, Scale bar 7.5μm

Table 6.1 Summary of the validation of the specificity of CAR CT antiserum with the wild-type and truncated CAR-SIV constructs

Assays	CAR CT binding	
	(CAR-SIV construct)	(Truncated CAR-SIV mutant construct)
Immunocytochemistry	+	-
Western blotting	+	-
Flow cytometry	+	-
Proximity ligation assay	+	-

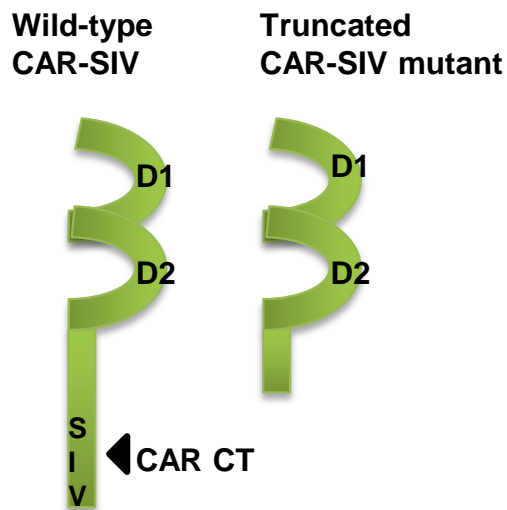


Figure 6.5 Schematic diagram of both CAR constructs

Diagram showing the extracellular domains (D1 & D2) with the C terminal end in the wild-type CAR-SIV (full length) indicating CAR CT epitope recognition and a truncated terminal end in truncated CAR-SIV mutant

6.2.3 CAR-SIV colocalises with insulin in wild-type CAR-SIV construct in the human pancreatic beta cell line 1.1B4

To assess the extent of colocalisation of insulin and CAR-SIV in 1.1B4 cells expressing the wild-type CAR-SIV construct, triple staining with anti-insulin, anti-CAR RmcB and anti-CAR CT was employed. This revealed that CAR-SIV isoform and insulin were colocalised to a significant extent in 1.1B4 cells (*Figure 6.6*). This therefore prompted us to use a system to assess CAR-SIV's involvement in insulin secretion in the subsequent section.

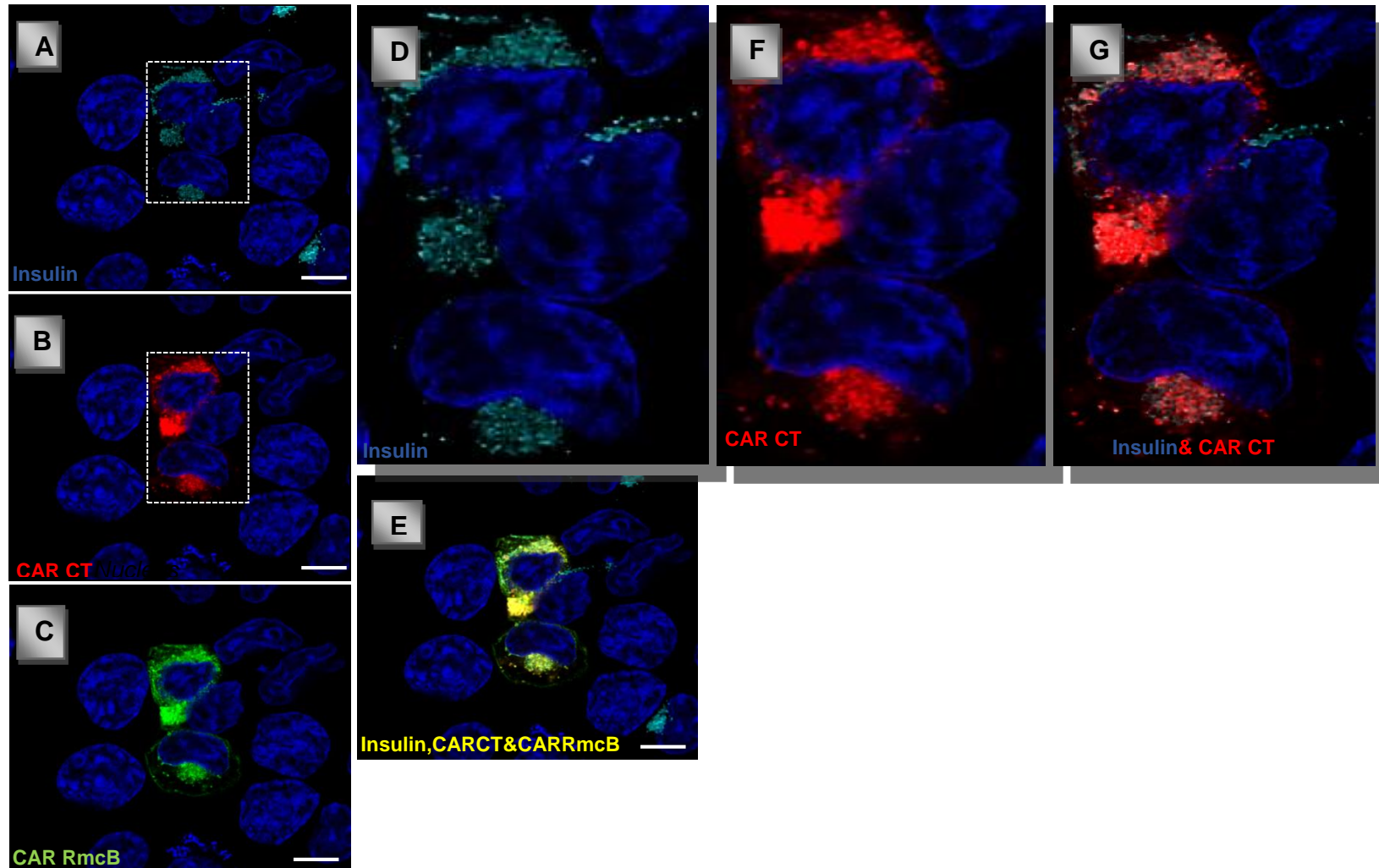


Figure 6.6 CAR-SIV co-localises with insulin in the wild-type CAR-SIV transfected 1.1B4 cells.

Immunocytochemical analysis utilised to detects the expression of (A) insulin (anti-insulin; light blue), (B) CAR-SIV (anti-CAR CT; red) and (C)(anti-CAR RmcB; green). Magnified images (Broken lines) displays (D) insulin and (F) CAR-SIV and (G) colocalisation of CAR CT and insulin (E) Colocalisation of insulin, CAR CT and CAR RmcB (yellow). Nuclei were stained with DAPI (blue). Data are representative of three replicates, Scale bar 5μm

6.2.4 Investigating insulin secretion in transfected 1.1B4 cells

In order to assess the effects of changes in CAR expression on insulin secretion from transfected 1.1B4 cells it was necessary to devise a method to distinguish between secretions from untransfected vs transfected cells. To achieve this, we made use of a previously established human Growth Hormone assay system. Human Growth Hormone (hGH) was first used in rodent beta cells as a means to monitor secretory activity and it was shown to be co-sorted and secreted with insulin (Iezzi et al., 1999). Cells are transfected with a vector encoding hGH and the secreted product is assayed by ELISA in the cell supernatant (Chapter 2, section 2.23). This is then taken as a surrogate for insulin release. In order to utilise this system, the hGH construct encoding plasmid pXGH5 (Varadi et al., 2002) provided as a gift by Prof. Guy Rutter (Imperial College London) was transfected into 1.1B4 cells.

In order to determine the suitable combination of insulin secretion stimuli that would provide greatest hGH secretion from 1.1B4 cells, hGH construct was transiently transfected and assayed in the supernatant after 1hr. Cells were treated with 0mM and 20mM glucose, 25mM KCl alone or together with a combination of agents that raise cAMP (200µM IBMX and 10µM forskolin). The results revealed that the cells responded with a two-fold increase in hGH secretion when exposed to 20mM glucose and 25mM KCl when compared to 0mM glucose. Moreover, combinations of (200µM IBMX+ 10µM forskolin+ 20mM glucose) and (200µM IBMX+ 10µM forskolin+ 25mM KCl) yielded a further two-fold increase above than achieved with 20mM glucose or 25mM KCl alone (*Figure 6.7*). This result implies that a combination of 20mM glucose, 25mM KCl, 10µM forskolin and 200µM IBMX yielded the greatest hGH release.

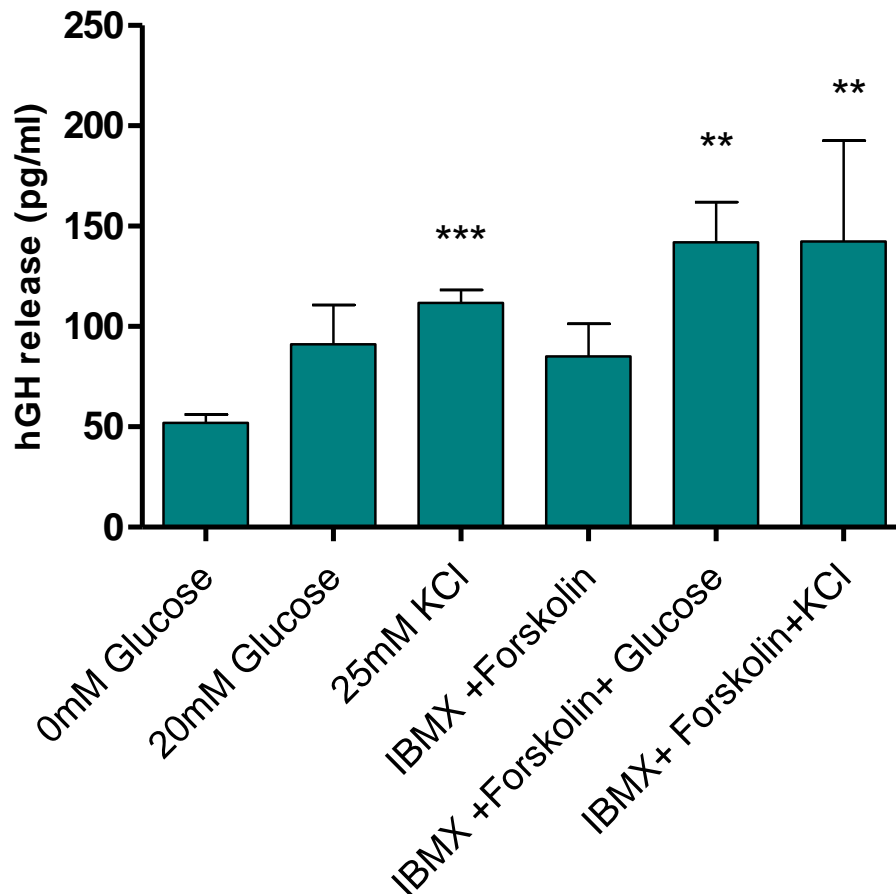


Figure 6.7 Effect of different combinations of insulin secretion stimuli on human Growth Hormone (hGH) release in hGH transfected 1.1B4 cells.

Transfected hGH 1.1B4 cells were starved for 90mins followed by treatment with 0mM or 20mM glucose, 25mM KCl, 200 μ M IBMX and 10 μ M forskolin for 60mins. Hgh secreted into collected supernatant was determined by hGH ELISA assay. Data represents fold change versus control treatment, mean \pm SEM (n=3).

**p<0.01 relative to 0mM glucose (control)

***p<0.001 relative to 0mM glucose (control)

6.2.5 Effects of transfection with CAR-SIV on human growth hormone (hGH) release from 1.1B4 cells

To examine whether transfection with CAR-SIV leads to any change in hormone secretion, 1.1B4 cells were co-transfected with 0.7 μ g of hGH and 0.3 μ g of either wild-type CAR-SIV, truncated CAR-SIV mutant or empty vector prior to stimulation of secretion. Growth hormone release into the cell supernatant was then assessed. The results demonstrate that hGH release was increased robustly (2-3 fold) by the stimulation cocktail (20mM glucose, 25mM KCl, 200 μ M IBMX and 10 μ M forskolin) in cells transfected with human Growth Hormone alone (*Figure 6.8A*). Surprisingly, co-transfection of hGH with any other DNA species resulted in a decrease in absolute hormone release. However, when the values were normalised to the relevant control as a means to yield an estimate of relative secretion rates with reference to basal secretion, no difference in the extent of growth hormone released was evident with any of the constructs tested (*Figure 6.8B*).

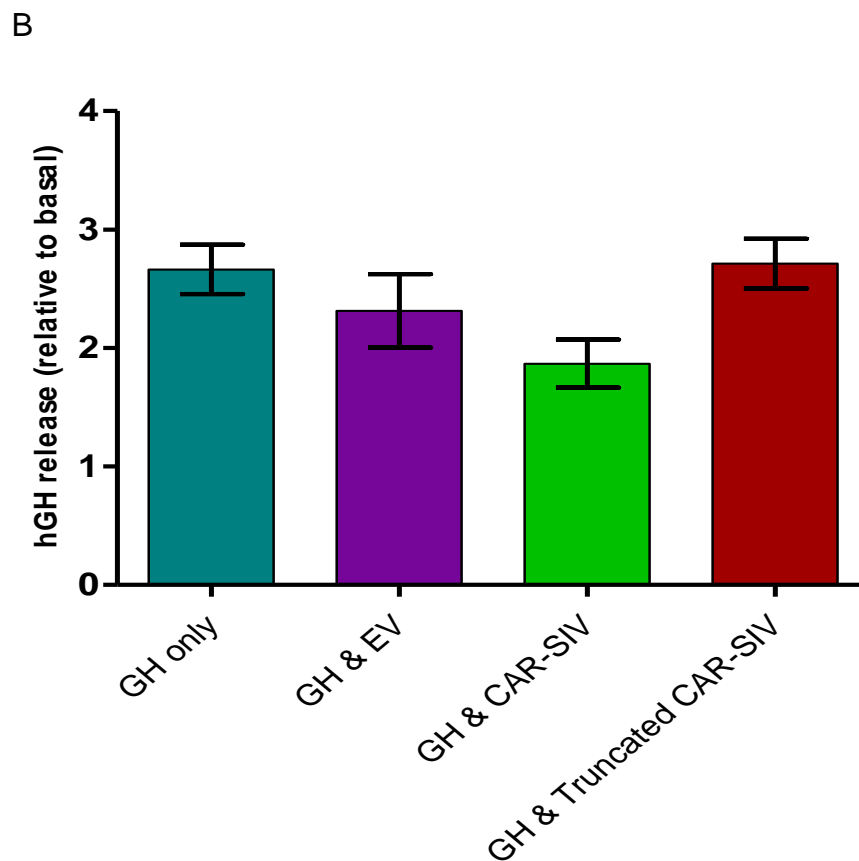
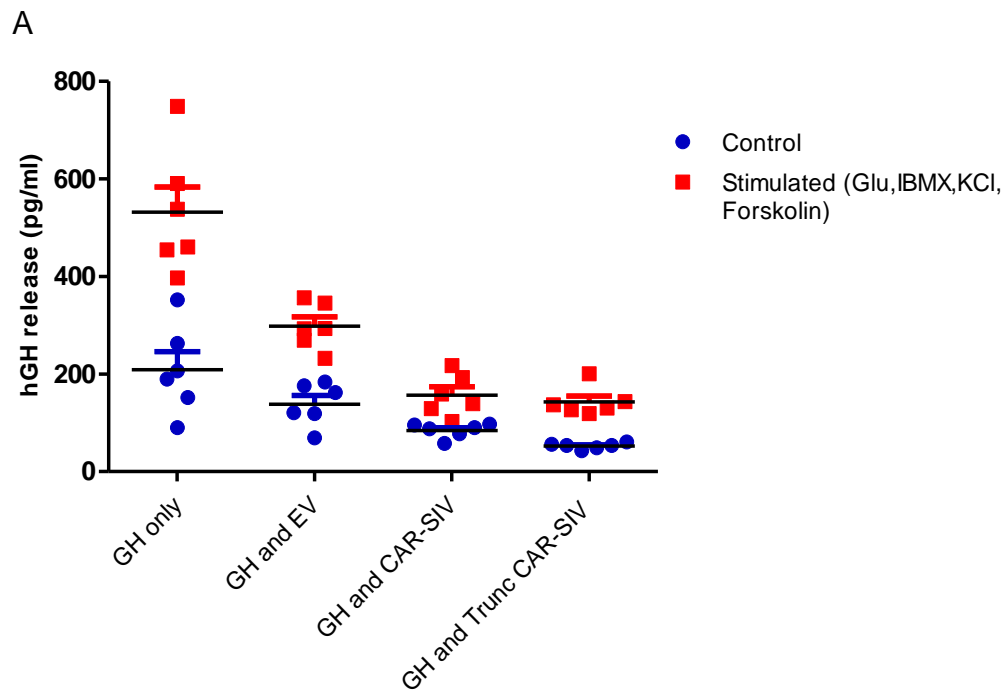


Figure 6.8 Effect of the different CAR-SIV constructs on human growth Hormone (hGH) release in 1.1B4 cells

Cells were co-transfected with of 0.7µg of hGH and 0.3µg of corresponding constructs (empty vector, wild-type CAR-SIV and truncated CAR-SIV mutants and then hGH release was assessed with hGH ELISA (A) Total hGH release (B) Fold change in reference to basal secretion, values are presented as mean ± SEM (n=3)

To explore these relationships further, the ratio of hGH to other vectors was varied. Initially, an equal ratio of hGH and the corresponding constructs was employed. Thus, 0.5µg of hGH in combination with 0.5µg of wild-type CAR-SIV, truncated CAR-SIV mutant or empty vector was transfected and the hGH release was monitored. The data show that, using this protocol, a decrease in the absolute amount of growth hormone released occurred (78pg/ml vs 550pg/ml; when compared to the previous results in Figure 6.8A & Figure 6.9A. However, as noted previously, when the “fold change” was measured with reference to basal secretion, there was no difference in the amount of growth hormone released when comparing cells transfected with the wild-type CAR-SIV, truncated CAR-SIV mutant or empty vector (*Figure 6.9B*).

Collectively, these results revealed that CAR-SIV does not have a marked effect on human growth hormone release under the conditions of these studies.

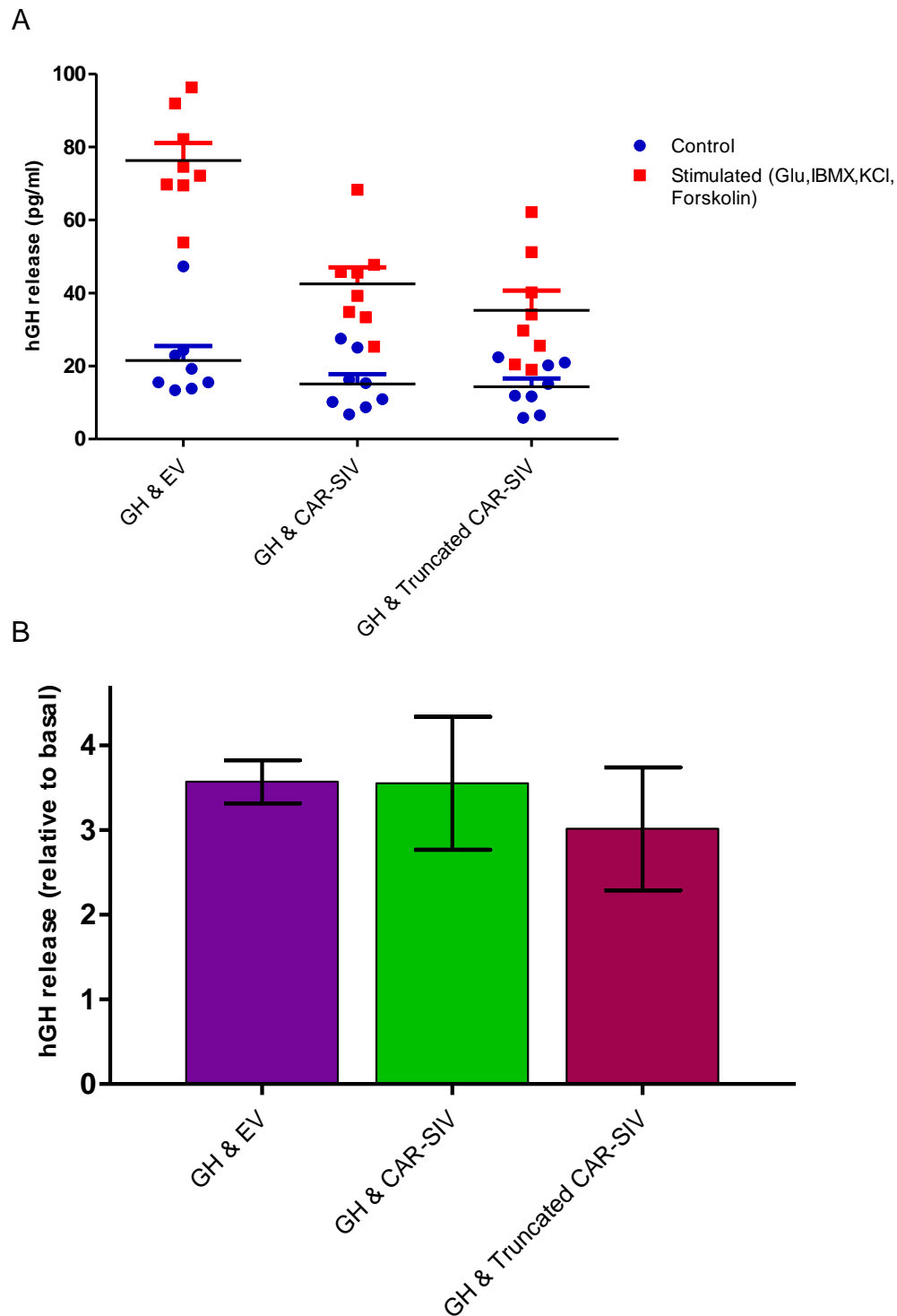


Figure 6.9 Effect of the equal ratio of human growth hormone (hGH) and different CAR-SIV constructs on hGH release in 1.1B4 cells

Cells were co-transfected with of 0.5µg of hGH and 0.5µg of corresponding constructs (empty vector, wild-type CAR-SIV and truncated CAR-SIV mutants) and then hGH release was assessed with hGH ELISA (A) Total hGH release (B) Fold change in reference to basal secretion presented as the mean ± SEM (n=3)

6.2.6 Investigation of the human growth hormone (hGH) system in the rodent pancreatic INS-1E cell line

The results obtained with 1.1B4 cells prompted an assessment of parallel studies using a rodent beta cell, INS-1E, since earlier reports have utilised the hGH assay in rodent pancreatic beta cell lines (da Silva Xavier et al., 2003, Varadi et al., 2002). INS-1E cells were co-transfected with 0.7 μ g hGH and 0.3 μ g empty vector and the release of growth hormone was evaluated. The results showed a robust increase in growth hormone release compared to control when cells were treated with the “stimulation cocktail” (Figure 6.10). This concurs with the hGH release observed from 1.1B4 cells shown below in Figure 6.11.

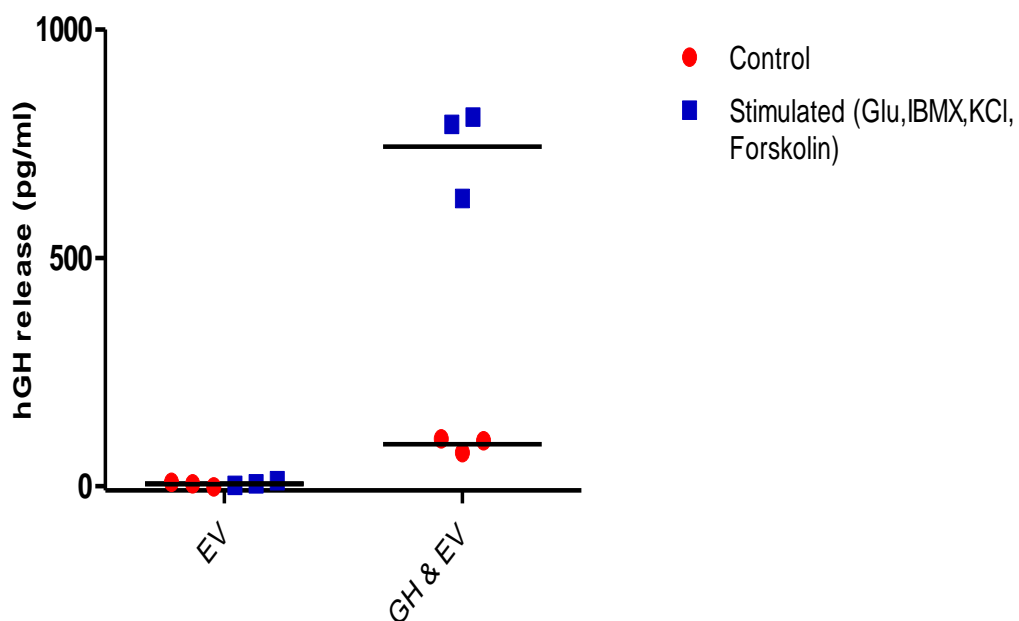


Figure 6.10 hGH is released in INS1E cells co-transfected with 0.5 μ g of hGH and 0.3 μ g empty constructs.

Transfected hGH construct and empty vector INS-1E cells were starved for 90mins followed by treatment with 0mM or 20mM glucose, 25mM KCl, 200 μ M IBMX and 10 μ M forskolin for 60mins. The hGH secreted into collected supernatant was determined by hGH ELISA. Data are represented as mean \pm SEM (n=3)

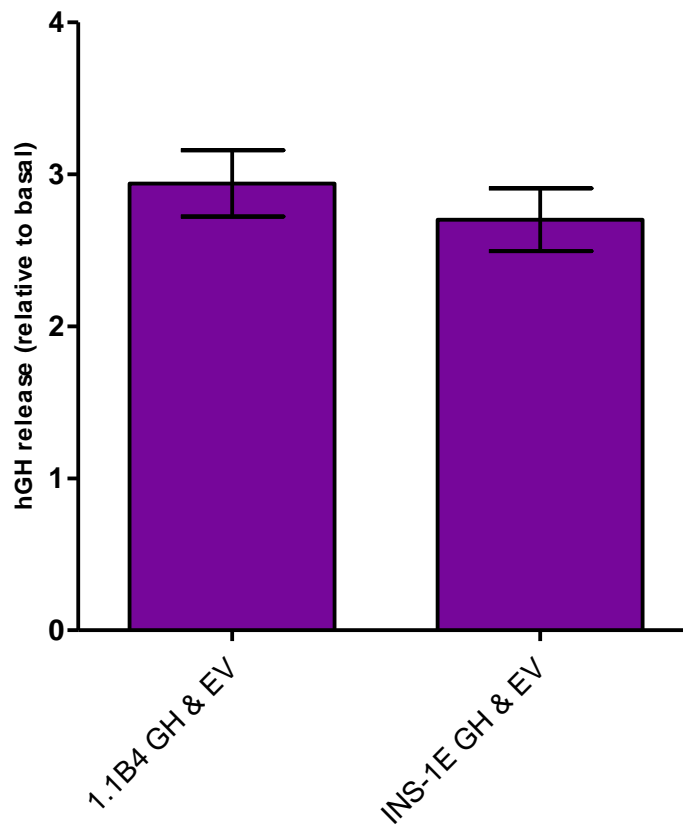


Figure 6.11 The hGH release from the hGH transfected 1.1B4 cells is similar to the INS1-E cells.

1.1B4 and INS-1E cells were co-transfected with 0.7 μ g of hGH and 0.3 μ g of empty vector and then hGH release was assessed with hGH ELISA. Fold change in reference to basal secretion was assessed in both 1.1B4 and INS1-E cells. Each data set are presented as mean \pm SEM

To determine if indeed the hGH and insulin are co-localised in transfected cells, immunocytochemical (ICC) analysis was employed by co-staining INS-1E cells with anti-hGH and anti-insulin. High resolution confocal microscopy revealed that insulin was present in many more cells than expressed hGH (*Figure 6.12*). Moreover, where these were present in the same cells, hGH and insulin did not always co-localise (*Figure 6.13*). These results suggest that insulin and hGH may be routed differentially through the regulated secretory pathway in INS-1E cells but this remains to be confirmed.

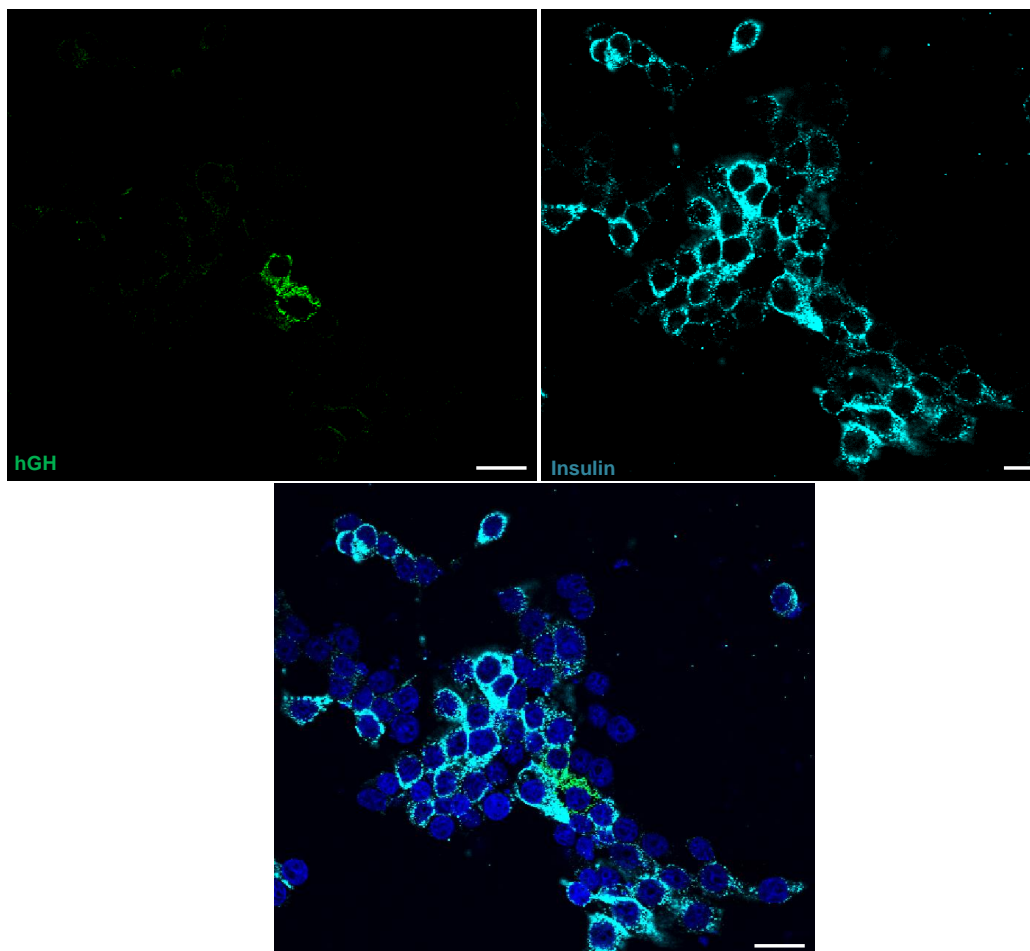


Figure 6.12 Insulin is present in many more INS-1E cells than expressed hGH. Representative confocal immunocytochemical imaging showing staining with anti-hGH (green) and insulin (light blue). Nuclei were stained with DAPI (blue). Data are representative of three replicates. Scale bar 50 μ m

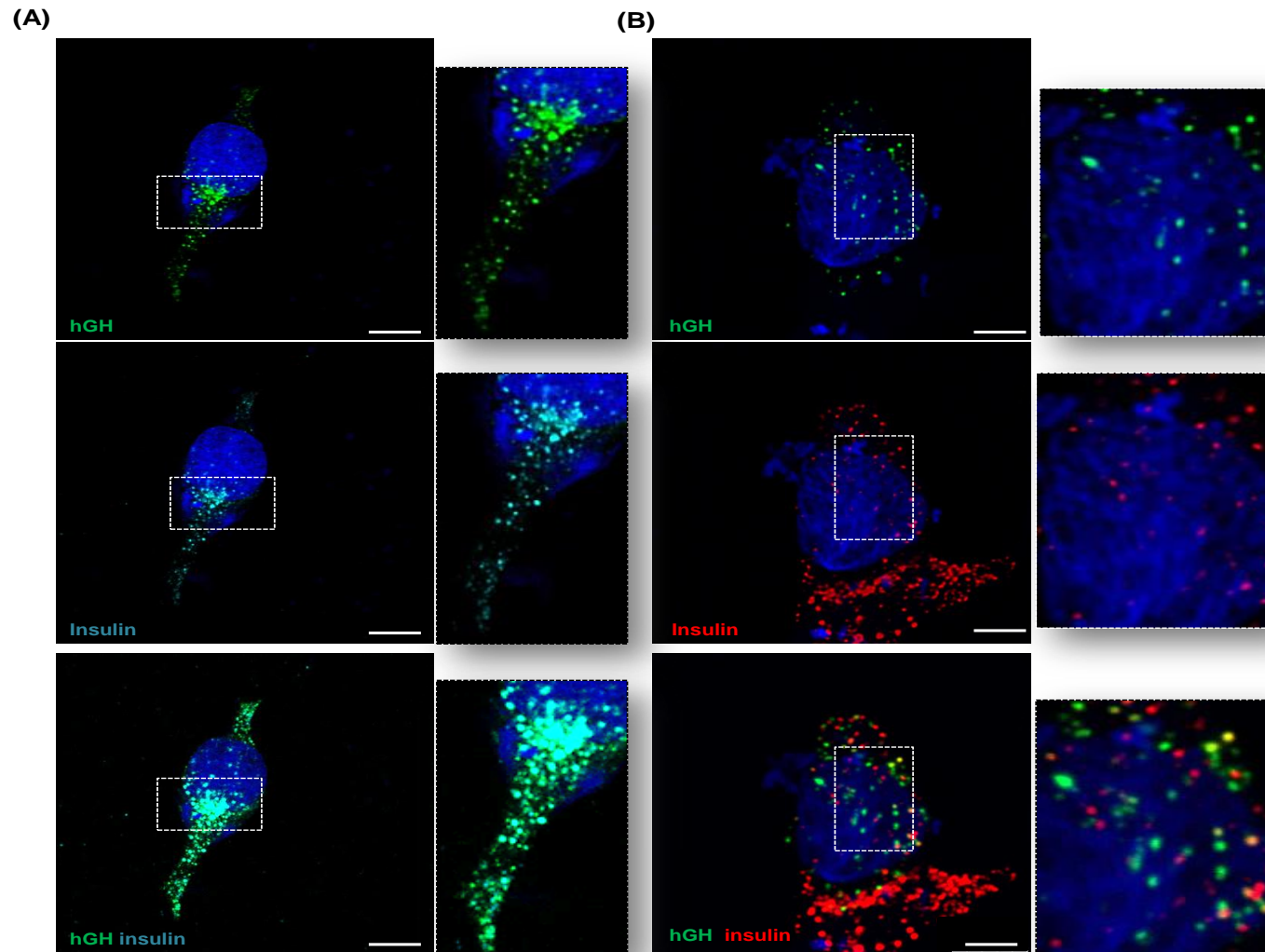


Figure 6.13 hGH co-localises with insulin in some, but not in all INS-1E cells.

Representative immunohistochemical analysis of (A) anti-hGH (green) and insulin (light blue) (B) anti-hGH (green) and anti-insulin (red), Magnified images (white broken box) displaying co-localisation. Nuclei are stained with DAPI (blue). Data are representative of three replicates. Scale Bar 7.5 μ m

6.2.7. Immunocytochemical detection of human growth hormone (hGH) and CAR-SIV in the human pancreatic beta cell line 1.1B4

To further explore the co-localisation of hGH and insulin in the wild type CAR-SIV construct in 1.1B4 cells, cells that had been co-transfected with growth hormone were examined by immunocytochemistry using anti-growth hormone, anti-CAR CT and anti-insulin. The staining pattern demonstrates that CAR-SIV co-localised with human growth hormone in certain regions in some cells but this was not always the case (*Figure 6.14A*). In other cells, that were negative for insulin, CAR-SIV and growth hormone co-localised partially (*Figure 6.14B*).

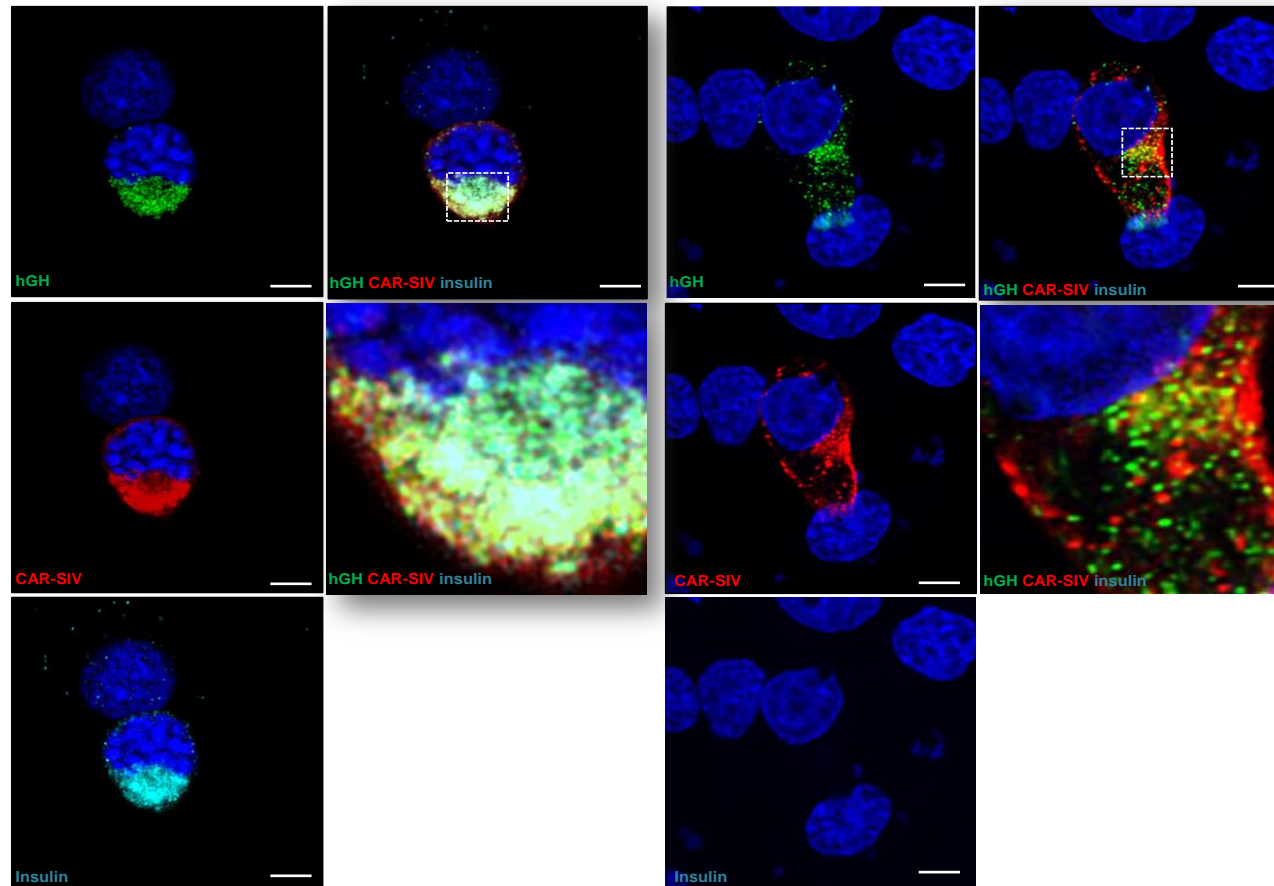


Figure 6.14 ICC staining reveals hGH partial co-localisation with CAR-SIV in insulin containing beta cells in 1.1B4 cells.

Representative immunocytochemical analysis of (A) hGH (anti-hGH; green), CAR-SIV (anti-CAR CT; red) and insulin (anti-insulin; light blue) (B) anti-hGH (green), CAR-SIV (anti-CAR CT; red) and anti-insulin (negative). Magnified images displays degree of co-localisation, Nuclei is stained with DAPI (blue). Data are representative of images from three replicates. Scale Bar 5 μ m, 7.5 μ m

6.3 Discussion

6.3.1 Generation of wild-type and mutant CAR-SIV constructs

The employment of a site directed mutagenesis strategy resulted in the successful generation of wild-type CAR-SIV and truncated CAR-SIV mutant constructs. Visualisation of these constructs by immunocytochemistry (ICC), western blotting and flow cytometry revealed that transfected CAR-SIV was robustly detected in the 1.1B4 cells when immunolabelled with the anti-CAR CT serum. Indeed, a similar pattern was achieved with either CAR CT or CAR RmcB antisera. As expected, the CAR CT antiserum did not detect the truncated CAR-SIV mutant from which the C terminal “SIV” motif had been removed. This was confirmed by ICC, western blotting and flow cytometry. In addition, it was also found that attachment of a Myc-tag to the C’ terminal end of wild-type CAR-SIV created a molecule in which steric hindrance prevented the CAR CT antiserum from binding.

6.3.2 Validation of the specificity of the CAR CT antiserum using the mutant CAR-SIV construct

As demonstrated in this study, the CAR CT antiserum failed to recognise the truncated CAR-SIV mutant when tested via ICC, western blotting or flow cytometry. Consistent with this, a proximity ligation assay which relies upon the close proximity of two antisera provided an independent confirmation since no labelling was achieved with a combination of the CAR RmcB and CAR CT antisera in cells expressing truncated CAR-SIV. By contrast, a positive signal was obtained with these antisera in cells expressing the wild-type CAR-SIV construct. This implies that CAR CT and CAR RmcB antisera will only interact when the “SIV” residue is intact.

Overall, these studies have validated the specificity of CARCT antiserum and shown that it does not cross react with other CAR isoforms.

6.3.3 CAR-SIV overexpression did not impact on insulin granule secretion in this model-but is it the right model?

The wild-type CAR-SIV construct was observed to be localised in a similar subcellular compartment to insulin in the 1.1B4 cells (*Figure 6.6*). Thus, to assess whether the presence of CAR-SIV had a functional impact on insulin secretion, a human Growth Hormone assay was utilised in the 1.1B4 cells because it has been reported that growth hormone is co-secreted with insulin following transfection and that hGH secretion is stimulated in a calcium dependent manner (Sugita et al., 1999). Interestingly, results of the trial with different stimuli revealed that indeed the 1.1B4 cells were responsive in that growth hormone release was increased by 2-4 fold under stimulating conditions, by comparison with the basal levels.

One feature of the responses described here is that hGH secretion appeared to be decreased in absolute terms as the amount of DNA was varied in transfection experiments. However, when the growth hormone release was normalised by reference to the basal level, it was seen that the stimulation index was essentially unchanged under conditions when each of the forms of CAR-SIV was introduced.

This finding is rather disappointing as, when taken at face value, the results suggest that CAR-SIV may not be involved in controlling insulin secretion. However, we note that the hGH release in these cells is utilised as a surrogate for insulin release and examination of the co-localisation of insulin and hGH revealed that, in many 1.1B4 cells and INS-1E cells, the transfected hGH did not fully co-localise with insulin. This suggests the surprising possibility that the granules

containing insulin and growth hormone may be different and as such each granule pool could be regulated differentially. Thus, this suggests that it may not be completely accurate to measure insulin secretion from growth hormone release.

Another important issue is that many of the 1.1B4 cells were not immunopositive for insulin (*Figure 6.14B*) and may therefore mean that this cell model is not ideal for assessing the potential role of CAR-SIV in insulin secretion. An alternative human model that could be examined in the future is the EndoC- β H1, however, studies from other members from our laboratory utilising this model have shown that they are difficult to transfect.

Together these arguments suggest that the hGH assay might not be an efficient system to study insulin secretion and other alternative human pancreatic beta cell model would need to be pursued for future experiments in clarifying the CAR-SIV functional impact in insulin secretion.

6.3.4 Future work to assess the effect of CAR-SIV in insulin secretion

Initially the first objective would be to confirm more fully whether insulin and growth hormone utilise the same granule pools and this might be best achieved by using EM studies to label both insulin and growth hormone in beta cells to observe if they are both co-localised in the same pool of granules.

Unfortunately it may not be ideal to utilise a rodent beta cell line to understand the role of CAR-SIV in insulin secretion because immunostaining with anti-CAR CT in chapter 3 in murine pancreas suggests that CAR-SIV is not normally expressed in the endocrine cells and therefore may not form part of the insulin

secretion machinery in rodents. In other words, the rodent beta cell line will not be ideal for studying the role of CAR in insulin secretion.

Potentially, knocking down CAR-SIV in isolated human islets by the transfection of siRNA's and assessment of the impact on insulin secretion would, however, be an appropriate approach. In a similar vein, an endogenous regulator of CAR has recently been described which is known as "hsa-miR-466d". This was shown to downregulate CAR expression in human A549 cell line (Lam et al., 2015) and could be of value in beta cells if similar regulatory mechanisms are present.

Another option would be to inhibit the interaction between CAR-SIV and PICK1 in isolated human islets or EndoC- β H1 by utilising a cell permeable, small molecule PDZ domain inhibitor (*E*)-ethyl 2-cyano-3-(3,4-dichlorophenyl acryloylcarbamate) which has been shown to specifically target PICK1 PDZ domain (Bach et al., 2010).

However, the above experiments mentioned are problematic in that obtaining isolated human islets is not trivial. Moreover, physically knocking down genes in a human islet would require significant optimisation. Furthermore, a human islets would require further isolation of functional beta cells which is intricate as islets are a mixed population consisting of both beta islets cells and exocrine cells.

In conclusion, this chapter has been able to validate the CAR CT antiserum and has recommended that a system to assess CAR-SIV role in insulin secretion would need to be developed to clarify the functional importance.

CHAPTER 7

Conclusion

7.0 Summary

This is the first study to comprehensively investigate which CAR isoforms are expressed in the human pancreas. Immunological and molecular approaches reveal the selective expression of a specific CAR isoform “CAR-SIV” in the human pancreatic beta cell, at both the RNA and protein level. The specificity of the CAR antiserum (CAR CT), used for the characterisation of CAR-SIV was validated and proven not to react with other CAR isoforms by site-directed mutagenesis. Unexpectedly, we discovered that the subcellular localisation of CAR-SIV in the human pancreatic beta cell was not at the plasma membrane. Rather, it was found to be intracellular within a granular distribution in the cytoplasm suggesting a distinct physiological role. Intriguingly, assessment of a human microarray revealed that CAR-SIV was expressed in a variety of other tissues that have a biological secretory function and in these cells it tended to have a granular localisation. In the pancreatic beta cell, CAR-SIV colocalised with insulin and other insulin secretory granule proteins ZnT8 and PC1/3 but less so with proinsulin. It was also found to interact and co-localise with PICK1, a cytosolic protein involved in the budding, maturation and trafficking of insulin secretory granules. Direct confirmation by Cryo-immuno EM revealed that CAR-SIV is localised to both maturing insulin secretory granules and to fully mature, dense core (insulin) secretory granules. These intriguing findings may have several implications in type 1 diabetes which are discussed below.

7.0.1 The localisation of CAR-SIV may explain the susceptibility of human beta cells to enteroviral infection

Coxsackie B viruses (1-6) have been associated with the pathogenesis of autoimmune type 1 diabetes although, the mechanisms by which these viruses could contribute to type 1 diabetes are not fully understood. CVB can gain entry into cells via CAR and therefore I propose that CAR-SIV localisation to the mature dense core insulin granules may facilitate enteroviral entry into the beta cells during exocytosis, which is summarised in Figure 7.1.

I predict that the orientation of CAR-SIV is such that the C' terminus (with the PDZ binding domain) is located in the cytoplasm environment making it available to other proteins containing PDZ domains while the extracellular domain (important for virus binding) is in the lumen of the granule. Thus, during maturation of the granule, the extracellular domain of CAR is in the interior of the granule and only becomes available to the external face of the plasma membrane during exocytosis. This would suggest that enteroviral entry into the beta cells might be facilitated when secretory exocytosis occurs, leading to increased externalisation of CAR-SIV and therefore increased viral entry. In support of this, Ylipaasto *et al* (2004) demonstrated that pre-treatment of human islets with a CAR blocking antiserum (CAR RmcB) directed towards epitopes in the extracellular domain of CAR attenuated Coxsackie virus infection (Ylipaasto *et al.*, 2004). This is consistent with the present study where the majority of CAR is localised intracellularly in the islet cells implying that externalisation of CAR-SIV facilitates viral entry.

Furthermore, Hodik *et al* (2016) demonstrated that stimulation of insulin secretion 3 days after infection of isolated human islets with CVB-5 led to the formation of

enterovirus replication complexes and CVB-5 viral particle lattices on or near insulin secretory granules (Hodik et al., 2016b). This evidence supports the hypothesis that CAR-SIV localisation in the beta cells may enhance their susceptibility to enteroviral infection.

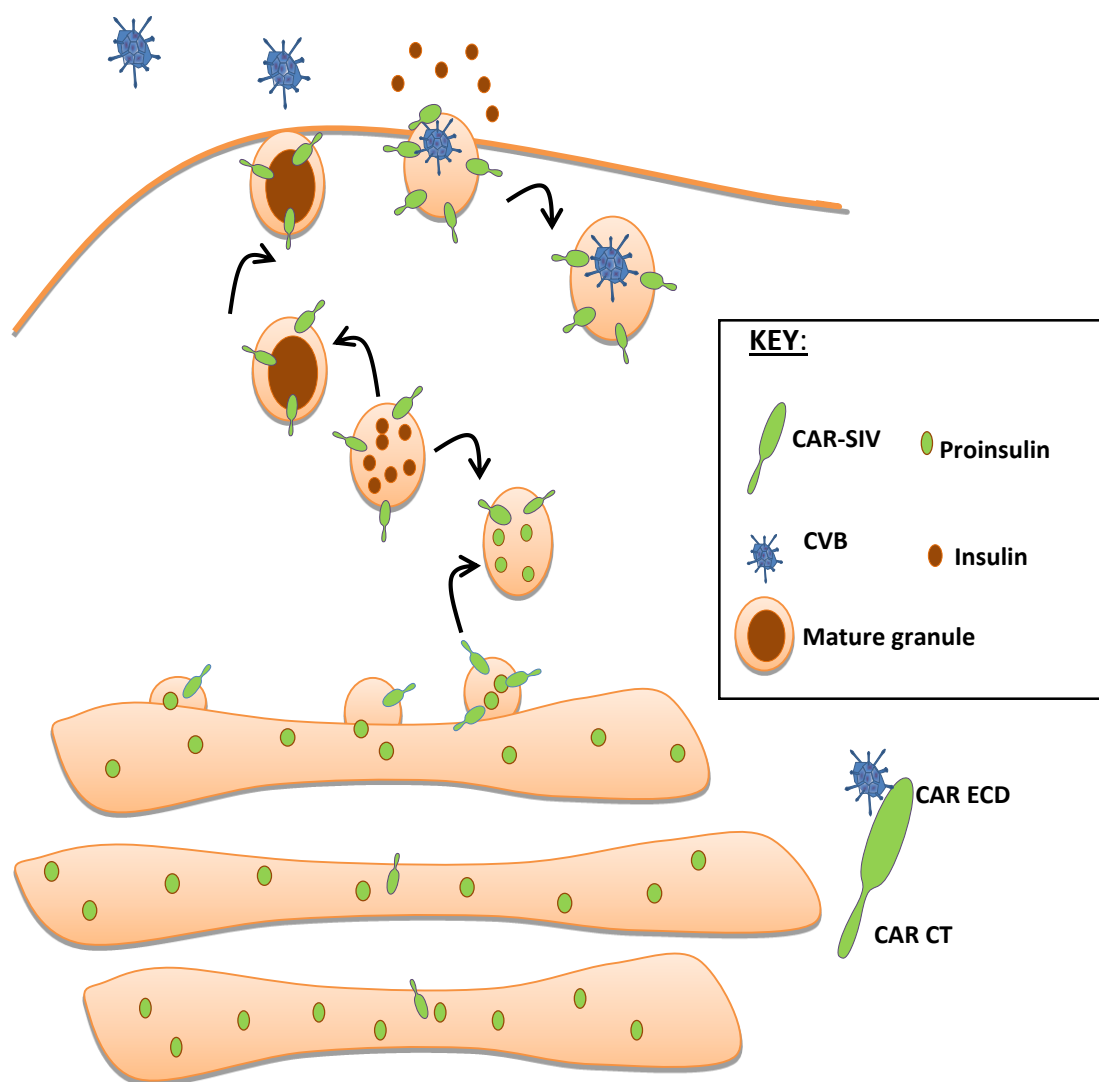


Figure 7.1 Proposed model of enteroviral entry in the beta cell through CAR-SIV.

7.0.2 CAR-SIV may have a role in vesicle maturation and trafficking in human pancreatic beta cells

This study revealed that CAR-SIV is expressed in a variety of tissues involved in exocytotic secretion; for example the testis and brain. Previous work has demonstrated that the testis secretes proacrosomal granules that are involved in fertilisation (Berruti and Paiardi, 2011) while neuronal cells secrete neurotransmitters by exocytosis (De Camilli and Jahn, 1990).

In this study, CAR-SIV was reported to co-localise and interact with the PDZ domain cytosolic protein PICK1 in human beta cells. PICK1 has a unique combination of PDZ and BAR domains (Xu and Xia, 2006) and plays a specific role in budding and trafficking of immature secretory granules from the trans-Golgi network (Holst et al., 2013). Electrophysiological and Cryo-EM analysis in adrenal chromaffin cells from PICK1 KO mice revealed aberrant biogenesis of secretory granules and impaired catecholamine secretion (Pinheiro et al., 2014). Furthermore, PICK1 knockout mice demonstrated impaired trafficking of proacrosomal granules in the testis and abnormal acrosome formation in sperm, directly affecting male infertility (Xiao et al., 2009). These studies provide strong evidence to support a role for PICK1 in the trafficking and maturation of secretory granules. It is conceivable from our study that CAR-SIV orientation in the insulin granule enables PICK1 interaction and this association with the insulin secretory granules could facilitate the maturation of the insulin secretory granules after their emergence from the trans-Golgi network (see Figure 7.2, below)

Furthermore, via its BAR domain PICK1 interacts with a microtubule trafficking associated protein, syntabulin, which functions as a linker molecule for the attachment of cargo vesicles to the molecular motor, conventional kinesin 1,

mediating vesicle transport (Su et al., 2004). In rat hippocampal neuronal cells, time lapse live imaging demonstrated that syntabulin regulates the trafficking of PICK1 containing vesicles along axons (Xu et al., 2016). Since, syntabulin is expressed in beta cells and was shown to mediate glucose stimulated insulin secretion (Ying et al., 2012), we speculate that PICK1 and CAR-SIV may interact in the insulin granules to favour syntabulin binding to the PICK1 and CAR-SIV complex thereby promoting the tethering of insulin secretory granules to microtubules. CAR-SIV has also been shown to have high affinity for microtubules and it was revealed that its cytoplasmic domain is required for the interaction with microtubules (Fok et al., 2007). Thus, microtubule dependent ATPases such as kinesins could then assist in the transport of tethered insulin granules along microtubules to the cortical F actin filamentous web located near the cell periphery, in preparation for exocytosis (docking and SNARE protein complex formation) (Thurmond et al., 2003). At this point, we suspect that PICK1 is lost as it is not required for exocytosis (Cao et al., 2013, Pinheiro et al., 2014) with CAR-SIV still intact in the secretory granule. Depolymerisation of the F-actin network at the plasma membrane occurs disrupting its interaction with the SNARE protein complex leading to the mobilisation of the insulin granule for exocytosis.

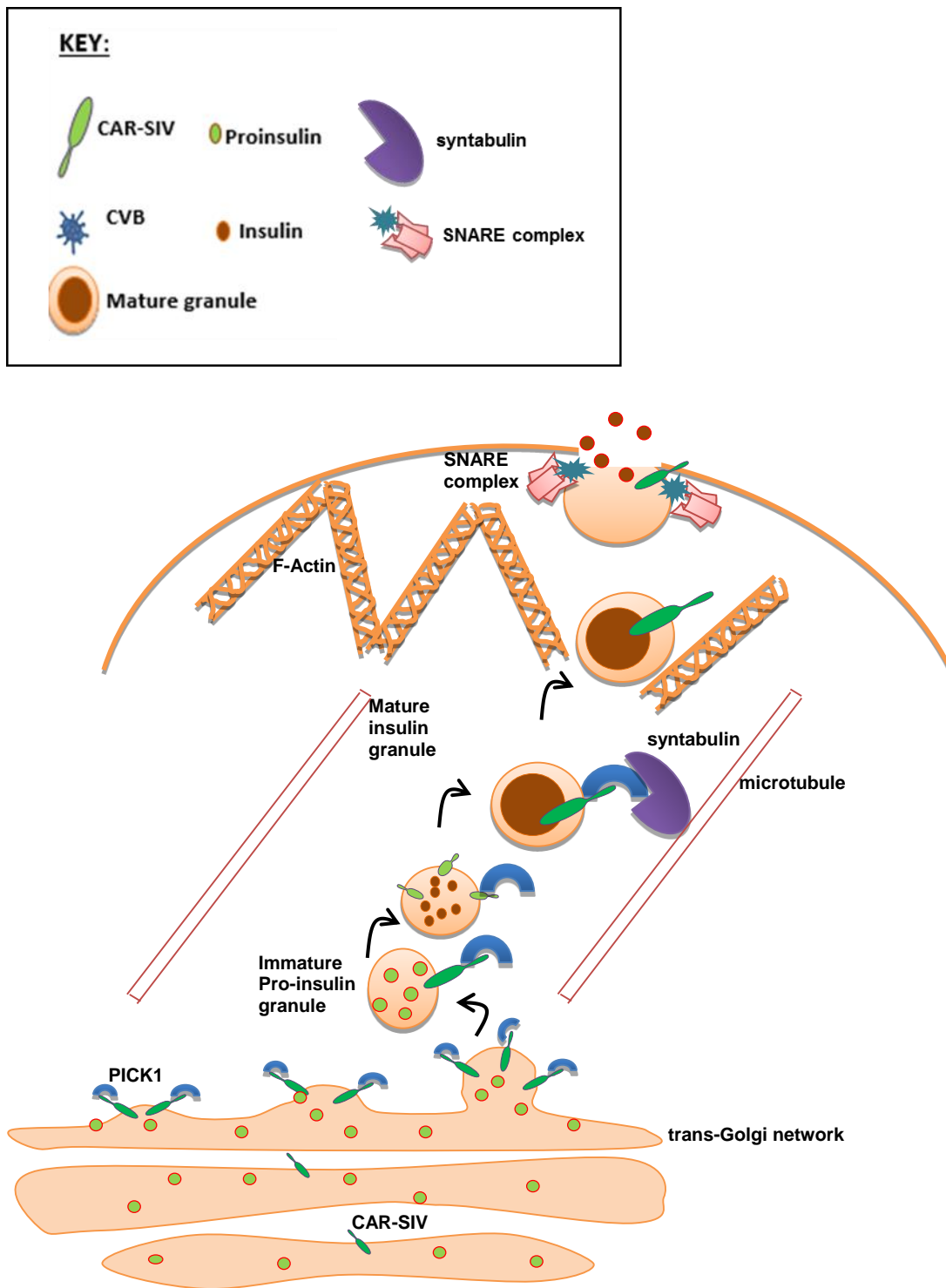


Figure 7.2 CAR-SIV and PICK1 interaction in the beta cell may be involved in the maturation and trafficking of the insulin secretory vesicle. Hypothesis: PICK1 interacts with CAR-SIV through its PDZ domain to facilitate the maturation of the insulin secretory granules after their emergence from the trans-Golgi network. PICK1 then interacts via its BAR domain with syntabulin, mediating insulin vesicle transport on microtubules to F-actin near the cell periphery. In preparation for exocytosis, PICK1 is lost and there is depolymerisation of the F-actin network at the plasma membrane, allowing mobilisation of the insulin granule for exocytosis.

7.1 Limitation of study

Whilst this work predominantly focuses on the expression of CAR-SIV in the human pancreatic beta cell, the other transmembrane isoform CAR-TVV is also present as shown by RNA analysis in either isolated human islets or from laser-captured microdissected islets. The use of less selective antisera (CAR RmcB and CAR ECD) cannot differentiate between these isoforms, therefore the possibility that CAR-TVV is present and functional in beta cells cannot be excluded. Unfortunately, a specific CAR-TVV antiserum is neither commercially available nor was I able to obtain it from authors of publications describing such antisera.

7.2 Future Work

To test the models presented in this thesis in isolated human beta cell or a suitable pancreatic beta cell line by;

- Assessing the impact on insulin secretion of wild-type CAR-SIV and truncated CAR-SIV constructs
- Knocking down the CAR-SIV isoform and studying the effects on insulin secretion.
- Examining if the level of viral infection under high and low glucose conditions is impacted by treatment with a CAR blocking antibody. If my model is correct, high glucose treatment should enhance viral infection and if CAR is mediating this, treatment with the blocking antibody should reduce infection. In addition, to confirm that viral infection of beta cells can be mediated by CAR-SIV, I would transfect cells with both the wild-type CAR-SIV and the truncated CAR-SIV constructs, to demonstrate that CAR

is mediating the infection. This will also confirm the importance of the terminal three amino acids in this process.

- Disrupting the interaction between CAR-SIV and PICK1 by utilising a small cell permeable PDZ domain inhibitor (*E*-ethyl 2-cyano-3-(3,4-dichlorophenyl acryloylcarbamate), which has been shown to specifically target PICK1 PDZ domain (Bach et al., 2010). This could be used to confirm the importance of the CAR-SIV and PICK1 interaction in mediating both insulin secretion and/ or viral infection.

APPENDIX

APPENDIX

Table 8.1 Tissue Samples, Patient Information

Case ID	Case Type	Cohort	Age	Sex	Duration of disease
12425	No diabetes	EADB	Neonate		
8582	No diabetes	EADB	1	N/A	
150/88	No diabetes	EADB	3	F	
274/91	No diabetes	EADB	6	M	
245/90	No diabetes	EADB	6	M	
8651	No diabetes	EADB	6	N/A	
12229	No diabetes	EADB	10	N/A	
540/91	No diabetes	EADB	11	M	
6099-06	No diabetes	nPOD	14.2	M	
PM146/66	No diabetes	EADB	18	F	
PAN 8	No diabetes	EADB	19	N/A	
PAN 1	No diabetes	EADB	22	N/A	
6160-06	No diabetes	nPOD	22.1	M	
329/72	No diabetes	EADB	24	M	
191/67	No diabetes	EADB	25	M	
PM132/67	No diabetes	EADB	46	M	
330/71	No diabetes	EADB	47	M	
186/74	No diabetes	EADB	55	F	
77/6/87	No diabetes	EADB	57	F	
332/66	No diabetes	EADB	59	M	
6098	No diabetes	nPOD	17.8	M	
6153	No diabetes	nPOD	15.2	M	
6027	AAb+	nPOD	18.8	M	
6167	AAb+	nPOD	37	M	
E236	T1D	EADB	7	F	'Recent'
SC41	T1D	EADB	4	F	3 weeks
11746	T1D	EADB	6	M	<1 week
11713	T1D	EADB	3	M	3mth
E375	T1D	EADB	11	F	1 week
E560	T1D	EADB	42	F	18mths
6041	T1D	nPOD	26.3	M	23y
6087	T1D	nPOD	17.5	M	4y
6113	T1D	nPOD	13.1	F	1.58y
6161	T1D	nPOD	19.2	F	7y

EADB – Exeter Archival Diabetes Biobank; AAb+ - Autoantibody positive no diabetes; N/A – not available

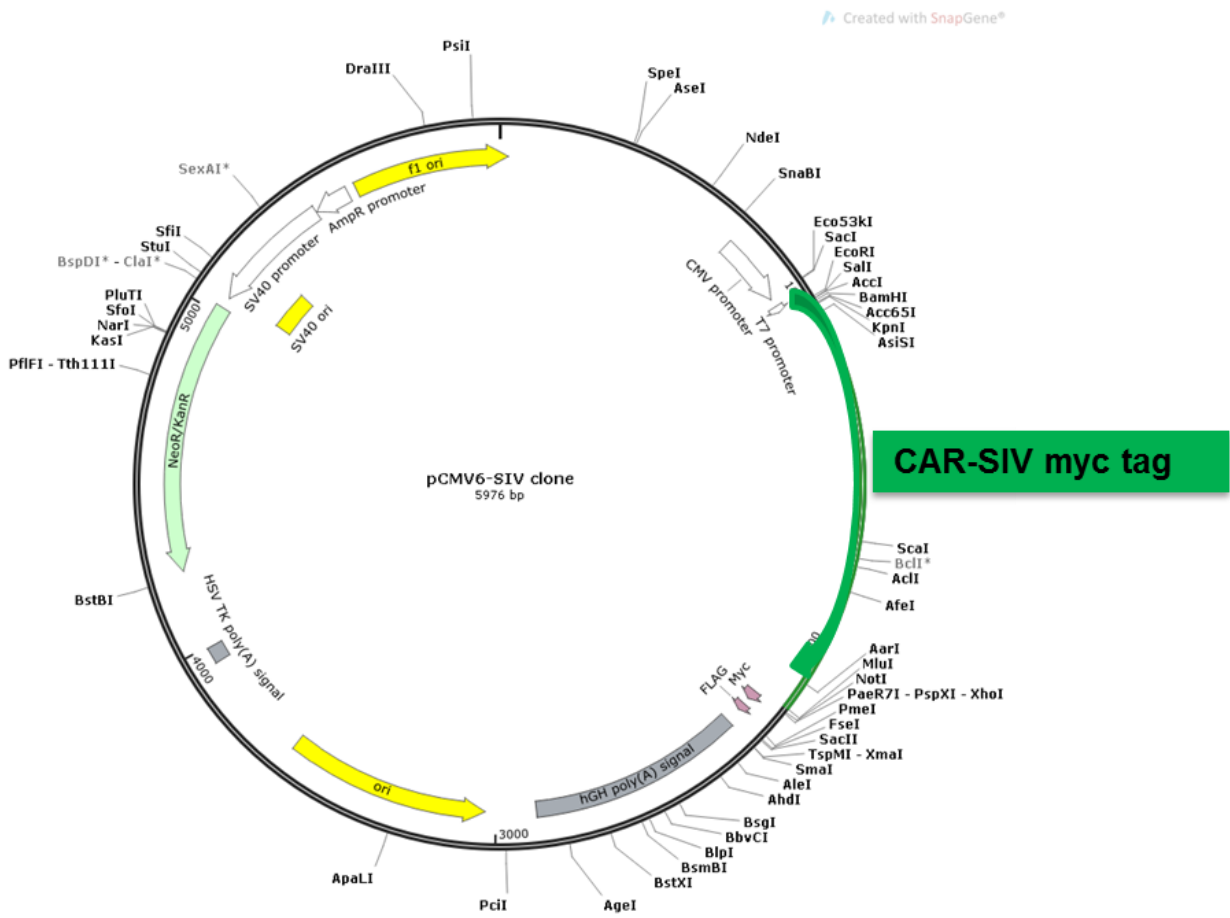


Figure 8.1 Map of the pCMV6 vector

The vector map depicts where CAR-SIV Myc-tag is inserted (green). This vector was purchased from ORIGENE. Map was created with version 4.1.2 SnapGene.com software

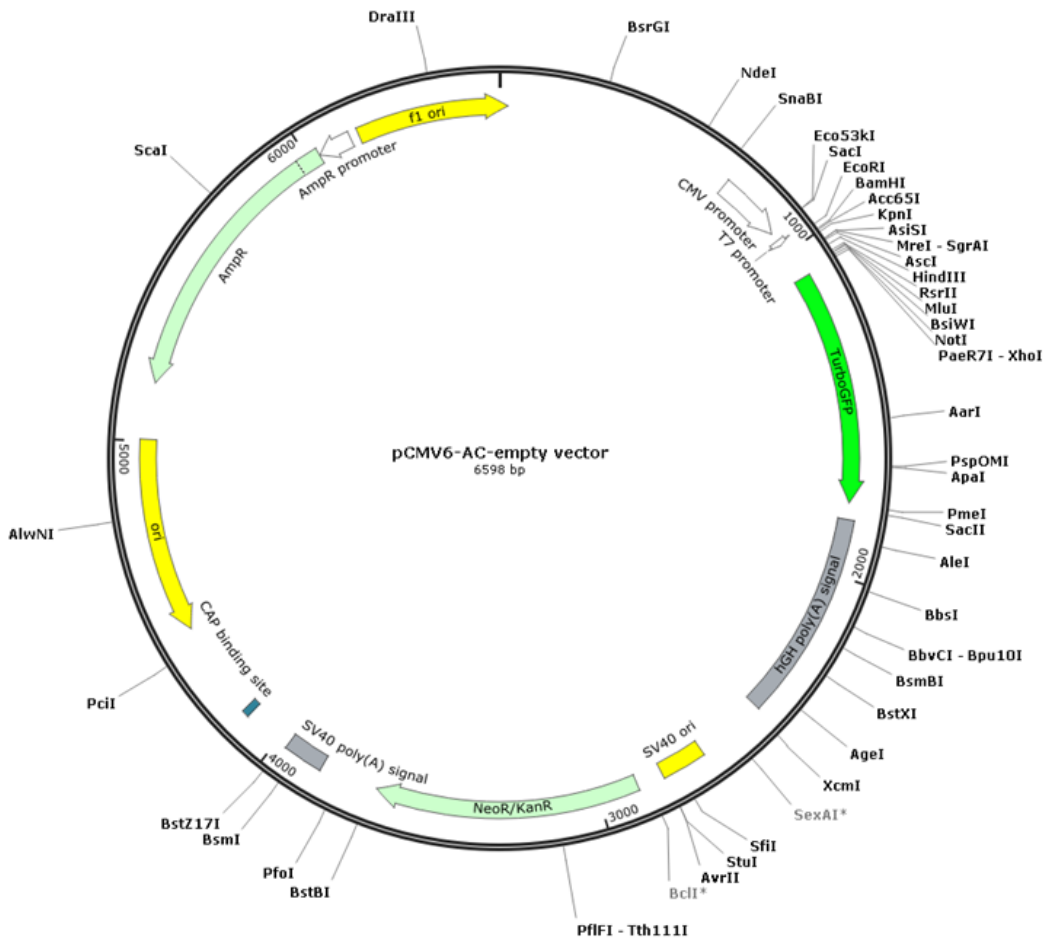


Figure 8.2 Map of the pCMV6 empty vector

This vector was purchased from ORIGENE. Map was created with version 4.1.2 SnapGene.com software

Table 8.2 Primers used for site directed mutagenesis

Target sequence	Primers
Wild-type CAR-SIV	
Exon 7Fd (stop codon insert) <i>Shown in bold italics above</i>	GTCTATAGTA ta GCGTACG
Exon 7Rv	CCATCCTTGCTCTGTGCT
Truncated CAR-SIV mutant	
Exon 7Fd (stop codon insert) <i>Shown in bold italics above</i>	GAGCAAGGAT ta GTCTATA
Exon 7RV	TGTGCTGGAATCATCACAG

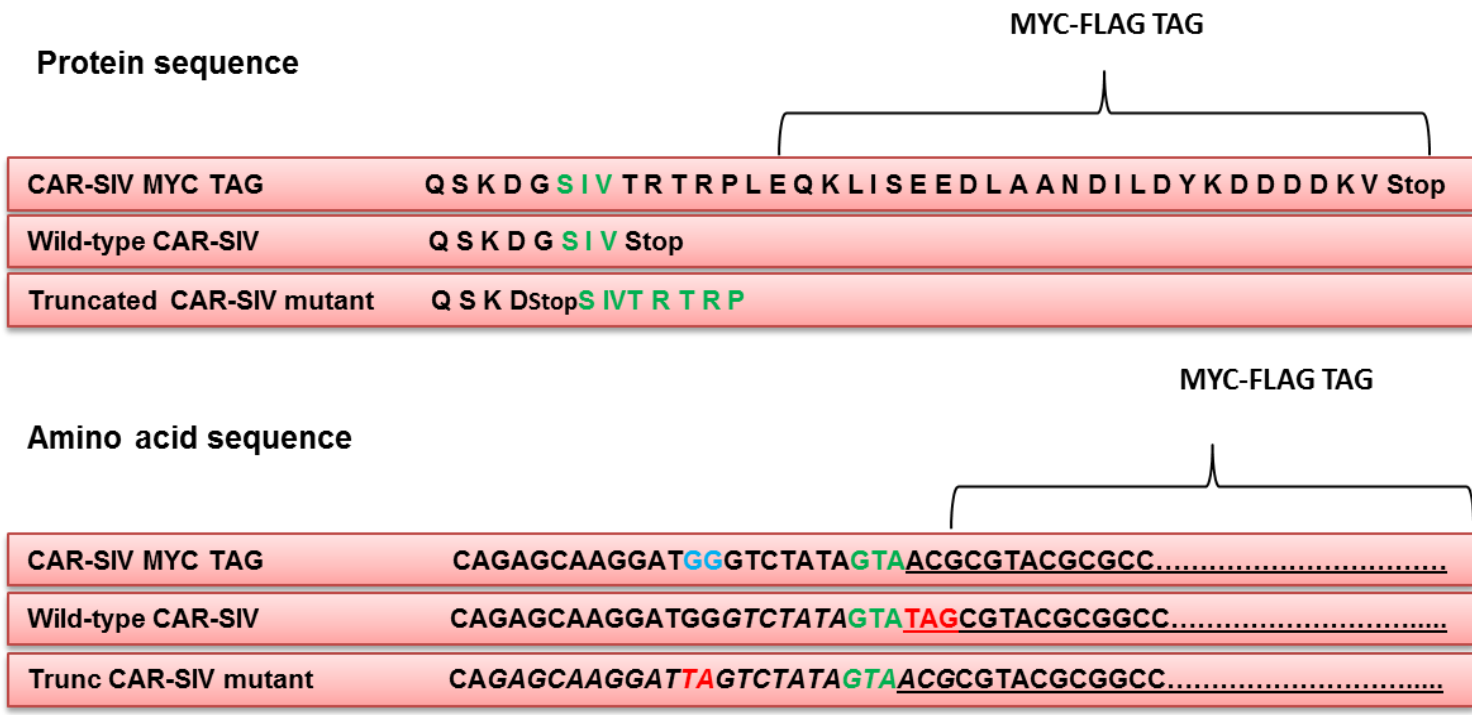


Figure 8.3 Site directed mutagenesis strategy creating the Wild-type CAR-SIV and truncated CAR-SIV mutant construct

REFERENCES

- AHMED, A. M. 2002. History of diabetes mellitus. *Saudi medical journal*, 23, 373-378.
- AHRÉN, B. 2000. Autonomic regulation of islet hormone secretion—implications for health and disease. *Diabetologia*, 43, 393-410.
- AKERBLOM, H. K. & KNIP, M. 1998. Putative environmental factors in Type 1 diabetes. *Diabetes-Metabolism Reviews*, 14, 31-67.
- ALASBAHI, R. H. & MELZIG, M. F. 2012. Forskolin and derivatives as tools for studying the role of cAMP. *Pharmazie*, 67, 5-13.
- ALIDJINO, E. K., ENGELMANN, I., BOSSU, J., VILLENET, C., FIGEAC, M., ROMOND, M. B., SANÉ, F. & HOBER, D. 2017. Persistence of Coxsackievirus B4 in pancreatic ductal-like cells results in cellular and viral changes. *Virulence*, 1-16.
- ANAGANDULA, M., RICHARDSON, S. J., OBERSTE, M. S., SIOOFY-KHOJINE, A.-B., HYOTY, H., MORGAN, N. G., KORSGREN, O. & FRISK, G. 2014a. Infection of Human Islets of Langerhans With Two Strains of Coxsackie B Virus Serotype 1: Assessment of Virus Replication, Degree of Cell Death and Induction of Genes Involved in the Innate Immunity Pathway. *Journal of Medical Virology*, 86, 1402-1411.
- ANAGANDULA, M., RICHARDSON, S. J., OBERSTE, M. S., SIOOFY-KHOJINE, A. B., HYÖTY, H., MORGAN, N. G., KORSGREN, O. & FRISK, G. 2014b. Infection of human islets of Langerhans with two strains of Coxsackie B virus serotype 1: assessment of virus replication, degree of cell death and induction of genes involved in the innate immunity pathway. *Journal of medical virology*, 86, 1402-1411.
- AMERICAN DIABETES ASSOCIATION, 2010. Diagnosis and classification of diabetes mellitus. *Diabetes care*, 33(Suppl 1)p.S62
- AMERICAN DIABETES ASSOCIATION, 2018.2. Classification and Diagnosis of Diabetes: Standards of Medical Care in Diabetes 2018. *Diabetes Care*, 41(Supplement 1), pp S13-S2
- ANDERS, M., VIETH, M., RÖCKEN, C., EBERT, M., PROSS, M., GRETSCHEL, S., SCHLAG, P., WIEDENMANN, B., KEMMNER, W. & HÖCKER, M. 2009. Loss of the coxsackie and adenovirus receptor contributes to gastric cancer progression. *British journal of cancer*, 100, 352.
- ANDERSON, M. S. & BLUESTONE, J. A. 2005. THE NOD MOUSE: A Model of Immune Dysregulation. *Annual Review of Immunology*, 23, 447-485.
- ARIAS, A. E., VÉLEZ-GRANELL, C. S., MAYER, G. & BENDAYAN, M. 2000. Colocalization of chaperone Cpn60, proinsulin and convertase PC1 within immature secretory granules of insulin-secreting cells suggests a role for Cpn60 in insulin processing. *J Cell Sci*, 113, 2075-2083.
- AROLA, A., KALIMO, H., RUUSKANEN, O. & HYYPIÄ, T. 1995. Experimental myocarditis induced by two different coxsackievirus B3 variants: aspects of pathogenesis and comparison of diagnostic methods. *Journal of medical virology*, 47, 251-259.
- ASFARI, M., JANJIC, D., MEDA, P., LI, G., HALBAN, P. A. & WOLLHEIM, C. B. 1992. Establishment of 2-mercaptoethanol-dependent differentiated insulin-secreting cell lines. *Endocrinology*, 130, 167-178.
- ASHCROFT, F. M. & ASHCROFT, S. J. 1992. *Insulin: molecular biology to pathology*, IRL Press.
- ASHCROFT, F. M. & RORSMAN, P. 1989. Electrophysiology of the pancreatic β -cell. *Progress in biophysics and molecular biology*, 54, 87-143.
- ASHCROFT, F. M. & RORSMAN, P. 2012. Diabetes mellitus and the β cell: the last ten years. *Cell*, 148, 1160-1171.
- ASSOCIATION, A. D. 2010. Diagnosis and classification of diabetes mellitus. *Diabetes care*, 33, S62.

- ATKINSON, M. A., BOWMAN, M. A., CAMPBELL, L., DARROW, B. L., KAUFMAN, D. L. & MACLAREN, N. K. 1994. Cellular immunity to a determinant common to glutamate decarboxylase and coxsackie virus in insulin-dependent diabetes. *The Journal of clinical investigation*, 94, 2125-2129.
- ATKINSON, M. A. & EISENBARTH, G. S. 2001. Type 1 diabetes: new perspectives on disease pathogenesis and treatment. *The Lancet*, 358, 221-229.
- ATKINSON, M. A., VON HERRATH, M., POWERS, A. C. & CLARE-SALZLER, M. 2015. Current Concepts on the Pathogenesis of Type 1 Diabetes—Considerations for Attempts to Prevent and Reverse the Disease. *Diabetes Care*, 38, 979-988.
- BACH, A., STUHR-HANSEN, N., THORSEN, T. S., BORK, N., MOREIRA, I. S., FRYDENVANG, K., PADRAH, S., CHRISTENSEN, S. B., MADSEN, K. L., WEINSTEIN, H., GETHER, U. & STRØMGAARD, K. 2010. Structure–activity relationships of a small-molecule inhibitor of the PDZ domain of PICK1. *Organic & biomolecular chemistry*, 8, 4281-4288.
- BAGGEN, J., THIBAUT, H., STRATING, J. R. & VAN KUPPEVELD, F. J. 2018. The life cycle of non-polio enteroviruses and how to target it. *Nature Reviews Microbiology*, 1.
- BANTING, F. G., BEST, C. H., COLLIP, J. B., CAMPBELL, W. R. & FLETCHER, A. A. 1922. Pancreatic extracts in the treatment of diabetes mellitus. *Canadian Medical Association Journal*, 12, 141.
- BARG, S., LINDQVIST, A. & OBERMÜLLER, S. 2008. Granule docking and cargo release in pancreatic β -cells. Portland Press Limited.
- BENSLEY, R. R. 1914. *Structure and relationships of the islets of Langerhans*.
- BERGELSON, J. M., CHAN, M., SOLOMON, K. R., ST JOHN, N. F., LIN, H. & FINBERG, R. W. 1994. Decay-accelerating factor (CD55), a glycosylphosphatidylinositol-anchored complement regulatory protein, is a receptor for several echoviruses. *Proceedings of the National Academy of Sciences*, 91, 6245-6248.
- BERGELSON, J. M., CUNNINGHAM, J. A., DROGUETT, G., KURT-JONES, E. A., KRITHIVAS, A., HONG, J. S., HORWITZ, M. S., CROWELL, R. L. & FINBERG, R. W. 1997. Isolation of a common receptor for Coxsackie B viruses and adenoviruses 2 and 5. *Science*, 275, 1320-1323.
- BERGELSON, J. M., KRITHIVAS, A., CELI, L., DROGUETT, G., HORWITZ, M. S., WICKHAM, T., CROWELL, R. L. & FINBERG, R. W. 1998. The murine CAR homolog is a receptor for coxsackie B viruses and adenoviruses. *Journal of virology*, 72, 415-419.
- BERINSTEIN, A., ROIVAINEN, M., HOVI, T., MASON, P. & BAXT, B. 1995. Antibodies to the vitronectin receptor (integrin alpha V beta 3) inhibit binding and infection of foot-and-mouth disease virus to cultured cells. *Journal of Virology*, 69, 2664-2666.
- BERRUTI, G. & PAIARDI, C. 2011. Acrosome biogenesis: Revisiting old questions to yield new insights. *Spermatogenesis*, 1, 95-98.
- BLANTON, D., HAN, Z., BIERSCHENK, L., LINGA-REDDY, M. P., WANG, H., CLARE-SALZLER, M., HALLER, M., SCHATZ, D., MYHR, C. & SHE, J.-X. 2011. Reduced Serum Vitamin D–Binding Protein Levels Are Associated With Type 1 Diabetes. *Diabetes*, 60, 2566-2570.
- BOPEGAMAGE, S., KOVACOVA, J., VARGOVA, A., MOTUSOVA, J., PETROVICOVA, A., BENKOVICOVA, M., GOMOLCAK, P., BAKKERS, J., VAN KUPPEVELD, F. & MELCHERS, W. J. 2005a. Coxsackie B virus infection of mice: inoculation by the oral route protects the pancreas from damage, but not from infection. *Journal of general virology*, 86, 3271-3280.
- BOPEGAMAGE, S., KOVACOVA, J., VARGOVA, A., MOTUSOVA, J., PETROVICOVA, A., BENKOVICOVA, M., GOMOLCAK, P., BAKKERS, J., VAN KUPPEVELD, F., MELCHERS, W. J. & GALAMA, J. M. 2005b. Coxsackie B virus infection of mice: inoculation by the oral route protects the pancreas from damage, but not from infection. *J Gen Virol*, 86, 3271-80.

- BOSCO, D., ARMANET, M., MOREL, P., NICLAUSS, N., SGROI, A., MULLER, Y. D., GIOVANNONI, L., PARNAUD, G. & BERNEY, T. 2010. Unique arrangement of α - and β -cells in human islets of Langerhans. *Diabetes*, 59, 1202-1210.
- BRUNS, D. & JAHN, R. 2002. Molecular determinants of exocytosis. *Pflügers Archiv*, 443, 333-338.
- BUCHANAN, T. A., XIANG, A., KJOS, S. L. & WATANABE, R. 2007. What is gestational diabetes? *Diabetes care*, 30, S105-S111.
- CANIVELL, S. & GOMIS, R. 2014. Diagnosis and classification of autoimmune diabetes mellitus. *Autoimmunity reviews*, 13, 403-407.
- CAO, M., MAO, Z., KAM, C., XIAO, N., CAO, X., SHEN, C., CHENG, K. K., XU, A., LEE, K.-M. & JIANG, L. 2013. PICK1 and ICA69 control insulin granule trafficking and their deficiencies lead to impaired glucose tolerance. *PLoS Biol*, 11, e1001541.
- CAO, M., XU, J., SHEN, C., KAM, C., HUGANIR, R. L. & XIA, J. 2007. PICK1-ICA69 heteromeric BAR domain complex regulates synaptic targeting and surface expression of AMPA receptors. *Journal of Neuroscience*, 27, 12945-12956.
- CARMODY, D., STØY, J., GREELEY, S. A. W., BELL, G. I. & PHILIPSON, L. H. 2015. A clinical guide to monogenic diabetes. *Genetic Diagnosis of Endocrine Disorders (Second Edition)*. Elsevier.
- CHAPMAN, N. M., KIM, K.-S., DRESCHER, K. M., OKA, K. & TRACY, S. 2008. 5' terminal deletions in the genome of a coxsackievirus B2 strain occurred naturally in human heart. *Virology*, 375, 480-491.
- CHEN, J.-W., GHOSH, R., FINBERG, R. W. & BERGELSON, J. M. 2003. Structure and chromosomal localization of the murine coxsackievirus and adenovirus receptor gene. *DNA and cell biology*, 22, 253-259.
- CHIMIENTI, F., DEVERGNAS, S., PATTOU, F., SCHUIT, F., GARCIA-CUENCA, R., VANDEWALLE, B., KERR-CONTE, J., VAN LOMMEL, L., GRUNWALD, D. & FAVIER, A. 2006. In vivo expression and functional characterization of the zinc transporter ZnT8 in glucose-induced insulin secretion. *Journal of cell science*, 119, 4199-4206.
- CHRÉTIEN, I., MARCUZ, A., COURTET, M., KATEVUO, K., VAINIO, O., HEATH, J. K., WHITE, S. J. & DU PASQUIER, L. 1998. CTX, a *Xenopus* thymocyte receptor, defines a molecular family conserved throughout vertebrates. *European journal of immunology*, 28, 4094-4104.
- COHEN, C. J., GAETZ, J., OHMAN, T. & BERGELSON, J. M. 2001a. Multiple regions within the coxsackievirus and adenovirus receptor cytoplasmic domain are required for basolateral sorting. *Journal of Biological Chemistry*, 276, 25392-25398.
- COHEN, C. J., SHIEH, J. T., PICKLES, R. J., OKEGAWA, T., HSIEH, J. T. & BERGELSON, J. M. 2001b. The coxsackievirus and adenovirus receptor is a transmembrane component of the tight junction. *Proc Natl Acad Sci U S A*, 98, 15191-6.
- COOK, D. L., SATIN, L. S., ASHFORD, M. L. & HALES, C. N. 1988. ATP-sensitive K⁺ channels in pancreatic β -cells: spare-channel hypothesis. *Diabetes*, 37, 495-498.
- COPPIETERS, K. T., BOETTLER, T. & VON HERRATH, M. 2012. Virus infections in type 1 diabetes. *Cold Spring Harbor perspectives in medicine*, 2, a007682.
- CRAMERI, A., WHITEHORN, E., TATE, E., STEMMER, W., CRAMERI, A., KITTS, P. & KITTS, P. 1996. Improved green fluorescent protein by molecular evolution using. *Nat. Biotechnol*, 14, 315-319.
- CUNNINGHAM, L., BOWLES, N., LANE, R., DUBOWITZ, V. & ARCHARD, L. 1990. Persistence of enteroviral RNA in chronic fatigue syndrome is associated with the abnormal production of equal amounts of positive and negative strands of enteroviral RNA. *Journal of General Virology*, 71, 1399-1402.
- DA SILVA XAVIER, G., LECLERC, I., VARADI, A., TSUBOI, T., MOULE, S. K. & RUTTER, G. A. 2003. Role for AMP-activated protein kinase in glucose-stimulated insulin secretion and preproinsulin gene expression. *Biochem J*, 371, 761-74.

- DABELEA, D., REWERS, A., STAFFORD, J. M., STANDIFORD, D. A., LAWRENCE, J. M., SAYDAH, S., IMPERATORE, G., D'AGOSTINO, R. B., MAYER-DAVIS, E. J. & PIHOKER, C. 2014. Trends in the prevalence of ketoacidosis at diabetes diagnosis: the SEARCH for diabetes in youth study. *Pediatrics*, 133, e938-e945.
- DANESHTALAB, N., DORÉ, J. J. E. & SMEDA, J. S. 2010. Troubleshooting tissue specificity and antibody selection: Procedures in immunohistochemical studies. *Journal of Pharmacological and Toxicological Methods*, 61, 127-135.
- DAVIDSON, H. W., RHODES, C. J. & HUTTON, J. C. 1988. Intraorganellar calcium and pH control proinsulin cleavage in the pancreatic β cell via two distinct site-specific endopeptidases. *Nature*, 333, 93.
- DE BEECK, A. O. & EIZIRIK, D. L. 2016. Viral infections in type 1 diabetes mellitus [mdash] why the [beta] cells? *Nat Rev Endocrinol*, advance online publication.
- DE CAMILLI, P. & JAHN, R. 1990. Pathways to regulated exocytosis in neurons. *Annual Review of Physiology*, 52, 625-645.
- DE VOS, A., HEIMBERG, H., QUARTIER, E., HUYPENS, P., BOUWENS, L., PIPELEERS, D. & SCHUIT, F. 1995. Human and rat beta cells differ in glucose transporter but not in glucokinase gene expression. *The Journal of clinical investigation*, 96, 2489-2495.
- DEAN, P. M. 1973. Ultrastructural morphometry of the pancreatic β -cell. *Diabetologia*, 9, 115-119.
- DEV, K. K., NISHIMUNE, A., HENLEY, J. M. & NAKANISHI, S. 1999. The protein kinase α binding protein PICK1 interacts with short but not long form alternative splice variants of AMPA receptor subunits. *Neuropharmacology*, 38, 635-644.
- DODSON, G. & STEINER, D. 1998. The role of assembly in insulin's biosynthesis. *Current opinion in structural biology*, 8, 189-194.
- DÖRNER, A., GRUNERT, H.-P., LINDIG, V., CHANDRASEKHARAN, K., FECHNER, H., KNOWLTON, K., ISIK, A., PAUSCHINGER, M., ZEICHHARDT, H. & SCHULTHEISS, H.-P. 2006. Treatment of coxsackievirus-B3-infected BALB/c mice with the soluble coxsackie adenovirus receptor CAR4/7 aggravates cardiac injury. *Journal of molecular medicine*, 84, 842-851.
- DÖRNER, A., XIONG, D., COUCH, K., YAJIMA, T. & KNOWLTON, K. U. 2004. Alternatively spliced soluble coxsackie-adenovirus receptors inhibit coxsackievirus infection. *Journal of Biological Chemistry*, 279, 18497-18503.
- DORNER, A. A., WEGMANN, F., BUTZ, S., WOLBURG-BUCHHOLZ, K., WOLBURG, H., MACK, A., NASDALA, I., AUGUST, B., WESTERMANN, J. & RATHJEN, F. G. 2005. Coxsackievirus-adenovirus receptor (CAR) is essential for early embryonic cardiac development. *J Cell Sci*, 118, 3509-3521.
- DOYLE, M. E. & EGAN, J. M. 2007. Mechanisms of action of glucagon-like peptide 1 in the pancreas. *Pharmacology & therapeutics*, 113, 546-593.
- DUNN, M. F. 2005. Zinc–Ligand Interactions Modulate Assembly and Stability of the Insulin Hexamer – A Review. *Biometals*, 18, 295-303.
- EIZIRIK, D. L., SAMMETH, M., BOUCKENOOGHE, T., BOTTU, G., SISINO, G., IGOILLO-ESTEVE, M., ORTIS, F., SANTIN, I., COLLI, M. L., BARTHSON, J., BOUWENS, L., HUGHES, L., GREGORY, L., LUNTER, G., MARSELLI, L., MARCHETTI, P., MCCARTHY, M. I. & CNOP, M. 2012. The Human Pancreatic Islet Transcriptome: Expression of Candidate Genes for Type 1 Diabetes and the Impact of Pro-Inflammatory Cytokines. *PLOS Genetics*, 8, e1002552.
- EL-GOHARY, Y. & GITTES, G. 2018. Structure of Islets and Vascular Relationship to the Exocrine Pancreas. *Pancreapedia: The Exocrine Pancreas Knowledge Base*.
- ELAYAT, A. A., EL-NAGGAR, M. M. & TAHIR, M. 1995. An immunocytochemical and morphometric study of the rat pancreatic islets. *Journal of anatomy*, 186, 629.
- ELDING LARSSON, H., VEHIK, K., HALLER, M. J., LIU, X., AKOLKAR, B., HAGOPIAN, W., KRISCHER, J., LERNMARK, Å., SHE, J.-X., SIMELL, O., TOPPARI, J., ZIEGLER, A.-G., REWERS, M. & FOR THE, T. S. 2016. Growth and risk for islet autoimmunity and progression to type 1 diabetes in early childhood: The Environmental Determinants of Diabetes in the Young Study. *Diabetes*.

- ELIASSON, L., ABDULKADER, F., BRAUN, M., GALVANOVSKIS, J., HOPPA, M. B. & RORSMAN, P. 2008. Novel aspects of the molecular mechanisms controlling insulin secretion. *The Journal of physiology*, 586, 3313-3324.
- ELSHEBANI, A., OLSSON, A., WESTMAN, J., TUVEMO, T., KORSGREN, O. & FRISK, G. 2007. Effects on isolated human pancreatic islet cells after infection with strains of enterovirus isolated at clinical presentation of type 1 diabetes. *Virus Research*, 124, 193-203.
- EXCOFFON, K. J., BOWERS, J. R. & SHARMA, P. 2014. 1. Alternative splicing of viral receptors: A review of the diverse morphologies and physiologies of adenoviral receptors. *Recent research developments in virology*, 9, 1.
- EXCOFFON, K. J., GANSEMER, N. D., MOBILY, M. E., KARP, P. H., PAREKH, K. R. & ZABNER, J. 2010. Isoform-specific regulation and localization of the coxsackie and adenovirus receptor in human airway epithelia. *PLoS One*, 5, e9909.
- EXCOFFON, K. J., TRAVER, G. L. & ZABNER, J. 2005. The role of the extracellular domain in the biology of the coxsackievirus and adenovirus receptor. *American journal of respiratory cell and molecular biology*, 32, 498-503.
- EXCOFFON, K. J. A., GANSEMER, N., TRAVER, G. & ZABNER, J. 2007. Functional effects of coxsackievirus and adenovirus receptor glycosylation on homophilic adhesion and adenoviral infection. *Journal of virology*, 81, 5573-5578.
- EXCOFFON, K. J. A., HRUSKA-HAGEMAN, A., KLOTZ, M., TRAVER, G. L. & ZABNER, J. 2004. A role for the PDZ-binding domain of the coxsackie B virus and adenovirus receptor (CAR) in cell adhesion and growth. *Journal of cell science*, 117, 4401-4409.
- EXCOFFON, K. J. A., MONINGER, T. & ZABNER, J. 2003. The coxsackie B virus and adenovirus receptor resides in a distinct membrane microdomain. *Journal of virology*, 77, 2559-2567.
- FANG, J., LIU, M., ZHANG, X., SAKAMOTO, T., TAATJES, D. J., JENA, B. P., SUN, F., WOODS, J., BRYSON, T. & KOWLURU, A. 2015. COPII-dependent ER export: a critical component of insulin biogenesis and β -cell ER homeostasis. *Molecular Endocrinology*, 29, 1156-1169.
- FEHMANN, H. C. & HABENER, J. F. 1992. Insulinotropic hormone glucagon-like peptide-1(7-37) stimulation of proinsulin gene expression and proinsulin biosynthesis in insulinoma beta TC-1 cells. *Endocrinology*, 130, 159-166.
- FIELDS, B., KNIPE, D., HOWLEY, P. & GRIFFIN, D. 2007. *Fields virology*. 5th. Philadelphia: Wolters Kluwer Health/Lippincott Williams & Wilkins.
- FOK, P. T., HUANG, K.-C., HOLLAND, P. C. & NALBANTOGLU, J. 2007. The Coxsackie and adenovirus receptor binds microtubules and plays a role in cell migration. *Journal of Biological Chemistry*, 282, 7512-7521.
- FOULIS, A., MCGILL, M., FARQUHARSON, M. & HILTON, D. 1997. A search for evidence of viral infection in pancreases of newly diagnosed patients with IDDM. *Diabetologia*, 40, 53-61.
- FREDRIKSSON, S., GULLBERG, M., JARVIUS, J., OLSSON, C., PIETRAS, K., GUSTAFSDOTTIR, S. M., OSTMAN, A. & LANDEGREN, U. 2002. Protein detection using proximity-dependent DNA ligation assays. *Nat Biotechnol*, 20, 473-7.
- FRISK, G. & DIDERHOLM, H. 2000. Tissue culture of isolated human pancreatic islets infected with different strains of coxsackievirus B4: assessment of virus replication and effects on islet morphology and insulin release. *Int J Exp Diabetes Res*, 1, 165-75.
- FURUTA, M., YANO, H., ZHOU, A., ROUILLÉ, Y., HOLST, J. J., CARROLL, R., RAVAZZOLA, M., ORCI, L., FURUTA, H. & STEINER, D. F. 1997. Defective prohormone processing and altered pancreatic islet morphology in mice lacking active SPC2. *Proceedings of the National Academy of Sciences*, 94, 6646-6651.
- GAISANO, H. Y. 2014. Here come the newcomer granules, better late than never. *Trends in Endocrinology & Metabolism*, 25, 381-388.

- GALLAGHER, G. R., BREHM, M. A., FINBERG, R. W., BARTON, B. A., SHULTZ, L. D., GREINER, D. L., BORTELL, R. & WANG, J. P. 2014. Viral infection of engrafted human islets leads to diabetes. *Diabetes*, DB_141020.
- GAMBLE, D. R., KINSLEY, M. L., FITZGERA.MG, BOLTON, R. & TAYLOR, K. W. 1969. Viral Antibodies in Diabetes Mellitus. *British Medical Journal*, 3, 627-&.
- GAN, W. J., ZAVORTINK, M., LUDICK, C., TEMPLIN, R., WEBB, R., WEBB, R., MA, W., PORONNIK, P., PARTON, R. G. & GAISANO, H. Y. 2017. Cell polarity defines three distinct domains in pancreatic β -cells. *J Cell Sci*, 130, 143-151.
- GAO, Y. & LUI, W.-Y. 2014. Synergistic effect of interferon-gamma and tumor necrosis factor-alpha on coxsackievirus and adenovirus receptor expression: an explanation of cell sloughing during testicular inflammation in mice. *Biology of reproduction*, 90.
- GERLING, I., CHATTERJEE, N. K. & NEJMAN, C. 1991. Coxsackievirus B4-Induced Development of Antibodies to 64,000-Mr Islet Autoantigen and Hyperglycemia in Mice. *Autoimmunity*, 10, 49-56.
- GILLESPIE, K. M. 2006. Type 1 diabetes: pathogenesis and prevention. *Canadian Medical Association Journal*, 175, 165-170.
- GILON, P. & HENQUIN, J.-C. 2001. Mechanisms and physiological significance of the cholinergic control of pancreatic β -cell function. *Endocrine reviews*, 22, 565-604.
- GLAUNSINGER, B. A., LEE, S. S., THOMAS, M., BANKS, L. & JAVIER, R. 2000. Interactions of the PDZ-protein MAGI-1 with adenovirus E4-ORF1 and high-risk papillomavirus E6 oncoproteins. *Oncogene*, 19, 5270.
- GOODFELLOW, I. G., EVANS, D. J., BLOM, A. M., KERRIGAN, D., MINERS, J. S., MORGAN, B. P. & SPILLER, O. B. 2005. Inhibition of Coxsackie B Virus Infection by Soluble Forms of Its Receptors: Binding Affinities, Altered Particle Formation, and Competition with Cellular Receptors. *Journal of Virology*, 79, 12016-12024.
- GOODGE, K. A. & HUTTON, J. C. Translational regulation of proinsulin biosynthesis and proinsulin conversion in the pancreatic β -cell. *Seminars in cell & developmental biology*, 2000. Elsevier, 235-242.
- GRAHAM, F., SMILEY, J., RUSSELL, W. & NAIRN, R. 1977. Characteristics of a human cell line transformed by DNA from human adenovirus type 5. *Journal of General Virology*, 36, 59-72.
- GRAHAM, K. L., SUTHERLAND, R. M., MANNERING, S. I., ZHAO, Y., CHEE, J., KRISHNAMURTHY, B., THOMAS, H. E., LEW, A. M. & KAY, T. W. H. 2012. Pathogenic Mechanisms in Type 1 Diabetes: The Islet is Both Target and Driver of Disease. *The Review of Diabetic Studies : RDS*, 9, 148-168.
- GREITZER-ANTES, D., XIE, L., QIN, T., XIE, H., ZHU, D., DOLAI, S., LIANG, T., KANG, F., HARDY, A. B. & HE, Y. 2018. Kv2. 1 clusters on β -cell plasma membrane act as reservoirs that replenish pools of newcomer insulin granule through their interaction with syntaxin-3. *Journal of Biological Chemistry*, jbc. RA118. 002703.
- GUT, A., KIRALY, C. E., FUKUDA, M., MIKOSHIBA, K., WOLLHEIM, C. B. & LANG, J. 2001. Expression and localisation of synaptotagmin isoforms in endocrine (β)-cells: their function in insulin exocytosis. *Journal of Cell Science*, 114, 1709-1716.
- HASTOY, B., CLARK, A., RORSMAN, P. & LANG, J. 2017. Fusion pore in exocytosis: More than an exit gate? A β -cell perspective. *Cell calcium*, 68, 45-61.
- HATLAPATKA, K., WILLENBORG, M. & RUSTENBECK, I. 2009. Plasma membrane depolarization as a determinant of the first phase of insulin secretion. *Am J Physiol Endocrinol Metab*, 297, E315-22.
- HATTERSLEY, A., BRUINING, J., SHIELD, J., NJOLSTAD, P. & DONAGHUE, K. C. 2009. The diagnosis and management of monogenic diabetes in children and adolescents. *Pediatric diabetes*, 10, 33-42.
- HE, Y., CHIPMAN, P. R., HOWITT, J., BATOR, C. M., WHITT, M. A., BAKER, T. S., KUHN, R. J., ANDERSON, C. W., FREIMUTH, P. & ROSSMANN, M. G. 2001. Interaction of coxsackievirus B3 with the full length coxsackievirus-adenovirus receptor. *Nature structural biology*, 8, 874-878.

- HELLMAN, B. 1959. The frequency distribution of the number and volume of the islets Langerhans in man. I. Studies on non-diabetic adults. *Acta Societatis Medicorum Upsaliensis*, 64, 432.
- HENDERSON, J. & MOSS, M. 1985. A morphometric study of the endocrine and exocrine capillaries of the pancreas. *Experimental Physiology*, 70, 347-356.
- HENQUIN, J.-C., ISHIYAMA, N., NENQUIN, M., RAVIER, M. A. & JONAS, J.-C. 2002. Signals and pools underlying biphasic insulin secretion. *Diabetes*, 51, S60-S67.
- HENQUIN, J.-C. & NENQUIN, M. 2014. Activators of PKA and Epac distinctly influence insulin secretion and cytosolic Ca²⁺ in female mouse islets stimulated by glucose and tolbutamide. *Endocrinology*, 155, 3274-3287.
- HILTON, D. A., DAY, C., PRINGLE, J. H., FLETCHER, A. & CHAMBERS, S. 1992. Demonstration of the distribution of coxsackie virus RNA in neonatal mice by non-isotopic in situ hybridization. *Journal of virological methods*, 40, 155-162.
- HOANG DO, O. & THORN, P. 2015. Insulin secretion from beta cells within intact islets: location matters. *Clinical and Experimental Pharmacology and Physiology*, 42, 406-414.
- HOBER, D., SANÉ, F., RIEDWEG, K., MOUMNA, I., GOFFARD, A., CHOTEAU, L., ALIDJINO, E. K. & DESAILLOUD, R. 2013. Viruses and type 1 diabetes: focus on the enteroviruses. *Type 1 diabetes*. InTech.
- HODIK, M., ANAGANDULA, M., FUXE, J., KROGVOLD, L., DAHL-JØRGENSEN, K., HYÖTY, H., SARMIENTO, L., FRISK, G. & CONSORTIUM, P.-V. 2016a. Coxsackie-adenovirus receptor expression is enhanced in pancreas from patients with type 1 diabetes. *BMJ Open Diabetes Research & Care*, 4, e000219.
- HODIK, M., SKOG, O., LUKINIUS, A., ISAZA-CORREA, J. M., KUIPERS, J., GIEPMANS, B. N. G. & FRISK, G. 2016b. Enterovirus infection of human islets of Langerhans affects β -cell function resulting in disintegrated islets, decreased glucose stimulated insulin secretion and loss of Golgi structure. *BMJ Open Diabetes Research & Care*, 4.
- HOGLE, J. M. 2002. Poliovirus cell entry: common structural themes in viral cell entry pathways. *Annual Reviews in Microbiology*, 56, 677-702.
- HOLST, B., MADSEN, K. L., JANSEN, A. M., JIN, C., RICKHAG, M., LUND, V. K., JENSEN, M., BHATIA, V., SØRENSEN, G. & MADSEN, A. N. 2013. PICK1 deficiency impairs secretory vesicle biogenesis and leads to growth retardation and decreased glucose tolerance. *PLoS Biol*, 11, e1001542.
- HOLZ, G. G. 2004. Epac: a new cAMP-binding protein in support of glucagon-like peptide-1 receptor-mediated signal transduction in the pancreatic β -cell. *Diabetes*, 53, 5-13.
- HONDA, T., SAITOH, H., MASUKO, M., KATAGIRI-ABE, T., TOMINAGA, K., KOZAKAI, I., KOBAYASHI, K., KUMANISHI, T., WATANABE, Y. G. & ODANI, S. 2000a. The coxsackievirus-adenovirus receptor protein as a cell adhesion molecule in the developing mouse brain. *Molecular brain research*, 77, 19-28.
- HONDA, T., SAITOH, H., MASUKO, M., KATAGIRI-ABE, T., TOMINAGA, K., KOZAKAI, I., KOBAYASHI, K., KUMANISHI, T., WATANABE, Y. G., ODANI, S. & KUWANO, R. 2000b. The coxsackievirus-adenovirus receptor protein as a cell adhesion molecule in the developing mouse brain. *Brain Res Mol Brain Res*, 77, 19-28.
- HOTTA, Y., HONDA, T., NAITO, M. & KUWANO, R. 2003. Developmental distribution of coxsackie virus and adenovirus receptor localized in the nervous system. *Developmental brain research*, 143, 1-13.
- HOU, J. C., MIN, L. & PESSIN, J. E. 2009. Insulin granule biogenesis, trafficking and exocytosis. *Vitamins & Hormones*, 80, 473-506.
- HOURI, N., HUANG, K. C. & NALBANTOGLU, J. 2013. The Coxsackievirus and Adenovirus Receptor (CAR) undergoes ectodomain shedding and regulated intramembrane proteolysis (RIP). *PLoS One*, 8, e73296.
- HUANG, K. C., ALTINOZ, M., WOSIK, K., LAROCHELLE, N., KOTY, Z., ZHU, L., HOLLAND, P. C. & NALBANTOGLU, J. 2005. Impact of the coxsackie and

- adenovirus receptor (CAR) on glioma cell growth and invasion: Requirement for the C-terminal domain. *International journal of cancer*, 113, 738-745.
- HUANG, Q., BAUM, L. & FU, W.-L. 2010. Simple and practical staining of DNA with GelRed in agarose gel electrophoresis.
- HUOVILA, A.-P. J., TURNER, A. J., PELTO-HUIKKO, M., KÄRKKÄINEN, I. & ORTIZ, R. M. 2005. Shedding light on ADAM metalloproteinases. *Trends in Biochemical Sciences*, 30, 413-422.
- HUTTON, J. C. 1994. Insulin secretory granule biogenesis and the proinsulin-processing endopeptidases. *Diabetologia*, 37, S48-S56.
- HYÖTY, H. 2002. Enterovirus infections and type 1 diabetes. *Annals of Medicine*, 34, 138-147.
- HYÖTY, H. 2016. Viruses in type 1 diabetes. *Pediatric diabetes*, 17, 56-64.
- HYPPÖNEN, E., LÄÄRÄ, E., REUNANEN, A., JÄRVELIN, M.-R. & VIRTANEN, S. M. 2001. Intake of vitamin D and risk of type 1 diabetes: a birth-cohort study. *The Lancet*, 358, 1500-1503.
- IEZZI, M., ESCHER, G. R., MEDA, P., CHAROLLAIS, A., BALDINI, G., DARCHEN, F. O., WOLLHEIM, C. B. & REGAZZI, R. 1999. Subcellular distribution and function of Rab3A, B, C, and D isoforms in insulin-secreting cells. *Molecular Endocrinology*, 13, 202-212.
- IEZZI, M., KOURI, G., FUKUDA, M. & WOLLHEIM, C. B. 2004. Synaptotagmin V and IX isoforms control Ca²⁺-dependent insulin exocytosis. *Journal of cell science*, 117, 3119-3127.
- ITO, M., KODAMA, M., MASUKO, M., YAMAURA, M., FUSE, K., UESUGI, Y., HIRONO, S., OKURA, Y., KATO, K., HOTTA, Y., HONDA, T., KUWANO, R. & AIZAWA, Y. 2000. Expression of Coxsackievirus and Adenovirus Receptor in Hearts of Rats With Experimental Autoimmune Myocarditis. *Circulation Research*, 86, 275.
- JAIDANE, H. & HOBER, D. 2008. Role of coxsackievirus B4 in the pathogenesis of type 1 diabetes. *Diabetes & metabolism*, 34, 537-548.
- JEE, Y. S., LEE, S. G., LEE, J. C., KIM, M. J., LEE, J. J., KIM, D. Y., PARK, S. W., SUNG, M.-W. & HEO, D. S. 2002. Reduced expression of coxsackievirus and adenovirus receptor (CAR) in tumor tissue compared to normal epithelium in head and neck squamous cell carcinoma patients. *Anticancer research*, 22, 2629-2634.
- JIN, W., GE, W.-P., XU, J., CAO, M., PENG, L., YUNG, W., LIAO, D., DUAN, S., ZHANG, M. & XIA, J. 2006. Lipid binding regulates synaptic targeting of PICK1, AMPA receptor trafficking, and synaptic plasticity. *Journal of Neuroscience*, 26, 2380-2390.
- JMII, H., HALOUANI, A., ELMASTOUR, F., IFIE, E., RICHARDSON, S. J., SANE, F., MOKNI, M., AOUNI, M., HOBER, D. & JAÏDANE, H. 2016. Central nervous system infection following vertical transmission of Coxsackievirus B4 in mice. *FEMS Pathogens and Disease*, 74, ftw096.
- JUN, H.-S. & YOON, J.-W. 2004. A new look at viruses in type 1 diabetes. *ILAR journal*, 45, 349-374.
- KAHN, S. E., D'ALESSIO, D. A., SCHWARTZ, M. W., FUJIMOTO, W. Y., ENSINCK, J. W., TABORSKY, G. J. & PORTE, D. 1990. Evidence of cosecretion of islet amyloid polypeptide and insulin by β -cells. *Diabetes*, 39, 634-638.
- KALLEWAARD, N. L., ZHANG, L., CHEN, J.-W., GUTTENBERG, M., SANCHEZ, M. D. & BERGELSON, J. M. 2009. Tissue-specific deletion of the coxsackievirus and adenovirus receptor protects mice from virus-induced pancreatitis and myocarditis. *Cell host & microbe*, 6, 91-98.
- KALWAT, M. A. & THURMOND, D. C. 2013. Signaling mechanisms of glucose-induced F-actin remodeling in pancreatic islet β cells. *Experimental & molecular medicine*, 45, e37.
- KATZ, J., BENOIST, C. & MATHIS, D. 1993. Major histocompatibility complex class I molecules are required for the development of insulinitis in non-obese diabetic mice. *European journal of immunology*, 23, 3358-3360.

- KIM, K.-S., TRACY, S., TAPPRICH, W., BAILEY, J., LEE, C.-K., KIM, K., BARRY, W. & CHAPMAN, N. 2005. 5'-Terminal deletions occur in coxsackievirus B3 during replication in murine hearts and cardiac myocyte cultures and correlate with encapsidation of negative-strand viral RNA. *Journal of virology*, 79, 7024-7041.
- KLINGEL, K., HOHENADL, C., CANU, A., ALBRECHT, M., SEEMANN, M., MALL, G. & KANDOLF, R. 1992. Ongoing enterovirus-induced myocarditis is associated with persistent heart muscle infection: quantitative analysis of virus replication, tissue damage, and inflammation. *Proceedings of the National Academy of Sciences*, 89, 314-318.
- KLINGEL, K., STEPHAN, S., SAUTER, M., ZELL, R., MCMANUS, B. M., BÜLTMANN, B. & KANDOLF, R. 1996. Pathogenesis of murine enterovirus myocarditis: virus dissemination and immune cell targets. *Journal of virology*, 70, 8888-8895.
- KOBAYASHI, T., TAMEMOTO, K., NAKANISHI, K., KATO, N., OKUBO, M., KAJIO, H., SUGIMOTO, T., MURASE, T. & KOSAKA, K. 1993. Immunogenetic and clinical characterization of slowly progressive IDDM. *Diabetes care*, 16, 780-788.
- KOTHA, P. L., SHARMA, P., KOLAWOLE, A. O., YAN, R., ALGHAMRI, M. S., BROCKMAN, T. L., GOMEZ-CAMBRONERO, J. & EXCOFFON, K. J. 2015. Adenovirus entry from the apical surface of polarized epithelia is facilitated by the host innate immune response. *PLoS pathogens*, 11, e1004696.
- KROGVOLD, L., SKOG, O., SUNDSTRÖM, G., EDWIN, B., BUANES, T., HANSEN, K. F., LUDVIGSSON, J., GRABHERR, M., KORSGREN, O. & DAHL-JØRGENSEN, K. 2015. Function of Isolated Pancreatic Islets From Patients at Onset of Type 1 Diabetes: Insulin Secretion Can Be Restored After Some Days in a Nondiabetogenic Environment In Vitro Results From the DiViD Study. *Diabetes*, 64, 2506-2512.
- KUNIN, C. M. 1964. Cellular susceptibility to enteroviruses. *Bacteriological reviews*, 28, 382.
- LAM, W., CHEUNG, A. C., TUNG, C. K., YEUNG, A., NGAI, K. L., LUI, V. W., CHAN, P. K. & TSUI, S. K. 2015. miR-466 is putative negative regulator of Coxsackie virus and Adenovirus Receptor. *FEBS letters*, 589, 246-254.
- LANE, M. A. 1907. The cytological characters of the areas of Langerhans. *Developmental Dynamics*, 7, 409-422.
- LANG, J. 1999. Molecular mechanisms and regulation of insulin exocytosis as a paradigm of endocrine secretion. *The FEBS Journal*, 259, 3-17.
- LEBOVITZ, H. E. 1999. Type 2 Diabetes: An Overview. *Clinical Chemistry*, 45, 1339.
- LESLIE, R. D. G., WILLIAMS, R. & POZZILLI, P. 2006. Type 1 Diabetes and Latent Autoimmune Diabetes in Adults: One End of the Rainbow. *The Journal of Clinical Endocrinology & Metabolism*, 91, 1654-1659.
- LEVENTAL, I., LINGWOOD, D., GRZYBEK, M., COSKUN, Ü. & SIMONS, K. 2010. Palmitoylation regulates raft affinity for the majority of integral raft proteins. *Proceedings of the National Academy of Sciences*, 107, 22050-22054.
- LI, J., MAO, Z., HUANG, J. & XIA, J. 2018. PICK1 is Essential for Insulin Production and the Maintenance of Glucose Homeostasis. *Molecular biology of the cell*, mbc. E17-03-0204.
- LI, J., OUYANG, Q., CHEN, C.-W., CHEN, Q.-B., LI, X.-N., XIANG, Z.-H. & YUAN, H.-B. 2017. Neuron-Derived ADAM10 Production Stimulates Peripheral Nerve Injury-Induced Neuropathic Pain by Cleavage of E-Cadherin in Satellite Glial Cells. *Pain Medicine*, 18, 1752-1766.
- LIEBER, M., MAZZETTA, J., NELSON-REES, W., KAPLAN, M. & TODARO, G. 1975. Establishment of a continuous tumor-cell line (PANC-1) from a human carcinoma of the exocrine pancreas. *International Journal of Cancer*, 15, 741-747.
- LILLIOJA, S., MOTT, D. M., SPRAUL, M., FERRARO, R., FOLEY, J. E., RAVUSSIN, E., KNOWLER, W. C., BENNETT, P. H. & BOGARDUS, C. 1993. Insulin resistance and insulin secretory dysfunction as precursors of non-insulin-dependent diabetes mellitus. Prospective studies of Pima Indians. *N Engl J Med*, 329, 1988-92.

- LIM, B.-K., XIONG, D., DORNER, A., YOUN, T.-J., YUNG, A., LIU, T. I., GU, Y., DALTON, N. D., WRIGHT, A. T. & EVANS, S. M. 2008. Coxsackievirus and adenovirus receptor (CAR) mediates atrioventricular-node function and connexin 45 localization in the murine heart. *The Journal of clinical investigation*, 118, 2758-2770.
- LINDEN, L. V. D., WOLTERS, K. C. & VAN KUPPEVELD, F. J. 2015. Replication and inhibitors of enteroviruses and parechoviruses. *Viruses*, 7, 4529-4562.
- LINDSAY, T., HALVORSON, K., PETERS, C., GHILARDI, J., KUSKOWSKI, M., WONG, G. & MANTYH, P. 2006. A quantitative analysis of the sensory and sympathetic innervation of the mouse pancreas. *Neuroscience*, 137, 1417-1426.
- LIU, M., WRIGHT, J., GUO, H., XIONG, Y. & ARVAN, P. 2014. Proinsulin entry and transit through the endoplasmic reticulum in pancreatic beta cells. *Vitamins & Hormones*. Elsevier.
- LONGNECKER, D. S. 2014. Anatomy and Histology of the Pancreas. *Pancreapedia: The Exocrine Pancreas Knowledge Base*.
- LOU, X. & SHIN, Y.-K. 2016. SNARE zippering. *Bioscience reports*, 36, e00327.
- LOUSTALOT, F., KREMER, E. J. & SALINAS, S. 2016. Membrane dynamics and signaling of the coxsackievirus and adenovirus receptor. *International review of cell and molecular biology*. Elsevier.
- LOVE, J. A., YI, E. & SMITH, T. G. 2007. Autonomic pathways regulating pancreatic exocrine secretion. *Autonomic Neuroscience: Basic and Clinical*, 133, 19-34.
- LOW, J. T., ZAVORTINK, M., MITCHELL, J. M., GAN, W. J., DO, O. H., SCHWIENING, C. J., GAISANO, H. Y. & THORN, P. 2014. Insulin secretion from beta cells in intact mouse islets is targeted towards the vasculature. *Diabetologia*, 57, 1655-1663.
- LUCEY, B. P., NELSON-REES, W. A. & HUTCHINS, G. M. 2009. Henrietta Lacks, HeLa Cells, and Cell Culture Contamination. *Archives of Pathology & Laboratory Medicine*, 133, 1463-1467.
- LUOPAJÄRVI, K., SAVILAHTI, E., VIRTANEN, S. M., ILONEN, J., KNIP, M., ÅKERBLOM, H. K. & VAARALA, O. 2008. Enhanced levels of cow's milk antibodies in infancy in children who develop type 1 diabetes later in childhood. *Pediatric diabetes*, 9, 434-441.
- MACDONALD, P. E., BRAUN, M., GALVANOVSKIS, J. & RORSMAN, P. 2006. Release of small transmitters through kiss-and-run fusion pores in rat pancreatic β cells. *Cell metabolism*, 4, 283-290.
- MACFARLANE, W., READ, M., GILLIGAN, M., BUJALSKA, I. & DOCHERTY, K. 1994. Glucose modulates the binding activity of the β -cell transcription factor IUF1 in a phosphorylation-dependent manner. *Biochemical Journal*, 303, 625-631.
- MACFARLANE, W. M., CAMPBELL, S. C., ELRICK, L. J., OATES, V., BERMANO, G., LINDLEY, K. J., AYSLEY-GREEN, A., DUNNE, M. J., JAMES, R. F. & DOCHERTY, K. 2000. Glucose regulates islet amyloid polypeptide gene transcription in a PDX1- and calcium-dependent manner. *Journal of Biological Chemistry*, 275, 15330-15335.
- MADSEN, K. L., ERIKSEN, J., MILAN-LOBO, L., HAN, D. S., NIV, M. Y., AMMENDRUP-JOHNSEN, I., HENRIKSEN, U., BHATIA, V. K., STAMOU, D. & SITTE, H. H. 2008. Membrane localization is critical for activation of the PICK1 BAR domain. *Traffic*, 9, 1327-1343.
- MANN, E. & BELLIN, M. D. 2016. Secretion of Insulin in Response to Diet and Hormones. *Pancreapedia: The Exocrine Pancreas Knowledge Base*.
- MARRIF, H. I. & AL-SUNOUSI, S. I. 2016. Pancreatic β cell mass death. *Frontiers in pharmacology*, 7, 83.
- MARTINO, T. A., PETRIC, M., WEINGARTL, H., BERGELSON, J. M., OPAVSKY, M. A., RICHARDSON, C. D., MODLIN, J. F., FINBERG, R. W., KAIN, K. C. & WILLIS, N. 2000. The coxsackie-adenovirus receptor (CAR) is used by reference strains and clinical isolates representing all six serotypes of coxsackievirus group B and by swine vesicular disease virus. *Virology*, 271, 99-108.

- MATSCHINSKY, F. M. 1990. Glucokinase as glucose sensor and metabolic signal generator in pancreatic β -cells and hepatocytes. *Diabetes*, 39, 647-652.
- MATSUMOTO, K., SHARIAT, S. F., AYALA, G. E., RAUEN, K. A. & LERNER, S. P. 2005. Loss of coxsackie and adenovirus receptor expression is associated with features of aggressive bladder cancer. *Urology*, 66, 441-446.
- MATTHÄUS, C., LANGHORST, H., SCHÜTZ, L., JÜTTNER, R. & RATHJEN, F. G. 2017. Cell-cell communication mediated by the CAR subgroup of immunoglobulin cell adhesion molecules in health and disease. *Molecular and Cellular Neuroscience*, 81, 32-40.
- MCCLUSKEY, J. T., HAMID, M., GUO-PARKE, H., MCCLENAGHAN, N. H., GOMIS, R. & FLATT, P. R. 2011. Development and functional characterization of insulin-releasing human pancreatic beta cell lines produced by electrofusion. *Journal of Biological Chemistry*, 286, 21982-21992.
- MCDONALD, A., FOGARTY, S., LECLERC, I., HILL, E. V., HARDIE, D. G. & RUTTER, G. A. 2009. Control of insulin granule dynamics by AMPK dependent KLC1 phosphorylation. *Islets*, 1, 198-209.
- MCDONALD, D., STOCKWIN, L., MATZOW, T., ZAJDEL, M. B. & BLAIR, G. 1999. Coxsackie and adenovirus receptor (CAR)-dependent and major histocompatibility complex (MHC) class I-independent uptake of recombinant adenoviruses into human tumour cells. *Gene therapy*, 6, 1512.
- MCSHARRY, J. J. 1994. Uses of flow cytometry in virology. *Clinical Microbiology Reviews*, 7, 576-604.
- MENA, I., FISCHER, C., GEBHARD, J. R., PERRY, C. M., HARKINS, S. & WHITTON, J. L. 2000. Coxsackievirus Infection of the Pancreas: Evaluation of Receptor Expression, Pathogenesis, and Immunopathology. *Virology*, 271, 276-288.
- MENDELSON, C. L., WIMMER, E. & RACANIELLO, V. R. 1989. Cellular receptor for poliovirus: molecular cloning, nucleotide sequence, and expression of a new member of the immunoglobulin superfamily. *Cell*, 56, 855-865.
- MIRZA, M., PANG, M.-F., ZAINI, M. A., HAIKO, P., TAMMELA, T., ALITALO, K., PHILIPSON, L., FUXE, J. & SOLLERBRANT, K. 2012. Essential role of the coxsackie-and adenovirus receptor (CAR) in development of the lymphatic system in mice. *PloS one*, 7, e37523.
- MIRZA, M., RASCHPERGER, E., PHILIPSON, L., PETTERSSON, R. F. & SOLLERBRANT, K. 2005. The cell surface protein coxsackie-and adenovirus receptor (CAR) directly associates with the Ligand-of-Numb Protein-X2 (LNX2). *Experimental cell research*, 309, 110-120.
- MITRA, N., SINHA, S., RAMYA, T. N. & SUROLIA, A. 2006. N-linked oligosaccharides as outfitters for glycoprotein folding, form and function. *Trends in biochemical sciences*, 31, 156-163.
- MORGAN, N. G. & RICHARDSON, S. J. 2014. Enteroviruses as causative agents in type 1 diabetes: loose ends or lost cause? *Trends in Endocrinology & Metabolism*, 25, 611-619.
- MORIN, R., BAINBRIDGE, M., FEJES, A., HIRST, M., KRZYWINSKI, M., PUGH, T., MCDONALD, H., VARHOL, R., JONES, S. & MARRA, M. 2008. Profiling the HeLa S3 transcriptome using randomly primed cDNA and massively parallel short-read sequencing. *Biotechniques*, 45, 81-94.
- MORTON, P. E., HICKS, A., NASTOS, T., SANTIS, G. & PARSONS, M. 2013. CAR regulates epithelial cell junction stability through control of E-cadherin trafficking. *Scientific reports*, 3, 2889.
- NAGGERT, J. K., FRICKER, L. D., VARLAMOV, O., NISHINA, P. M., ROUILLE, Y., STEINER, D. F., CARROLL, R. J., PAIGEN, B. J. & LEITER, E. H. 1995. Hyperproinsulinaemia in obese fat/fat mice associated with a carboxypeptidase E mutation which reduces enzyme activity. *Nature genetics*, 10, 135.
- NAIK, R. G. & PALMER, J. P. 2003. Latent autoimmune diabetes in adults (LADA). *Reviews in Endocrine and Metabolic Disorders*, 4, 233-241.

- NATHANS, D. & DANNA, K. J. 1972. SPECIFIC ORIGIN IN SV40 DNA-REPLICATION. *Nature-New Biology*, 236, 200-&.
- NEHER, E. 1998. Vesicle Pools and Ca^{2+} Microdomains: New Tools for Understanding Their Roles in Neurotransmitter Release. *Neuron*, 20, 389-399.
- NESHER, R. & CERASI, E. 2002. Modeling phasic insulin release: immediate and time-dependent effects of glucose. *Diabetes*, 51, S53-S59.
- NEWGARD, C. B. & MCGARRY, J. D. 1995. Metabolic coupling factors in pancreatic β -cell signal transduction. *Annual review of biochemistry*, 64, 689-719.
- NGUYEN, D. H., ZHOU, T., SHU, J. & MAO, J. 2013. Quantifying chromogen intensity in immunohistochemistry via reciprocal intensity. *Cancer InCytes*, 2, e.
- NOBLE, J. A. & ERLICH, H. A. 2012. Genetics of type 1 diabetes. *Cold Spring Harbor perspectives in medicine*, 2, a007732.
- NOUSIAS, M., FECHNER, H., DE JONGE, H., WANG, X., DEKKERS, D., HOUTSMULLER, A., PAUSCHINGER, M., BERGELSON, J., WARRAICH, R. & YACOUB, M. 2001. Human coxsackie-adenovirus receptor is colocalized with integrins $\alpha\beta3$ and $\alpha\beta5$ on the cardiomyocyte sarcolemma and upregulated in dilated cardiomyopathy: implications for cardiotropic viral infections. *Circulation*, 104, 275-280.
- OIKARINEN, S., TAURIAINEN, S., HOBER, D., LUCAS, B., VAZEOU, A., SIOOFY-KHOJINE, A., BOZAS, E., MUIR, P., HONKANEN, H. & ILONEN, J. 2014. Virus antibody survey in different European populations indicates risk association between coxsackievirus B1 and type 1 diabetes. *Diabetes*, 63, 655-662.
- OKEGAWA, T., LI, Y., PONG, R.-C., BERGELSON, J. M., ZHOU, J. & HSIEH, J.-T. 2000. The dual impact of coxsackie and adenovirus receptor expression on human prostate cancer gene therapy. *Cancer research*, 60, 5031-5036.
- OKEGAWA, T., PONG, R.-C., LI, Y., BERGELSON, J. M., SAGALOWSKY, A. I. & HSIEH, J.-T. 2001. The mechanism of the growth-inhibitory effect of coxsackie and adenovirus receptor (CAR) on human bladder cancer: a functional analysis of car protein structure. *Cancer research*, 61, 6592-6600.
- OLOFSSON, C. S., GÖPEL, S. O., BARG, S., GALVANOVSKIS, J., MA, X., SALEHI, A., RORSMAN, P. & ELIASSON, L. 2002. Fast insulin secretion reflects exocytosis of docked granules in mouse pancreatic B-cells. *Pflügers Archiv*, 444, 43-51.
- OLSSON, A., JOHANSSON, U., KORSGREN, O. & FRISK, G. 2005. Inflammatory gene expression in Coxsackievirus B-4-infected human islets of Langerhans. *Biochemical and biophysical research communications*, 330, 571-576.
- OMASITS, U., AHRENS, C. H., MÜLLER, S. & WOLLSCHIED, B. 2014. Protter: interactive protein feature visualization and integration with experimental proteomic data. *Bioinformatics*, 30, 884-886.
- ORCI, L., RAVAZZOLA, M., AMHERDT, M., MADSEN, O., PERRELET, A., VASSALLI, J. D. & ANDERSON, R. G. 1986. Conversion of proinsulin to insulin occurs coordinately with acidification of maturing secretory vesicles. *J Cell Biol*, 103, 2273-81.
- ORGANTINI, L. J., MAKHOV, A. M., CONWAY, J. F., HAFENSTEIN, S. & CARSON, S. D. 2014. Kinetic and structural analysis of coxsackievirus B3 receptor interactions and formation of the A-particle. *Journal of virology*, 88, 5755-5765.
- PANDOL, S. J. The exocrine pancreas. Colloquium Series on Integrated Systems Physiology: From Molecule to Function, 2011. Morgan & Claypool Life Sciences, 1-64.
- PATTERSON, C., GUARIGUATA, L., DAHLQUIST, G., SOLTÉSZ, G., OGLE, G. & SILINK, M. 2014. Diabetes in the young—a global view and worldwide estimates of numbers of children with type 1 diabetes. *Diabetes research and clinical practice*, 103, 161-175.
- PATTERSON, C., GYÜRÜS, E., ROSENBAUER, J., CINEK, O., NEU, A., SCHOBER, E., PARSLAW, R., JONER, G., SVENSSON, J. & CASTELL, C. 2012. Trends in childhood type 1 diabetes incidence in Europe during 1989–2008: evidence of non-uniformity over time in rates of increase. *Diabetologia*, 55, 2142-2147.

- PATTERSON, C. C., DAHLQUIST, G. G., GYÜRÜS, E., GREEN, A., SOLTÉSZ, G. & GROUP, E. S. 2009. Incidence trends for childhood type 1 diabetes in Europe during 1989–2003 and predicted new cases 2005–20: a multicentre prospective registration study. *The Lancet*, 373, 2027-2033.
- PAZIRANDEH, A., SULTANA, T., MIRZA, M., ROZELL, B., HULTENBY, K., WALLIS, K., VENNSTRÖM, B., DAVIS, B., ARNER, A. & HEUCHEL, R. 2011. Multiple phenotypes in adult mice following inactivation of the Coxsackievirus and Adenovirus Receptor (Car) gene. *PLoS one*, 6, e20203.
- PELLEGRINI, S., SORDI, V., BOLLA, A. M., SAITA, D., FERRARESE, R., CANDUCCI, F., CLEMENTI, M., INVERNIZZI, F., MARIANI, A. & BONFANTI, R. 2017. Duodenal mucosa of patients with type 1 diabetes shows distinctive inflammatory profile and microbiota. *The Journal of Clinical Endocrinology & Metabolism*, 102, 1468-1477.
- PERSSON, A., FAN, X., WIDEGREN, B. & ENGLUND, E. 2006. Cell type-and region-dependent coxsackie adenovirus receptor expression in the central nervous system. *Journal of neuro-oncology*, 78, 1-6.
- PHILIPSON, L. & PETTERSSON, R. 2004. The coxsackie-adenovirus receptor—a new receptor in the immunoglobulin family involved in cell adhesion. *Adenoviruses: Model and Vectors in Virus-Host Interactions*. Springer.
- PINHEIRO, P. S., JANSEN, A. M., DE WIT, H., TAWFIK, B., MADSEN, K. L., VERHAGE, M., GETHER, U. & SØRENSEN, J. B. 2014. The BAR domain protein PICK1 controls vesicle number and size in adrenal chromaffin cells. *Journal of Neuroscience*, 34, 10688-10700.
- PINKERT, S., DIERINGER, B., DIEDRICH, S., ZEICHHARDT, H., KURRECK, J. & FECHNER, H. 2016. Soluble coxsackie- and adenovirus receptor (sCAR-Fc); a highly efficient compound against laboratory and clinical strains of coxsackie-B-virus. *Antiviral Research*, 136, 1-8.
- POLACEK, C., EKSTRÖM, J.-O., LUNDGREN, A. & LINDBERG, A. M. 2005. Cytolytic replication of coxsackievirus B2 in CAR-deficient rhabdomyosarcoma cells. *Virus research*, 113, 107-115.
- POOLA-KELLA, S., STEINMAN, R. A., MESMAR, B. & MALEK, R. 2018. Gestational diabetes mellitus: post-partum risk and follow up. *Reviews on recent clinical trials*, 13, 5-14.
- RASCHPERGER, E., THYBERG, J., PETTERSSON, S., PHILIPSON, L., FUXE, J. & PETTERSSON, R. F. 2006. The coxsackie-and adenovirus receptor (CAR) is an in vivo marker for epithelial tight junctions, with a potential role in regulating permeability and tissue homeostasis. *Experimental cell research*, 312, 1566-1580.
- RAVASSARD, P., HAZHOUS, Y., PECHBERTY, S., BRICOUT-NEVEU, E., ARMANET, M., CZERNICHOW, P. & SCHARFMANN, R. 2011. A genetically engineered human pancreatic β cell line exhibiting glucose-inducible insulin secretion. *The Journal of clinical investigation*, 121, 3589-3597.
- REDA, T. K., GELIEBTER, A. & PI-SUNYER, F. X. 2002. Amylin, food intake, and obesity. *Obesity*, 10, 1087-1091.
- REDONDO, M. J., REWERS, M., YU, L., GARG, S., PILCHER, C. C., ELLIOTT, R. B. & EISENBARTH, G. S. 1999. Genetic determination of islet cell autoimmunity in monozygotic twin, dizygotic twin, and non-twin siblings of patients with type 1 diabetes: prospective twin study. *Bmj*, 318, 698-702.
- RHOADES, R. E., TABOR-GODWIN, J. M., TSUENG, G. & FEUER, R. 2011. Enterovirus Infections of the Central Nervous System Review. *Virology*, 411, 288-305.
- RICHARDSON, S. J. & HORWITZ, M. S. 2014. Is type 1 diabetes “going viral”? *Diabetes*, 63, 2203-2205.
- RICHARDSON, S. J., LEETE, P., BONE, A. J., FOULIS, A. K. & MORGAN, N. G. 2013. Expression of the enteroviral capsid protein VP1 in the islet cells of patients with

- type 1 diabetes is associated with induction of protein kinase R and downregulation of Mcl-1. *Diabetologia*, 56, 185-93.
- RICHARDSON, S. J., MORGAN, N. G. & FOULIS, A. K. 2014. Pancreatic Pathology in Type 1 Diabetes Mellitus. *Endocrine Pathology*, 25, 80-92.
- RICHARDSON, S. J., RODRIGUEZ-CALVO, T., GERLING, I. C., MATHEWS, C. E., KADDIS, J. S., RUSSELL, M. A., ZEISSLER, M., LEETE, P., KROGVOLD, L., DAHL-JORGENSEN, K., VON HERRATH, M., PUGLIESE, A., ATKINSON, M. A. & MORGAN, N. G. 2016. Islet cell hyperexpression of HLA class I antigens: a defining feature in type 1 diabetes. *Diabetologia*, 59, 2448-2458.
- RICHARDSON, S. J., WILLCOX, A., BONE, A., FOULIS, A. K. & MORGAN, N. G. 2009. The prevalence of enteroviral capsid protein vp1 immunostaining in pancreatic islets in human type 1 diabetes. *Diabetologia*, 52, 1143-1151.
- RODRIGUEZ-CALVO, T., SABOURI, S., ANQUETIL, F. & VON HERRATH, M. G. 2016. The viral paradigm in type 1 diabetes: Who are the main suspects? *Autoimmunity reviews*, 15, 964-969.
- RODRIGUEZ-DIAZ, R. & CAICEDO, A. 2013. Novel approaches to studying the role of innervation in the biology of pancreatic islets. *Endocrinology and Metabolism Clinics*, 42, 39-56.
- ROIVAINEN, M., RASILAINEN, S., YLIPAASTO, P., NISSINEN, R., USTINOV, J., BOUWENS, L., EIZIRIK, D. L., HOVI, T. & OTONKOSKI, T. 2000. Mechanisms of Coxsackievirus-Induced Damage to Human Pancreatic β -Cells 1. *The Journal of Clinical Endocrinology & Metabolism*, 85, 432-440.
- RORSMAN, P. & BRAUN, M. 2013. Regulation of insulin secretion in human pancreatic islets. *Annual review of physiology*, 75, 155-179.
- RORSMAN, P., ELIASSON, L., RENSTROM, E., GROMADA, J., BARG, S. & GOPEL, S. 2000. The cell physiology of biphasic insulin secretion. *Physiology*, 15, 72-77.
- RORSMAN, P. & RENSTRÖM, E. 2003. Insulin granule dynamics in pancreatic beta cells. *Diabetologia*, 46, 1029-1045.
- ROSS, M. E., HAYASHI, K. & NOTKINS, A. L. 1974. Virus-induced pancreatic disease: alterations in concentration of glucose and amylase in blood. *Journal of Infectious Diseases*, 129, 669-676.
- SACHS, M. D., RAUEN, K. A., RAMAMURTHY, M., DODSON, J. L., DE MARZO, A. M., PUTZI, M. J., SCHOENBERG, M. P. & RODRIGUEZ, R. 2002. Integrin α v and coxsackie adenovirus receptor expression in clinical bladder cancer. *Urology*, 60, 531-536.
- SAITO, K., YAGINUMA, N. & TAKAHASHI, T. 1979. Differential volumetry of A, B and D cells in the pancreatic islets of diabetic and nondiabetic subjects. *The Tohoku journal of experimental medicine*, 129, 273-283.
- SAKULA, A. 1988. Paul Langerhans (1847-1888): a centenary tribute. *Journal of the Royal Society of Medicine*, 81, 414-415.
- SANTIN, I. & EIZIRIK, D. L. 2013. Candidate genes for type 1 diabetes modulate pancreatic islet inflammation and β -cell apoptosis. *Diabetes, Obesity and Metabolism*, 15, 71-81.
- SCHLOOT, N. C., WILLEMEN, S., DUINKERKEN, G., DRIJFHOUT, J., DE VRIES, R. & ROEP, B. 2001. Molecular mimicry in type 1 diabetes mellitus revisited: T-cell clones to GAD65 peptides with sequence homology to Coxsackie or proinsulin peptides do not crossreact with homologous counterpart. *Human immunology*, 62, 299-309.
- SCHREIBER, J., LANGHORST, H., JÜTTNER, R. & RATHJEN, F. G. 2014. The IgCAMs CAR, BT-IgSF, and CLMP: structure, function, and diseases. *Cell Adhesion Molecules*. Springer.
- SCHULTE, B. M., BAKKERS, J., LANKE, K. H., MELCHERS, W. J., WESTERLAKEN, C., ALLEBES, W., AANSTOOT, H.-J., BRUINING, G. J., ADEMA, G. J. & VAN KUPPEVELD, F. J. 2010. Detection of enterovirus RNA in peripheral blood mononuclear cells of type 1 diabetic patients beyond the stage of acute infection. *Viral Immunology*, 23, 99-104.

- SHAFREN, D. R., BATES, R. C., AGREZ, M. V., HERD, R. L., BURNS, G. F. & BARRY, R. D. 1995. Coxsackieviruses B1, B3, and B5 use decay accelerating factor as a receptor for cell attachment. *Journal of virology*, 69, 3873-3877.
- SHAFREN, D. R., DORAHY, D. J., INGHAM, R. A., BURNS, G. F. & BARRY, R. D. 1997. Coxsackievirus A21 binds to decay-accelerating factor but requires intercellular adhesion molecule 1 for cell entry. *Journal of virology*, 71, 4736-4743.
- SHAW, C., HOLLAND, P., SINNREICH, M., ALLEN, C., SOLLERBRANT, K., KARPATI, G. & NALBANTOGLU, J. 2004. Isoform-specific expression of the Coxsackie and adenovirus receptor (CAR) in neuromuscular junction and cardiac intercalated discs. *BMC Cell Biology*, 5, 42.
- SHEVTSOVA, Z., MALIK, J., MICHEL, U., SCHÖLL, U., BÄHR, M. & KÜGLER, S. 2006. Evaluation of epitope tags for protein detection after in vivo CNS gene transfer. *European Journal of Neuroscience*, 23, 1961-1969.
- SHI, S. R., KEY, M. E. & KALRA, K. L. 1991. Antigen retrieval in formalin-fixed, paraffin-embedded tissues: an enhancement method for immunohistochemical staining based on microwave oven heating of tissue sections. *Journal of Histochemistry & Cytochemistry*, 39, 741-748.
- SHI, Y., CHEN, C., LISEWSKI, U., WRACKMEYER, U., RADKE, M., WESTERMANN, D., SAUTER, M., TSCHÖPE, C., POLLER, W., KLINGEL, K. & GOTTHARDT, M. 2009. Cardiac Deletion of the Coxsackievirus-Adenovirus Receptor Abolishes Coxsackievirus B3 Infection and Prevents Myocarditis In Vivo. *Journal of the American College of Cardiology*, 53, 1219-1226.
- SHIBASAKI, T., SUNAGA, Y., FUJIMOTO, K., KASHIMA, Y. & SEINO, S. 2004. Interaction of ATP sensor, cAMP sensor, Ca²⁺ sensor, and voltage-dependent Ca²⁺ channel in insulin granule exocytosis. *Journal of Biological Chemistry*, 279, 7956-7961.
- SHIELDS, B. M., HICKS, S., SHEPHERD, M. H., COLCLOUGH, K., HATTERSLEY, A. T. & ELLARD, S. 2010. Maturity-onset diabetes of the young (MODY): how many cases are we missing? *Diabetologia*, 53, 2504-2508.
- SIOOFY-KHOJINE, A.-B., LEHTONEN, J., NURMINEN, N., LAITINEN, O. H., OIKARINEN, S., HUHTALA, H., PAKKANEN, O., RUOKORANTA, T., HANKANIEMI, M. M. & TOPPARI, J. 2018. Coxsackievirus B1 infections are associated with the initiation of insulin-driven autoimmunity that progresses to type 1 diabetes. *Diabetologia*, 1-10.
- SLOT, J. W. & GEUZE, H. J. 2007. Cryosectioning and immunolabeling. *Nat Protoc*, 2, 2480-91.
- SMEETS, S. 2015. Microscopic anatomy of the human islet of Langerhans. *Islets of Langerhans*. Springer.
- STECKER, K., VIETH, M., KOSCHEL, A., WIEDENMANN, B., RÖCKEN, C. & ANDERS, M. 2011. Impact of the coxsackievirus and adenovirus receptor on the adenoma-carcinoma sequence of colon cancer. *British journal of cancer*, 104, 1426.
- STEFAN, Y., ORCI, L., MALAISSE-LAGAE, F., PERRELET, A., PATEL, Y. & UNGER, R. H. 1982. Quantitation of endocrine cell content in the pancreas of nondiabetic and diabetic humans. *Diabetes*, 31, 694-700.
- STONE, V. M., HANKANIEMI, M. M., SVEDIN, E., SIOOFY-KHOJINE, A., OIKARINEN, S., HYÖTY, H., LAITINEN, O. H., HYTÖNEN, V. P. & FLODSTRÖM-TULLBERG, M. 2018. A Coxsackievirus B vaccine protects against virus-induced diabetes in an experimental mouse model of type 1 diabetes. *Diabetologia*, 61, 476-481.
- SU, Q., CAI, Q., GERWIN, C., SMITH, C. L. & SHENG, Z.-H. 2004. Syntabulin is a microtubule-associated protein implicated in syntaxin transport in neurons. *Nature cell biology*, 6, 941.
- SUGITA, S., JANZ, R. & SÜDHOF, T. C. 1999. Synaptogyrins regulate Ca²⁺-dependent exocytosis in PC12 cells. *Journal of Biological Chemistry*, 274, 18893-18901.
- SZOPA, T., DRONFIELD, D., WARD, T. & TAYLOR, K. 1989. In Vivo Infection of Mice with Coxsackie B4 Virus Induces Long-term Functional Changes in Pancreatic Islets with Minimal Alteration in Blood Glucose. *Diabetic medicine*, 6, 314-319.

- TAJADINI, M., PANJEHPOUR, M. & JAVANMARD, S. H. 2014. Comparison of SYBR Green and TaqMan methods in quantitative real-time polymerase chain reaction analysis of four adenosine receptor subtypes. *Adv Biomed Res*, 3, 85.
- TAKAHASHI, N., KISHIMOTO, T., NEMOTO, T., KADOWAKI, T. & KASAI, H. 2002. Fusion pore dynamics and insulin granule exocytosis in the pancreatic islet. *Science*, 297, 1349-1352.
- TAM, P. E. & MESSNER, R. P. 1999. Molecular mechanisms of coxsackievirus persistence in chronic inflammatory myopathy: viral RNA persists through formation of a double-stranded complex without associated genomic mutations or evolution. *Journal of virology*, 73, 10113-10121.
- TARASKA, J. W., PERRAIS, D., OHARA-IMAIZUMI, M., NAGAMATSU, S. & ALMERS, W. 2003. Secretory granules are recaptured largely intact after stimulated exocytosis in cultured endocrine cells. *Proceedings of the National Academy of Sciences*, 100, 2070-2075.
- THOELN, I., MAGNUSSON, C., TÅGERUD, S., POLACEK, C., LINDBERG, M. & VAN RANST, M. 2001. Identification of alternative splice products encoded by the human coxsackie-adenovirus receptor gene. *Biochemical and biophysical research communications*, 287, 216-222.
- THORENS, B. 1992. Molecular and Cellular Physiology of GLUT-2, a High-Km Facilitated Diffusion Glucose Transporter. *International review of cytology*. Elsevier.
- THURMOND, D. C., GONELLE-GISPERT, C., FURUKAWA, M., HALBAN, P. A. & PESSIN, J. E. 2003. Glucose-stimulated insulin secretion is coupled to the interaction of actin with the t-SNARE (target membrane soluble N-ethylmaleimide-sensitive factor attachment protein receptor protein) complex. *Molecular endocrinology*, 17, 732-742.
- TODD, J. A. 2010. Etiology of Type 1 Diabetes. *Immunity*, 32, 457-467.
- TOKARZ, V. L., MACDONALD, P. E. & KLIP, A. 2018. The cell biology of systemic insulin function. *J Cell Biol*, jcb. 201802095.
- TOMKO, R. P., XU, R. & PHILIPSON, L. 1997. HCAR and MCAR: the human and mouse cellular receptors for subgroup C adenoviruses and group B coxsackieviruses. *Proceedings of the National Academy of Sciences*, 94, 3352-3356.
- TRACY, S., SMITHEE, S., ALHAZMI, A. & CHAPMAN, N. 2015. Coxsackievirus can persist in murine pancreas by deletion of 5' terminal genomic sequences. *Journal of medical virology*, 87, 240-247.
- TRIVEDI, P., GRAHAM, K. L., KRISHNAMURTHY, B., FYNCH, S., SLATTERY, R. M., KAY, T. W. & THOMAS, H. E. 2016. Perforin facilitates beta cell killing and regulates autoreactive CD8+ T-cell responses to antigen in mouse models of type 1 diabetes. *Immunology & Cell Biology*, 94, 334-341.
- TSUBOI, T. & RUTTER, G. A. 2003. Multiple forms of "kiss-and-run" exocytosis revealed by evanescent wave microscopy. *Current Biology*, 13, 563-567.
- V. MERING, J. & MINKOWSKI, O. 1890. Diabetes mellitus nach Pankreasexstirpation. *Archiv für experimentelle Pathologie und Pharmakologie*, 26, 371-387.
- VAN'T HOF, W. & CRYSTAL, R. G. 2002. Fatty acid modification of the coxsackievirus and adenovirus receptor. *Journal of virology*, 76, 6382-6386.
- VARADI, A., AINSCOW, E. K., ALLAN, V. J. & RUTTER, G. A. 2002. Involvement of conventional kinesin in glucose-stimulated secretory granule movements and exocytosis in clonal pancreatic β -cells. *Journal of cell science*, 115, 4177-4189.
- VERHAGE, M. & SØRENSEN, J. B. 2008. Vesicle docking in regulated exocytosis. *Traffic*, 9, 1414-1424.
- VON ENGELHARDT, D. 1989. Outlines of Historical Development. In: VON ENGELHARDT, D. (ed.) *Diabetes Its Medical and Cultural History: Outlines — Texts — Bibliography*. Berlin, Heidelberg: Springer Berlin Heidelberg.
- VOSBERG, H.-P. 1977. Molecular cloning of DNA. *Human Genetics*, 40, 1-72.
- WANG, X. & BERGELSON, J. M. 1999. Coxsackievirus and adenovirus receptor cytoplasmic and transmembrane domains are not essential for coxsackievirus and adenovirus infection. *Journal of virology*, 73, 2559-2562.

- WEIR, G. C. & BONNER-WEIR, S. 2013. Islet β cell mass in diabetes and how it relates to function, birth, and death. *Annals of the New York Academy of Sciences*, 1281, 92-105.
- WILLCOX, A., RICHARDSON, S. J., BONE, A. J., FOULIS, A. K. & MORGAN, N. G. 2009. Analysis of islet inflammation in human type 1 diabetes. *Clinical & Experimental Immunology*, 155, 173-181.
- XIA, J., ZHANG, X., STAUDINGER, J. & HUGANIR, R. L. 1999. Clustering of AMPA receptors by the synaptic PDZ domain-containing protein PICK1. *Neuron*, 22, 179-187.
- XIAO, N., KAM, C., SHEN, C., JIN, W., WANG, J., LEE, K. M., JIANG, L. & XIA, J. 2009. PICK1 deficiency causes male infertility in mice by disrupting acrosome formation. *The Journal of clinical investigation*, 119, 802-812.
- XU, J., WANG, N., LUO, J.-H. & XIA, J. 2016. Syntabulin regulates the trafficking of PICK1-containing vesicles in neurons. *Scientific reports*, 6, 20924.
- XU, J. & XIA, J. 2006. Structure and function of PICK1. *Neurosignals*, 15, 190-201.
- YANAGAWA, B., SPILLER, O. B., PROCTOR, D. G., CHOY, J., LUO, H., ZHANG, H. M., SUAREZ, A., YANG, D. & MCMANUS, B. M. 2004. Soluble Recombinant Coxsackievirus and Adenovirus Receptor Abrogates Coxsackievirus B3-Mediated Pancreatitis and Myocarditis in Mice. *The Journal of Infectious Diseases*, 189, 1431-1439.
- YANG, Y., HUA, Q.-X., LIU, J., SHIMIZU, E. H., CHOQUETTE, M. H., MACKIN, R. B. & WEISS, M. A. 2010. Solution structure of proinsulin connecting domain flexibility and prohormone processing. *Journal of Biological Chemistry*, 285, 7847-7851.
- YEUNG, W.-C. G., RAWLINSON, W. D. & CRAIG, M. E. 2011. Enterovirus infection and type 1 diabetes mellitus: systematic review and meta-analysis of observational molecular studies. *Bmj*, 342, d35.
- YING, Y., LI, L., CAO, W., YAN, D., ZENG, Q., KONG, X., LU, L., YAN, M., XU, X. & QU, J. 2012. The microtubule associated protein syntabulin is required for glucose-stimulated and cAMP-potentiated insulin secretion. *FEBS letters*, 586, 3674-3680.
- YLIPAASTO, P., KLINGEL, K., LINDBERG, A. M., OTONKOSKI, T., KANDOLF, R., HOVI, T. & ROIVAINEN, M. 2004. Enterovirus infection in human pancreatic islet cells, islet tropism in vivo and receptor involvement in cultured islet beta cells. *Diabetologia*, 47, 225-239.
- YONELINAS, A. P. 2013. The Hippocampus Supports High-Resolution Binding in the Service of Perception, Working Memory and Long-Term Memory. *Behavioural brain research*, 254, 34-44.
- YOON, J.-W., AUSTIN, M., ONODERA, T. & NOTKINS, A. L. 1979. Virus-induced diabetes mellitus: isolation of a virus from the pancreas of a child with diabetic ketoacidosis. *New England Journal of Medicine*, 300, 1173-1179.
- ZEN, K., LIU, Y., MCCALL, I. C., WU, T., LEE, W., BABBIN, B. A., NUSRAT, A. & PARKOS, C. A. 2005. Neutrophil migration across tight junctions is mediated by adhesive interactions between epithelial coxsackie and adenovirus receptor and a junctional adhesion molecule-like protein on neutrophils. *Molecular biology of the cell*, 16, 2694-2703.
- ZIEGLER, A. G., REWERS, M., SIMELL, O., SIMELL, T., LEMPAINEN, J., STECK, A., WINKLER, C., ILONEN, J., VEIJOLA, R. & KNIP, M. 2013. Seroconversion to multiple islet autoantibodies and risk of progression to diabetes in children. *Jama*, 309, 2473-2479.
- ZUSSY, C., LOUSTALOT, F., JUNYENT, F., GARDONI, F., BORIES, C., VALERO, J., DESARMÉNIEN, M. G., BERNEX, F., HENAFF, D. & BAYO-PUXAN, N. 2016. Coxsackievirus adenovirus receptor loss impairs adult neurogenesis, synapse content, and hippocampus plasticity. *Journal of Neuroscience*, 36, 9558-9571.